GEOLOGICAL SURVEY OF DENMARK AND GREENLAND BULLETIN 15 • 2008

Review of Survey activities 2007

Edited by
Ole Bennike and A. K. Higgins

GEOLOGICAL SURVEY OF DENMARK AND GREENLAND
MINISTRY OF CLIMATE AND ENERGY

Geological Survey of Denmark and Greenland Bulletin 15

Keywords
Geological Survey of Denmark and Greenland, survey organisations, current research, Denmark, Greenland.

Cover photographs from left to right

1. Field work in West Greenland. Photo: Jakob Lautrup.
2. Field work in the mo-clay region of Denmark. Photo: Stig A. Schack Pedersen.
3. Wind mills in Denmark. GEUS has been mapping the geology of new offshore wind mill farm areas. Photo: Jørn Bo Jensen.
4. Launching of seismic equipment from the Swedish icebreaker *Oden* during the LOMROG (**Lom**onosov **R**idge **o**ff **G**reenland) cruise to the Arctic Ocean in 2007. Photo: Martin Jakobsson, Stockholm University.

Frontispiece: facing page
As part of the Danish Continental Shelf Project (http://a76.dk) bathymetric, seismic and gravimetric data were acquired in August and September 2007 during the LOMROG cruise in the Arctic Ocean north of Greenland. The LOMROG project is a co-operation between institutions in Denmark, Sweden and other nations. Results from the LOMROG cruise will be published in forthcoming years. Photo: Martin Jakobsson, Stockholm University.

Chief editor of this series: Adam A. Garde
Editorial board of this series: John A. Korstgård, Department of Earth Sciences, University of Aarhus; Minik Rosing, Geological Museum, University of Copenhagen; Finn Surlyk, Department of Geography and Geology, University of Copenhagen
Scientific editors: Ole Bennike and A.K. Higgins
Editorial secretaries: Jane Holst and Esben W. Glendal
Referees: (DK = Denmark; numbers refer to first page of reviewed article): Troels Aagaard, DK (85); Anonymous (41, 45, 53, 61, 89); Geo Arnold, Holland (81); Niels Balling, DK (53); Björn E. Berglund, Sweden (57); Morten Bjerager, DK (13); Lars Ole Boldreel, DK (37); Ilke Borowski, Germany (81); Jens Bruun-Petersen, DK (37); Bjørn Buchardt, DK (13, 89); Ashton Embry, Canada (65); Ida Fabricius, DK (17); Clark Friend, UK (73); Henrik Friis, DK (9); Thomas Frisch, Canada (77); Ole Graversen, DK (25); Bent Hasholt, DK (61); Claus Heilmann-Clausen, DK (29); Claus Heinberg, DK (29); Julie A. Hollis, Australia (69, 73); Mads Huuse, UK (33); Rasmus Jacobsen, DK (45); Kurt Kjær, DK (33); Jens Konnerup-Madsen, DK (69); John A. Korstgård, DK (25); Lars Kristiansen, DK (21); Nicolaj Krog Larsen, Sweden (41, 49); Ole Bjørslev Nielsen, DK (21); Henrik Olsen, DK (49); Ian Parsons, UK (9); John S. Peel, Sweden (77); Heikki Seppä, Finland (57); Martin Sønderholm, DK (65, 93); Ole V. Vejbæk, DK (17); Jim Williamson, UK (93). (Page nos corrected Aug. 2009)
Illustrations: Jette Halskov
Lay-out and graphic production: Annabeth Andersen
Printers: Schultz Grafisk, Albertslund, Denmark
Manuscripts submitted: 4 February – 17 March 2008
Final versions approved: 28 May 2008
Printed: 10 July 2008

ISSN 1603-9769 (Review of Survey activities)
ISSN 1604-8156 (Geological Survey of Denmark and Greenland Bulletin)
ISBN 978-87-7871-213-4

Citation of the name of this series
It is recommended that the name of this series is cited in full, viz. *Geological Survey of Denmark and Greenland Bulletin*.
If abbreviation of this volume is necessary, the following form is suggested: *Geol. Surv. Den. Green. Bull.* 15, 96 pp.

Available from
Geological Survey of Denmark and Greenland (GEUS) • Øster Voldgade 10 • DK-1350 Copenhagen K • Denmark
Phone: +45 38 14 20 00, fax: +45 38 14 20 50, e-mail: geus@geus.dk


IMO 9152959
50 ЛЕТ ПОБЕДЫ

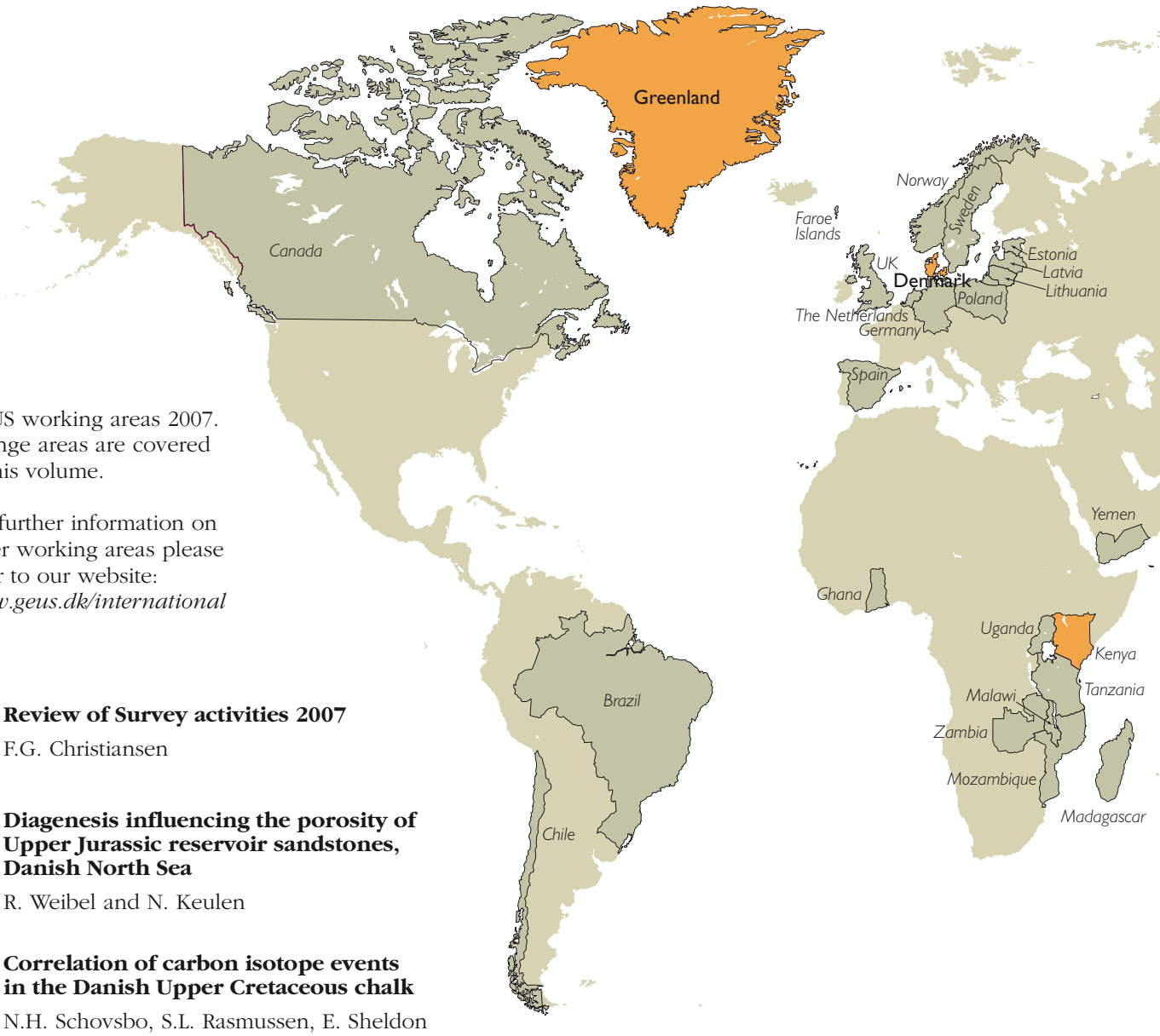

GEUS working areas 2007. Orange areas are covered in this volume.

For further information on other working areas please refer to our website: *www.geus.dk/international*

Review of Survey activities 2007

Flemming G. Christiansen
Deputy Director

After a very critical period with a major reorganisation of the scientific environment in Denmark, 2007 created new stability for the Geological Survey of Denmark and Greenland (GEUS). A new law describing the role of GEUS was passed by the Danish Parliament in the spring, followed by changes in top management and a newly formalised collaboration between GEUS, the University of Copenhagen and the University of Aarhus – the so-called Geocenter Denmark. This collaboration is very promising and will provide a much better chance of integrating young scientists in research activities.

This fifth annual issue describes selected activities that GEUS and its partners carry out in Denmark, Greenland and internationally. Together with the previous four issues it provides a good overview of the many different types of activities and projects, the advisory capacity and analytical services available from GEUS.

This 2007 review contains a total of 22 four-page papers, 13 on Denmark, five on Greenland and four with the focus on methodology or international work. Compared to the previous four that were biased towards Greenland, this issue has a majority of papers related to activities in Denmark: oil and gas, deep crustal structure, offshore wind farms, coastal processes in the Danish Wadden Sea (Vadehavet), groundwater vulnerability, raw materials, Neogene and Quaternary history, and palaeoclimate.

Chalk is the main key to the good national economy of Denmark. Better understanding of the depositional and diagenetic processes that formed the chalk and the petrophysical properties of this prolific rock is necessary to exploit the petroleum potential offshore. Chalk is covered in two papers in this issue, while two other papers on diagenesis and exhumation are also important for understanding the petroleum potential of Denmark. The deep crustal structure under Denmark is presented in one paper and Danish raw materials are described in a paper on the diatomite deposits of the Palaeogene Fur Formation.

Today climate changes and resultant adaptation are in focus. Several papers are important in this context, especially on coastal processes, understanding of the Neogene and Quaternary history, variation in palaeoclimate and monitoring of the ice sheet in Greenland.

A dramatic increase in oil and metal prices in recent years – together with abundant new targets for exploration – is the background for the boom within the oil and mining industries in Greenland. The number of licences – and the area covered by them – is historically large. Previous and ongoing research and mapping activities together with an easy access to critical data at GEUS have been very important in the process of attracting industry to Greenland. New possibilities within both the oil and mineral industries are described in papers on the sedimentary basins of Baffin Bay and on the basement terrains in south-western Greenland. The research history of the disputed island Hans Ø in Nares Strait between Greenland and Canada is also outlined in one article.

Two papers describe the development of new analytical techniques, one on the automatic use of computer-controlled scanning electron microscopy (CCSEM) very important in exploration and for quality control of industrial materials; and the other one on the use of laser ablation - inductively coupled plasma - mass spectrometry (LA-ICP-MS) for environmental studies of bivalves.

GEUS is active in international collaboration through the EU and has ongoing activities in many different countries, especially in south-east Asia and Africa. In this issue there is one paper on tsunami damage modelling in Kenya and another on implementing the EU's Water Framework Directive.

In the summer of 2007 GEUS in collaboration with other Danish and Swedish institutions and the Swedish Polar Research Secretariat acquired data in the area north of Greenland as part of the Danish Continental Shelf Project (see frontispiece). This project aims to acquire the necessary technical data to support a Danish claim for extending the juridical continental shelf beyond 200 nautical miles before 2014.

Diagenesis influencing the porosity of Upper Jurassic reservoir sandstones, Danish North Sea

Rikke Weibel and Nynke Keulen

Upper Jurassic quartz-rich sandstones in the North Sea Basin are important reservoir rocks for oil and gas, and one of the latest discoveries of oil in the Danish sector was made in the area of the Hejre wells that penetrated such sediments (Fig. 1). The reservoir properties of sandstones are strongly influenced by diagenetic alteration, i.e. the mineralogical changes that take place during burial of the sediments. The diagenetic features depend on the source area, depositional setting, facies architecture and burial history of the sediment. The major diagenetic features influencing porosity in Upper Jurassic reservoir sandstones are feldspar dissolution and precipitation, preci-pitation of illite, calcite and quartz, and quartz stylolite formation. With regard to the Upper Jurassic sandstones in the Danish sector of the North Sea, the important question is: how can porosity be preserved in sediments buried at depths of more than 5 km?

The Hejre-2 well penetrated the Upper Jurassic sediments (Fig. 2) before reaching pre-Upper Jurassic volcaniclastic conglomerates. The diagenetic features were studied in thin sections of core samples with traditional petrographic techniques using transmitted light microscopy supplemented by scanning electron microscopy (SEM) of rock chips and thin sections.

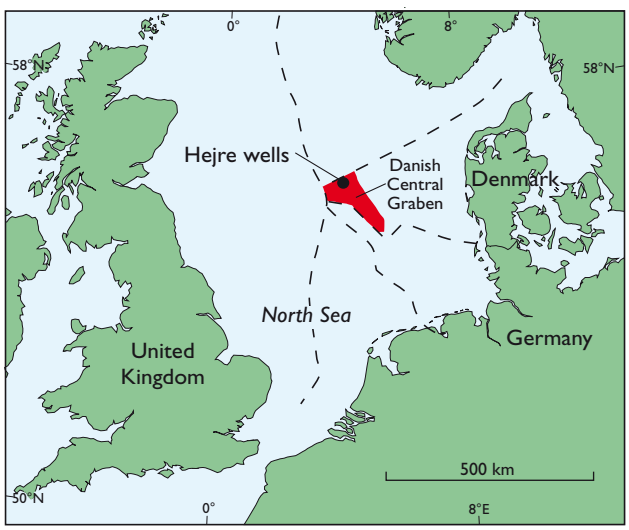

Fig. 1. Sketch map of the North Sea region showing the location of the Hejre wells. The dashed lines show the borders between the national sectors.

Feldspar dissolution and precipitation

Previous studies of feldspar diagenesis have generally focused on the albitisation of K-feldspar, the dissolution and replacement of plagioclase with clay at deep burial depths, and their importance for the generation of secondary porosity (e.g. Surdam *et al.* 1984; Bjørlykke *et al.* 1992). Recent investigations show that the formation of feldspar overgrowths may also be a significant early diagenetic phenomenon (Lee & Parsons 2003). Early diagenetic authigenic K-feldspar has also played an important role in the Upper Jurassic sandstones investigated here, although the volume of precipitated material is not nearly as high as the succeeding calcite and quartz cementation.

Detrital feldspar, and notably K-feldspar, is a common constituent of Upper Jurassic sediments. Authigenic K-feldspar may have formed during early diagenesis, but is now mainly preserved in calcite-cemented parts of the sandstones, where it forms overgrowths on detrital K-feldspar, perthite and albite grains (Fig. 3A, B). Authigenic K-feldspar is com-

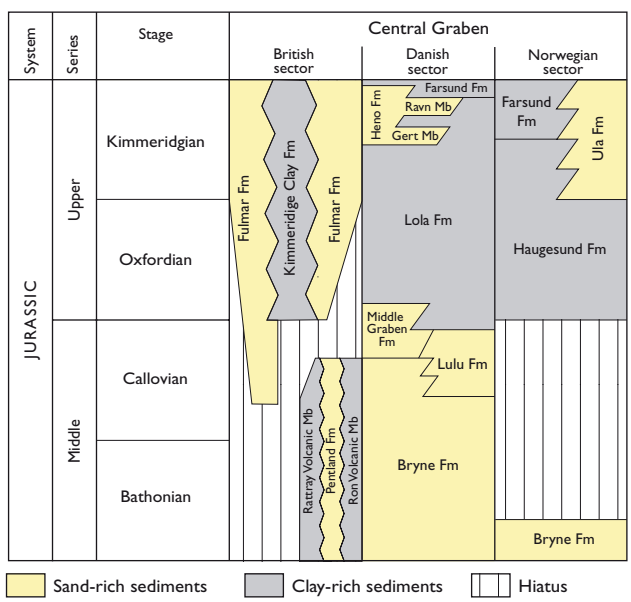

Fig. 2. Middle and Upper Jurassic lithostratigraphy of the British, Danish and Norwegian sectors of the Central Graben in the North Sea. The Hejre-2 well penetrated the Farsund Formation, the Ravn Member of the Heno Formation, the Lola Formation and the Gert Member of the Heno Formation. Simplified after Johannesen *et al.* (2003) and Michelsen *et al.* (2003).

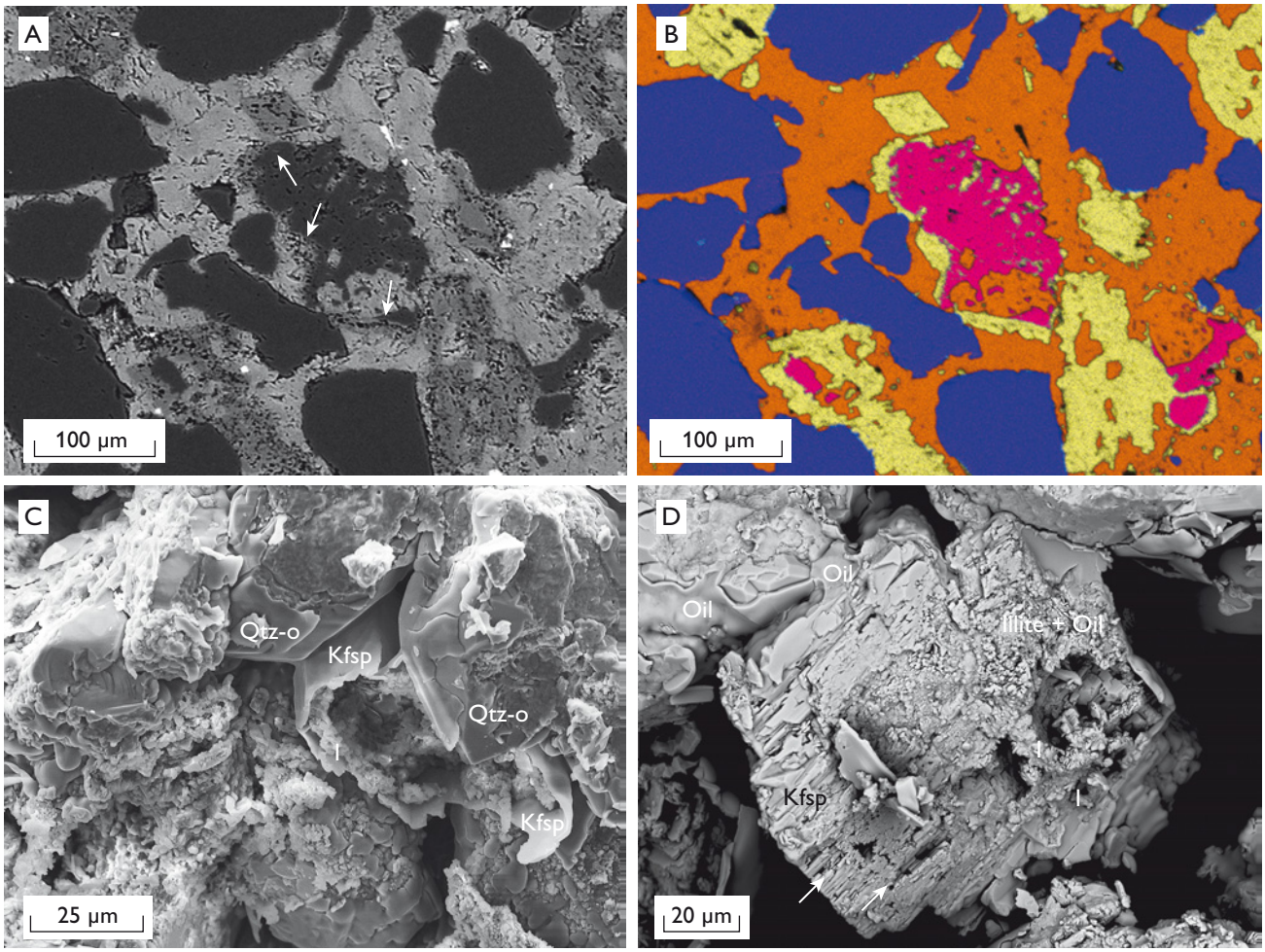

Fig. 3. Images showing diagenetic alteration of feldspars in Upper Jurassic sandstones that resulted in both reduction and increase of porosity. **A**: Abundant detrital K-feldspar and K-feldspar overgrowths (arrows) on detrital albite in calcite-cemented parts of the sandstones. Back-scattered electron SEM image. **B**: Combined element maps of the area shown in Fig. 3A. Orange, calcium; yellow, potassium; pink, sodium; blue, quartz. **C**: K-feldspar overgrowths (**Kfsp**) most likely formed on an original plagioclase grain prior to its dissolution and replacement by illite (**I**) during which substantial secondary porosity was created. Subsequent quartz overgrowths (**Qtz-o**) and compression may have reduced this porosity. Secondary electron SEM image. **D**: Detrital K-feldspar (**Kfsp**) partly dissolved (white arrows) and replaced by illite (**I**). Some oil droplets (**Oil**) can be observed. Secondary electron SEM image.

mon in the vicinity of K-bearing clay-rich intervals and in the sandstone immediately overlying volcaniclastic conglomerates.

Element mapping of the calcite-cemented parts of the sandstones shows the volumetric importance of the early authigenic K-feldspar phase (Fig. 3B). The marine Upper Jurassic sediments (Johannessen 2003) are expected to have had relatively high concentrations of potassium in the original pore fluids, in the K-feldspar stability field (e.g. Worden & Morad 2000). However, the large proportions of authigenic K-feldspar associated with clay-rich intervals and the underlying volcaniclastic conglomerates could indicate an additional external supply of potassium. The volcaniclastic conglomerates have a very high K-content and must originate from a potassic alkaline volcanic source. Lee & Parsons (2003) found exceptionally high proportions of sanidine cryptoperthites in the Upper Jurassic Humber Group, inferred to have an ultra-potassic volcanic source. Potassic volcanic sources of Early and Middle Jurassic (Furnes *et al.* 1982) or Permian age (Aghabawa 1993) are present in the North Sea area, but a determination of the age and location of the actual volcanic source of potassium for the Upper Jurassic reservoir sandstones require further investigations.

Remnants of albite grains are only preserved in the calcite-cemented parts of the sandstones, whereas more calcium-rich plagioclase detrital grains are almost completely lacking in the sandstones. These parts of the sandstone are instead characterised by K-feldspar overgrowths around voids of approximately the size of average detrital grains (Fig. 3C). These voids are often partly filled with illite and occasionally authigenic quartz. The K-feldspar overgrowths presumably precipi-

tated around detrital albite or Ca-rich plagioclase grains that were subsequently dissolved or replaced by clay minerals, mainly illite. It appears that dissolution of detrital albite and Ca-rich plagioclase grains led to substantial secondary porosity in the non-calcite cemented parts of the sandstones; even K-feldspar shows partial dissolution and illitisation (Fig. 3D). However, subsequent compaction and growth of authigenic phases have reduced this secondary porosity (Fig. 3B). Furthermore, it is possible that the relatively high porosity in the lower parts of the sandstones originates from early precipitation of authigenic K-feldspar cement, which, similar to the detrital feldspars, was subsequently dissolved or replaced by illite resulting in major secondary porosity.

Quartz diagenesis: stylolites, pressure solution and overgrowth

Quartz cementation by development of stylolites, pressure solution between adjacent quartz grains and precipitation of macro-overgrowths are important in deeper (3–5 km) buried siliciclastic reservoirs (e.g. Bjørlykke *et al.* 1992; Worden & Morad 2000). The investigated Upper Jurassic sediments are no exception, as detrital quartz grains are the major constituent of the Upper Jurassic sediments and quartz diagenesis is the major porosity-reducing feature outside the calcite-cemented areas. However, parts of the sandstones show a high porosity and are without major quartz or calcite cement. The porosity is reduced by the formation of stylolites (Fig. 4A), pressure solution and by precipitation of quartz overgrowths (Fig. 4B, C); all late diagenetic processes that took place after authigenic K-feldspar precipitation, calcite cementation and feldspar dissolution and illitisation. The stylolites appear to have evolved from primary mica-rich and detrital clay-rich (mainly illitic) laminae (Fig. 4A).

Quartz pressure solution and stylolite formation may be related to the local microphysiochemical environment where alkaline conditions formed around clays, which could lead to enhanced pressure solution of quartz through increased solubility or an increased dissolution rate (Tada & Siever 1989). Pressure solution has also been related to the surface charge of the illitic clays or mica (Walderhaug *et al.* 2006). Illitic clays are quite common in the investigated Upper Jurassic sandstones and may have led to enhanced development of stylolites. On the other hand, in sediments with high concentrations of clay and rock fragments, stylolites may be completely absent, due to the cushioning effect of the clay matrix and ductile lithic fragments (cf. Tada & Siever 1989).

The pressure solution of detrital quartz grains and stylolite formation may have released silica for the quartz overgrowths. Syntaxial quartz overgrowths are found in all parts of the Upper Jurassic sediments except for the calcite-cemented areas.

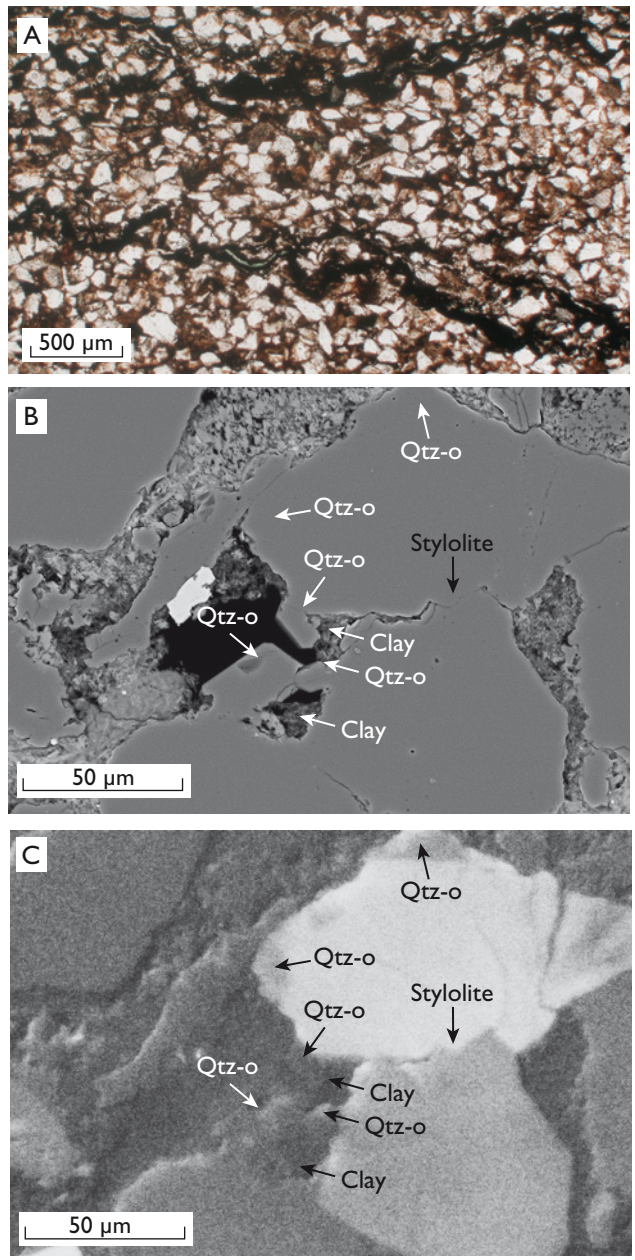

Fig. 4. Images showing development of quartz stylolites, quartz pressure solution and quartz overgrowths that are the main diagenetic features affecting the porosity outside the calcite-cemented parts of the sandstones. **A**: Quartz stylolite formation is enhanced by the presence of detrital clays and mica. Non-calcite cemented parts of the sandstones. Transmitted light microscope image. **B**: Quartz pressure solution between adjacent detrital quartz grains (black arrows) and quartz overgrowths (**Qtz-o**) that locally appear to be partly inhibited due to thick coatings of authigenic illite (white arrows). Non-calcite cemented sandstone. Back-scattered electron SEM image. **C**: Same area as Fig. 4B, but cathodoluminescence SEM image.

Peculiar, irregularly shaped quartz overgrowths are found in those parts of the sediments that show the highest present-day porosities (Fig. 4B, C). These peculiar quartz overgrowths

can be interpreted as an indication of three completely different processes. They could either be caused by an incipient introduction of hydrocarbons, which partly covered the overgrowth (cf. Marchand *et al.* 2000). In other cases, it has been suggested that authigenic chlorite rims have inhibited or retarded quartz overgrowth (Aase *et al.* 1996). Aase & Walderhaugh (2005) argued that the delay of such quartz precipitation was caused by thin coatings of micron-scale quartz crystals (microquartz). In sandstones of the Hejre-2 well abundant illite, formed during alteration of feldspar, may have inhibited pressure solution and stylolite formation, as a result of the cushioning effect of the clays, and furthermore have delayed the growth of authigenic quartz in the Upper Jurassic sediments.

Summary and perspectives

The quartz-rich Upper Jurassic reservoir sandstones in the Hejre-2 well are characterised by relatively high amounts of detrital K-feldspar, which most likely come from a volcanic source. Authigenic K-feldspar grew on detrital K-feldspar, perthite and albite grains and possibly Ca-rich plagioclase. The potassium for the K-feldspar overgrowths probably comes from marine pore fluids, detrital clay minerals and the underlying volcaniclastic conglomerates. The K-feldspar overgrowths were initially abundant, but were later dissolved except for the calcite-cemented parts of the sandstones. The formation of secondary porosity in the sandstones in the Hejre-2 well was mainly caused by dissolution of detrital feldspars and authigenic K-feldspar.

Quartz diagenesis prevails in the Upper Jurassic sediments in the Hejre-2 well where carbonates are absent and where illitic clays are restricted. Pressure solution and stylolite formation provide abundant silica, which is precipitated as quartz overgrowths. The presence of small amounts of illitic clays and mica may have enhanced the development of stylolites. On the other hand, relatively large amounts of illitic coatings seem to have inhibited or retarded the formation of quartz overgrowths, which otherwise could have reduced the porosity. Consequently, sandstone intervals in the Hejre-2 well with high porosities are the result of dissolution and illite replacement of detrital feldspars and early authigenic K-feldspar cement, thus secondary porosity was created; together with illite coatings that inhibited the formation of quartz overgrowths.

Future investigations may reveal whether the diagenetic evolution of Upper Jurassic sediments in other wells is similar to that encountered in the Hejre-2 well. Another aspect worth pursuing is to investigate if bulk rock geochemistry can be correlated with major diagenetic phenomena.

Acknowledgement

DONG Energy is thanked for permission to publish the present information on the Hejre-2 well prior to public release of the data.

References

Aase, N.E., Bjørkum, P.A. & Nadeau, P.H. 1996: The effect of grain-coating microquartz on preservation of reservoir porosity. American Association of Petroleum Geologists Bulletin **80**, 1654–1673.

Aase, N.E. & Walderhaug, O. 2005: The effect of hydrocarbons on quartz cementation: diagenesis in the Upper Jurassic sandstone of the Miller Fields, North Sea, revisited. Petroleum Geoscience **11**, 215–223.

Aghabawa, M.A. 1993: Petrology and geochemistry of the Rotliegendes volcanic rocks in Denmark and their tectonic implications. Dynmaisk/Stratigrafisk analyse af Palæozoikum i Danmark. EFP-89; område 1: Olie og Naturgas, 3, DGU Kunderapport **1993/35**, 351 pp.

Bjørlykke, K., Nedkvitne, T., Ramm, M. & Saigal, G.C. 1992: Diagenetic processes in the Brent Group (Middle Jurassic) reservoirs of the North Sea: an overview. In: Morton, A.C. *et al.* (eds): Geology of the Brent Group. Geological Society Special Publication (London) **61**, 263–287.

Furnes, H., Elvsborg, A. & Malm, O.A. 1982: Lower and Middle Jurassic alkaline magmatism in the Egersund sub-basin, North Sea. Marine Geology **46**, 53–69.

Johannessen, P.N. 2003: Sedimentology and sequence stratigraphy of paralic and shallow marine Upper Jurassic sandstones in the northern Danish Central Graben. In: Ineson, J.R. & Surlyk, F. (eds): The Jurassic of Denmark and Greenland. Geological Survey of Denmark and Greenland Bulletin **1**, 367–402.

Lee, M.R. & Parsons, I. 2003: Microtextures of authigenic Or-rich feldspar in the Upper Jurassic Humber Group, UK North Sea. Sedimentology **50**, 597–608.

Marchand, A.M.E., Haszeldine, R.S., MacAulay, C.I., Swennen, R. & Fallick, A.E. 2000: Quartz cementation inhibited by crestal oil charge: Miller deep water sandstone, UK North Sea. Clay Minerals **35**, 201–210.

Michelsen, O., Nielsen, L.H., Johannessen, P.N. Andsbjerg, J. & Surlyk, F. 2003: Jurassic lithostratigraphy and stratigrafic development onshore and offshore Denmark. In: Ineson, J.R. & Surlyk, F. (eds): The Jurassic of Denmark and Greenland. Geological Survey of Denmark and Greenland Bulletin **1**, 147–216.

Surdam, R.C., Boese, S.W. & Crossey, L.J. 1984: The chemistry of secondary porosity. In: McDonald, D.A. & Surdam, R.C. (eds): Clastic diagenesis. American Association of Petroleum Geologists Memoir **37**, 127–149.

Tada, R. & Siever, R. 1989: Pressure solution during diagenesis. Annual Review of Earth and Planetary Science **17**, 89–118.

Walderhaug, O., Bjørkum, P.A. & Aase, N.E. 2006: Kaolin-coating of stylolites, effect on quartz cementation and general implications for dissolutions at mineral interfaces. Journal of Sedimentary Research **76**, 234–243.

Worden, R.H. & Morad, S. 2000: Quartz cementation in oil field sandstones: a review of the key controversies. In: Worden, R.H. & Morad, S. (eds): Quartz cementation in sandstones. Special Publication of the International Association of Sedimentologists **29**, 1–20. Oxford: Blackwell Science.

Authors' address

Geological Survey of Denmark and Greenland, Øster Voldgade 10, DK-1350 Copenhagen K, Denmark. E-mail: *rwh@geus.dk*

Correlation of carbon isotope events in the Danish Upper Cretaceous chalk

Niels H. Schovsbo, Susanne Lil Rasmussen, Emma Sheldon and Lars Stemmerik

A high resolution carbon isotope ($\delta^{13}C$) profile through the upper Campanian to Maastrichtian chalk was recently completed based on material from the Stevns-1 core from the Stevns peninsula, eastern Denmark. The $\delta^{13}C$ variation of marine carbonates essentially reflects global perturbations in the carbon cycle, i.e. the burial fluxes of carbonate carbon versus organic carbon. It is widely observed that the $\delta^{13}C$ variation broadly tracks the eustatic sea-level curve, and that $\delta^{13}C$ curves can be used for stratigraphic correlation (e.g. Jarvis *et al.* 2002). In the Stevns-1 core, a total of 29 notable isotope changes have been identified in the upper Campanian to Maastrichtian succession. In order to evaluate the stratigraphic significance of the isotope changes, the variation in $\delta^{13}C$ values of the mid-Maastrichtian chalk from cores in eastern Denmark and the Danish North Sea, and from outcrops at Rørdal, northern Jylland has been examined (Fig. 1). The selected interval is characterised by distinct chalk and marl cycles in the Stevns-1 and Karlslunde-1 cores and in the Rørdal quarry (Fig. 2), whereas a non-cyclic clean chalk is found in the M-10X well from the North Sea. In the Rørdal quarry, the chalk–marl unit spans the upper–lower Maastrichtian boundary in the Boreal brachiopod and belemnite stratigraphies (Surlyk 1984; unpublished data, B. Lauridsen & F. Surlyk). In Stevns-1 and Karlslunde-1 the chalk–marl unit was deposited during the younger part of nannofossil subzone UC20b (Sheldon 2006, in press).

This paper presents preliminary results of a high-resolution study of carbon isotopes, carried out by the Geological Survey of Denmark and Greenland (GEUS) in co-operation with partners from the Department of Geography and Geology at the University of Copenhagen. This paper is a product of the Cretaceous Research Centre (CRC) at Geocenter Denmark.

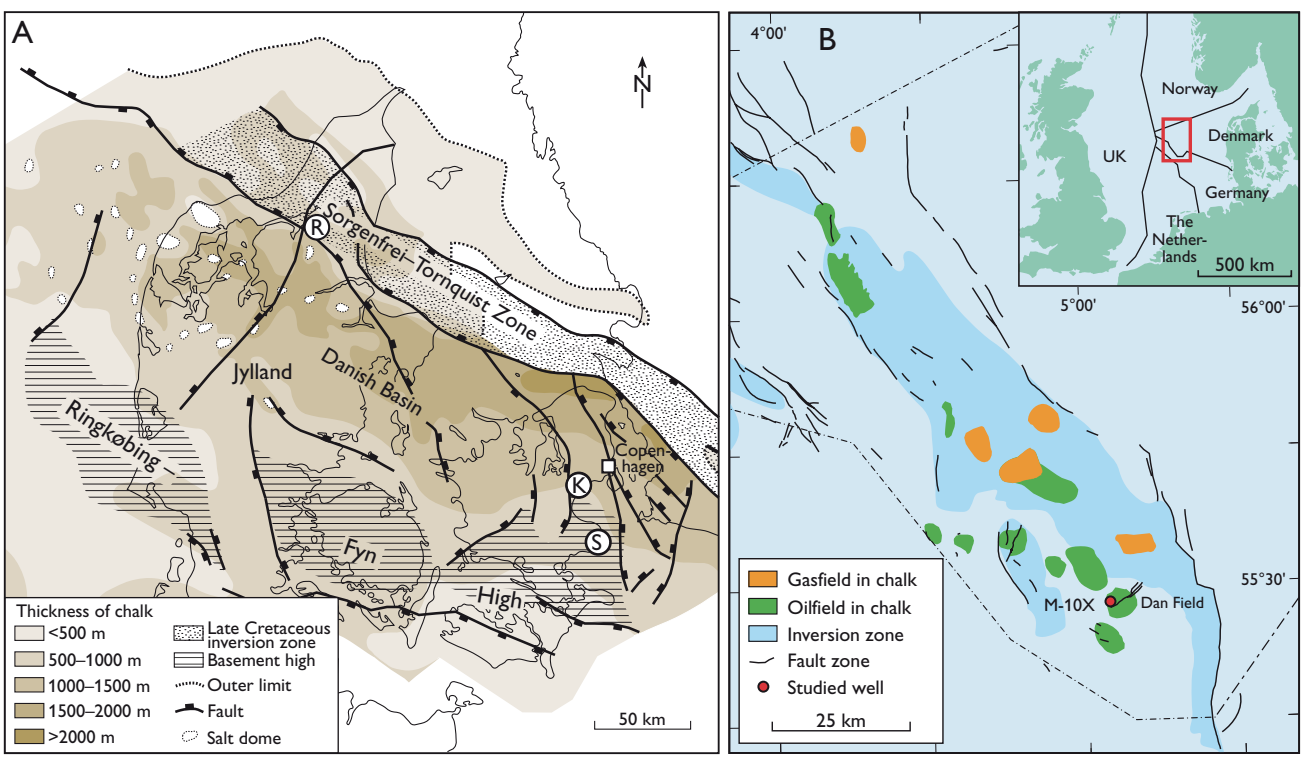

Fig. 1. **A**: Thickness of the Upper Cretaceous to Danian carbonates in the Danish area. **K**, Karlslunde-1 borehole; **S**, Stevns-1 borehole; **R**, Rørdal quarry. Modified from Stemmerik *et al.* (2006). **B**: Location of the M-10X well and the dominant Late Cretaceous structural elements in the Danish Central Graben (modified from Ineson *et al.* 2006). The inset shows the territorial borders in the North Sea.

Stevns-1 carbon isotope curve

The Stevns-1 borehole represents the first continuously cored Maastrichtian section in north-western Europe (Stemmerik *et al*. 2006). The borehole is located close to the Stevns Klint coastal cliff section (Fig. 1) and penetrated 456.1 m of Lower Danian bryozoan limestone and uppermost Maastrichtian to Campanian chalk with 100% core recovery. The Campanian to Maastrichtian chalk is composed of very pure carbonate (90–95%) and consists mainly of coccoliths. Marl beds (1–10 cm thick) occur in two intervals, in the Campanian to Maastrichtian boundary interval and within the mid-Maastrichtian. The $\delta^{13}C$ values in the Stevns-1 core have been measured on bulk sediment samples collected with a density of approximately four samples per metre. Isotope measurements were made at the Department of Geography and Geology. The analytical precision of the $\delta^{13}C$ values is better than ±0.05‰. All carbon isotope results are given relative to the V-PDB standard.

The mid-Maastrichtian marl succession in Stevns-1, from 90–110 m, forms part of a 120 m thick interval characterised by high $\delta^{13}C$ values that range between 2.2 and 2.5‰ (Fig. 3). The interval is characterised by a gentle upward decrease in $\delta^{13}C$ values terminated by a marked fall at 85 m, near the boundary between the nannofossil subzones UC20b and UC20c. The overlying chalk, referred to subzone UC20c, is characterised by lower and more variable $\delta^{13}C$ values between 1.7 and 2.2‰, and shows a general fall towards a distinct low at the UC20c–d boundary (Fig. 3). Within the interval from 135 m to 60 m in Stevns-1, we have defined seven conspicuous isotope events in chalk belonging to subzones UC20b and UC20c (Fig. 3). The three lower events, UC20b1–UC20b3, all predate the onset of marl deposition. Isotope event UC20b1, at 131 m, is characterised by a slight increase in $\delta^{13}C$ values followed by a decrease of 0.2‰. UC20b2, at 118 m, is reflected by a change in $\delta^{13}C$ values of 0.2‰. UC20b3 occurs immediately prior to the onset of marl deposition and is characterised by two short-term fluctuations in $\delta^{13}C$ values of 0.2‰ each. The upper six events all post-date the marly interval. UC20c1, near the boundary between subzones UC20b and UC20c, is characterised by a drop in $\delta^{13}C$ values and marks the termination of the early Maastrichtian $\delta^{13}C$ high. Similarly UC20d1 is characterised by a marked fall in $\delta^{13}C$ values immediately above the boundary between subzones UC20c and UC20d (Fig. 3). Isotope event UC20c2, at 72 m, is characterised by a change in $\delta^{13}C$ values of 0.2‰. UC20c3, at 68 m, is reflected by a decrease in $\delta^{13}C$ values of 0.3‰ and UC20c4 is characterised by a 0.3‰ increase in $\delta^{13}C$ values.

Correlation to adjacent areas

Carbon isotope data also have been aquired from the Maastrichtian chalk of the 250 m long Karlslunde-1 core (eastern Sjælland), from mid-Maastrichtian chalk and marl from the Rørdal quarry (Fig. 3), and from upper Maastrichtian chalk from the M-10X well in the Danish North Sea (Figs 1, 3).

Fig. 2. Chalk and cyclical chalk–marl succession spanning the macrofossil defined lower–upper Maastrichtian boundary exposed in the Rørdal quarry. The exposed section consists of a lower homogeneous chalk unit, a middle cyclic chalk–marl unit and an upper unit of homogeneous chalk. The light beds are marl and the darker beds chalk. This 'inversion' of colour is due to surface weathering. The height of the section is 20 m.

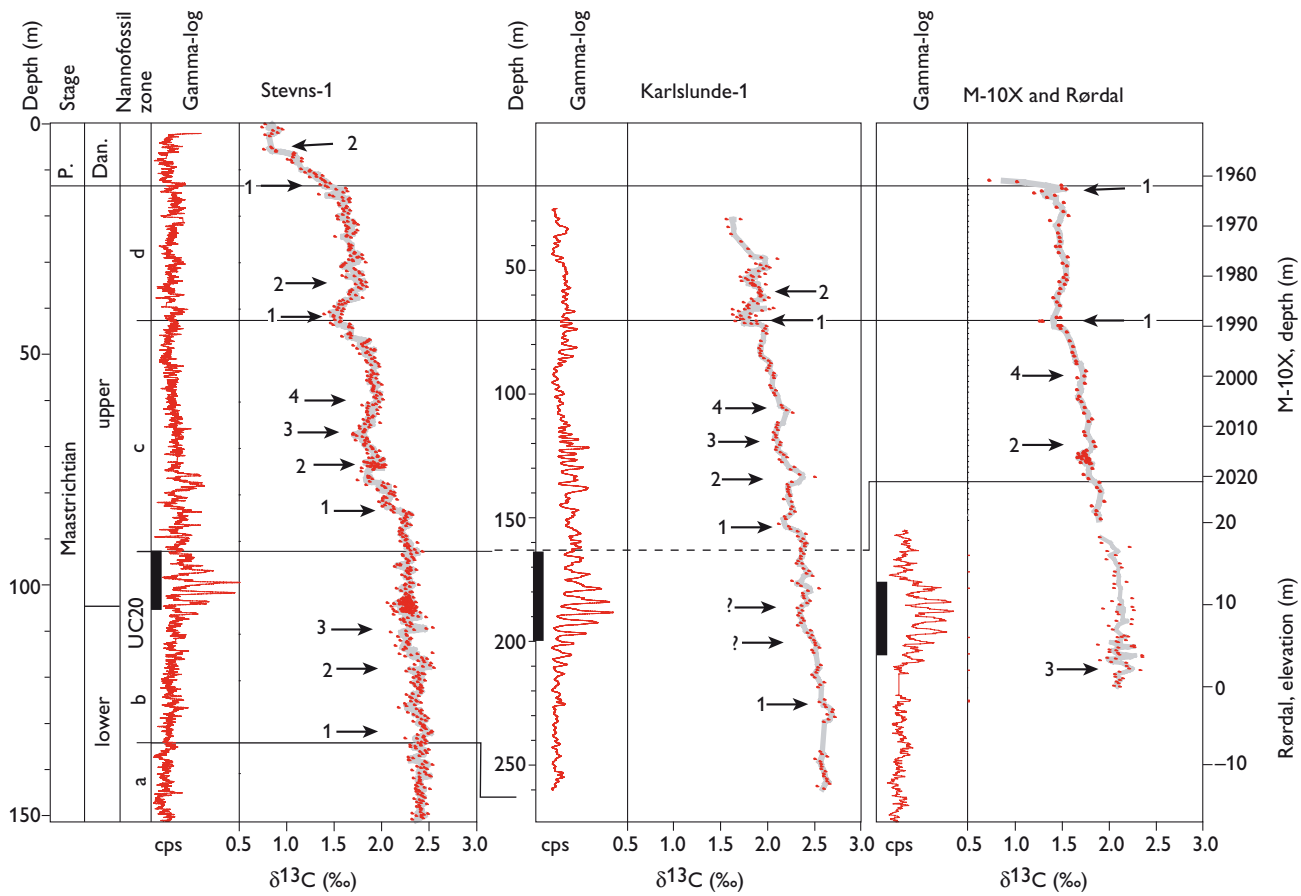

Fig. 3. Gamma-ray log and carbon isotope variation of the Stevns-1, the Karlslunde-1 and the M-10X (gamma-ray log not shown) and the Rørdal section (gamma-log for Stevns-1 obtained from core scanning (Stemmerik *et al.* 2006)). The thick black vertical lines indicate recognised cyclic chalk–marl intervals. The full black horizontal lines represent correlation based on nannofossils (Sheldon 2006). The stippled line shows the uncertain position of the nannofossil boundary. The thick grey lines represent running average of the data points. Note the difference in vertical scale between the wells. 11 marked isotope changes out of the 29 changes occur in the depicted interval. **P**, Paleocene; **Dan**, Danian; **cps**, counts per second.

Sedimentological and log data indicate that cyclically deposited chalk and marl are present in UC20b in both Stevns-1 and Karlslunde-1. The $\delta^{13}C$ curve for Karlslunde-1, although less densely sampled, displays the same overall pattern as the Stevns-1 curve with an overall decrease in the $\delta^{13}C$ values during the Maastrichtian, starting with a stable early Maastrichtian high followed by an interval with more fluctuating $\delta^{13}C$ values (Fig. 3). Isotope events UC20c1-4 and UC20d1-2 are also easily identified in the Karlslunde-1 succession whereas it has only been possible to identify the lowermost UC20b1 event in the interval below the chalk–marl cycles (Fig. 3). The $\delta^{13}C$ values in Karlslunde-1 are approximately 0.1‰ higher than those in Stevns-1.

In the Rørdal section it has been possible to identify isotope event UC20b3 immediately below an interval of interbedded chalk and marl of mid-Maastrichtian age. At Rørdal, UC20b3 is characterised by short-term changes of 0.2‰ in the 2–6 m interval (Fig. 3). The $\delta^{13}C$ values are approximately 0.2‰ more negative than those from the Stevns-1 core.

The upper Maastrichtian chalk in the M-10X well was deposited in relatively deep water and differs from the time-equivalent onshore successions by the absence of flint nodules and layers (Ineson *et al.* 2006). We have identified isotope events UC20c2, UC20c4 and UC20d1 in the cored interval (Fig. 3). The UC20d1 event at 1990 m ends a long-term fall in $\delta^{13}C$ values similar to those recognised in Stevns-1 and Karlslunde-1 (Fig. 3). The absolute $\delta^{13}C$ values are approximately 0.2‰ more negative than those recorded in Stevns-1. Isotope events UC20c2 and UC20c4 are both identified as short-term positive $\delta^{13}C$ excursions of 0.1–0.2‰, similar to those seen in Stevns-1 and Karlslunde-1.

Variation in sedimentation rates

The correlation of $\delta^{13}C$ events across the Danish area allows a refined stratigraphic subdivision of the chalk compared with the present nannofossil zonation, and thus leads to a more detailed model of sedimentation rates across the region.

The present data set indicates that the accumulation rate in the Karlslunde area was almost twice as high as at Stevns-1 during subzone UC20c. The interval starting at UC20c1 and terminating at UC20d1 is 45 m thick in Stevns-1 and 80 m thick in Karlslunde-1. In both cores the sediment consists of flint-rich chalk. Surprisingly, sedimentation rates for the upper Maastrichtian in the North Sea offshore area seem not to differ much from those recorded in the Stevns-1 core. The interval from UC20c2 to UC20d1 is 25 m in M-10X and 35 m in Stevns-1, and the thickness of the interval from UC20d1 to the Maastrichtian–Danian boundary is approximately 25 m in both areas.

Lateral variation of carbon isotopes

The $\delta^{13}C$ values in the cyclic chalk–marl interval in Stevns-1 and Karlslunde-1 show variations of up to 0.2‰, with a mean value of 2.3‰. In the Rørdal quarry, the $\delta^{13}C$ values in the time-equivalent interval also show variations of 0.2‰, but the mean value is 2.1‰. Similarly, the average $\delta^{13}C$ value of the chalk belonging to nannofossil subzone UC20c in M-10X is 0.2‰ lower than that of the time-equivalent chalk in Stevns-1 and Karlslunde-1. This east–west, intra-basinal variation in $\delta^{13}C$ values most likely reflects compositional differences of the chalk, being richer in macrofossils towards the east.

Conclusions

The high-resolution carbon isotope curve constructed for the upper Campanian to uppermost Maastrichtian chalk in Stevns-1 allows 29 isotope events to be identified. The regional significance of eight of these events has been tested using isotope data from onshore and offshore cores and an outcrop. Most isotope events are readily identified in the wells and sections though they are generally less densely sampled. It is evident that $\delta^{13}C$ data can be used for correlation of chalk at nannofossil subzone level, and give a better understanding of lateral variations in sedimentation rates.

Acknowledgement

The Danish Natural Science Research Council supported the project financially.

References

Ineson, J.R., Buchardt, B., Lassen, S., Rasmussen, J.A., Schiøler, P., Schovsbo, N.H., Sheldon, E. & Surlyk, F. 2006: Stratigraphy and palaeoceanography of upper Maastrichtian chalks, southern Danish Central Graben. Geological Survey of Denmark and Greenland Bulletin **10**, 9–12.

Jarvis, I., Mabrouk, A., Moody, R.T.J. & de Cabrera, S. 2002: Late Cretaceous (Campanian) carbon isotope events, sea-level change and correlation of the Tethyan and Boreal realms. Palaeogeography, Palaeoclimatology, Palaeoecology **188**, 215–248.

Sheldon, E. 2006: Upper Maastrichtian–Danian nannofossils of the Danish Central Graben and the Danish Basin: a combined biostratigraphic-palaeoecological approach, 354 pp. Unpublished Ph.D. thesis, University College London, UK.

Sheldon, E. in press: Upper Campanian calcareous nannofossil biostratigraphy of the Stevns-1 borehole, Denmark. Journal of Nannoplankton Research **30**.

Stemmerik, L., Surlyk, F., Klitten, K., Rasmussen, S.L. & Schovsbo, N. 2006: Shallow core drilling of the Upper Cretaceous Chalk at Stevns Klint, Denmark. Geological Survey of Denmark and Greenland Bulletin **10**, 13–16.

Surlyk, F. 1984: The Maastrichtian stage in NW Europe, and its brachiopod zonation. Bulletin of the Geological Society of Denmark **33**, 217–223.

Authors' addresses

N.H.S., S.L.R. & E.S., *Geological Survey of Denmark and Greenland, Øster Voldgade 10, DK-1350 Copenhagen K, Denmark.* E-mail: *nsc@geus.dk*

L.S., *Department of Geography and Geology, University of Copenhagen, Øster Voldgade 10, DK-1350 Copenhagen K, Denmark.*

Geophysical imaging of porosity variations in the Danish North Sea chalk

Tanni Abramovitz

More than 80% of the present-day oil and gas production in the Danish part of the North Sea is extracted from fields with chalk reservoirs of late Cretaceous (Maastrichtian) and early Paleocene (Danian) ages (Fig. 1). Seismic reflection and inversion data play a fundamental role in mapping and characterisation of intra-chalk structures and reservoir properties of the Chalk Group in the North Sea. The aim of seismic inversion is to transform seismic reflection data into quantitative rock properties such as acoustic impedance (AI) that provides information on reservoir properties enabling identification of porosity anomalies that may constitute potential reservoir compartments. Petrophysical analyses of well log data have shown a relationship between AI and porosity. Hence, AI variations can be transformed into porosity variations and used to support detailed interpretations of porous chalk units of possible reservoir quality.

This paper presents an example of how the chalk team at the Geological Survey of Denmark and Greenland (GEUS) integrates geological, geophysical and petrophysical information, such as core data, well log data, seismic 3-D reflection and AI data, when assessing the hydrocarbon prospectivity of chalk fields.

Chalk

Chalk is a pelagic carbonate sediment, formed from settling of calcareous phytoplankton remains (i.e. coccoliths). The North Sea chalk is practically a monomineralic carbonate reservoir rock that consists of 96–99% calcite ($CaCO_3$), opal (radiolarians, diatoms and sponge spicules) and small amounts of clay minerals washed into the basin from land (Håkansson *et al.* 1974; Hancock 1975). As a reservoir rock, chalk is characterised by high porosity (25–50%) and low permeability (0.1–10 millidarcies, mD; Jørgensen & Andersen 1991). Depending on permeability, chalk can be either a reservoir or a seal.

Due to the dominating calcitic nature of chalk, a robust empirical correlation exists between AI and total porosity (PHIT). Hence, AI values can be transformed to PHIT and the relationship can be visualised by cross-plots of PHIT versus AI. Variations in porosity obtained from inverted seismic data reflect changes in clay content or clay mineralogy, pore geometry, pore fluid and fracture characteristics (Anderson 1999). Using seismic attributes, it is also possible to distinguish between clean porous chalk with high-amplitude continuous reflectivity and clean tight chalk with low-amplitude discontinuous reflectivity. Furthermore, the gamma-ray log – sonic-log correlation method can be used to distinguish between reservoir and non-reservoir intervals within the Chalk Group. The gamma-ray log can distinguish clean chalk intervals from more clay-rich chalk intervals, and the sonic log can be used as a porosity indicator. The gamma-ray log – sonic-log correlation method has been developed because gamma-ray and sonic logs are the most commonly available log types for North Sea wells (Britze *et al.* 2000).

Multi-disciplinary approach

The Kraka Field

An example from the Kraka Field in the southern part of the Salt Dome province in the Danish North Sea illustrates how a multidisciplinary approach can be used to identify and delineate porosity anomalies in the Maastrichtian reservoir interval. A combination of detailed seismic interpretation,

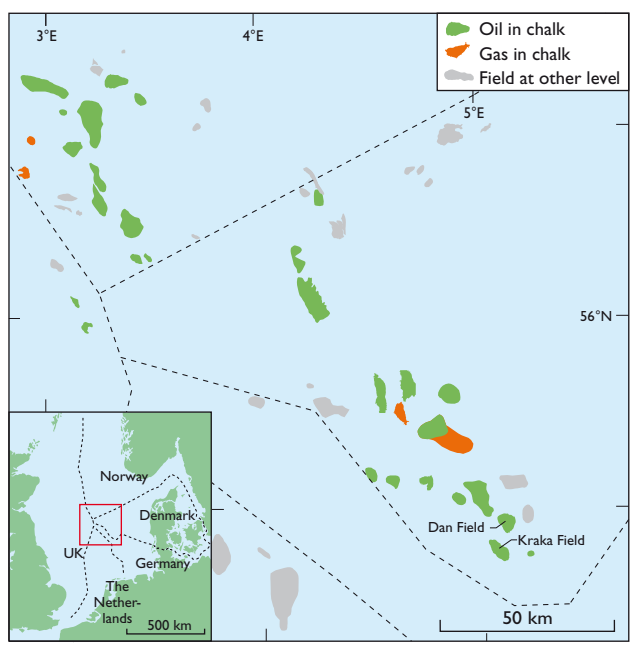

Fig. 1. Map of the central part of the North Sea, showing the distribution of oil- and gasfields. Modified from Vejbæk *et al.* (2007).

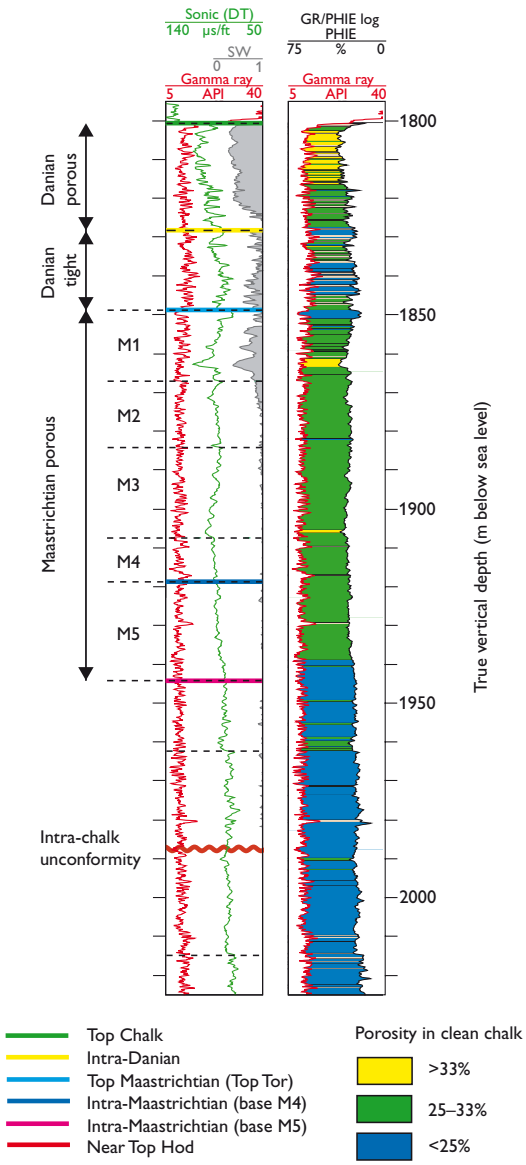

Fig. 2. GR-DT log for the Anne-3 well, Kraka Field. Gamma-ray, sonic, effective porosity and water saturation log curves are shown for the different reservoir units of the Danian–Maastrichtian reservoir interval. High GR chalk is shown in brown. **DT**, sonic; **GR**, gamma ray; **SW**, total water saturation; **PHIE**, effective porosity. Modified from Klinkby *et al.* (2005).

analysis of AI variations obtained from seismic inversion data, stratigraphic log correlation, petrophysical log analysis and rock physics analysis was used.

The Kraka Field is a 60 km^2 anticlinal structure with a four-way dip closure at top-chalk level. It has been induced through salt tectonics by up-doming of the chalk layers over a salt pillow (Klinkby *et al.* 2005). The main chalk reservoir units are found in the Danian Ekofisk Formation and the Maastrichtian Tor Formation, which are characterised by high porosity (24–32%) on the crest of the structure and low matrix permeability of less than 1 mD in the Danian and 2–3 mD in the Maastrichtian units, and an effective permeability of 8–10 mD due to fracturing. The oil zone is characterised by high water content (>50%) and limited thickness (70 m), and the gas cap is thin, less than 8 m. The free water level in the Kraka Field dips to the south-east according to Thomasen & Jacobsen (1994).

Geophysical interpretation

Integrating detailed seismic horizon interpretation and gamma-ray log/sonic-log correlation enables a consistent division of the Chalk Group and correlation of the Chalk Group units between wells in the study area. The interpretation of the gamma-ray log/sonic log of the Anne-3 well in the Kraka Field (Figs 1, 2) illustrates how reservoir and non-reservoir intervals can be identified. The Maastrichtian units M1 to M4 were described by Klinkby *et al.* (2005), who interpreted an intra-Maastrichtian seismic horizon (base of unit M4; Fig. 2) as the base of the reservoir interval in the Kraka–Dan area, separating porous chalk from tighter chalk below. As part of a major study of the internal chalk structures in the southern part of the Danish North Sea, several additional seismic horizons have been mapped including a porous unit (M5 on Fig. 2) in the Maastrichtian chalk reservoirs, which is present at a slightly deeper level than the previously interpreted base of the reservoir interval.

The base of the M5 unit is seen as a distinct, relatively high-amplitude continuous reflection (trough) in the seismic data. The horizon can be correlated from the Kraka wells to Olga-1X and the Dan Field wells (M-1X, M-2X, M-8X, M-9X and M-10X), where it corresponds to a consistent regional reflection between two intra-Maastrichtian intervals. The reflector marking the base of the M5 unit changes character and becomes weaker towards the north-east in the direction of the Alma-1X and Alma-2X wells. Near the Anne-3 well and farther to the south-west, it merges with a deeper lying intra-chalk seismic horizon (Near Top Hod; Fig. 3). Here, an E–W-striking AI profile crossing the Anne-3 well shows pronounced lateral variability in AI values within the M5 unit. On the eastern flank of the Kraka structure, the M5 unit is dominated by low AI values, corresponding to higher porosities. In general, to the north and to the west the base of the M5 unit separates the porous Maastrichtian units with lower AI values from the underlying units with higher AI values (Figs 3, 4).

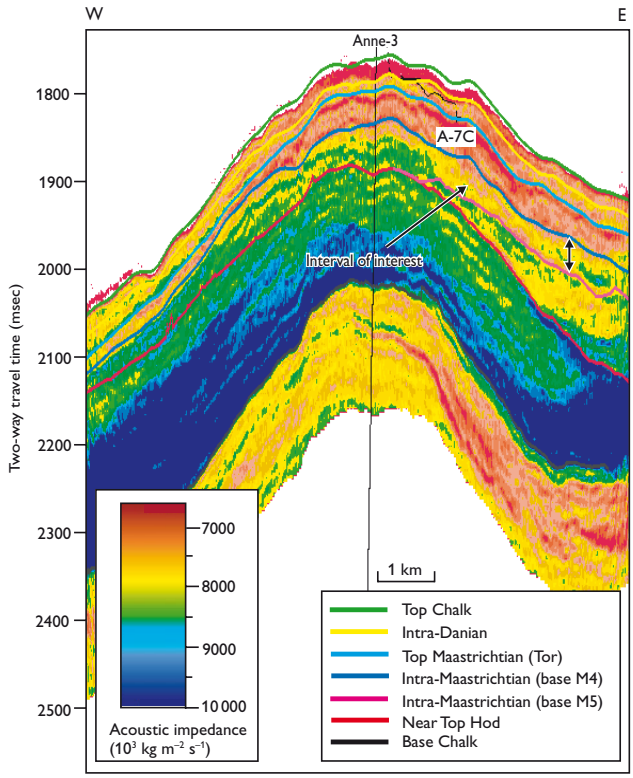

Fig. 3. An E–W-orientated acoustic impedance profile extracted from the inverted seismic data of the merged 3-D survey (produced for Mærsk Oil and Gas AS) crossing the Anne-3 well, Kraka Field.

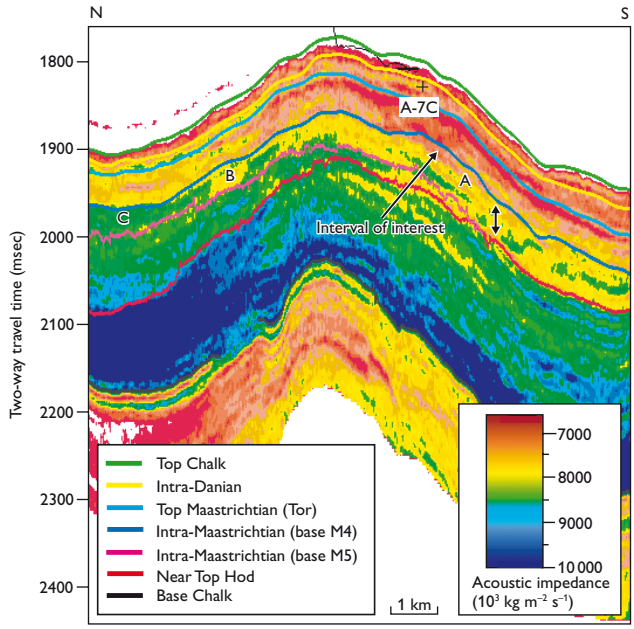

Fig. 4. A N–S-orientated acoustic impedance section from the Dan to Kraka Fields. Labels **A**, **B** and **C** are discussed in the text.

Transforming acoustic impedance to porosity

Based on petrophysical log-porosity evaluations of 14 wells from the southern part of the Danish Central Graben, a robust relationship between log-derived AI and PHIT has been established for the Chalk Group (Kristensen & Andersen 2008). AI can be converted to PHIT using a second order polynomial regression. The following relationship was found for clean chalk (<2% clay) where PHIT is close to the effective porosity (PHIE):

$$PHIT = 0.729 - 7.08 \times 10^{-5} AI + 1.55 \times 10^{-9} AI^2$$

where porosity is given in fraction and AI in g cm^{-3} × msec^{-1}. In order to display the AI variations of the M5 unit on a map, the lowest AI values were extracted from the inverted seismic data within the target interval. The AI map of the M5 unit shows the presence of an area with low AI values on the south-eastern flank of the Kraka structure (Fig. 5).

The AI–PHIT relationship allowed the generation of a total porosity map (Fig. 6) for the target interval using the seismically derived AI values (Fig. 5). The porosity map shows an area with higher porosities (30–35%) east of the Anne-3 well on the south-eastern flank of the Kraka structure. This indicates the existence of high porosity values in the deeper part of the M5 unit. In addition, the seismically derived PHIT values show good agreement with the GR-DT log values estimated for the M5 unit (Fig. 2).

The area with low AI values (labelled A on the map; Fig. 5) corresponds to label A on the north–south orientated, inverted seismic profile (Fig. 4) and to the high porosity area labelled A' on the porosity map (Fig. 6). The area labelled B on the N–S-orientated inverted, seismic profile (Fig. 4) illustrates the abrupt transition from higher to lower AI values within the mapped unit (equal to B on Fig. 6). This corresponds to an area with relatively low porosity marked by B' on Fig. 6. Similarly, the lower porosities (<25%) labelled C' on Fig. 6 and located in the saddle between the Kraka and Dan structures correspond to an area with high AI values, labelled C on Figs 4, 5.

Conclusions and outlook

A multi-disciplinary approach is a powerful method for detecting and predicting intervals of high porosity of chalk in the North Sea. This study indicates the existence of high porosity values at a slightly deeper level than the previously interpreted base of the reservoir interval on the south-eastern flank of the Kraka Field.

A porosity map based on inverted seismic data may contribute as input to a 3-D reservoir model for further calculation of hydrocarbon volumes at different reservoir property and FWL scenarios.

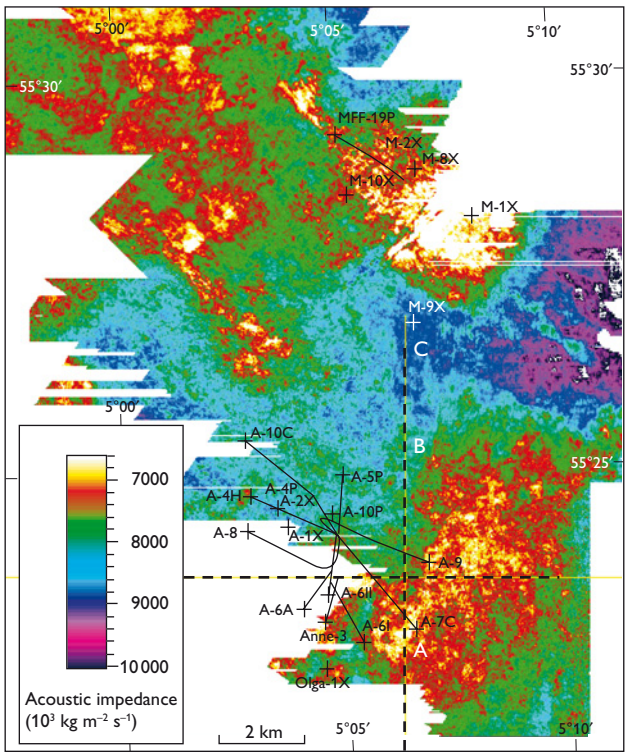

Fig. 5. Map showing the distribution of the lowest acoustic impedance values in unit M5 in the area of the Kraka and Dan fields. Labels A, B and C correspond to the labels on Fig. 4. The black stippled lines show the position of the two profiles shown in Figs 3 and 4. For location see Fig. 1.

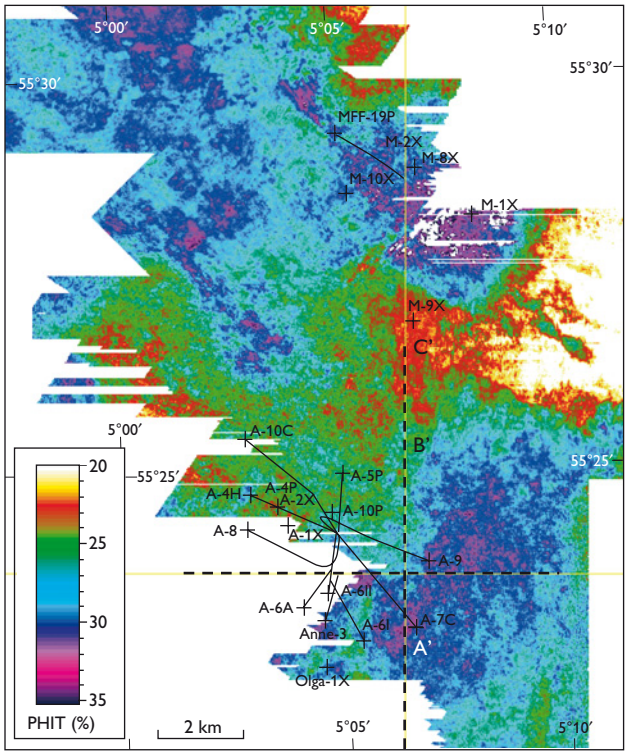

Fig. 6. Porosity map for the M5 unit in the area of the Kraka and Dan fields derived from the AI-PHIT transform. Porosity anomalies labelled A', B' and C' correspond to A, B and C on Figs 4 and 5 as discussed in the text. The black stippled lines show the position of the two profiles shown in Figs 3 and 4. For location see Fig. 1.

References

Anderson, J.K. 1999: The capabilities and challenges of the seismic method in chalk exploration. In: Fleet, A.J. & Boldy, S.A.R. (eds): Petroleum geology of North-West Europe. Proceedings of the 5th petroleum geology conference, 939–947. London: Geological Society.

Britze, P., Nielsen, E.B., Dahl, N. & Haug, S. 2000: North Sea chalk porosity resolved by integration of seismic reflectivity and well log data. Abstract P100, 64th EAGE conference & exhibition, Florence. Abstract P100, 4 pp.

Håkansson, E., Bromley, E.G. & Perch-Nielsen, K. 1974: Maastrichtian chalk from North West Europe – a pelagic shelf sediment. Special Publication, International Association of Sedimentologists **1**, 211–233.

Hancock, J.M. 1975: The petrology of the chalk. Proceedings of the Geologists' Association **86**, 499–535.

Jørgensen, L.N. & Andersen, P.M. 1991: Integrated study of the Kraka Field. Society of Petroleum Engineers paper, 14 pp. (http://dx.doi.org/10.2118/23082-MS).

Klinkby, L., Kristensen, L., Nielsen, E.B., Zinck-Jørgensen, K. & Stemmerik, L. 2005: Mapping and characterisation of thin chalk reservoirs using data integration: the Kraka Field, Danish North Sea. Petroleum Geoscience **11**, 113–124.

Kristensen, L. & Andersen, C. 2008: Log-derived acoustic impedance versus porosity and porosity versus depth trends in the Chalk Group: examples from the southern Danish Central Graben. Danmarks og Grønlands Geologiske Undersøgelse Rapport **2008/13**, 33 pp.

Thomasen, J.B. & Jacobsen, N.L. 1994: Dipping fluid contacts in the Kraka Field, Danish North Sea. Society of Petroleum Engineers paper, 10 pp. (http://dx.doi.org/10.2118/28435-MS).

Vejbæk, O.V., Bidstrup, T., Britze, P., Erlström, M., Rasmussen, E.S. & Sivhed, U. 2007: Chalk depth structure maps, central to eastern North Sea, Denmark. Geological Survey of Denmark and Greenland Bulletin **13**, 9–12.

Author's address

Geological Survey of Denmark and Greenland, Øster Voldgade 10, DK-1350 Copenhagen K, Denmark. E-mail: *tab@geus.dk*

Palaeogene diatomite deposits in Denmark: geological investigations and applied aspects

Stig A. Schack Pedersen

The Danish term 'moler' is the name for a special and unique marine deposit of Lower Eocene age found in the northern part of Denmark and the Danish North Sea. In the literature it is often referred to as mo-clay, the English translation of 'moler' – a whitish, powdery sediment that lithologically is a clayey diatomite. The deposit, which is defined as the Fur Formation, is also well known for its 180 volcanic ash beds, increasing in number towards the top of the formation (Pedersen & Surlyk 1983). Due to Pleistocene glaciotectonic deformations the diatomite deposits crop out at the surface in the Limfjorden area (Gry 1940; Klint & Pedersen 1995; Pedersen 1996, 2000). Prior to the deformations the Fur Formation was situated at about 50–100 m below sea level, but during the deformations the diatomite was displaced upwards into glaciotectonic complexes. The complexes form elongate parallel hills up to 80 m a.s.l. in the western Limfjord region (Fig. 1).

The clayey diatomite attracts attention because it is a valuable raw material for production of insulation bricks and absorbing granulates, which are mainly used as cat litter. In addition, the exposed Fur Formation is a unique reference for investigations of the Palaeogene stratigraphy in the North Sea, where mudstones and shales with ash layers are known as the Sele and Balder Formations (Schiøler *et al.* 2007). In a tectonic framework the ash layers provide a unique addition to the understanding of the development of the North Atlantic igneous province at the time when Greenland and Norway began to drift away from each other (Larsen *et al.* 2003). Moreover, the Fur Formation is especially noted for its rich fossil fauna, which comprises remarkably well-preserved specimens of birds, fish and insects. Due to the public interest two museum exhibitions have been established, on Mors and Fur, and the geological features are so evident that numerous geological field trips have benefited from the success of well-displayed geology seen in exposures along the coastal cliffs and in the mo-clay pits. At present a Norwegian drilling company is planning to use the Fur Formation outcrops at Skarrehage for testing before applying their new drilling method offshore. In 2007, GEUS has continued many years of mo-clay investigations, and this paper presents some results from the 2007 activities, in addition to a review on the geology of the mo-clay.

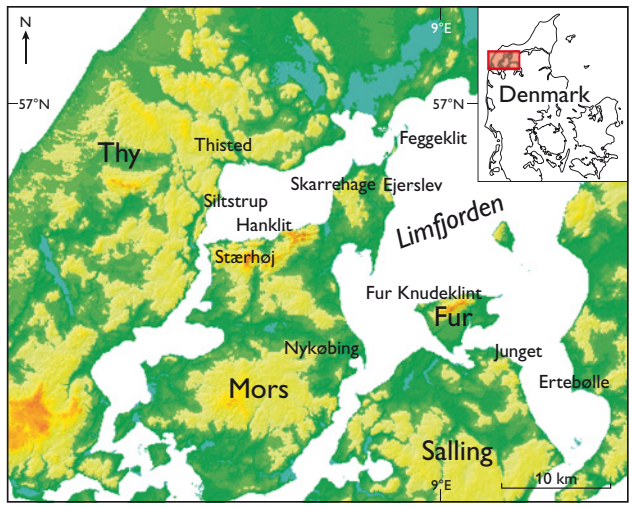

Fig. 1. Map of the western Limfjorden region with place names. Note the hilly landscapes on the islands of Mors and Fur.

Sedimentology of the Fur Formation

The Fur Formation is *c.* 60 m thick at the type locality in the north-west corner of the island of Fur. The sedimentology of the formation was described by Pedersen (1981) and Pedersen & Surlyk (1983), who demonstrated that parallel well-laminated intervals alternate with structureless intervals. Due to the exact identification and numbering of the ash layers the two sediment types can be followed throughout the diatomite basin. The laminated mo-clay formed during anoxic periods, whereas the structureless mo-clay represents oxic events, during which a rich bottom fauna inhabited the seabed. In many layers the ash grains fill the burrows facilitating the recognition of the trace fossils (Pedersen 1981).

Petrologically, diatom opal frustules make up 65% of the sediment. The dominant diatom is *Coscinodiscus* (Fig. 2). The clay content is about 28%, but varies, and the clay fraction comprises the clay mineral smectite (Pedersen *et al.* 2004); the remainder is mainly disseminated pyrite. Mo-clay situated above the groundwater level has been depleted of pyrite, but mo-clay situated below the groundwater level shows a pyrite content that varies from 5 to 8%. This gives the diatomite a black colour. Above the redox level the diatomite is light coloured due to the depletion of pyrite, which is corroded and transformed into sulphates (jarosite and gypsum)

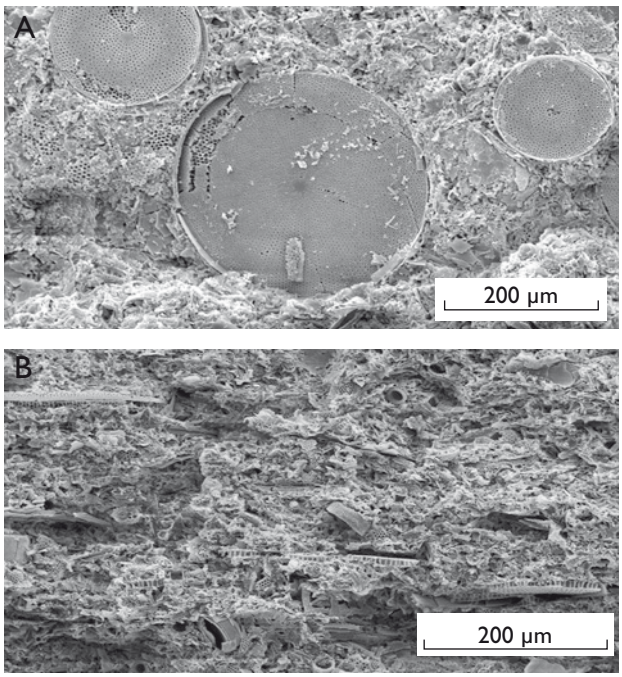

Fig. 2. Scanning electron microscope images of clayey diatomite from the Fur Formation. The upper image is a plan view, where the large diatom frustules of *Coscinodiscus* are seen. The lower image is perpendicular to the lamination and shows some diatom frustules in cross-section.

and limonite. Part of the latter is transported out to the slopes and cliffs at the coast, where it cements the Quaternary deposits, mainly the glaciofluvial sand and gravel, to form the so called 'red stone'.

During diagenesis amorphous opal A is transformed to microcrystalline opal C/T, and in the lower part of the formation cherty shales (skiferlag) have formed (Pedersen *et al.* 1998). In the middle and upper part of the formation calcareous concretions are seen. The concretions are found in about five marker levels, they are ellipsoid in shape and their size range from 0.3 to 0.75 m in thickness and one to a few metres in lateral extent. One exception is the calcareous concretion cementing the ash layer +101, which is a 35 cm thick marker bed in the upper part of the formation. Gypsum is sometimes found as small rosettes up to 5 cm in size, often concentrated in glaciotectonic shear zones.

Volcanic ash layers

The volcanic ash layers were stratigraphically logged and numbered by Bøggild (1918), who also published the first data on the petrological composition and is responsible for the division of the ash layers into a negative and a positive series. From their geochemical characteristics, four stages of volcanic activity can be recognised (Pedersen *et al.* 1975).

Stage 1 corresponds to the ash layers from –39 to –22, which vary in composition from rhyolitic to basaltic. The source of these ash layers was volcanic centres situated on the shelf west of the British Isles (Larsen *et al.* 2003). A volcanic stage pre-dating stage 1 is recorded from offshore Britain (Knox *et al.* 1997) and is probably responsible for the bentonite in the Holmehus Formation; it is well known that bentonite is a devitrification product of volcanic glass.

Stage 2 is represented by ash layers –21 to –15, which are variable in composition and comprise phonolites, nephelinites, trachytes and rhyolites. The peralkaline nephelinitic ash layer –19 is a remarkable blue ash layer, easily recognisable, and the very distinct, 4 cm thick, orange coloured –17 is a diagenitically altered trachyte, formerly thought to be rhyolitic. The source of the stage 2 ash layers was either the shelf area west of the British Isles or the Gardiner igneous complex in East Greenland (Larsen *et al.* 2003).

Stage 3 is represented by the three distinctive black alkali basalt ash layers –13, –12 and –11. The ash layers may originate from the opening rift between North-West Europe and Greenland (Larsen *et al.* 2003).

Stage 4 is the main tholeiitic basalt eruption, during which the positive numbered ash layers were formed. They correspond in composition to the basalts currently forming in Iceland. Thus the source could be regarded as a proto-Iceland situated in the middle of the incipient oceanic crust of the North Atlantic Ocean (Larsen *et al.* 2003). The most significant ash layer in this unit is the 20 cm grey rhyolitic andesite +19, which has been dated to 54 Ma (Larsen *et al.* 2003), and which is an important marker bed for the exploitation activities.

Glaciotectonic deformation

In the 1930s state-geologist H. Gry consulted the mo-clay companies, and from his co-operation with them he realised how important structural geology was for solving the exploration problems. In 1940 he summarised the structural knowledge of all the known outcrops of the Fur Formation and described their glaciotectonic framework (Gry 1940). Gry's model was monoglacial with a lobe-shaped body of ice advancing from the north. Pedersen (2000) demonstrated that the glaciotectonic structures were due to superimposed deformation. The Norwegian and Swedish advances spreading over the northern part of Denmark in the Weichselian at about 28–24 ka B.P. created the main structural features. However, evidence of older glaciations of Saalian age is also recorded, both as deposits (Hesselbjerg till and Harhøj sand series) and as minor deformations along the glaciotectonic unconformity truncating the Fur Formation (Fig. 3).

The advanced structural studies of the glaciotectonic complexes are based on the concept of thin-skinned thrust-fault

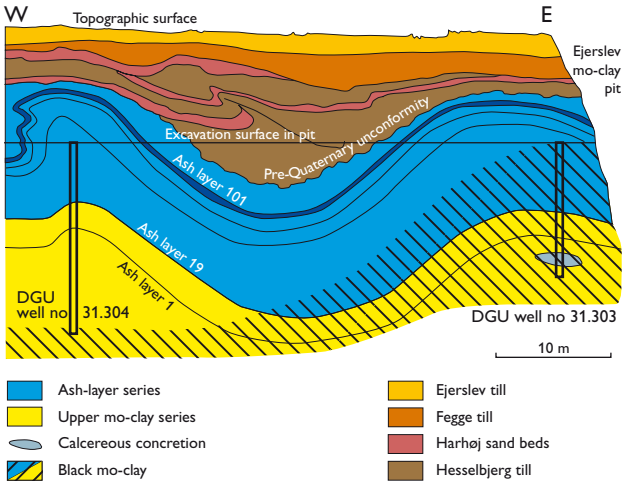

Fig. 3. Geological cross-section of the area with black diatomite. The location of the wells is shown in Fig. 4B (–303 and –304). The Hesselbjerg till and the Harhøj sand beds are of Saalian age, whereas the Fegge and Ejerslev tills represent, respectively, the Weichselian Norwegian and Swedish advances.

deformation and construction of balanced cross-sections. A prominent example of this is the Hanklit glaciotectonic complex, which constitutes three 60 m thick thrust sheets with a maximum displacement of about 300 m from the décollement surface at 80–100 m below sea level (Klint & Pedersen 1995). Before the displacement the upper surface of the Fur Formation was situated 20 m below sea level, from where it was displaced to 60 m above sea level to form the elongated E–W-trending hills of northern Mors (Fig. 1). A similar depth to the décollement surface (about 100 m b.s.l.) was calculated from area balance of the Feggeklit cross-section (Fig. 1). This study also demonstrated that the sequential deformations within a glaciotectonic propagation were related to one ice advance (Pedersen 1996). A number of advanced glaciotectonic studies are described in the series Danmarks og Grønlands Geologiske Undersøgelse Rapport from 1996 to 2007, and document the structural framework of the areas planned for future excavation of the clayey diatomite.

Raw material investigation

In general all the mo-clay pits are located within elongate hanging-wall anticlines in thrust sheets of the Fur Formation. Thus the basic problem is to identify the trend of the anticlines in order to locate the boundaries of the excavation areas. When this has been solved, the important two questions to be answered are: How much diatomite is present, and how much cover has to be removed during the excavation?

The answers are provided by construction of isopach maps of the excavation areas and volume calculation with application of kriging (Cressie 1990). The data applied for the kriging are based on the information from the exploration wells (Fig. 4), where the depth to ash layer +19 is the most important parameter. The ash layers above +19 are included in the

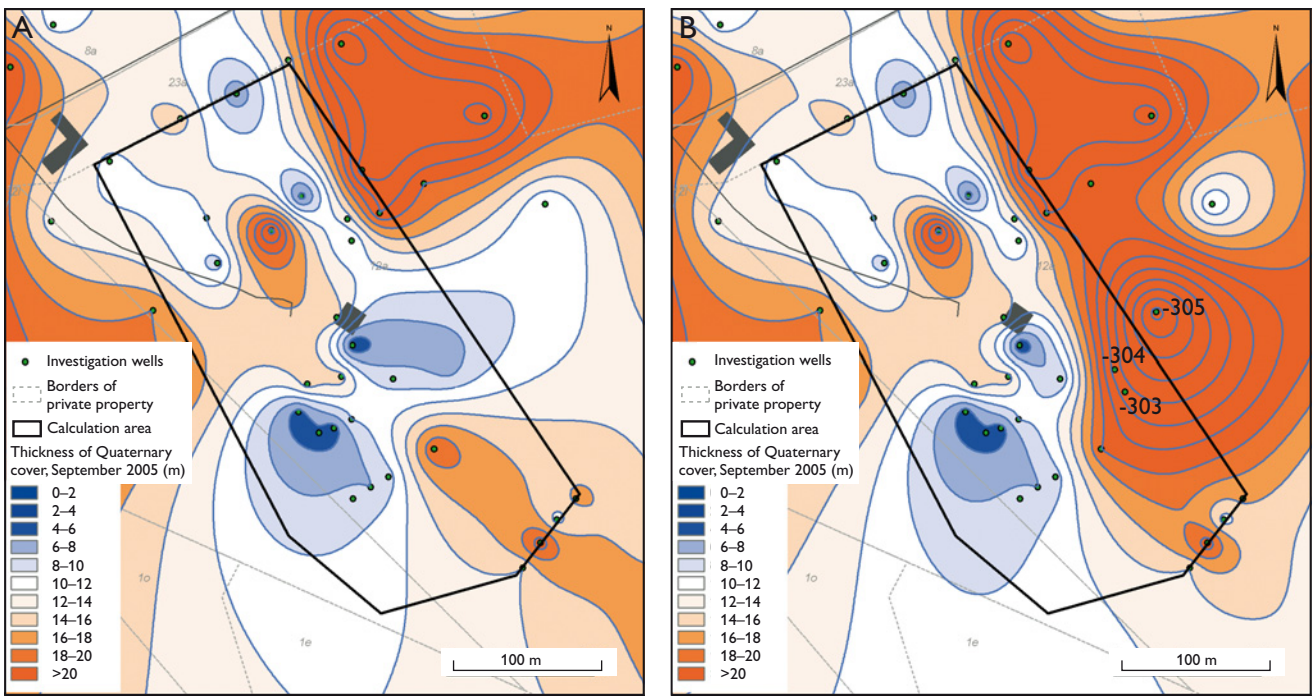

Fig. 4. Two isopach maps constructed by kriging calculation based on well data. **A**: Gives an unrealistic NE-trend of the raw material deposit. **B**: Improves the reliability of the isopach map by including data from the three new wells, –303, –304 and –305, in the calculation. This map agrees well with the original structural model for the area.

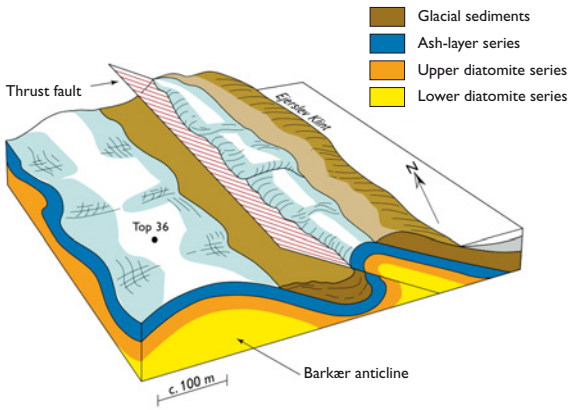

Fig. 5. Structural model for the northern part of the Ejerslev field. The Barkær anticline is the main target for exploitation. In the syncline east of the Barkær anticline, a more than 20 m thick sequence of Quaternary deposits is found, which makes this area uneconomic for excavation. Moreover, the diatomite here is probably also of a black variety unsuitable for production.

Fig. 6. Drill operation in the Ejerslev clay pit. The vehicles are parked on the top of the Barkær anticline (see Fig. 5), which is seen in front of the drill rig. Note the black colour of the diatomite, which is caused by a high content of disseminated pyrite. Till deposits occur behind and above the drill rig. Compare with Fig. 3.

unutilised cover, which is dominated by Quaternary deposits (Fig. 3). Only few and thin ash layers are found below ash layer +19, and they do not affect the production. The lower boundary of the excavation is either at the groundwater level or at the occurrence of black diatomite, which usually coincide. However, exceptions occur as illustrated below.

The Ejerslev field is currently the main production area on Mors. For the production planning, an isopach map (Fig. 4A) was constructed in the spring of 2005. However, the density of data points is crucial for the calculation of the exploitation area, and the resulting map contradicted the structural model for the area (Fig. 5). In the spring of 2007 an unusual occurrence of black diatomite cropped out during excavation of the uppermost part of the Fur Formation (Fig. 6). Based on three new wells, combined with field investigations, it was concluded that the black diatomite is preserved in an anticlinal structure (Fig. 3). Since the late Weichselian (*c.* 20 ka) this dome feature had been protected from percolating groundwater and no leaching of the pyrite had taken place. The subsequent kriging analysis had an important new data point in the most poorly covered area. The new isopach map (Fig. 4B) supports the original structural model for the area (Fig. 5) demonstrating the importance of using structural models.

References

Bøggild, O.B. 1918: Den vulkanske Aske i Moleret. Danmarks Geologiske Undersøgelse II. Række **33**, 84 pp.

Cressie, N.A.C. 1990: The origins of kriging. Mathematical Geology **22**, 239–252.

Gry, H. 1940: De istektoniske Forhold i Molerområdet. Meddelelser fra Dansk Geologisk Forening **9**, 586–627.

Klint, K.E.S. & Pedersen, S.A.S. 1995: The Hanklit glaciotectonic thrust fault complex, Mors, Denmark. Danmarks Geologiske Undersøgelse Serie A **35**, 30 pp.

Knox, R.W.O'B., Holloway, S., Kirby, G.A. & Bailey, H.E. 1997: Stratigraphic nomenclature of the UK North West Margin: **2**. Early Paleogene lithostratigraphy and sequence stratigraphy, 58 pp. Nottingham: British Geological Survey.

Larsen, L.M., Godfrey Fitton, J. & Pedersen, A.K. 2003: Paleogene volcanic ash layers in the Danish Basin: compositions and source areas in the North Atlantic Igneous Province. Lithos **71**, 47–80.

Pedersen, A.K., Engell, J. & Rønsbo, J.G. 1975: Early Tertiary volcanism in the Skagerrak: new chemical evidence from ash layers in the moclay of northern Denmark. Lithos **8**, 255–268.

Pedersen, G.K. 1981: Anoxic events during sedimentation of a Palaeogene diatomite in Denmark. Sedimentology **28**, 487–504.

Pedersen, G.K. & Surlyk, F. 1983: The Fur Formation, a late Paleocene ash-bearing diatomite from northern Denmark. Bulletin of the Geological Society of Denmark **32**, 43–65.

Pedersen, G.K., Pedersen S.A.S., Steffensen, J. & Pedersen, C.S. 2004: Clay content of a clayey diatomite, the Early Eocene Fur Formation, Denmark. Bulletin of the Geological Society of Denmark **51**, 159–177.

Pedersen, S.A.S. 1996: Progressive glaciotectonic deformation in Weichselian and Palaeogene deposits at Feggeklit, northern Denmark. Bulletin of the Geological Society of Denmark **42**, 153–174.

Pedersen, S.A.S. 2000: Superimposed deformation in glaciotectonics. Bulletin of the Geological Society of Denmark **46**, 125–144.

Pedersen, S.A.S., Lindgreen, H. & Pedersen, G.K. 1998: Amorphous silica and hydrous aluminosilicates for production of construction materials. INCO-Copernicus project No. ERBIC15CT96 0712. Danmarks og Grønlands Geologiske Undersøgelse Rapport **1998/3**, 47 pp.

Poul Schiøler *et al.* 2007: Lithostratigraphy of the Palaeogene – Lower Neogene succession of the Danish North Sea. Geological Survey of Denmark and Greenland Bulletin **12**, 77 pp.

Author's address

Geological Survey of Denmark and Greenland, Øster Voldgade 10, DK-1350 Copenhagen K, Denmark, E-mail: *sasp@geus.dk*

Cenozoic palaeogeography and isochores predating the Neogene exhumation of the eastern North Sea Basin

Peter Japsen, Erik S. Rasmussen, Paul F. Green, Lars Henrik Nielsen and Torben Bidstrup

Denmark is a key region for studies of the Cenozoic development of Scandinavia because Paleocene to Upper Miocene sediments crop out across the country and because it is possible to correlate these occurrences with the up to 3 km thick Cenozoic succession of the North Sea Basin. However, the reason why the Cenozoic deposits occur close to the surface of the Earth in Denmark is that the sediments have been exhumed from their cover of younger rocks. This implies that a reconstruction of the Cenozoic development across Denmark – involving both burial and exhumation – must rely on sedimentological and seismic studies of preserved sediments as well as on physical parameters that may yield evidence of the postdepositional history of the sediments now at the surface. Only if the burial and exhumation history of the basins can be deciphered is it possible to infer the geological development in the Scandinavian hinterland where Cenozoic sediments are rarely preserved.

We have identified four Mesozoic–Cenozoic palaeothermal phases related to burial and subsequent exhumation, and one phase reflecting climate change during the Eocene. This is based on new apatite fission-track analyses (AFTA) and vitrinite reflectance data from eight Danish wells (Japsen *et al.* 2007a). The study combined thermal history reconstruction with exhumation studies based on palaeoburial (sonic velocity), stratigraphic and seismic data (cf. Japsen & Bidstrup 1999; Green *et al.* 2002; Nielsen 2003; Rasmussen 2004; Japsen *et al.* 2007b). Two of the exhumation phases occurred during the mid-Jurassic and the mid-Cretaceous. In this study we focus on the Cenozoic development and on the early and late Neogene exhumation phases during which up to 1 km of sediments were removed across most of the Danish region (Fig. 1).

Early and late Neogene exhumation

A major phase of exhumation of the parts of the eastern North Sea Basin adjacent to the presently exposed basement areas in Norway and Sweden began between 30 and 20 Ma ago according to the AFTA data (Fig. 1). We suggest that this phase corresponds to the Oligocene–Miocene unconformity (*c.* 24 Ma). Prior to this early Neogene exhumation phase, the Mesozoic sediments in the Felicia-1 well were at maximum burial. The maximum burial of the Mesozoic sediments in the Hans-1 well occurred during the mid-Cretaceous, prior to inversion along the Sorgenfrei–Tornquist Zone, whereas maximum burial during the Cenozoic occurred prior to the early Neogene exhumation phase.

Late Neogene exhumation began between 10 and 5 Ma ago according to the AFTA data from e.g. the Års-1 and Felicia-1 wells. Only one sample limits the onset of this phase to begin before 5 Ma, and the onset of the exhumation probably began in the early Pliocene at *c.* 4 Ma as suggested by the prominent unconformity of this age. After 4 Ma significant progradation from Scandinavia into the North Sea Basin and increased subsidence in the central North Sea were initiated. A section of 450–850 m was removed in the central part of the Norwegian–Danish Basin in association with this reshaping of the North Sea Basin. The exhumation affected extensive regions where Neogene strata are truncated, and in southern Norway and Sweden a sub-Cretaceous etched surface was re-exposed along the coasts (Lidmar-Bergström *et al.* 2000).

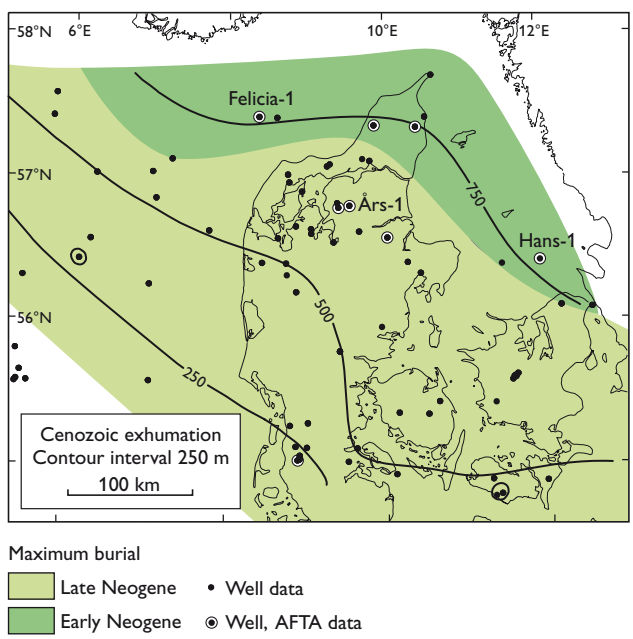

Fig. 1. Thickness of the section removed during Cenozoic exhumation. Maximum burial of the Mesozoic sediments took place during the late Neogene in most of the study area. Near the present coasts of Norway and Sweden, however, maximum burial occurred subsequent to deposition of the Oligocene wedges and prior to early Neogene exhumation. Only in the Hans-1 well did maximum burial occur during the Mesozoic. Modified from Japsen *et al.* (2007a).

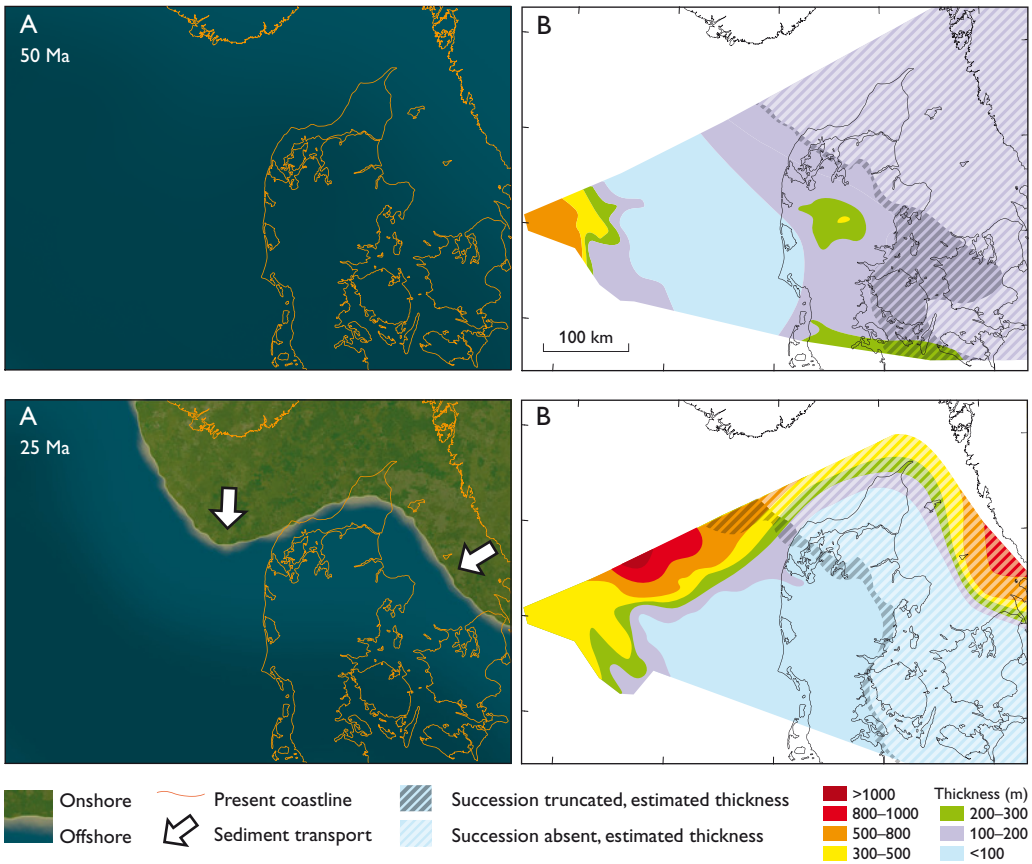

Fig. 2. **A**: Early Eocene palaeogeography, 50 Ma. **B**: Upper Paleocene – Eocene isochore prior to Neogene exhumation. Modified from Japsen *et al.* (2007a).

Fig. 3. **A**: Late Oligocene palaeogeography, 25 Ma. **B**: Oligocene isochore prior to Neogene exhumation. Modified from Japsen *et al.* (2007a).

Legend to Figs 2–6.

Maps of palaeogeography and isochores prior to the Neogene exhumation phases

We have compiled a series of maps to illustrate the Cenozoic development of the eastern North Sea Basin (Figs 2–6). The isochore maps are based on present thicknesses and estimates of the removed sections constrained by the total amount of section removed by Cenozoic exhumation. The estimates of the removed sections of specific ages are furthermore constrained by the known geology and our interpretation of the depositional pattern. Each isochore map shows the thicknesses prior to the first phase of exhumation that affected the distribution of the unit; i.e. prior to early Neogene exhumation (starting at *c.* 24 Ma) in the case of the Palaeogene units and prior to late Neogene exhumation (starting at *c.* 4 Ma) for the Neogene units. The palaeogeographical maps show the distribution of onshore and offshore areas separated by the coastline based on the known geology. In the areas where the deposits of a given age have been removed, the map has been drawn from an estimate based on our interpretation of the depositional system and on the inferred burial and exhumation history.

In the early Eocene, the study region was covered by a deep sea as demonstrated by hemipelagic deep-marine sedimentation that lasted until latest Eocene times (Fig. 2A; Heilmann-Clausen *et al.* 1985; Michelsen *et al.* 1998). Parts of Scandinavia were probably covered by Eocene sediments because Eocene deposits within the Norwegian–Danish Basin contain a deep marine fauna close to the Sorgenfrei–Tornquist Zone with no signs of a near-shore fauna (C. Heilmann-Clausen, personal communication 2005). Furthermore, reworked Eocene dinocysts and clasts of Eocene muds interbedded with Miocene deltaic sediments in Denmark clearly indicate the presence of marine Eocene deposits in the Scandinavian hinterland (Rasmussen 2004). The thickness of the Upper Paleocene – Eocene sediments that was removed during the Neogene rise of Scandinavia was probably limited (<200 m; Fig. 2B).

During the Oligocene, major clastic wedges prograded into the Norwegian–Danish Basin from present-day Norway (Fig. 3A; Michelsen *et al.* 1998; Clausen *et al.* 1999; Faleide *et al.* 2002). This change in depositional environment from Eocene times indicates a phase of tectonic uplift of southern Norway (*c.* 33 Ma) (e.g. Michelsen *et al.* 1998; Lidmar-Bergström *et al.* 2000; Faleide *et al.* 2002). This tectonic activity is shown by reactivation of faults on the Ringkøbing–Fyn High and by movements of salt structures in the Norwegian–Danish Basin (Rasmussen 2004). We suggest that a thick succession of Oligocene shelf and delta sediments that

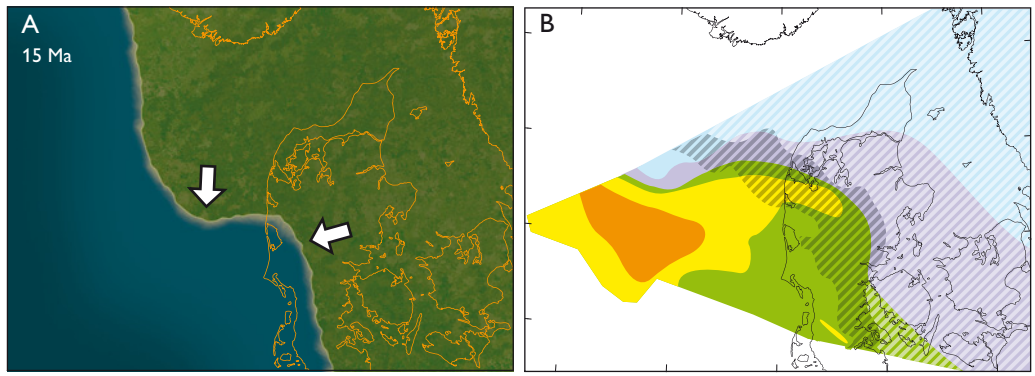

Fig. 4. **A**: Middle Miocene palaeogeography, 15 Ma. **B**: Lower – lower Middle Miocene isochore prior to late Neogene exhumation. Modified from Japsen *et al.* (2007a).

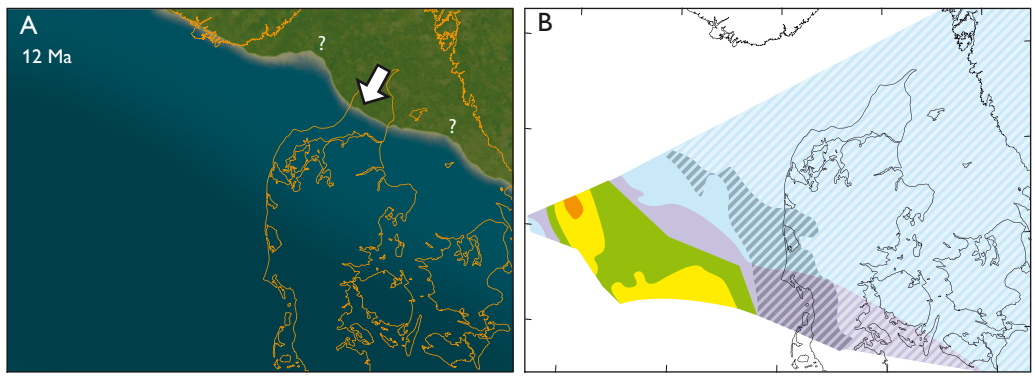

Fig. 5. **A**: Late Miocene palaeogeography, 12 Ma. **B**: Upper Middle – lower Upper Miocene isochore prior to late Neogene exhumation. Modified from Japsen *et al.* (2007a).

prograded southwards from southern Norway and westwards from southern Sweden made up a substantial part of the section that was removed during the Neogene exhumation at the locations of the Felicia-1 and Hans-1 wells, respectively (>1 km) (Fig. 3B).

During the early Miocene, deltas prograded to the south and south-west and reached a thickness up to 300 m (Fig. 4A). The deposition of coarse-grained sediments reached the southern part of the Norwegian–Danish Basin and the Ringkøbing–Fyn High during the Neogene (Rasmussen 2004). These prograding systems reflect a redistribution of sediments caused by uplift in the Scandinavian hinterland that resulted in the early Neogene exhumation near the craton. The occurrence of both immature and mature sediments reflects erosion of weathered as well as newly exposed basement. In the Danish area, the early Miocene tectonic activity is demonstrated by coarse-grained, braided fluvial systems and later by a sudden increase in the heavy mineral content at *c.* 17 Ma (Rasmussen 2004). The thickness of the Lower – lower Middle Miocene sediments that was removed during late Neogene exhumation was probably limited (<500 m), because mainly the onshore part of these deposits were affected by exhumation (Fig. 4B).

In the middle Miocene, at *c.* 15 Ma, a distinct marine flooding of the area took place, and up to 150 m of clayey sediments were deposited in south-western Denmark during the middle–late Miocene (Fig. 5A) (Rasmussen 2005). The flooding was caused partly by eustatic sea-level rise related to the mid-Miocene climatic optimum and partly by increased subsidence in the eastern North Sea Basin in the late Miocene (Rasmussen 2004). The thickness of the upper Middle – lower Upper Miocene sediments that was removed during late Neogene exhumation was limited (<200 m; Fig. 5B).

At the end of the Miocene resumed delta progradation from north-east and in particular the east occurred (Fig. 6A) (Rasmussen 2005). The infilling of the North Sea Basin continued during the Pliocene where up to 500 m were deposited in the central North Sea Basin. Substantial thicknesses (<500 m) of upper Upper Miocene – Pliocene sediments were removed during late Neogene exhumation across an extensive region of the eastern North Sea (Fig. 6B).

Summary and implications

This study emphasises that the tectonic development of a region cannot be reconstructed solely on evidence from the sedimentary record. Such reconstructions need also to be based on the record of physical indicators of palaeothermal and palaeoburial phases related to the former presence of geological units now removed. We have found evidence for three tectonic phases that have affected southern Scandinavia during the Cenozoic: (1) A phase that began at the Eocene–Oligocene transition at *c.* 33 Ma as indicated by the onset of progradation of clastic wedges away from southern Norway and

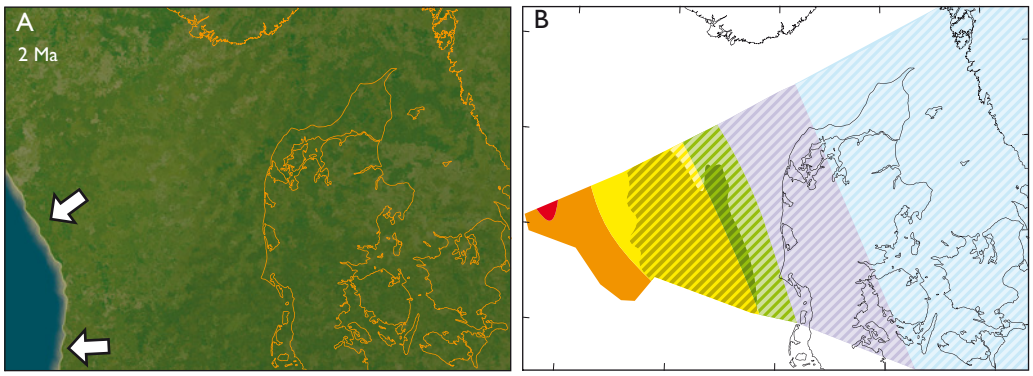

Fig. 6. **A**: Pliocene palaeogeography, 2 Ma. **B**: Upper Upper Miocene – Pliocene isochore prior to late Neogene exhumation. Modified from Japsen *et al.* (2007a).

inferred progradation away from southern Sweden. (2) A phase that began at the Oligocene–Miocene transition at *c.* 24 Ma, as indicated by early Neogene exhumation of the areas adjacent to the presently exposed basement areas and by early Miocene coarse-grained braided fluvial systems south of Scandinavia. (3) A phase that began in the early Pliocene at *c.* 4 Ma, as indicated by the widespread, late Neogene exhumation, the intra-Pliocene unconformity and subsequent tilting of the Neogene succession in the eastern North Sea.

These phases are consistent with the stratigraphy in the north-east Atlantic Ocean (Stoker *et al.* 2005) and around southern Norway (e.g. Michelsen *et al.* 1998; Faleide *et al.* 2002; Rasmussen 2004). The observations thus suggest that southern Norway, with peaks higher than 2 km above sea level, emerged during several phases since Eocene times, when a deep ocean covered much of the region.

References

Clausen, O.R., Gregersen, U., Michelsen, O. & Sørensen, J.C. 1999: Factors controlling the Cenozoic sequence development in the eastern parts of the North Sea. Journal of the Geological Society of London **156**, 809–816.

Faleide, J.I., Kyrkejbø, R., Kjennerud, T., Gabrielsen, R.H., Jordt, H., Fanavoll, S. & Bjerke, M. 2002: Tectonic impact on sedimentary processes during Cenozoic evolution of the northern North Sea and surrounding areas. In: Doré, A.G. *et al.* (eds): Exhumation of the North Atlantic Margin: Timing, Mechanisms and Implications for Petroleum Exploration. Geological Society Special Publications (London) **196**, 235–269.

Green, P.F., Duddy, I.R. & Hegarty, K.A. 2002: Quantifying exhumation from apatite fission-track analysis and vitrinite reflectance data: precision, accuracy and latest results from the Atlantic margin of NW Europe. In: Doré, A.G. *et al.* (eds.): Exhumation of the North Atlantic margin: timing, mechanisms and implications for petroleum exploration. Geological Society Special Publications (London) **196**, 331–354.

Heilmann-Clausen, C., Nielsen, O.B. & Gersner, F. 1985: Lithostratigraphy and depositional environments in the upper Palaeocene and Eocene of Denmark. Bulletin of the Geological Society of Denmark **33**, 287–323.

Japsen, P. & Bidstrup, T. 1999: Quantification of late Cenozoic erosion in Denmark based on sonic data and basin modelling. Bulletin of the Geological Society of Denmark **46**, 79–99.

Japsen, P., Green, P.F., Nielsen, L.H., Rasmussen, E.S. & Bidstrup, T. 2007a: Mesozoic–Cenozoic exhumation in the eastern North Sea Basin: a multi-disciplinary study based on palaeo-thermal, palaeo-burial, stratigraphic and seismic data. Basin Research **19**, 451–490.

Japsen, P., Mukerji, T. and Mavko, G. 2007b: Constraints on velocity-depth trends from rock physics models. Geophysical Prospecting **55**, 135–154.

Lidmar-Bergström, K., Ollier, C.D. & Sulebak, J.C. 2000: Landforms and uplift history of southern Norway. Global and Planetary Change **24**, 211–231.

Michelsen, O., Thomsen, E., Danielsen, M., Heilmann-Clausen, C., Jordt, H. & Laursen, G. 1998: Cenozoic sequence stratigraphy in the eastern North Sea. In: de Graciansky, P.-C. *et al.* (eds): Mesozoic and Cenozoic sequence stratigraphy of European basins. Society of Economic Paleontologists and Mineralogists Special Publication **60**, 91–118.

Nielsen, L.H. 2003: Late Triassic – Jurassic development of the Danish Basin and Fennoscandian Border Zone, southern Scandinavia. In: Ineson, J. & Surlyk, F. (eds): The Jurassic of Denmark and Greenland. Geological Survey of Denmark and Greenland Bulletin **1**, 459–526.

Rasmussen, E.S. 2004: The interplay between true eustatic sea-level changes, tectonics, and climatical changes: What is the dominating factor in sequence formation of the Upper Oligocene–Miocene succession in the eastern North Sea Basin, Denmark? Global and Planetary Change **41**, 15–30.

Rasmussen, E.S. 2005: The geology of the upper Middle – Upper Miocene Gram Formation in the Danish area. Palaeontos **7**, 5–18.

Stoker, M.S., Praeg, D., Shannon, P.M., Hjelstuen, B.O., Laberg, J.S., Nielsen, T., van Weering, T.C.E., Sejrup, H.P. & Evans, D. 2005: Neogene evolution of the Atlantic continental margin of NW Europe Lofoten Islands to SW Ireland: anything but passive. In: Doré, A.G. & Vining, B.A. (eds): Petroleum geology: North-West Europe and global perspectives. Proceedings of the 6th Petroleum Geology Conference, 1057–1076. London: Geological Society.

Zachos, J.C., Pagani, M., Sloan, L.C., Thomas, E. & Billups, K. 2001: Trends, rythms, and aberrations in global climate 65 Ma to present. Science **292**, 686–693.

Authors' addresses

P.J., E.S.R., L.H.N. & T.B., *Geological Survey of Denmark and Greenland, Øster Voldgade 10, DK-1350 Copenhagen K, Denmark.* E-mail: *pj@geus.dk*

P.F.G., *Geotrack International, 37 Melville Road, Brunswick West, Victoria 3055, Australia.*

A new Neogene biostratigraphy for Denmark

Karen Dybkjær and Stefan Piasecki

In Denmark most of the water used in private households, in the industry and for irrigation in agriculture comes from subsurface aquifers. Some of the most important aquifers in Jylland, western Denmark, are sand layers deposited from 23 to 15 Ma ago, in the Early Neogene (Early to Middle Miocene). About 23 Ma ago, in the Early Miocene, the coastline ran NW–SE across present-day Jylland (Rasmussen 2004). Global climatic variations led to major sea-level changes (Zachos *et al.* 2001), which in combination with increased sediment transport from the north (the present Norway) resulted in deposition of several huge, fluvio-deltaic sand systems intercalated with marine clay (e.g. Rasmussen 1961; Rasmussen 2004; Rasmussen & Dybkjær 2005).

The Geological Survey of Denmark and Greenland (GEUS) and the regional Environment Centres (the former counties (amter)) in Jylland are working in close cooperation to study the Early Neogene succession; the main purposes are: (1) to find new aquifers, (2) to map the extent of known aquifers and clarify their mutual relationships, in order to evaluate the size of the water resources and optimise production, and (3) to protect the aquifers from pollution due to leaching from the surface.

In order to map the complex sedimentary succession, it has been necessary to combine several geological disciplines, including seismic interpretation, sedimentology, correlation of geophysical logs, and biostratigraphy (e.g. Dybkjær 2004; Rasmussen 2004; Rasmussen *et al.* 2004; Piasecki 2005; Rasmussen & Dybkjær 2005; Dybkjær & Rasmussen 2007). This article shows some results of a detailed dinoflagellate cyst stratigraphy, which is based on an extensive database (Fig. 1). We present here for the first time a dinoflagellate cyst zonation for the complete Neogene succession in the Danish area.

Dinoflagellates and their cysts

Dinoflagellates are eukaryotic, single-celled organisms that occur as motile cells with two flagella, one which encircles the cell, and one longitudinal flagellum. These organisms, which also occur abundantly at present, include autotrophs, phagotrophs, symbionts and parasites. Photosynthetic species (autotrophs) account for about half of the living genera and play an important role in the marine ecosystem as primary producers. Some marine species produce toxins or cause red tides and several types of shellfish poisoning. Dinoflagellates have left a rich fossil record, mainly of organic-walled cysts, in Mesozoic and Cenozoic rocks; examples of fossil dinoflagellate cysts are shown in Fig. 2. Some dinoflagellate species form cysts as part of their life-cycle; others form cysts as a survival strategy, during unfavourable environmental conditions (e.g. low sea surface temperatures or lack of nutrients). The morphology of a cyst reflects the morphology of the motile dinoflagellate. The rapid evolution of the relatively complex, fossilisable dinoflagellate cyst wall makes these fossils ideal for biostratigraphic purposes (e.g. Fensome *et al.* 1996).

Material and methods

The dinoflagellate cyst zonation scheme presented here is based on data from more than 50 onshore and offshore boreholes and a series of onshore exposures (Fig. 1). The sediment samples from the boreholes and exposures were processed at the palynological laboratory at GEUS using standard palynological preparation methods.

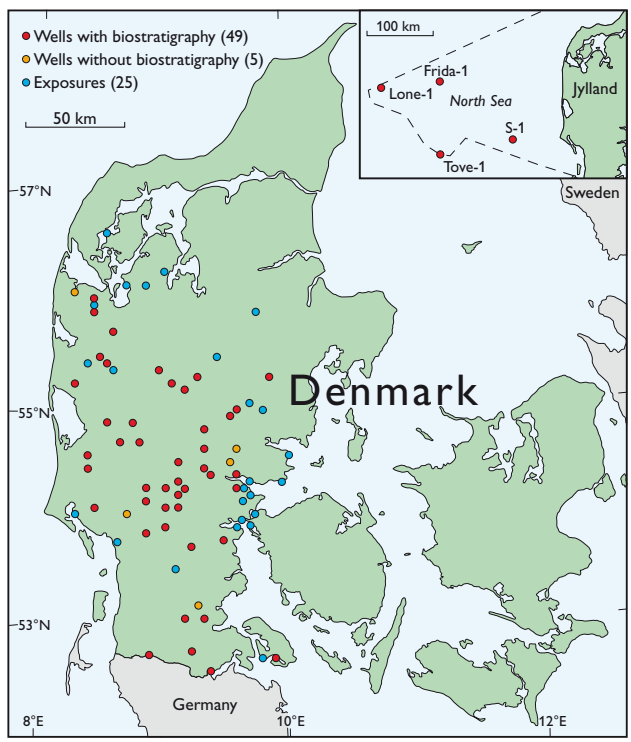

Fig. 1. Map of Denmark showing the location of studied wells and exposures. The insert map shows the location of the offshore exploration wells included in this study.

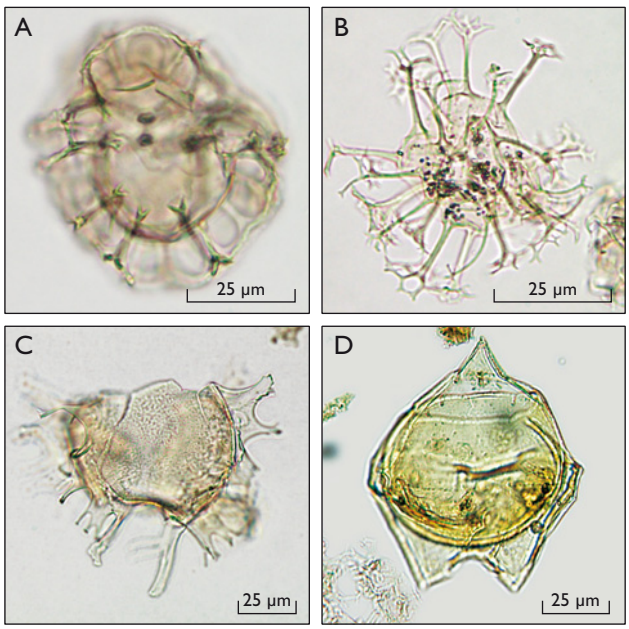

Fig. 2. Stratigraphically significant dinoflagellate cysts from the Miocene of Denmark. **A**: *Unipontidinium aquaeductum*. **B**: *Achomosphaera andalousiense*. **C**: *Chiropteridium galea*. **D**: *Deflandrea phosphoritica*.

The Danish Neogene stratigraphy has traditionally been based on molluscs and foraminifers whereas early studies of dinoflagellate floras were limited (Piasecki 1980). However, new comprehensive studies of dinoflagellate cysts throughout the Danish Neogene have resulted in a high-resolution stratigraphy of the succession, even in marginal marine deposits where foraminifers and molluscs rarely occur. Dinoflagellate cysts in strata of the central North Sea Basin were studied in offshore, hydrocarbon exploration wells, for comparison with the onshore, marginal, marine deposits and to obtain data from the youngest Neogene that is not represented by onshore strata. The resulting stratigraphy is a so-called interval zonation, i.e. all zones are defined as successions of rocks between a lower and an upper event of fossil appearance or disappearance. For example the *Unipontidinium aquaeductum* Zone is defined from the first appearance of *U. aquaeductum* to the first appearance of *Achomosphaera andalousiense* (Figs 2, 3). However, the zone is also characterised by other associated events (stratigraphic first and last occurrences of other characteristic species) and by the dinoflagellate cyst assemblage in general. Species with relatively common and consistent occurrence and with reported stratigraphic potential from outside the North Sea Basin, e.g. in the North Atlantic realm, were preferentially selected for the definition of the zones. The zonation can therefore easily be compared with other international/North Atlantic dinoflagellate zonations, despite the fact that much of the studied material was deposited in the relatively enclosed and possibly periodically brackish environments of the North Sea Basin.

Dinoflagellate cyst zonation

The Danish Neogene is formally divided into 19 dinoflagellate cyst zones from the uppermost Oligocene to the top of the Pliocene, with one zone in the Oligocene, 15 zones in the Miocene and three zones in the Pliocene (Fig. 3). The Pliocene is considered tripartite; Zanclean, Piacenzian and Gelasian (see Gradstein *et al.* 2004). The zonation has a high resolution in the uppermost Oligocene, the Lower Miocene and the Middle Miocene (1, 8 and 4 zones respectively) and a lower resolution in the Upper Miocene and Pliocene (3 and 3 zones respectively). The zones will be formally defined in a forthcoming paper. The proposed dinoflagellate cyst stratigraphy for Denmark correlates well with other formal stratigraphies in the North Sea Basin, e.g. in Germany (Köthe 2003), the Netherlands (Munsterman & Brinkhuis 2004), Belgium (e.g. Louwye *et al.* 1999) and the United Kingdom (e.g. Head 1998), as well as with dinoflagellate cyst stratigraphies outside this basin in the North Atlantic realm (de Verteuil & Norris 1996), in spite of differences in selection of diagnostic species. The new Danish biozonation is also correlated with Neogene chronostratigraphy and with nannoplankton biostratigraphy (see Gradstein *et al.* 2004).

Geological results

The new dinoflagellate cyst stratigraphy has been extensively tested in boreholes and exposures throughout Jylland (Fig. 1). The application provides a detailed stratigraphic framework for improved geological interpretations. Three major, prograding deltaic sand systems with excellent potential as reservoirs for drinking water are recognised in the Lower Miocene to lowermost Middle Miocene in the central parts of Jylland: the Billund sand, the Bastrup sand and the Odderup Formation (e.g. Dybkjær 2004; Rasmussen 2004). In addition, several problematic issues of Neogene geology in the Danish region have been solved:

1. The stratigraphic position of the Vejle Fjord Formation (Larsen & Dinesen 1959) is now definitively established as latest Oligocene (Brejning Clay) to earliest Miocene (Vejle Fjord Clay and Sand) (Dybkjær 2004; Dybkjær & Rasmussen 2007).
2. The upper, silty and sandy part of the Sofienlund Formation is time equivalent to the Vejle Fjord Clay and Sand. The lower Ulstrup Clay and the Sofienlund Clay are time equivalent with the Brejning Clay (Unpublished data 2006, K. Dybkjær).
3. The Oligocene–Miocene boundary can be recognised in the eastern North Sea Basin as the last occurrence of common *Deflandrea phosphoritica* (Figs 2, 3). This event corresponds to the transition from the Brejning Clay to the Vejle Fjord

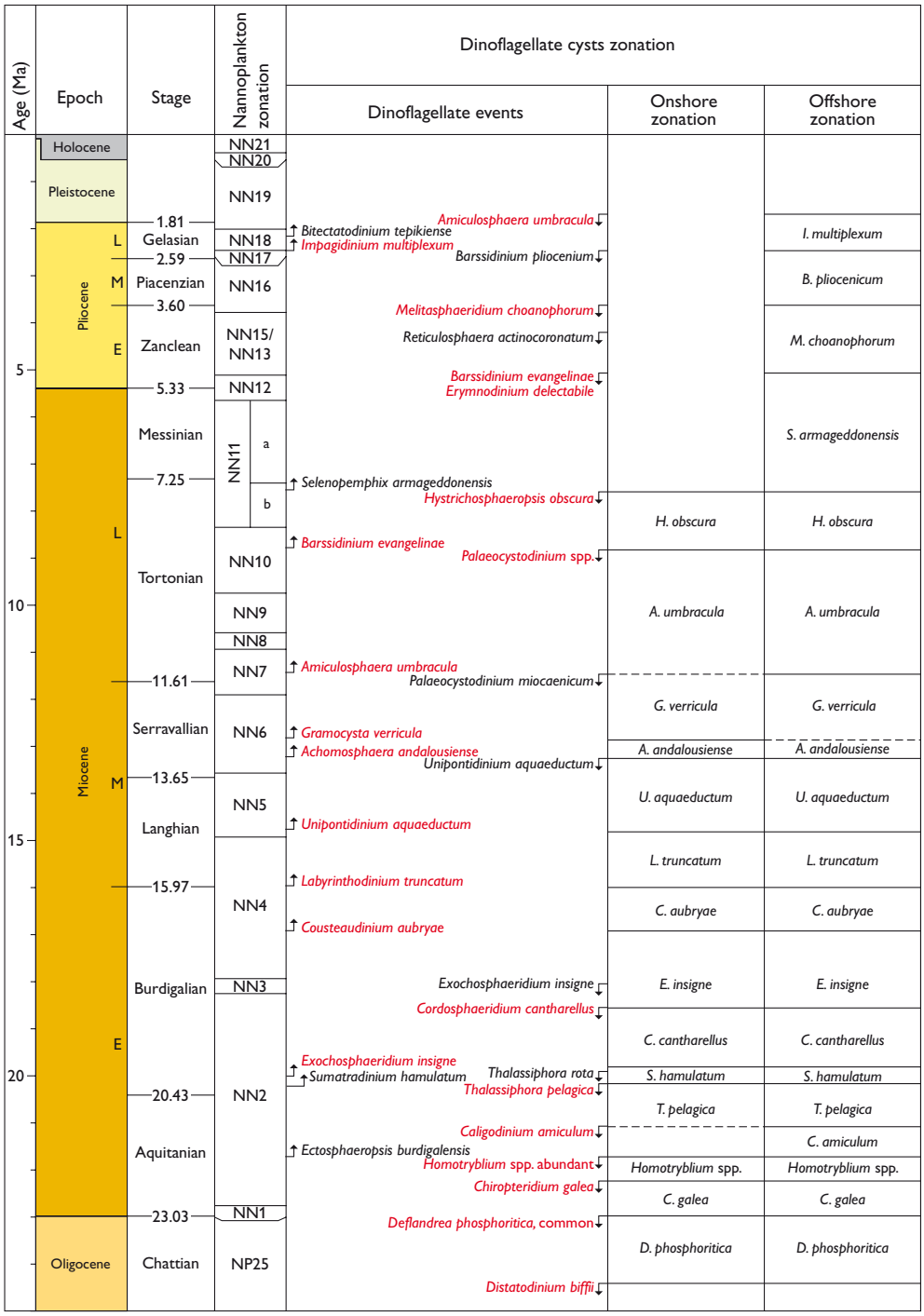

Fig. 3. Stratigraphic scheme presenting the new dinoflagellate cyst zonation correlated with the Neogene nannoplankton zonation and chronostratigraphy. The time scale is according to Gradstein *et al.* (2004). The diagnostic dinoflagellate cyst species are shown in red.

Clay and to the Sequence Boundary B (Rasmussen 2004; Dybkjær & Rasmussen 2007).

4. A significant hiatus is recognised between the Vejle Fjord and Arnum Formations in the northern and central parts of Jylland. In the southern parts of Jylland a time-equivalent fluvial-deltaic sand system, the Ribe Formation, was deposited (Dybkjær & Rasmussen 2000; Dybkjær 2004; Rasmussen 2004; Rasmussen & Dybkjær 2005).

5. The sand-rich succession in the Salten profile and in nearby gravel pits (Addit, Voervadsbro) was formerly referred to the late Early Miocene to early Middle Miocene Odderup Formation. Dinoflagellate cyst analysis has shown that this

succession is older than previously assumed and is part of the Vejle Fjord Formation/Billund sand system (Rasmussen *et al.* 2006).

6. The Hodde transgression occurred in the early Langhian, earliest Middle Miocene and limits the age of the underlying Odderup Formation to latest Early Miocene – earliest Middle Miocene (Piasecki 2005).

7. The youngest onshore Neogene deposits are of Tortonian age (Late Miocene) as no Messinian or Pliocene dinoflagellate cysts have been recorded. The earlier Sæd Formation, upper Gram Formation sand and the Neogene sand in cliffs at Ho Bugt are considered of Tortonian age and referred to the Gram Formation (Piasecki 2005).

8. A series of maps of the Cenozoic succession in the Danish North Sea area was produced by Rasmussen *et al.* (2005). The age determinations of the Neogene succession are based on the dinoflagellate cyst stratigraphy presented here.

Future perspectives

The new dinoflagellate cyst zonation is not only a valuable tool for unravelling the Danish Neogene succession. The Neogene succession in Denmark is presently being correlated with other Neogene successions, e.g. in Germany, the Netherlands and Poland, in order to elucidate the Neogene geology of the North Sea Basin.

The zonation also leads to an improved understanding of the subsidence and tilting of the North Sea Basin during the Neogene, and a better understanding of the petroleum systems in the hydrocarbon-producing provinces in the North Sea area. This may lead to new discoveries and increased production from known oil/gas-fields (Rasmussen *et al.* 2005). It is also an important tool for solving problems such as the evidence for and the timing of the Neogene uplift of Norway.

Acknowledgements

The Danish Environment Centres and the former counties are thanked for their cooperation and financial support.

References

De Verteuil, L. & Norris, G. 1996: Miocene dinoflagellate stratigraphy and systematics of Maryland and Virginia. Micropaleontology **42** (Supplement), 172 pp.

Dybkjær, K. 2004: Dinocyst stratigraphy and palynofacies studies used for refining a sequence stratigraphic model - uppermost Oligocene to Lower Miocene, Jylland, Denmark. Review of Palaeobotany and Palynology **131**, 201–249.

Dybkjær, K. & Rasmussen, E.S. 2000: Palynological dating of the Oligocene–Miocene successions in the Lille Bælt area, Denmark. Bulletin of the Geological Society of Denmark **47**, 87–103.

Dybkjær, K. & Rasmussen, E.S. 2007: Dinocyst stratigraphy in an expanded Oligocene–Miocene boundary section in the eastern North Sea Basin (the Frida-1 well, Denmark) and correlation from basinal to marginal areas. Journal of Micropalaeontology **26**, 1–17.

Fensome, R.A., Riding, J.B. & Taylor, F.J.R. 1996: Chapter 6. Dinoflagellates. In: Jansonius, J. & McGregor, D.C. (eds): Palynology: principles and applications. American Association of Stratigraphic Palynologists Foundation **1**, 107–169.

Gradstein, F.M., Ogg, J.G. & Smith, A.G. *et al.* 2004: A Geological Time Scale 2004, 589 pp. Cambridge: Cambridge University Press.

Head, M.J. 1998: Marine environmental change in the Pliocene and early Pleistocene of eastern England; the dinoflagellate evidence reviewed. In: van Kolfschoten, T. & Gibbard, P.L. (eds) The dawn of the Quaternary. Mededelingen Nederlands Instituut voor Toegepaste Geowettenschappen TNO **60**, 199–226.

Köthe, A. 2003: Dinozysten-Zonierung im Tertiär Norddeutschland. Revue Paléobiologie, Geneve **22**(2), 895–293.

Larsen, G. & Dinesen, A. 1959: Vejle Fjord Formationen ved Brejning. Sedimenterne og foraminiferfaunaen (Oligocæn-Miocæn). Danmarks Geologiske Undersøgelse II. Række **82**, 114 pp.

Louwye, S., de Coninck, J. & Verniers, J. 1999: Dinoflagellate cyst stratigraphy and depositional history of Miocene and Lower Pliocene formations in northern Belgium (southern North Sea Basin). Geologie en Mijnbouw **78**, 31–46.

Munsterman, D.K. & Brinkhuis, H. 2004: A southern North Sea Miocene dinoflagellate cyst zonation. Netherlands Journal of Geosciences / Geologie en Mijnbouw **83**, 267–285.

Piasecki, S. 1980: Dinoflagellate cyst stratigraphy of the Miocene Hodde and Gram Formations, Denmark. Bulletin of the Geological Society of Denmark **29**, 53–76.

Piasecki, S. 2005: Dinoflagellate cysts of the Middle – Upper Miocene Gram Formation, Denmark. In: Roth, F. & Hoedemarkers, K. (eds): The Gram Book. Palaeontos **7**, 29–45.

Rasmussen, E.S. 2004: Stratigraphy and depositional evolution of the uppermost Oligocene – Miocene succession in western Denmark. Bulletin of the Geological Society of Denmark **51**, 89–109.

Rasmussen, E.S. & Dybkjær, K. 2005: Sequence stratigraphy of the Upper Oligocene – Lower Miocene of eastern Jylland, Denmark: role of structural relief and variable sediment supply in controlling sequence development. Sedimentology **52**, 25–63.

Rasmussen, E.S., Dybkjær, K. & Piasecki, S. 2004: The Billund delta: a possible new giant aquifer in central and western Jutland. Geological Survey of Denmark and Greenland Bulletin **4**, 21–24.

Rasmussen, E.S., Piasecki, S., Andsbjerg, J., Dybkjær, K., Vejbæk, O.V., Jacobsen, C., Britze, P. & Bryde-Auken, M., 2005: Cenozoic maps of the Danish North Sea area. Danmarks og Grønlands Geologiske Undersøgelse Rapport **2005/33**, 8 pp.

Rasmussen, E.S., Dybkjær, K. & Piasecki, S. 2006: Neogene fluvial and nearshore marine deposits of the Salten section, central Jylland, Denmark. Bulletin of the Geological Society of Denmark **53**, 23–37.

Rasmussen, L.B. 1961: De Miocæne formationer i Danmark. Danmarks Geologiske Undersøgelse IV Række **4**(5), 45 pp.

Zachos, J.C., Pagani, M. Sloan, L.C. Thomas, E. & Billups, K. 2001: Trends, rhythms, and aberrations in global climate 65 Ma to present. Science **292**, 686–693.

Authors' address

Geological Survey of Denmark and Greenland, Øster Voldgade 10, DK-1350 Copenhagen K, Denmark. E-mail: *kd@geus.dk*

Mapping of buried tunnel valleys in Denmark: new perspectives for the interpretation of the Quaternary succession

Flemming Jørgensen and Peter B.E. Sandersen

Tunnel valleys eroded by subglacial meltwater underneath the Late Weichselian ice sheet are a common feature in the Danish landscape (Ussing 1907; Smed 1998). They occur as undulating elongate depressions with hollows and thresholds and without continuously descending floors. The valleys rise tens of metres before terminating in large outwash fans, primarily along the Main Stationary Line in Jylland, but also along younger ice-margin lines formed shortly after the Last Glacial Maximum. The meltwater was driven by hydrostatic pressure gradients below the glacier towards its margin leading to subglacial erosional features, partly in the form of valleys. The term 'tunnel valley' was first used by Madsen (1921), who referred to tunnel-like structures below glaciers that were expected to have carried the meltwater. Worldwide, this term is used for subglacially eroded valleys; however, other terms such as 'tunnel channel' and 'incision' are also widely used for such valleys.

There is general consensus that subglacial meltwater is the primary causative agent that has eroded the tunnel valleys (O'Cofaigh 1996; Huuse & Lykke-Andersen 2000; Jørgensen & Sandersen 2006). The subglacial origin is indicated by: (1) abrupt terminations at former ice margins and the association with the large outwash plains, (2) irregular longitudinal profiles, (3) the occurrence of small channels and eskers in the valleys, and (4) the non-meandering and non-dendritic appearance of the relatively straight-segmented valleys. The exact mode of meltwater erosion remains, however, poorly understood. Valleys are present not only in the landscape; they are also found buried in the subsurface. In Denmark, buried valleys have occasionally been described on the basis of borehole data and early geoelectrical methods (e.g. Sorgenfrei & Berthelsen 1954; Lykke-Andersen 1973; Binzer & Stockmarr 1994). Based on the large amount of newly collected hydrogeophysical data in Denmark, it has recently become possible to define such valleys as tunnel valleys and to acknowledge their wide distribution in the subsurface (Sandersen & Jørgensen 2003; Jørgensen *et al.* 2005; Jørgensen & Sandersen 2006). Analysis of these data has revealed dense networks of tunnel valleys and has significantly improved our understanding of their distribution, geometry and sedimentary infill. In the following, we review this work and identify new perspectives for the interpretation of the Quaternary succession in Denmark.

The work was initiated in 1998 by the former Danish counties (amter), and is currently continued by the Geological Survey of Denmark and Greenland and the 'miljøcentre' (environment centres). As part of this project, the buried valleys are continuously being mapped as new data are collected.

Data

The spacing between and the quality of deep boreholes in Denmark are generally insufficient to precisely delineate buried valleys (Thomsen *et al.* 2004). Borehole data are, however, important as they can often be used to verify the presence of valleys indicated from geophysical data, and provide valuable information about the sedimentary infill of the valleys.

Since the coverage of boreholes is generally too sparse for proper valley delineation, other types of data distributed in denser grids are needed. Densely spaced data can be collected using the Transient Electro-Magnetic (TEM) geophysical method (Sørensen & Auken 2004) that gives deep penetra-

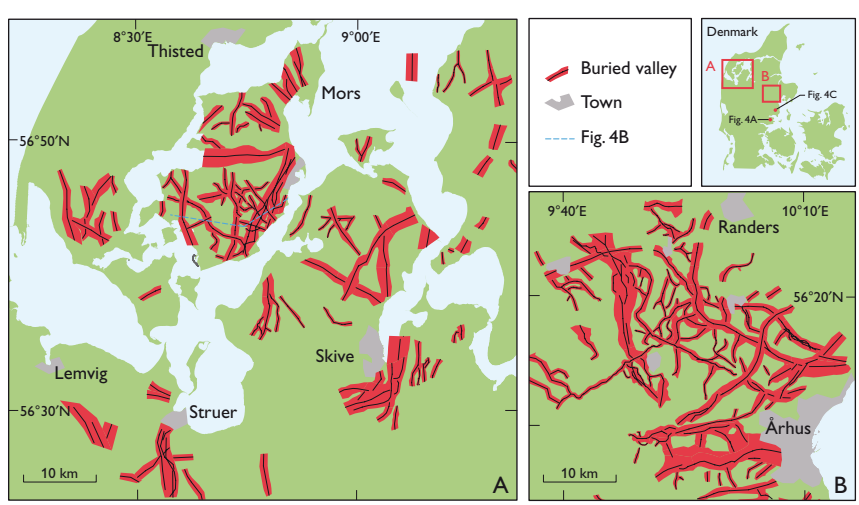

Fig. 1. Two selected areas with high densities of mapped buried valleys. **A**: North-western part of Jylland. **B**: North-west of Århus.

tion and an acceptable resolution. During the last ten years, this method has been extensively used in Denmark, allowing many buried valleys to be mapped.

High-resolution seismic data provide detailed 2D structural information of the valley architecture and allow detailed structural elements to be resolved, even in areas with poor lithological contrasts. However, data acquisition is costly and usually limited to widely spaced lines. The most effective method to map and investigate buried valleys is using a combination of the TEM method, seismic data and borehole data (Jørgensen *et al.* 2003).

In the present project, all available and relevant lithological and geophysical data from the Danish onshore area are being evaluated and examined in order to map and describe buried valleys (Sandersen & Jørgensen 2006). A set of criteria is used to obtain a high degree of certainty and objectivity in the valley delineation. The most important criterion is that the lateral extent and the orientation of the valleys must be unambiguously expressed in the available data. No interpolations between surveyed areas are made.

Valley characteristics

More than 2500 km of buried valleys have currently been mapped in Denmark using this procedure. The highest valley density is found in areas where TEM data have been collected in dense grids and where the conditions for this specific method are ideal. Such areas are found, for example, northwest of Århus and in the north-western part of Jylland (Fig. 1). Although many buried valleys have been mapped in these areas, even more are expected to exist because (1) not all valleys can be mapped with the methods in use, and (2) the study areas are not yet entirely covered by such data.

Only a minor part of the country has been surveyed by the TEM method and all valleys are not represented in the collected data, so the maps can at best be considered to show the minimum occurrence of buried valleys. The general distribution and density of buried valleys therefore cannot be directly seen from the maps. Thus, while a limited number of valleys have been mapped in western Jylland, seismic data and borehole data indicate that many more buried valleys are present in this part of Denmark than shown in Fig. 2. Delineation of buried valleys in western Jylland is difficult due to low data coverage.

The buried valleys can be divided into different generations that were formed during successive glaciations (Jørgensen *et al.* 2005; Jørgensen & Sandersen 2006). The valleys often cross-cut each other and sometimes they have different preferred orientations. A complicated pattern with three to five generations of valleys can often be distinguished in areas with high data resolution (Fig. 3). If the ice flows were parallel or

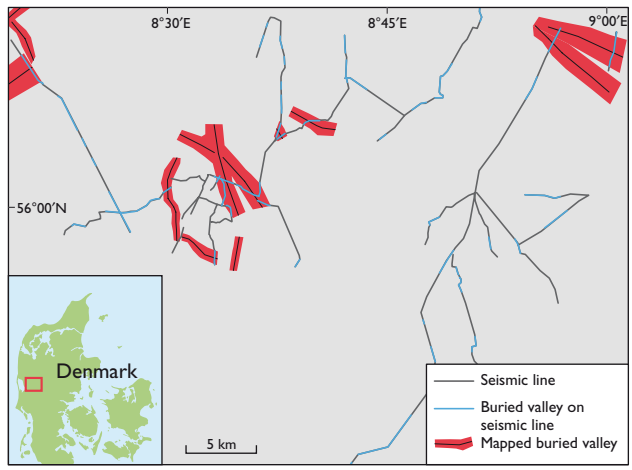

Fig. 2. Map of an area in western Jyllland, showing the location of high-resolution reflection seismic lines. The buried valleys cannot be accurately mapped from data obtained by this method alone, due to the wide line spacing. The valleys shown have mainly been mapped from data obtained by area-covering methods such as the TEM method. Modified from Sandersen & Jørgensen (2006).

nearly-parallel to pre-existing valleys, these valleys would be liable to repeated erosion and re-filling producing a complicated cut-and-fill setting within them. Multiple generations of valley erosion are therefore also often found within the buried valleys themselves. The valley architecture is normally complex due to this cut-and-fill history, but also due to glaciotectonic disturbances. This complexity can be observed in both seismic and TEM data (Fig. 4). The complex fill is also often indicated by borehole data that show strong lithological variations over short distances.

The valley fill is deposited in subglacial environments, in glacial lakes and rivers, in marine and terrestrial environments. Statistical analyses of borehole data in all the mapped valleys show that by far the most common infill sediment types are tills and meltwater deposits (Sandersen & Jørgensen 2006). In this group, 52% are coarse meltwater deposits (sand and gravel), 30% are clay-rich till and 18% are fine-grained meltwater deposits (silt and clay).

The mapped buried valleys vary in depth with the deepest features exceeding 350 m from valley floor to shoulder (Jørgensen & Sandersen 2006). The width is generally between 0.5 and 1.5 km, but widths of up to 4 km occur. The lengths of the valleys are difficult to evaluate, because many of the areas surveyed so far are small. However, some valleys in larger survey areas exceed 25–30 km in length. Some striking features of the valleys are that they often terminate abruptly and that they are highly irregular with depressions and thresholds along their floors.

It is difficult to determine the ages of the buried valleys. The infill sediments can be dated in some cases and provide a minimum age for the time of valley erosion. However, based on the

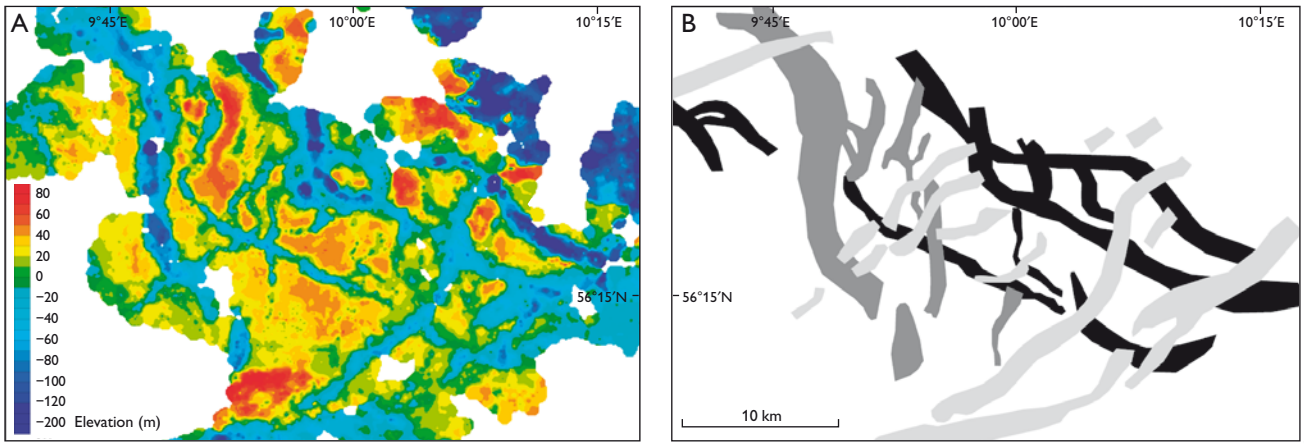

Fig. 3. **A**: Map of an area north-west of Århus showing the interpolated surface of a low-resistive bottom layer in TEM soundings. Large parts of the valleys have been eroded into this surface. **B**: Cross-cutting valley generations found in the same area. Black represents the oldest generation; light grey the youngest generation. Modified from Jørgensen & Sandersen (2006).

time gap between the age of the eroded sediments and the age of the infill sediments, buried valleys can be shown to have formed both during the Weichselian, the Saalian and the Elsterian glacial stages (Jørgensen & Sandersen 2006). Some of the valleys were probably formed during older glacial stages.

Valley formation

The mapped buried valleys are comparable to open tunnel valleys found in the present-day Danish landscape with respect to morphology and dimensions (Jørgensen & Sandersen 2006). Most likely, they therefore formed as tunnel valleys and were subsequently buried by younger sediments. Subglacial meltwater erosion is believed to have been responsible for most of the erosion, whereas direct glacial erosion may have contributed to the formation of the widest valleys. The presence of multiple generations of valleys shows that the area was repeatedly transgressed by glaciers during the Pleistocene (Jørgensen & Sandersen 2006). Tunnel valleys have a pronounced tendency to be re-used during repeated cycles of glacial erosion, which produces their cut-and-fill structure. The degree of re-use is presumably determined by differences in the morphology, erodibility and hydraulic conductivity of the substratum. However, the occurrence of pro- and subglacial permafrost may also have played an important role (Jørgensen & Sandersen 2006).

Consequences and perspectives

Buried valleys are widespread in the Danish subsurface, occurring as complex, cross-cutting structures established during repeated erosion and infill. These characteristics require close attention when stratigraphic correlations are made, because discontinuous and complex geological settings are to be expected.

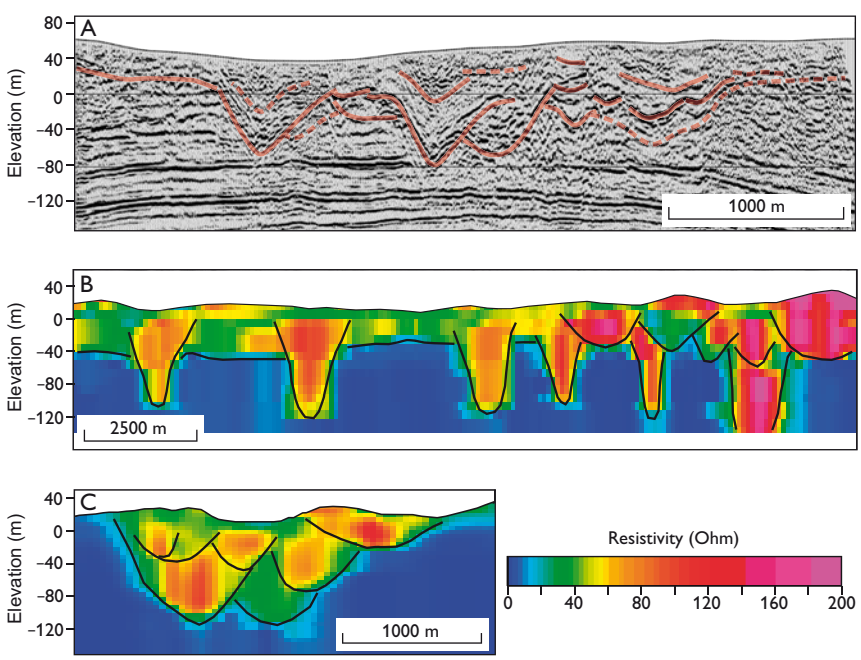

Fig. 4. Three profiles showing the complex geology related to buried valleys. **A**: A seismic profile across a buried valley with a cut-and-fill setting. Interpretation shown by a red line. **B**: TEM profile across a series of valleys. **C**: A TEM profile across a valley with a cut-and-fill setting. Interpretations on the TEM profiles are shown with black lines. See Fig. 1 for location of the profiles. Modified from Jørgensen *et al.* (2005) and Jørgensen & Sandersen (2006).

Correlation requires that the correlated sites are situated sufficiently close to each other so that they may not be significantly influenced by an unrecognised valley. The farther the valleys are apart, the more difficult correlation of their infill becomes. If one of the sites is situated inside an unrecognised or a poorly defined valley, stratigraphic correlations are likely to be erroneous, difficult or impossible to carry out. The discontinuous and complex geological setting of the valleys arises from the presence of unconformities produced by the valley erosion and from the limited lateral extent of the valleys and high variation of the sedimentary valley infill. Unconformities complicate correlations of the incised layers, and the limited lateral valley extent and high variation of the infill complicate the correlation of the infill sediments. Marked facies variations may make correlation of the infill sediments very difficult – even if the infill sediments were deposited simultaneously. The complications become even higher for valleys with cut-and-fill structures and when valleys cross-cut. Erosion of the valleys implies that much of the sedimentary record has been removed, but as erosion and sedimentation often occurred during successive events, sedimentary remnants are occasionally left behind between the unconformities. Therefore, the establishment of a coherent stratigraphy requires a dense data network and a large number of boreholes as well as a thorough knowledge of the outline and structure of the buried valleys and the relative age relationships between different valley generations in a given area. The challenges for stratigraphic correlations that arise from the presence of buried valleys as outlined above, also affect the construction of geological and hydrogeological models. Since the valleys often cross-cut older layers and contain aquifers as well as aquitards, they have the ability to significantly influence the flow regime of groundwater (e.g. Shaver & Pusc 1992). Furthermore, chances are high that buried valleys occur in almost all parts of Denmark. In order to construct such models it is crucial to know where the valleys occur and understand how they were formed.

While the occurrence of buried valleys imposes a series of new challenges, it may also provide new possibilities for the reconstruction of the Pleistocene record. Gradually increasing knowledge and overview of the erosional and depositional history of the valleys may lead to improved general understanding of the development of the Pleistocene. It is likely that the deeper parts of some deep valleys may have withstood events of extensive glacial erosion during the Pleistocene. Thus some valleys may contain remnants of glacial or interglacial sediments, and in that case, buried valleys may contain sedimentary records from the Early and early Middle Pleistocene. Such records are currently very rarely reported from the onshore parts of Denmark.

Acknowledgement

The project is supported by the Environmental Centres in Denmark.

References

Binzer, K. & Stockmarr, J. 1994: Geological map of Denmark, 1:500 000. Pre-Quaternary surface topography of Denmark. Danmarks Geologiske Undersøgelse Kortserie **44**, 10 pp., 2 maps.

Huuse, M. & Lykke-Andersen, H. 2000: Over-deepened Quaternary valleys in the eastern Danish North Sea: morphology and origin. Quaternary Science Reviews **19**, 1233–1253.

Jørgensen, F. & Sandersen, P.B.E. 2006: Buried and open tunnel valleys in Denmark – erosion beneath multiple ice sheets. Quaternary Science Reviews **25**, 1339–1363.

Jørgensen, F., Lykke-Andersen, H., Sandersen, P.B.E., Auken, E. & Normark, E. 2003: Geophysical investigations of buried Quaternary valleys in Denmark: an integrated application of transient electromagnetic soundings, reflection seismic surveys and exploratory drillings. Journal of Applied Geophysics **53**, 215–228.

Jørgensen, F., Sandersen, P.B.E., Auken, E., Lykke-Andersen, H. & Sørensen, K. 2005: Contributions to the geological mapping of Mors, Denmark – a study based on a large-scale TEM survey. Bulletin of the Geological Society of Denmark **52**, 53–75.

Lykke-Andersen, H. 1973: En begravet dal i Præ-kvartæret ved Århus. Dansk Geologisk Forening Årsskrift for **1972**, 111–118.

Madsen, V. 1921: Terrainformerne på Skovbjerg Bakkeø. Danmarks Geologiske Undersøgelse IV. Række **1**(12), 24 pp.

O'Cofaigh, C. 1996: Tunnel valley genesis. Progress in Physical Geography **20**, 1–19.

Sandersen, P.B.E. & Jørgensen, F. 2003: Buried Quaternary valleys in western Denmark – occurrence and inferred implications for groundwater resources and vulnerability. Journal of Applied Geophysics **53**, 229–248.

Sandersen, P.B.E. & Jørgensen, F. 2006: Kortlægning af begravede dale i Jylland og på Fyn. Opdatering 2005–2006, 201 pp. De jysk-fynske amters grundvandssamarbejde. Vejle: Vejle Amt & WaterTech A/S.

Shaver, R.B. & Pusc, S.W. 1992: Hydraulic barriers in Pleistocene buried-valley aquifers. Ground Water **30**, 21–28.

Smed, P. 1998: Die Entstehung der dänischen und norddeutschen Rinnentäler (Tunneltäler) – Glaziologische Gesichtspunkte. Eiszeitalter und Gegenwart **48**, 1–18.

Sørensen, K.I. & Auken, E. 2004: SkyTEM – a new high-resolution helicopter transient electromagnetic system. Exploration Geophysics **35**, 191–199.

Sorgenfrei, T. & Berthelsen, O. 1954: Geologi og vandboring. Danmarks Geologiske Undersøgelse III. Række **31**, 106 pp.

Thomsen, R., Søndergaard, V.H. & Sørensen, K.I. 2004: Hydrogeological mapping as a basis for establishing site-specific groundwater protection zones in Denmark. Hydrogeology Journal **12**, 550–562.

Ussing, N.V. 1907: Om Floddale og Randmoræner i Jylland. Oversigt over Det Kongelige Danske Videnskabernes Selskabs Forhandlinger **4**, 161–213.

Authors' addresses

F.J., *Geological Survey of Denmark and Greenland, Øster Voldgade 10, DK-1350 Copenhagen K, Denmark.* E-mail: *flj@geus.dk*

P.B.E.S., *Grontmij | Carl Bro A/S, Dusager 12, DK-8200 Århus N, Denmark.*.

Base Quaternary in the Danish parts of the North Sea and Skagerrak

Tove Nielsen, Anders Mathiesen and Malene Bryde-Auken

Over the years, several maps of the base Quaternary surface of the Danish area have been published. However, the maps have either been local in character (e.g. Håkansson & Pedersen 1992; Huuse *et al.* 2001) or have concentrated on special topics such as tunnel valleys (e.g. Huuse & Lykke-Andersen 2000) or glaciotectonic features (e.g. Klint & Pedersen 1995; Andersen *et al.* 2005). The only published map of a more regional character is that of Binzer & Stockmarr (1994) that covers onshore Denmark and eastern Danish waters. Here we present for the first time a regional map of the base Quaternary surface for the entire Danish sector of the North Sea and Skagerrak based on interpretations of reflection seismic data at the Geological Survey of Denmark and Greenland (GEUS) (Fig. 1). The new map has been depth-converted and merged with the onshore map of Binzer & Stockmarr (1994) and thus the first map covering the entire Danish land and sea areas has been compiled.

The definition of the base Quaternary is a current issue of debate. In this article, we follow Gradstein *et al.* (2004) who place the base Quaternary at base Gelasian, which is dated to 2.59 Ma. In parts of the studied area, glacial tectonic features in the form of thrust complexes can be seen on the seismic data. Here the base Quaternary surface has been placed at the base of the dislocated thrust units, corresponding to the basal décollement horizon.

The base Quaternary surface is of both academic and practical interest. The depth to the base Quaternary surface and its morphology are of interest to the understanding of

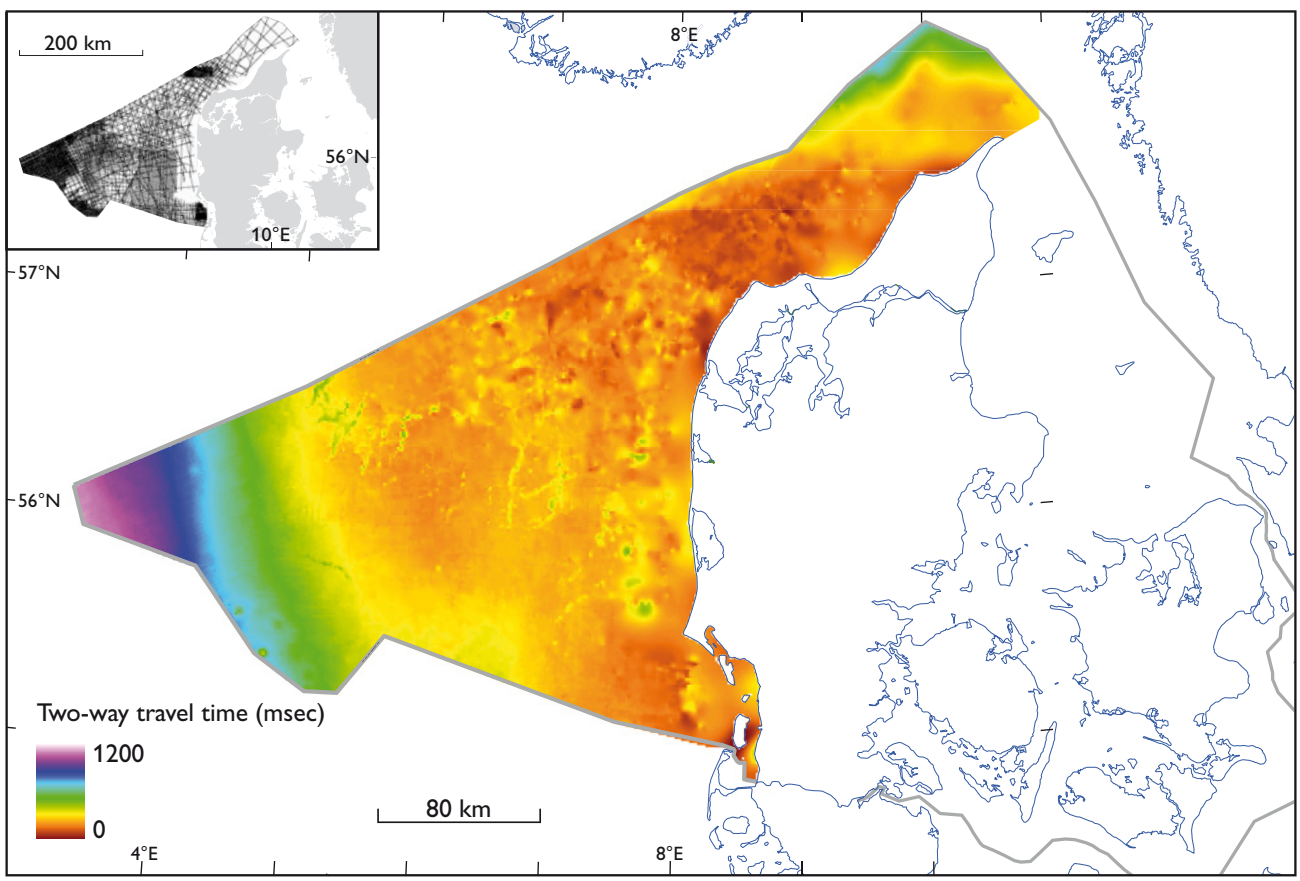

Fig. 1. The base Quaternary surface in the Danish sector of the North Sea and Skagerrak. The depth to the surface is shown in seismic two-way travel time in milliseconds below sea surface. The inset shows the line density of the seismic database.

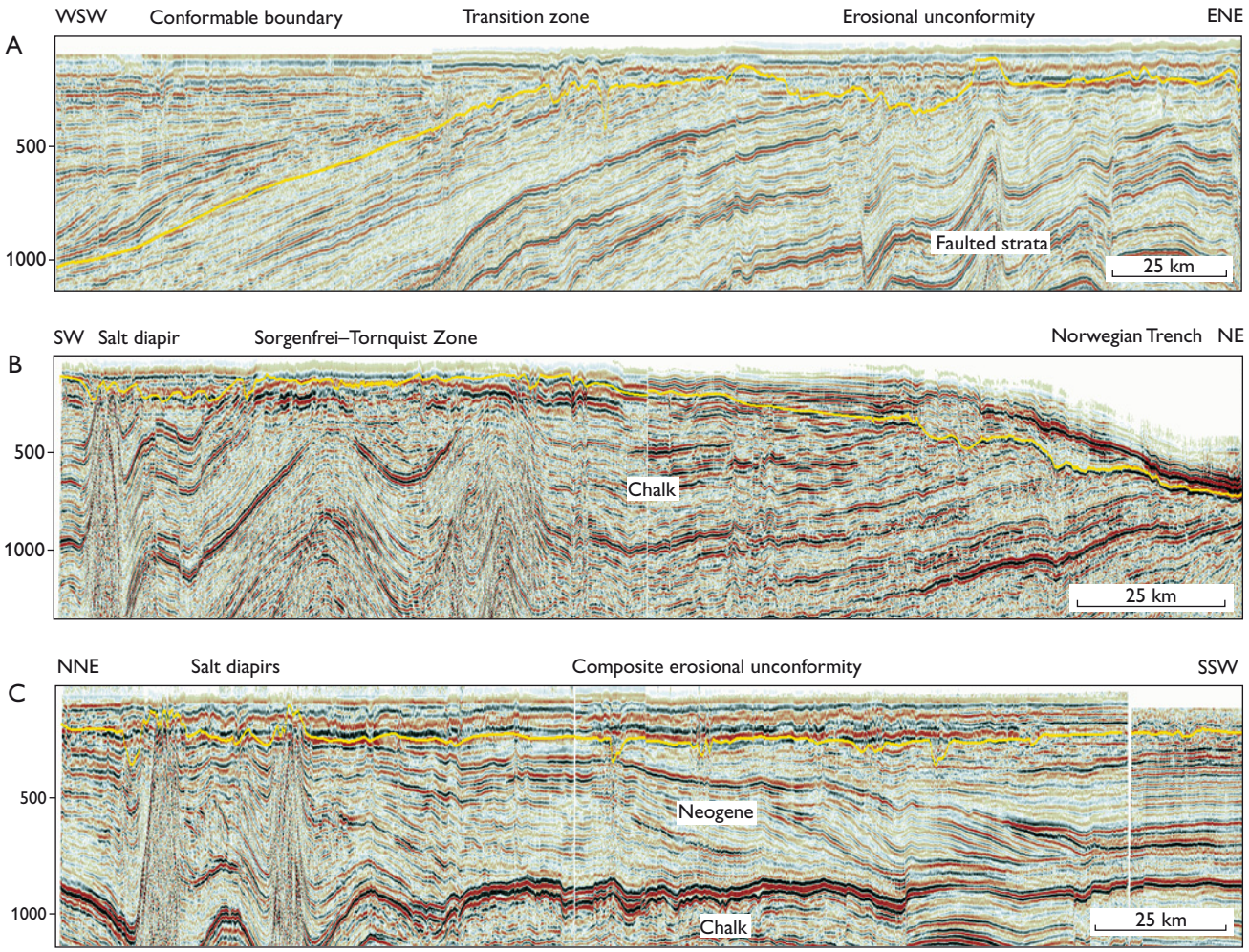

Fig. 2. Composite seismic profiles with the base Quaternary surface marked in yellow. The location of the profiles is shown in Fig. 3. **A**: Cross-section of the Danish North Sea sector. In the eastern part, the base Quaternary is seen as an erosional unconformity that cuts into mid- and late Cenozoic delta deposits. Towards the west, the base Quaternary becomes conformable with the underlying Lower Pliocene delta clinoforms. **B**: Cross-section of Skagerrak where the Quaternary deposits are relatively thin. The Quaternary is underlain by chalk and marks a major hiatus most likely formed by erosion during multiple glaciations. The high-lying chalk area towards the south is coincident with the Sorgenfrei–Tornquist Zone. Towards the north, the base Quaternary surface deepens and dips towards the Norwegian Trench. **C**: Cross-section of the Danish North Sea sector illustrating how in large parts of the North Sea the base Quaternary marks a change in depositional style from prograding pre-Quaternary delta deposits to aggradation or chaotic Quaternary till deposits. Towards the north, the shape of the base Quaternary surface implies that in this area the salt domes have been active during the Quaternary.

the Quaternary development of the region, but are also important in relation to offshore constructions such as oil and gas platforms, pipelines and wind mills.

Database and mapping procedure

The present seismic interpretation of the base Quaternary surface in the North Sea and Skagerrak (Fig. 1) forms part of a larger North-West Europe mapping project (*Petroleum geological atlas of the southern Permian Basin area* – SPBA), and the mapping is based on GEUS' digital 2D reflection seismic and well databases. The seismic interpretation is gridded in a 1000 × 1000 m grid and subsequently depth-converted using a linear time-depth function, ensuring that the resultant depth in metres fits available well data. In order to merge the new map with the pre-existing onshore map (Binzer & Stockmarr 1994), the latter has likewise been gridded into 1000 × 1000 m grids. To complete the composite map, a new seismic interpretation of the southern part of Bælthavet has been carried out, following the same interpretation procedure as for the North Sea and Skagerrak areas.

The base Quaternary surface

Using the 2.59 Ma age rather than the so far official 1.8 Ma age for the base of the Quaternary, only causes differences in the western North Sea where the mapped surface is deeply buried and lies conformably on Pliocene deltaic sediments

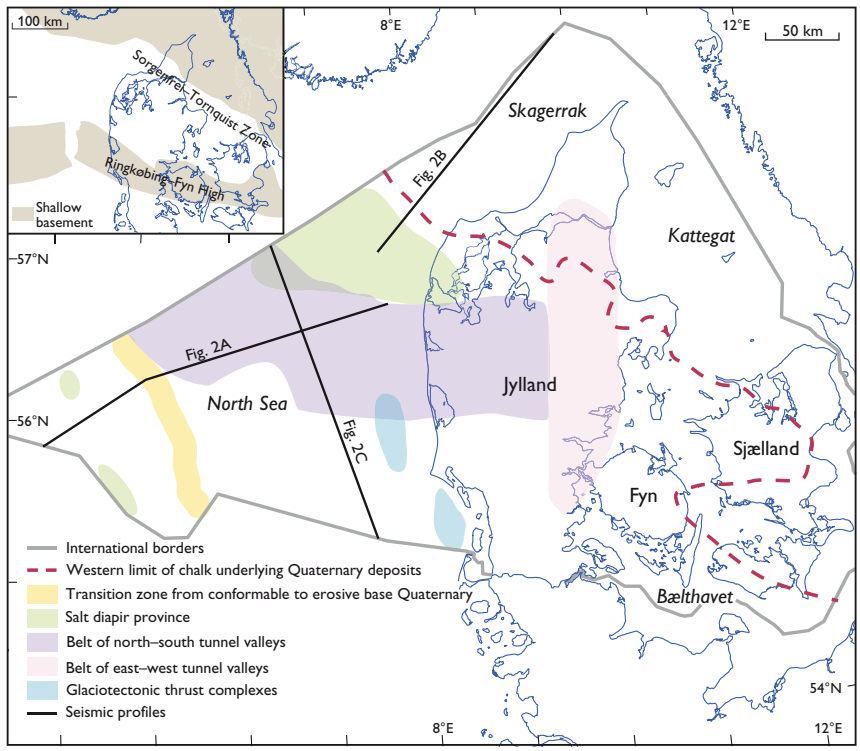

Fig. 3. Overview map showing areas and outline of features mentioned in the text. Also shown are the positions of the seismic profiles in Fig. 2. The inset shows the main structural elements and outline of shallow basement.

(Figs 1, 2). To the east, the base of the Quaternary shallows and becomes an erosional unconformity that cuts into pre-Quaternary deposits (Figs 1, 2). The transition zone from the conformable boundary to the erosional surface is marked in Fig. 3. The hiatus between the Quaternary and the underlying strata becomes greater towards the east (Rasmussen *et al.* 2005), and over large areas the base Quaternary surface is underlain by chalk (Fig. 2). This setting is a consequence of Neogene uplift and subsequent erosion.

The amount of glacial erosion during the Quaternary has been estimated to about one fifth of the total Neogene and Quaternary erosion (Japsen *et al.* 2002). The base Quaternary erosional surface east of the transition zone is most likely to be a composite unconformity created during multiple glaciations. West of the transition zone, the lower Quaternary deposits form a delta complex, and glacial erosion is only seen within the upper Quaternary deposits in the form of tunnel valleys and internal erosional surfaces (Fig. 2A). This depositional pattern shows that during the early Quaternary the glaciations did not extend into the central North Sea, and that full glaciation with grounding ice sheets did not occur in this area until later in the Quaternary.

In the north-eastern Danish North Sea, the base Quaternary surface displays an irregular morphology with several isolated, circular highs (Figs 1, 3). In the westernmost part of the Danish North Sea three similar highs are also seen. This pattern is the result of salt doming that was active during the Quaternary (Fig. 2C). Tunnel valleys occur in association with some of the salt domes, but few of them affect the base Quaternary surface. In the south-western Danish North Sea, the base Quaternary surface shows two elongated areas with depressions parallel to the coast of Jylland (Figs 1, 3). Here glaciotectonic deformation has taken place, resulting in the formation of major thrust complexes involving pre-Quaternary deposits with deep-lying décollement horizons. The trend of the thrust complexes and the internal pattern of the thrust faults indicate that they were formed by westward-moving ice.

In the central Danish North Sea, an E–W-trending belt of narrow, elongated incisions is seen in the base Quaternary surface (Figs 1, 3). This is a network of deep tunnel valleys that cuts into the pre-Quaternary deposits. The valleys have the same overall N–S trend, suggesting that they were formed below ice advancing over the area from the north. Some of the valleys are spatially associated with old fault systems (Fig. 2A), but usually there appear to be no pre-Quaternary features that can explain their location. It is worth noting that only few tunnel valleys incise the base Quaternary surface outside this approximately 80 km wide belt (Fig. 1), and hardly none on top of the Ringkøbing–Fyn High (Fig. 3, inset).

In most of the Skagerrak area, the Quaternary deposits rest unconformably on Cretaceous chalk (Figs 2B, 3). In the Sorgenfrei–Tornquist Zone in southern Skagerrak (Fig. 3, inset), the base Quaternary surface is relatively shallow due to up-thrusted chalk. Towards the north, the surface deepens and dips in the direction of the Norwegian trench (Figs 1, 2).

Figure 4 shows the base Quaternary composite depth map created by merging existing and new interpretations (see above). This map has been produced in order to place the interpretation of the North Sea and Skagerrak areas into a broader context. Differences in databases and mapping procedure have caused some discrepancies in the composite map. Nevertheless, some interesting observations can be made. The belt of distinct N–S-trending tunnel valleys incising the base Quaternary surface in the North Sea continues onshore in central Jylland, where it is cut by a N–S-trending belt of shallower, E–W-trending tunnel valleys (Figs 3, 4). The

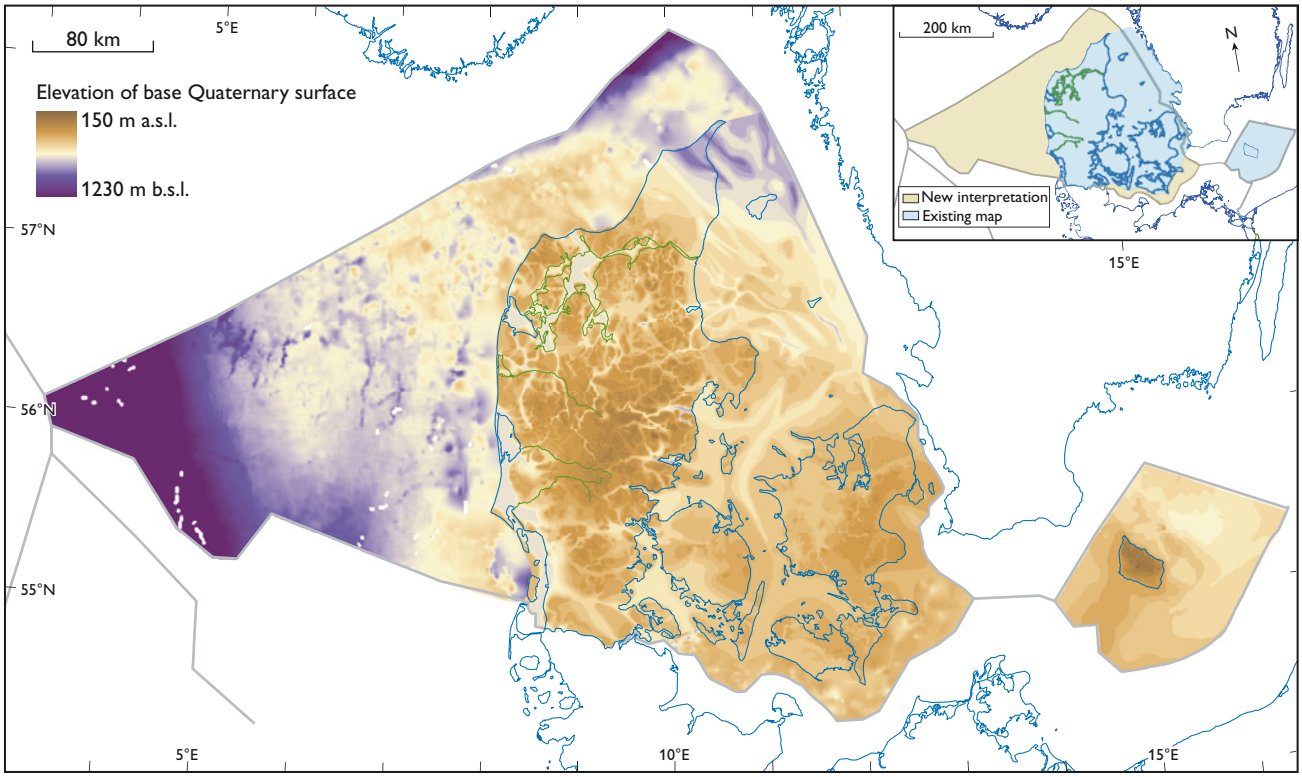

Fig. 4. Base Quaternary composite map. The map was created by merging the depth-converted new seismic mapping of the North Sea, Skagerrak and southern Bælthavet with an existing map of the Danish onshore, Kattegat and inner domestic marine areas (Binzer & Stockmarr 1994) (see text for details).

E–W-trending tunnel valleys (pink on Fig. 3) extend to the Main Stationary Line (MSL; the Last Glacial Maximum still-stand line, e.g. Houmark-Nielsen 2007), indicating a late Weichselian impact on the base Quaternary surface in this onshore region, while the deeper N–S-trending tunnel valleys (light purple on Fig. 3) lie south and west of the MSL, suggesting a pre-Weichselian age.

Acknowledgements

Fugro-Geoteam and Danpec A/S are thanked for permission to use their reprocessed 2D seismic data.

References

Andersen, L.T., Hansen, D.L. & Huuse, M. 2005: Numerical modelling of thrust structures in unconsolidated sediments: implications for glaciotectonic deformation. Journal of Structural Geology **27**, 587–596.

Binzer, K. & Stockmarr, J. 1994: Geological map of Denmark, 1:500 000. Pre-Quaternary surface topography of Denmark. Danmarks Geologiske Undersøgelse Kortserie **44**, 10 pp., 2 maps.

Gradstein, F.M., Ogg, J.G. & Smith A.G. (eds) 2004: A geological time scale, 610 pp. Cambridge: Cambridge University Press.

Håkansson, E. & Pedersen, S.A.S. (eds) 1992: Geologisk kort over den danske undergrund. Varv. Map sheet 1. København: Varv.

Houmark-Nielsen, M. 2007: Extent and age of Middle and Late Pleistocene glaciations and periglacial episodes in southern Jylland, Denmark. Bulletin of the Geological Society of Denmark **55**, 9–35.

Huuse, M. & Lykke-Andersen, H. 2000: Over-deepened Quaternary valleys in the eastern Danish North Sea: morphology and origin. Quaternary Science Reviews **19**, 1233–1253.

Huuse, M., Lykke-Andersen H. & Michelsen, O. 2001: Cenozoic evolution of the eastern Danish North Sea. Marine Geology **177**, 243–269.

Japsen, P., Bidstrup, T. & Lidmar-Bergström, K. 2002: Neogene uplift of southern Scandinavia induced by the rise of the south Swedish dome. In: Doré, A.G. *et al.* (eds): Exhumation of circum-Atlantic margins: timing mechanisms and implications for hydrocarbon exploration. Geological Society Special Publication (London) **196**, 183–207.

Klint, K.E.S. & Pedersen, S.A.S. 1995: The Hanklit glaciotectonic thrust fault complex, Mors, Denmark. Danmarks Geologiske Undersøgelse Serie A **35**, 30 pp.

Rasmussen, E.S., Vejbæk, O.V., Bidstrup, T., Piasecki, S. & Dybkjær, K. 2005: Late Cenozoic depositional history of the Danish North Sea Basin: implications for the petroleum systems in the Kraka, Halfdan, Siri and Nini fields. In: Doré, A.G. & Vining, B.A. (eds): Petroleum geology: North-West Europe and global perspectives. Proceedings of the 6th Petroleum Geology Conference, 1347–1358. London: Geological Society.

Salomonsen, I. & Jensen K.A. 1994: Quaternary erosional surfaces in the Danish North Sea. Boreas **23**, 244–253.

Authors' address

Geological Survey of Denmark and Greenland, Øster Voldgade 10, DK-1350 Copenhagen K, Denmark. E-mail: *tn@geus.dk*

Geology of outer Horns Rev, Danish North Sea

Jørn Bo Jensen, Peter Gravesen and Steen Lomholt

In 2006, Dong Energy initiated the development of the Horns Rev II offshore wind farm in the North Sea (Fig. 1). In order to evaluate and map the characteristics of the surface features of the sea bed and to characterise the subsurface in the wind farm area, the Geological Survey of Denmark and Greenland (GEUS) conducted a geophysical survey of the area. The survey utilised a variety of instruments: sparker, side-scan sonar, marine caesium magnetometer and a multibeam echo-sounder. In addition, information on the subsurface sediments was obtained by cone penetration tests (CPT) and by drilling to 30–50 m below the sea bottom. Geological correlation of the CPT results with the other survey results was extremely complicated but was required in order to understand the architecture of the ice marginal glaciotectonic complex. Information on the geology is crucial for evaluation of the geotechnical problems of the region.

Methods

Shallow seismic, multibeam and coring methods are well-established methods in marine geological research. In contrast, marine magnetometer and CPT studies are normally used to find iron objects and for the determination of geotechnical properties. However, both magnetometer and CPT data can yield valuable geological information, as described below.

The magnetometer, which gives information about the ambient magnetic field strength by measuring the variation in caesium electron energy level, is towed behind the survey vessel. Anomalies in the magnetic field are related to lithological differences in the area. The gridded variations in the strength of the magnetic field, as measured along the survey lines, revealed a spatial pattern. Some areas show homogeneous field strength, whereas other areas show a heterogeneous pattern of field strength. Initially, this pattern appeared to be spatially complex. However, we found that there is a close connection between the magnetic data and large-scale glaciotectonic deformations, as shown by comparisons with other geological and seismic data.

The CPT is carried out using a cylindrical penetrometer with a conical tip (cone) penetrating the ground at a constant rate (2 cm s^{-1}). During the penetration, the forces on the cone and the friction sleeve are measured. The CPT results at Horns Rev aid in the foundation design for each of the 98 windmills.

General geology

Horns Rev can be divided into an inner and outer part separated by a 20 m deep channel, Slugen (Fig. 1). A reef con-

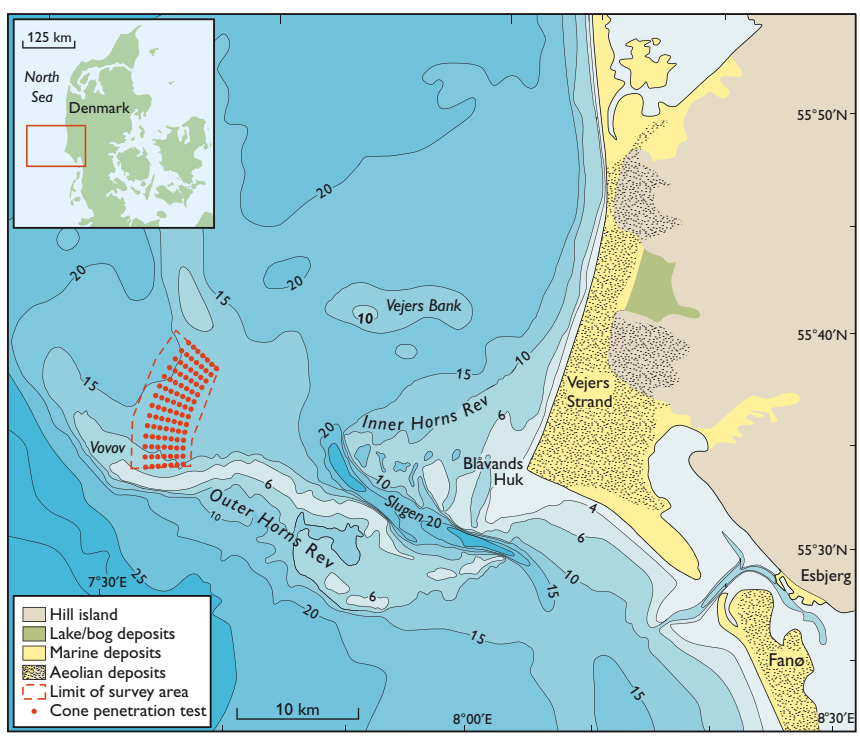

Fig. 1. Map of the Horns Rev region showing the survey area north of the outer part of Horns Rev. The plan is to build 98 windmills. The survey area covers approximately 58 km^2 with a length of 12 km from south to north and a width of 6 km from east to west. Modified from Larsen (2003).

sisting of Holocene shallow submarine sandbanks exists at a water depth of 2–7 m, whereas glacial and interglacial deposits occur in the surrounding area at a water depth of 20–30 m. Tertiary strata, most likely of Miocene age, comprise the basement to the Quaternary deposits located >50 m below the sea bed. The wind farm prospect area is located north of the Outer Horns Rev (Fig. 1), at a water depth of 7–18 m on the Vovov hill island (bakkeø).

Previous investigations have shown that the Horns Rev area was ice-covered during the Elsterian and Saalian glaciations (Larsen & Andersen 2005). Marine Late Elsterian – Holsteinian sediments that were deposited before the Saalian have also been identified in the central North Sea (Long *et al.* 1988) as well as onshore south-western Jylland (Knudsen 1987, 1994). Eemian marine interglacial sediments have also been recorded in the region (Konradi *et al.* 2005).

Saalian glacial deposits and other older Quaternary deposits

The detailed seismic survey results coupled with coring and CPT results (Fig. 2) show that it is possible to identify Elsterian glacial clay and sand till deposits that are overlain by Holsteinian interglacial marine clay, as confirmed by foraminiferal analyses.

The top of the glacial deposits is characterised by a regional erosion surface that appears as a notable seismic unconformity (Figs 2, 3). This reflector represents the surface of the Vovov hill island. Below the unconformity, chaotic seismic reflectors record the existence of small-scale hummocky clinoforms, vertical and sub-horizontal reflectors and channel-like features (Fig. 2). Similar structures that have been recognised in the southern North Sea have been interpreted as representing the ice margin of the Late Saalian Warthe advance (Andersen 2004). On Vovov hill island, the glacial top surface generally lies 18–20 m below sea level (b.s.l.). However, at the north-eastern rim of the wind farm where the western margin of the Horns Rev valley is situated, the surface drops to 39 m b.s.l.

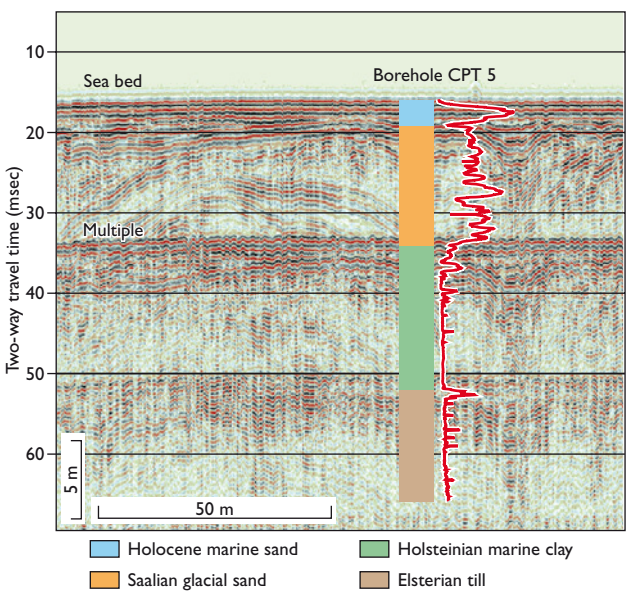

Fig. 2. Seismic example from sparker line 118 showing correlation to borehole and CPT data.

The Saalian glacial deposits consist mainly of medium- and coarse-grained sand and gravel with subordinate fine-grained sand and silt layers. In addition, fine-grained and silty sand with mica and plant fragments also occurs. This composition is similar to that of the onshore hill islands in western Jylland, where the deposits are also very sandy (Sjørring 1981). Sandy and clayey tills and diamictons with gravels, stones and boulders have also been found.

The chaotic seismic image suggests the presence of glaciotectonically deformed sand and gravel (and tills) that were dislocated at the end of the Saalian glacial stage (Fig. 2). The seismic sections also show several channels and valleys that have incised into the glacial hill (Fig. 3). The reflectors inside these depressions have parallel features that suggest the presence of water-lain sediments. The valleys, therefore, were filled with glaciofluvial sand and gravel, probably during the last phase of the Late Saalian Warthe advance and during decay of the ice. It is important to note, however, that the top sediment deposits in these valleys may also be younger in age.

Eemian deposits

Earlier studies of foraminiferal faunas from sediment cores suggested that Eemian deposits occur in the Horns Rev area. However, the seismic evidence for Eemian sediments is based on generally indistinct seismic reflectors that are often capped by a sharp top reflector (Konradi *et al.* 2005).

The Eemian sediments are up to 13 m thick, with the top of the unit located 11–14 m b.s.l. The deposition of the Eemian unit corresponds to a sea-level high-stand during the Eemian period when the sea covered almost the entire area. The only units not entirely transgressed by the sea were the Saalian glacial deposits at the Vovov hill island.

In the wind farm area, marine Eemian deposits have been identified using biostratigraphical data. The deposits are olive-grey silty clay and sandy silt with sand lenses. The sediments are often bioturbated and contain shells and shell fragments. The marine Eemian layers form a wedge that laps onto the Vovov hill island. Patchy channel infill occurs in the central part of the wind farm area (Fig. 3). Eemian freshwater lake deposits are found below the marine layers.

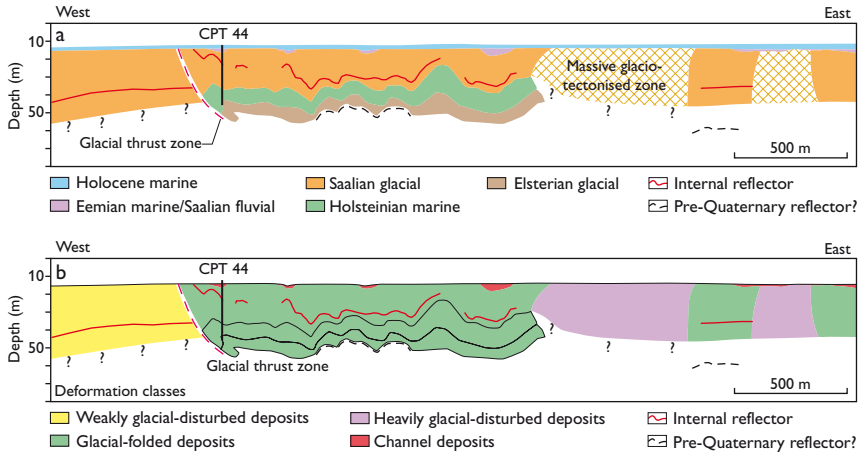

Fig. 3. Interpreted sparker line 102 illustrating (**a**) the seismic stratigraphy and (**b**) the different types of glaciotectonic deformation classes. For location see Fig. 4.

Holocene deposits

Due to the absence of Weichselian deposits, Holocene marine deposits directly overlie the Vovov hill island regional erosional surface (Fig. 3), as illustrated in the seismic pattern by internal horizontal layering (Fig. 2). The surface cuts into the Saalian deposits and also into the Eemian marine deposits when present. The Holocene marine deposits form a relatively thin sand cover over all of the glacial and interglacial sediments. In small depressions, early Holocene freshwater sediments with plant remains are occasionally noted. The thickness of the Holocene sand layers ranges from 1 to 2 m in most parts of the Vovov hill island. In contrast, the thickness of the Holocene deposits increases to 6 to 8 m in the northern margin of the wind farm area.

Hill island glacial deformations

Detailed seismic mapping reveals that the wind farm area is located in a complicated ice margin zone of Late Saalian age. The ridges were formed by ice push from the east (Fig. 4). Consequently, the wind farm area is characterised by ice marginal deformations that exhibit correlation with the gridded variations in magnetic field strength along the survey lines (Fig. 4).

Saalian glacio-fluvial sediments were deposited to the west of the glacier margin and are only weakly disturbed by glacial ice push. The deformations associated with the initial ice push mainly affected the central part of the wind farm area (Figs 3, 4). The western parts of the survey area are characterised by a veneer of Holocene deposits, which are underlain by non-disturbed deposits. On the magnetometer map the western survey areas show no magnetic anomalies due to the simple geology (Fig. 4). The eastern two thirds of the wind farm area are influenced by glacial deformation in the form of thrusting and folding. In the folded areas, the seismic reflectors have a characteristic wavy appearance (Figs 2, 3). It is in these areas that Holsteinian, interglacial clay deposits have been found folded into positions close to the sea bed in borehole 5 (Fig. 2). It is believed that soft Miocene clay acted as a décollement layer. On the magnetometer map, the lack of strong magnetic anomalies makes it possible to distinguish folded areas from severely glacially deformed areas (Fig. 4).

Severely disturbed areas interfinger with the folded areas, in a general SW–NE direction (Fig. 4). On the seismic profiles, the reflections are typically chaotic, with the deeper reflectors disappearing completely (Fig. 3). Consequently, the sediment layering would be expected to be chaotic, with many changes in lithology. The magnetometer map shows that anomalies are common in the severely disturbed areas, yielding an uneven map surface that is clearly related to the chaotic lithological distribution (Fig. 4).

Elongated depressions with a NW–SE trend are filled with fluvial deposits (Fig. 4). Examination of these depressions and their fill, as demonstrated in seismic line 102 (Fig. 3), shows that both the fluvial deposits and the channels follow the synclinal depressions of the folded areas. On the magnetometer map (Fig. 4), the fluvial deposits can be identified by relatively large NW–SE-trending anomalies.

Glacial deformation style

The combination of deformation classes reveals a SW–NE-trending border, separating deformed and undeformed deposits (Figs 3, 4). This distribution reveals an ice-push direction from the east and the Holsteinian marine sediments involved suggest that the deformations are associated with the Late Saalian Warthe ice margin, as no younger ice advance reached the area. The Horns Rev ice-margin push moraines can be classified as thin-skinned fold and thrust deformations following Bennett (2001). The large and well-developed fold deformation structures indicate that relatively high glacial stress (gravity spreading and/or push) was involved and that Miocene clay layers acted as an important décollement horizon. Outside the ice margin, the rather high foreland strength of the Warthe outwash fan resulted in a marginal zone dominated by thrust deformations. To the west only weakly deformed outwash fan deposits are found.

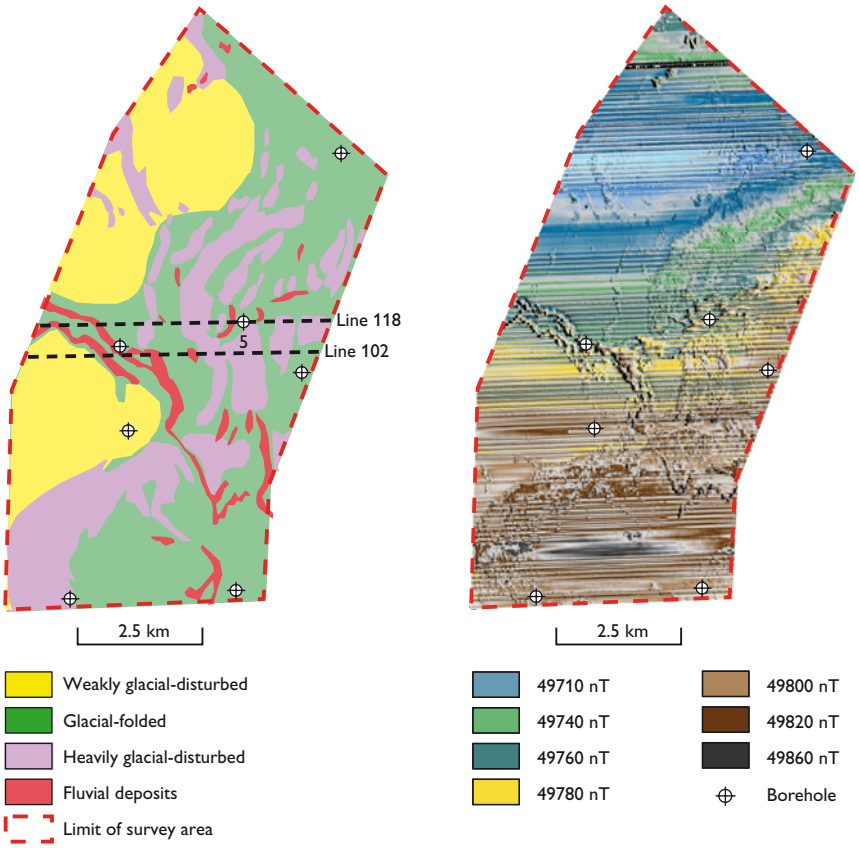

Fig. 4. Map distribution of the different types of glaciotectonic deformation structures and magnetometer anomalies. The locations of sparker line 102 and borehole 5 are shown.

Concluding remarks

Sediment cores and CPT tests from the Horns Rev II wind farm area show that the region is characterised by a complex geology. Large-scale glaciotectonic deformations are related to the Late Saalian Warthe advance with ice push from the east. This investigation also shows that there is a close correlation between magnetometer data and seismically mapped types of deformation structures.

The glacial push moraines developed under conditions of high glacial stress, with Miocene clay acting as décollement horizon. It is important to note that the new evidence from Outer Horns Rev moves the position of the Warthe ice margin more than 50 km further to the west than formerly suggested.

Acknowledgement

We thank Dong Energy for the opportunity to present the geological results from the Horns Rev II offshore wind farm project.

References

Andersen, L.T. 2004: The Fanø Bugt glaciotectonic thrust fault complex, southeastern Danish North Sea. Ph.D. thesis 2004. Danmarks og Grønlands Geologiske Undersøgelse Rapport **2004/30**, 143 pp.

Bennett, M.R. 2001: The morphology, structural evolution and significance of push moraines. Earth Science Reviews **53**, 197–236.

Knudsen, K.L. 1987: Foraminifera in the Late Elsterian – Holsteinian sequence at Tornskov in south Jutland, Denmark. Danmarks Geologiske Undersøgelse Serie B **10**, 7–31.

Knudsen, K.L. 1994: The marine Quaternary in Denmark: a review of new evidence from glacial – interglacial studies. Bulletin of the Geological Society of Denmark **41**, 203–218.

Konradi, P.B., Larsen, B. & Sørensen, Aa.B. 2005: Marine Eemian in the Danish eastern North Sea. Quaternary International **133**, 21–31.

Larsen, B. 2003: Blåvands Huk – Horns Rev området – et nyt Skagen? Geologi – Nyt fra GEUS **4**, 12 pp. København: Danmarks og Grønlands Geologiske Undersøgelse.

Larsen, B. & Andersen, L.T. 2005: Late Quaternary stratigraphy and morphogenesis in the Danish eastern North Sea and its relation to onshore geology. Geologie en Mijnbouw **84**, 113–128.

Long, D., Laban, C., Streif, H., Cameron, T.D.J. & Schüttenhelm, R.T.E. 1988: The sedimentary record of climatic variation in the southern North Sea. Philosophical Transactions of the Royal Society of London **B318**, 523–537.

Sjørring, S. 1981: Pre-Weichselian till stratigraphy in western Jutland, Denmark. Mededelingen Rijks Geologische Dienst **34**, 62–68.

Authors' address

Geological Survey of Denmark and Greenland, Øster Voldgade 10, DK-1350 Copenhagen K, Denmark. E-mail: *jbj@geus.dk*

Use of geochemistry in groundwater vulnerability mapping in Denmark

Birgitte Hansen and Lærke Thorling

The principal aim of mapping ground-water vulnerability in Denmark is to ensure optimal protection of present and future drinking-water resources. Groundwater vulnerability mapping of areas up to 1000 km^2 has been taking place over the past seven years. The scale of mapping has been adjusted to meet the demands for details of regulation of land use requested by Danish legislation. Groundwater vulnerability mapping comprises analyses and integration of geological, geophysical, hydrological and geochemical data. This paper focuses on the geochemical reactions between groundwater and sediment.

Geochemical knowledge may sometimes not be fully and systematically utilised in groundwater vulnerability mapping. This paper presents different geochemical approaches and demonstrates how these can be successfully integrated with geological, geophysical and hydrological data.

Groundwater vulnerability mapping

The national groundwater mapping project involves approximately 40% (17,476 km^2) of the total Danish land area classified as particularly valuable for groundwater abstraction, termed OSD in Danish. The mapping has been financed by a surcharge per cubic metre on consumed water. By 2007, approximately 17% (7066 km^2) of Denmark had been mapped (S. Midby, personal communication 2008).

Groundwater mapping in Denmark has focused on nitrate vulnerability mapping. The areas classified in 2005 as nitrate vulnerable OSDs, as based on pre-existing knowledge, or available intensive groundwater mapping, are shown in Fig. 1. In 2005, approximately 15% of Denmark had been delimitated as nitrate vulnerable OSDs according to the definitions given in Danish legislation. The evaluation of nitrate vulnerability follows a series of criteria, and includes geochemistry of groundwater and aquifer, and the protecting capabilities of the overlying aquitards (Miljøstyrelsen 2000).

Geochemical data types

The method of large-scale groundwater vulnerability mapping differs from that of a process-oriented scientific field investigation, and it relies extensively on pre-existing data due to the high costs of acquiring new data with sufficient spatial density. The pre-existing data are located in the databases at the Geological Survey of Denmark and Greenland (GEUS) and have been collected over the last century. The geochemical data types used are point information from boreholes and consist of (1) groundwater chemistry data, (2) geochemical sediment data, and (3) colour descriptions of soil layers.

The pre-existing geochemical data have been collected for other purposes than groundwater vulnerability mapping, e.g. drinking-water and irrigation wells. Today, some of these wells have been closed because of poor water quality, but the data are still useful. The distribution in space and time of data from abstraction wells is uneven and these data therefore cannot stand alone. Other existing data for vulnerability mapping come from the national groundwater monitoring network (Stockmarr 2005).

Acquisition of new geochemical data in an OSD area requires a detailed and carefully prepared strategy that presupposes a hydrogeological understanding of the area and an

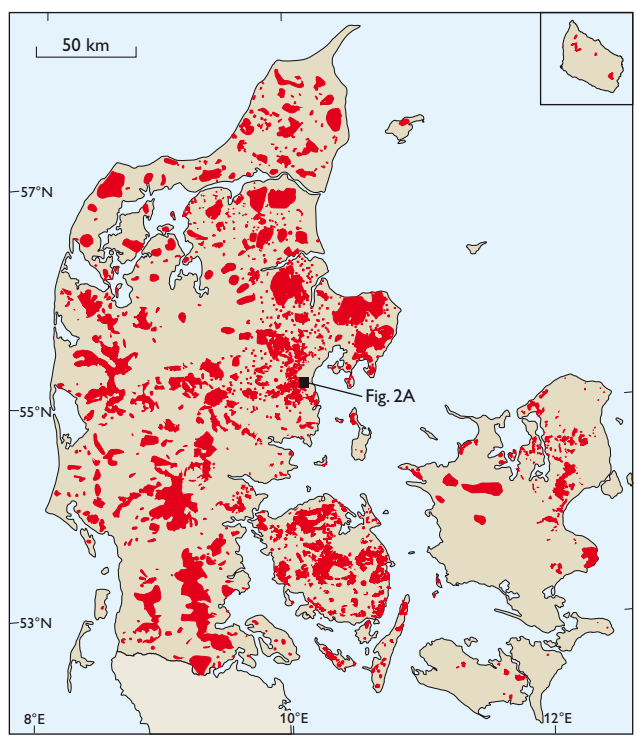

Fig. 1. Groundwater classification map showing abstraction areas that are vulnerable with respect to nitrate pollution of groundwater in Denmark. Modified from the region legislation plans from the county councils (amtsråd) from 2005.

evaluation of pre-existing geochemical data. New geochemical data are acquired by different techniques. The boreholes may be constructed by using the air-lift technique or conventional auger drilling. The wells are 5–200 m deep with 1–4 screens placed in the aquifer in order to cover the major groundwater quality variations.

The advantage of both air-lift and auger drilling lies in the possibility of obtaining sediment samples for geological interpretation and geochemical analysis of the nitrate reduction capacity. The disadvantage is low resolution of the variations of the groundwater chemistry. The ellog auger drilling method (Sørensen & Larsen 1999), which allows contemporary groundwater sampling while drilling, provides very important data on the vertical distribution of the groundwater quality (Thomsen *et al.* 2004). These data provide snapshots of the groundwater chemistry, because the techniques do not allow for permanent screens and soil sample collection.

Geochemical approaches

Groundwater chemistry

The interpretation of groundwater quality must take the geochemical processes between water and sediment in the aquifer into account. Each water analysis of redox-sensitive species reflects a certain redox state and can be used to evaluate nitrate vulnerability (Miljøstyrelsen 2000). Special attention must be paid to water samples showing signs of chemical disequilibrium between groundwater and sediment. Such disequilibrium may indicate that nitrate is penetrating into the anaerobic part of the aquifer (Thorling & Thomsen 2001). The interpretation of the chemical evolution in time series is also an important tool for discovering significant trends towards more subaerobic conditions. The spatial density of groundwater quality data is often poor compared with that of other data types, as the sampling points (screens) are often placed in clusters and only some levels of the aquifers are represented.

Geochemistry of sediments

The ability of the aquifer sediment to remove leached nitrate mainly depends on its concentration of reducing solid substances such as ferro-ions, pyrite and organic matter. Therefore, another geochemical approach in vulnerability mapping is to estimate the nitrate-reduction capacity based on analyses of the sedimentary content of these substances (e.g. Ernstsen *et al.* 2001). Sediment samples should be obtained according to a detailed sampling plan that ensures that they are statistically representative of the examined geological succession, for example in agreement with the theory of sampling (e.g. Petersen *et al.* 2005). It is important to obtain samples from both the aerobic and the anaerobic environment. If no detailed sampling plan has been worked out, we recommend collecting samples at one metre intervals in the borehole. The spatial density of the data points for determination of nitrate reduction capacity is often low compared to that obtained by means of other groundwater vulnerability mapping techniques, and this poses a general up-scaling problem (e.g. Hansen *et al.* 2006).

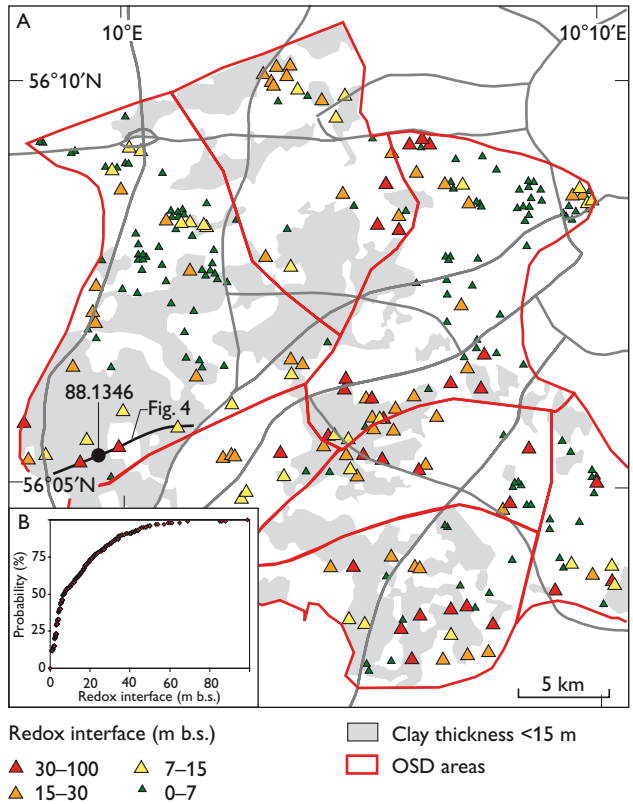

Fig. 2. **A**: The thickness of clay layers and the position of the redox interface in an area south-west of Århus, Denmark. **B**: Probability plot of the redox-interface data shown in **A**. The location of the area is shown in Fig. 1.

Interpretation of the redox interface from soil colours

The transition between aerobic sediment containing nitrate and anaerobic nitrate-free sediment is called the redox interface. Geologically, this interface slowly moves downward in sandy layers by 0.01 mm to 10 cm per year as the reductants are oxidised by oxygen and nitrate (Postma *et al.* 1991). The velocity of the downward movement of the redox interface depends on (1) the reactive content of nitrate-reducing matter; (2) the leaching of nitrate from land use; (3) the water flow and groundwater recharge; and (4) reaction kinetics.

Evaluation of the redox interface based on sedimentary colour descriptions is another feasible approach for nitrate vulnerability mapping. Yellow, red and brown colours indi-

cate aerobic conditions, while grey colours reflect anaerobic conditions. Colour determination is subjective and is usually done in the field, often by using Munsell soil colour charts. In areas with simple hydrogeological conditions, only one redox interface is found. Complex hydrogeological conditions often result in several redox interfaces in the same borehole, which indicates non-vertical infiltration in a heterogenous geological setting. The spatial density of the redox interface data is high compared with the density of groundwater chemistry data, and approaches the level of lithological data in an area. Thus, the redox-interface data are crucial in groundwater nitrate vulnerability mapping.

Integration of geochemical and geophysical data

In many areas, the thickness and composition of clay layers overlying aquifers play an important role in protecting groundwater against nitrate and other anthropogenic contaminants (Thomsen *et al.* 2004). Information about the nitrate vulnerability of an area can be obtained by combining data from geophysical mapping of the total clay content in the upper 30 m of the subsurface with area-distributed data of the redox interface based on soil colours. The geophysical data are commonly acquired using the pulled array continuous electrical sounding method (Sørensen 1996). Figure 2A shows an example from an approximately 150 km^2 OSD area in Jylland, Denmark. Colour descriptions come from about 460 boreholes made in the period 1930–2006. The large variations in the depth of the redox interfaces, even between closely situated data points, are a consequence of the geological heterogeneity in the area.

There is generally good agreement between areas where the redox interface has migrated to great depths (>7 m below surface: b.s.) and areas where the thickness of the clay layers is small (<15 m), presumably due to higher influx of oxidants because of high permeability. The depth of the redox interface in the area varies between the surface and *c.* 99 m b.s. In 50% of the investigated boreholes, the redox interface has migrated more than 7 m b.s. (the mean value in Fig. 2B). These areas mostly correlate with areas of low groundwater protection due to low clay content.

Integration of geochemical, geological and hydrological data

A borehole example

Appropriate mapping of groundwater nitrate vulnerability depends on integration of geochemical, geological, geophysical and hydrological data. Figure 3 shows data from a 150 m deep borehole with four screens. Data on water chemistry

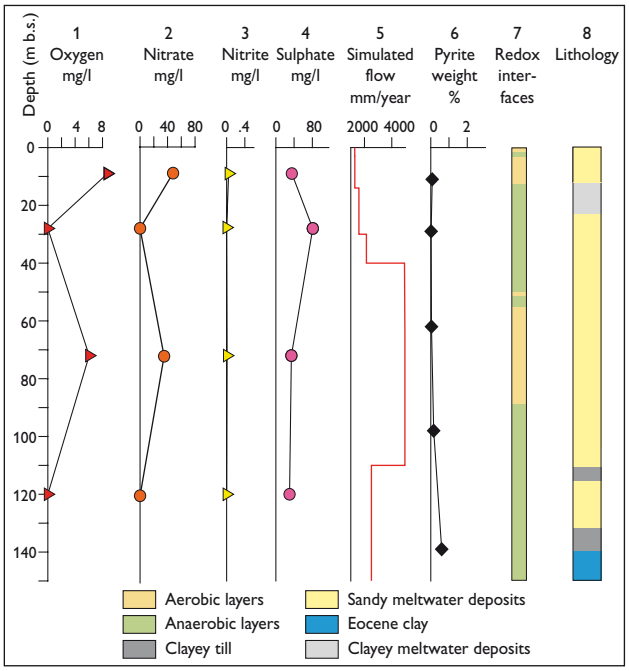

Fig. 3. Chemical, hydrological and geological data for the 150 m deep well DGU no. 88.1346 located south-west of Århus, Denmark. The location of the well is shown in Fig. 4.

(columns 1–4), groundwater flow simulations based on the MIKE SHE programme (mainly horizontal from 40 m b.s., column 5), sediment chemistry (column 6), redox interfaces (column 7), and lithology (column 8) are presented. The Quaternary deposits are dominated by sandy sediments with a composite thickness of about 100 m; with meltwater clay in the upper part and till beds in the lower part. The lowest part of the core penetrated impermeable Eocene clay of the Lillebælt Clay Formation. The colours of the sampled succession indicate seven redox interfaces in the borehole. The deepest one is at about 90 m b. s., and the aerobic/anaerobic zones correlate with the nitrate concentration in the groundwater. Sedimentary pyrite concentration is very low in the anaerobic sandy aquifer (0.02–0.16 wt%), which indicates a very low nitrate reduction capacity (up to 40 years per m) of the aquifer and a relatively fast-moving redox interface (*c.* 2.5 cm per year). The simulated, mainly horizontal groundwater flow in the primary aquifer in the area of the borehole is very high (up to 4 m per year). The presence of nitrate and the low nitrate reduction capacity support these hydrological findings.

Lithological analyses of the concentration of different unstable Ca-carbonate minerals in the fine gravel fraction show a high degree of weathering in the sandy meltwater deposits, although the groundwater remains saturated with calcite (Hansen *et al.* 2006). These data also correlate well with the water chemistry (nitrate concentration), geochemistry of the sediments (low pyrite concentration), and groundwater flow simulations (high groundwater flow).

A profile example

Figure 4 shows an example of geological and geochemical conceptual models from an approximately 4 km long profile through a buried valley in Jylland, Denmark (e.g. Jørgensen & Sandersen 2008 – this volume). The left borehole (DGU no. 88.1346) on the profile is also shown in Fig. 3. The boreholes and geophysical electrical data (see Fig. 2) show that clay is of limited extent, which makes the aquifer highly vulnerable to nitrate and pesticides. The depth of the redox interface varies significantly along the profile and several redox interfaces can be found in the same borehole indicating a heterogeneous flow regime.

Nitrate, pesticides (Des-Dip-Atrazine) and the pesticide degradation product BAM have penetrated deeply, to about 90 m b.s. into the aquifer as shown by the yellow areas in Fig. 4B. Vast parts of the aquifer are polluted by nitrate and pesticides. The groundwater chemistry support the understanding of the redox interface and the geological setting. Future extraction of groundwater from the deeper parts of the aquifer could worsen the nitrate and pesticide pollution of the primary aquifer due to increased flow.

Future perspectives

In order to improve mapping of groundwater nitrate vulnerability there is a general need to develop the sampling and interpretation techniques for sedimentary geochemical analysis. Up-scaling of geochemical data interpretation in groundwater mapping is also a scientific field with high potential. The development of new methods for integrating geological, geophysical, hydrological and geochemical data is also very important. Future focus should be on the development of guidelines for geochemical groundwater mapping and interpretation in a three dimensional perspective. The development and experience from Denmark described here could be very useful for the EU member states working with large-scale mapping under the Water Framework Directive.

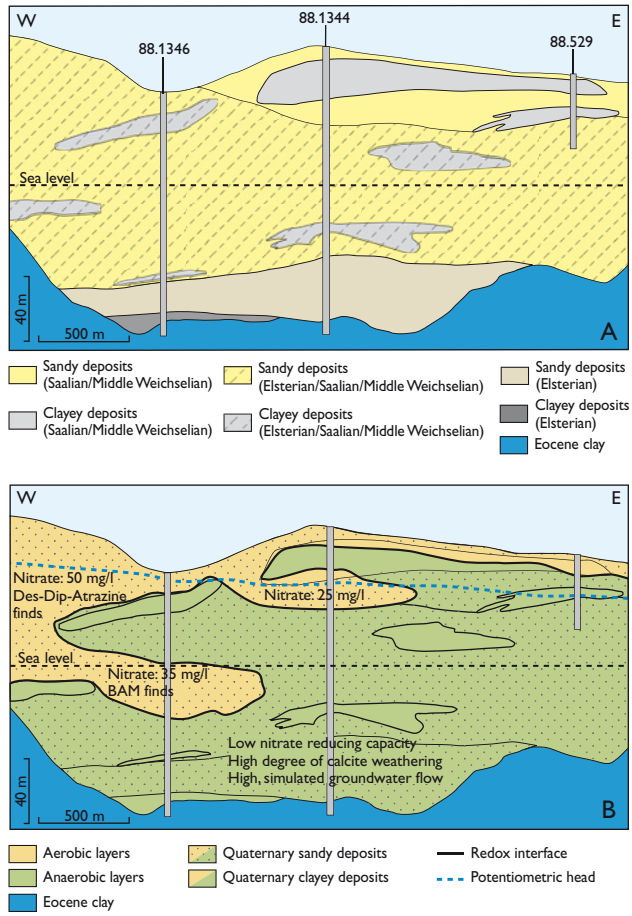

Fig. 4. A buried valley south of Århus, Denmark. **A**: Geological conceptual profile. **B**: Geochemical conceptual profile. The boreholes are identified with DGU numbers. The location of the profile is shown in Fig. 2A.

References

Ernstsen, V., Henriksen, H.J. & von Platen, F. 2001: Principper for beregning af nitratreduktion i jordlagene under rodzonen, 54 pp. Arbejdsrapport no. **24**. København: Miljøstyrelsen.

Hansen, B., Jordt, B.E., Thomsen, R., Sørensen, J., Kronborg, C. & Nielsen, O.B. 2006: Gebyrkortlægning i Århus Syd – Geologisk, kemisk og hydrologisk datasammenstilling. Geologisk Nyt **3/06**, 18–22.

Jørgensen, F. & Sandersen, P.B.E. 2008: Mapping of buried tunnel valleys in Denmark: new perspectives for interpretation of the Quaternary succession in Denmark. Geological Survey of Denmark and Greenland Bulletin **15**, 33–36.

Miljøstyrelsen 2000: Zonering. Detailkortlægning af arealer til beskyttelse af grundvandsressourcen. Vejledning fra Miljøstyrelsen **3**, 153 pp. København: Miljøstyrelsen.

Petersen, L., Minkkinen, P. & Esbensen, K.H. 2005: Representative sampling for reliable data analysis: theory of sampling. Chemometrics and Intelligent Laboratory Systems **77**, 262–277.

Postma, D., Boesen, C., Kristiansen, H. & Larsen, F. 1991: Nitrate reduction in an unconfined sandy aquifer: water chemistry, reduction processes, and geochemical modeling. Water Resources Research **27**, 2027–2045.

Sørensen, K. 1996: Pulled array continuous electrical sounding. First Break **14**, 85–90.

Sørensen, K.I. & Larsen, F. 1999: Ellog auger drilling: 3-in-one method for hydrogeological data collection. Ground Water Monitoring & Remediation **19**, 97–101.

Stockmarr, J. 2005: Groundwater quality monitoring in Denmark. Geological Survey of Denmark and Greenland Bulletin **7**, 33–36.

Thomsen, R., Søndergaard, V.H. & Sørensen, K.I. 2004: Hydrogeological mapping as a basis for establishing site-specific groundwater protection zones in Denmark. Hydrogeology Journal **12**, 550–562.

Thorling, L. & Thomsen, R. 2001: Tunø. Status report 1989–1999, 27 pp. Århus: Aarhus County, Environmental Division.

Authors' address

Geological Survey of Denmark and Greenland, Lyseng Allé 1, DK-8270 Højbjerg, Denmark. E-mail:*bgh@geus.dk*

Sedimentary facies and architecture of the Holocene to Recent Rømø barrier island in the Danish Wadden Sea

Peter N. Johannessen, Lars Henrik Nielsen, Lars Nielsen, Ingelise Møller, Morten Pejrup, Thorbjørn J. Andersen, Joakim Korshøj, Birger Larsen and Stefan Piasecki

This paper describes an ongoing multidisciplinary study on the development of the barrier islands in the Danish Wadden Sea (Vadehavet), carried out by the Department of Geography and Geology at the University of Copenhagen and the Geological Survey of Denmark and Greenland (GEUS). Nine sediment cores each *c.* 25 m long and a total of *c.* 45 km ground penetrating radar (GPR) profiles have been acquired on the islands of Rømø and Fanø. Geochemical and palaeontological analyses and dating of 150 core samples using optically stimulated luminescence (OSL) are in progress. This multidisciplinary approach has given new insights into the sedimentary architecture and development of the island, and the study is expected to result in a new detailed facies model. Such models are essential for an assessment of the effects of rising sea level associated with global warming. The new facies model can also be used as an analogue for subsurface oil or water reservoirs in similar sedimentary settings. This article presents selected core and GPR data from the Rømø barrier island.

Setting

The Rømø barrier island is situated in the northern part of the European Wadden Sea (Fig. 1). The maximum tidal amplitude is *c* 1.8 m (Andersen & Pejrup 2001). During the last *c.* 8000 years, the area has experienced an overall relative sea-level rise of ~15 m (Behre 2007).

The island of Rømø is *c.* 14 km long and *c.* 4 km wide and separated from the mainland by a *c.* 8 km wide lagoon (Figs 1, 2). The island is connected to the mainland by a dam. Tidal inlets, *c.* 1 km across, occur at the northern and southern tips of the island. The inlets continue as tidal channels into the lagoon and cut sand flats and mixed flats. Subtidal ebb-deltas are located where the tidal inlets terminate in the North Sea (Fig. 3). The inlets reach depths of up to 30 m, as in the Listerdyb south of Rømø, or 4–10 m in the Juvre Dyb north of the island. The salt marsh area fringing the lagoonal coast of the island is up to 2 km broad. Sand flats, up to 2.7 km wide, with three, 0.8–1.6 km broad bars that migrate towards the island, characterise the north-western and south-western parts of the island (Fig. 2). Tidal creeks, up to *c.* 50 m wide, separate the bars. Active eastward migrating aeolian dunes are found on large parts of the island.

Sedimentary facies of the Rømø barrier island

Core wells

Seven core wells were drilled on the island, and depositional units were defined on the basis of sedimentary structures, grain sizes, sorting, organic material, fossils, trace fossils and rootlets. Data from the Rømø-4 and -1 wells are presented here.

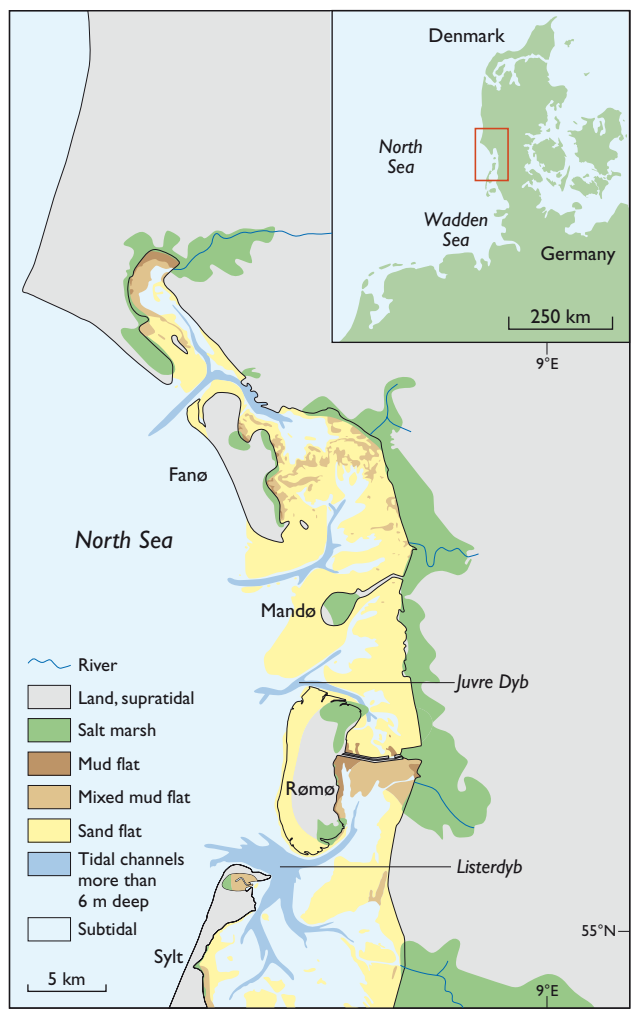

Fig. 1. The Danish Wadden Sea. The distribution of sediment types and subtidal channels are shown. The mainland of Jylland east of the lagoon consists of glacial deposits. Inset map shows the whole tidal Wadden Sea area. Modified from Pejrup (2006) and Sørensen *et al.* (2006).

Fig. 2. Orthophoto of the Rømø barrier island. The location of GPR reflection profiles and the seven core wells are shown. Very wide tidal sand flat characterise the north-western and south-western parts of Rømø. Rømø island is dominated by aeolian dunes that are migrating eastwards. Copyright Scankort.

In the Rømø-4 well the upper *c.* 3.5 m consist of well-sorted aeolian sand (Fig. 4). A mud bed, *c.* 20 cm thick and supposed to be deposited in a depression (swale) underlies the aeolian sand. About 11 m of medium-grained sand with numerous bivalve shells underlie the mud layer and are interpreted to have been deposited in a prograding to aggrading marine shoreface. At *c.* 2 m below mean s.l., a *c.* 0.3 m thick layer of coarse-grained sand may represent washover fans.

The Rømø-1 well that was drilled in the lagoon east of the island shows *c.* 8 m of bioturbated heteroliths of sand and mud with numerous bivalve shells, especially *Mytilus*, and gastropods below the dam (Figs 2, 4). The heteroliths represent back-barrier lagoonal mud- and sand flats and overlie 3 m of sand-streaked mud with numerous bivalve shells. Gyttja and peat layers, respectively 20 and 25 cm thick, underlie the mud (Fig. 4). The peat layer was probably deposited during the initial Holocene sea-level rise. Continued rise in sea level caused flooding of the peat swamp and formation of gytja, followed by lagoonal mud- and sand flats. The Holocene sediments overlie Pleistocene and Eeminan deposits.

The variation in composition of the dinoflagellate assemblages and other fossil algae from the core samples reflects shallow marine to lagoonal environments, in part with lowered salinity. The fauna of bivalves, snails and sea urchins in the cores is similar to that seen on the beaches of Rømø today. The rich but low-diversity fauna seen in the lagoonal deposit in the Rømø-1 well differs from the more diverse fauna with thick shells that is washed ashore on the open western coast at present. The fauna in the Rømø-4 well consists of small shells of the west coast fauna only. This suggests that the sand was deposited by washover events from the North Sea and that larger shells were left behind. The interpretations of the palynomorph assemblages and the macrofauna support the sedimentological interpretations and will be used in the reconstruction of the physical development of Rømø.

Ground penetrating radar (GPR)

W–E and N–S-trending GPR sections with a total length of *c.* 30 km were acquired from Rømø using unshielded 100 MHz antennae manufactured by Sensors & Software Inc.

Fig. 3. Landsat image (+ETM 9 May 2001) of the Danish Wadden Sea with distinct tidal sand flats and subtidal channels. Note the subtidal ebb-deltas where the main channels terminate in the North Sea.

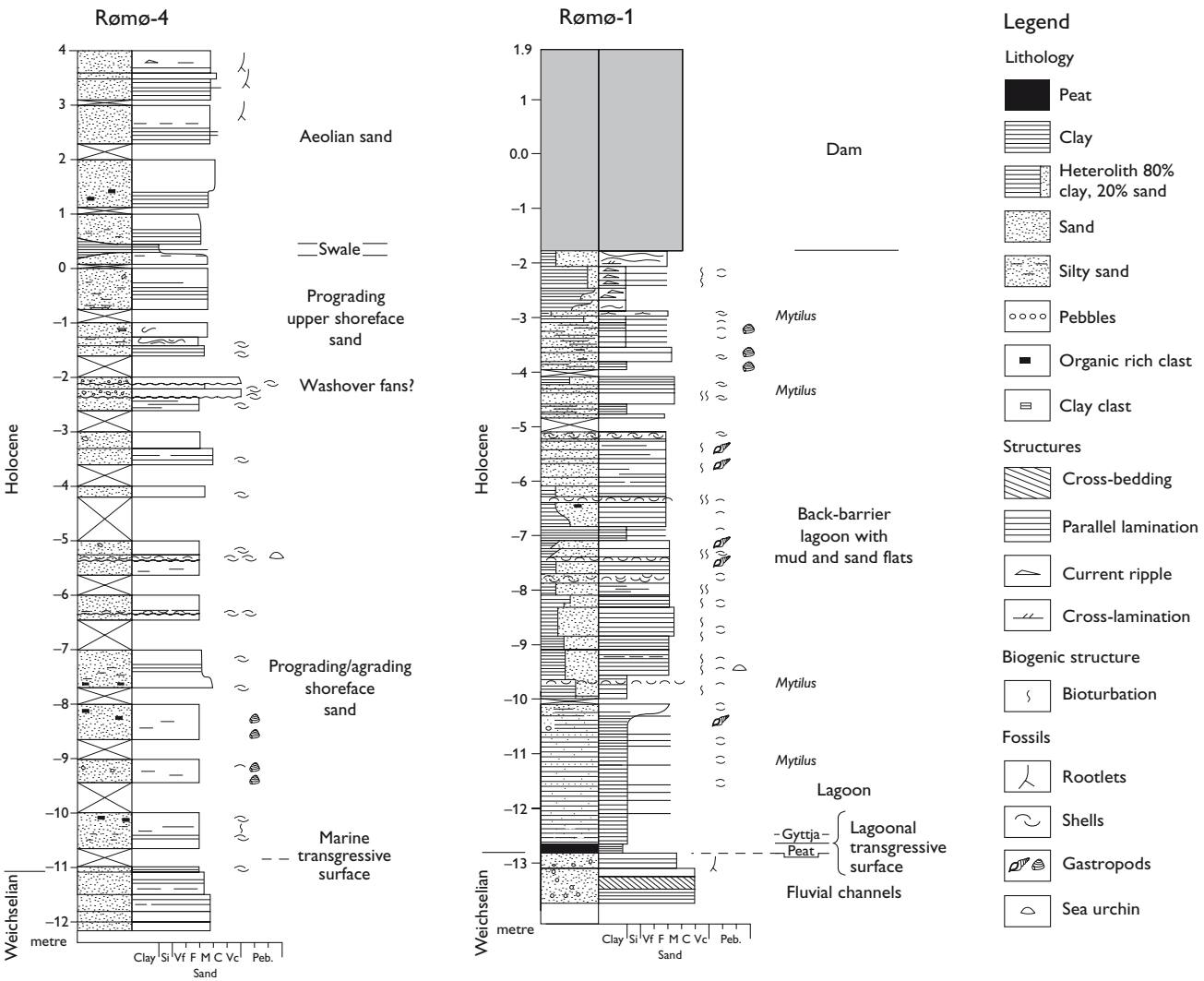

Fig. 4. Sedimentological core logs from the Rømø-1 and -4 wells, situated in the lagoon and the centre of Rømø, respectively. For locations see Fig. 2.

(Fig. 2; Nielsen *et al.* in press). Maximum signal penetration is *c.* 15 m in the central parts of the island where fresh groundwater is thickest, and the vertical resolution is 0.2–0.3 m. The reflected signal only reaches about 1 m depth at the margins of Rømø because of strong damping of the electromagnetic waves due to saltwater intrusion. Salt marsh, peat and mud layers also significantly reduce the signal penetration.

A GPR section from the central part of the island shows a beach ridge, *c.* 1.25 m high and *c.* 70 m wide, with a steep erosional side towards the west and a less steep side towards the east (Fig. 5). The top of the beach ridge is *c.* 0.5 m above mean s.l. Two superimposed cross-bedded units with east-dipping foresets occur upon the beach ridge. The lower unit is 0.8 m thick and *c.* 30 m long and the upper unit is *c.* 1 m thick and *c.* 50 m long (Fig. 5). East of the washover fans large, gently eastward-dipping clinoforms occur with much higher amplitude signal, which indicates that the sediments are organic or mud rich. Data from the Rømø-4 core well situated *c.* 75 m north of the section indicate that the high amplitude layer correlates with a 20 cm thick mud layer deposited in a swale (Fig. 4), consistent with previous findings elsewhere on the island (Nielsen *et al.* in press).

A more than 125 m wide set with clinoforms, *c.* 1.5 m thick, dipping in an eastward direction is found in the westernmost part of the section (Fig. 5). The set terminates eastwards in a channel-like structure. The clinoform set is interpreted as an eastward-migrating tidal bar filling in the western side of a 1.5 m deep tidal channel, forcing the channel eastwards, which is comparable to the modern situation illustrated in Fig. 3. The amplitude of the reflections in the channel sediments differs from those of the bar, suggesting that the channel fill is slightly muddier due to channel abandonment. The top of the channel and the bar are situated at the modern mean s.l.

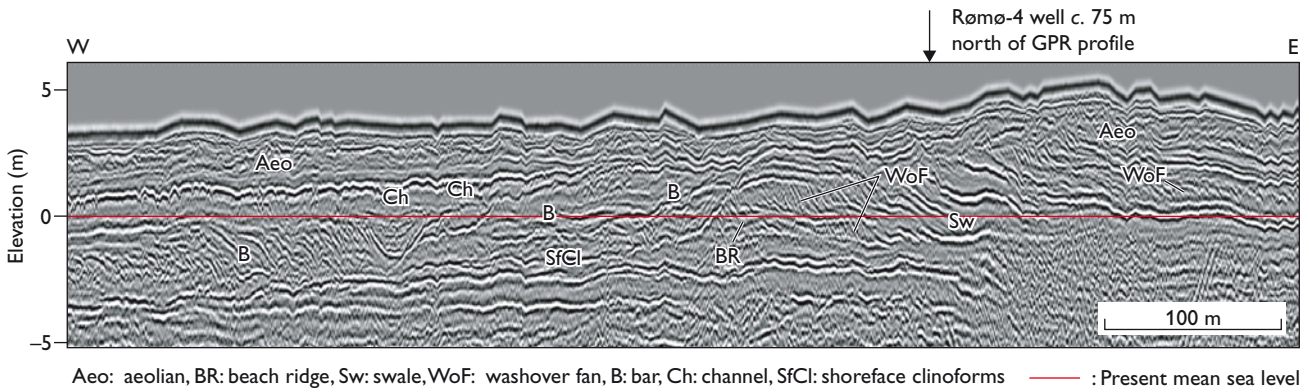

Fig. 5. West–east-trending ground penetrating radar profile T07a-1 from Rømø. The upper part of the section consists of aeolian sand. For location see Fig. 2.

Between the bar-channel complex and the beach ridge occur two sediment wedges, altogether *c.* 150 m across (Fig. 5). The eastern wedge onlaps the relatively steep western side of the beach ridge, whereas the western wedge onlaps the eastern wedge and is truncated by the channel to the west. The wedges were probably deposited by landward migrating bars that welded to the coast, causing a stepwise shoreface progradation. Aeolian sand lies on top of these foreshore sediments (Fig. 5). The gently westward dipping, high amplitude reflections in the deeper part of the section are interpreted as representing westward shoreface progradation, in agreement with the core data (Figs 4, 5).

Discussion and conclusions

The cores and GPR sections provide high quality data for the identification of the depositional units that compose the Rømø barrier island, and a few examples of the units are presented here. The interpretations of the cores and the GPR sections show that the Rømø barrier island was never located as far east as the Rømø-1 well. Furthermore, lagoonal sediments are not present at the position of the Rømø-4 well suggesting that lagoonal conditions were never established at this location. However, data from the cores of the Rømø-6 and -3 wells (to be described in forthcoming papers) suggest that the western fringe of the lagoon reached the positions of these wells, because lagoonal deposits are identified below aeolian sand (Nielsen *et al.* in press).

Samples of sand from the cores have been submitted for OSL dating, and shells and organic matter are being dated by the ^{14}C method. When the ages of the depositional units become available the development of the depositional units through time will be described in detail. Plots of sample depths against ages will be constructed to portray the relative sea level history and will, together with analyses of the mollusc fauna and palynomorph assemblages, provide additional constraints on the reconstructions of the development of the barrier island. The study will be concluded with a detailed reconstruction of the Holocene development of the Rømø barrier island.

Acknowledgements

The Danish Natural Science Research Council and Geocenter Copenhagen are thanked for financial support.

References

Andersen, T.J. & Pejrup, M. 2001. Suspended sediment transport on a temperate, microtidal mudflat, the Danish Wadden Sea. Marine Geology **173**, 69–85.

Behre, K.-E. 2007: A new Holocene sea-level curve for the southern North Sea. Boreas **36**, 82–102.

Nielsen, L., Møller, I., Nielsen, L.H., Johannessen, P.N., Pejrup, M., Korshøj, J.S. & Andersen, T.J. in press: Integrated ground-penetrating radar and sedimentological studies of Wadden Sea barrier islands. Journal of Applied Geophysics.

Pejrup, M. 2006: Det danske vadehav og store landvindingsprojekter. In: Sand-Jensen, K. & Fenchel, T. (eds): Naturen i Danmark: Havet, 433–415. København: Gyldendal.

Sørensen, T.H., Bartholdy, J. Christiansen, C. & Pedersen, J.B.T. 2006: Intertidal surface type mapping in the Danish Wadden Sea. Marine Geology **235**, 87–99.

Authors' addresses

P.N.J., L.H.N., I.M., B.L. & S.P.: *Geological Survey of Denmark and Greenland, Øster Voldgade 10, DK-1350 Copenhagen K, Denmark.* E-mail: *pjo@geus.dk*

L.N., M.P., T.J.A. & J.K.: *Department of Geography and Geology, Øster Voldgade 10, DK-1350 Copenhagen K, Denmark.*

Evidence of stretching of the lithosphere under Denmark

Søren Gregersen, Lene Vandur Nielsen and Peter Voss

The structure of the lithosphere under Denmark has been investigated in relation to adjacent regions of Sweden and Germany. The most interesting result of the study is that the 120 km thick lithosphere under Denmark appears to be a stretched version of the Swedish lithosphere, which is more than twice as thick. During the international project *Teleseismic Tomography across the Tornquist Zone* (Tor), field work and international interpretation were carried out between 1996 and 2002. Following the field work period, model-velocity computations were undertaken based on observations of distant earthquakes (e.g. Arlitt 1999; Shomali *et al.* 2002; Voss *et al.* 2006), and recently an evaluation of the Tor results was completed (Nielsen 2007).

The Tor project investigates deeper parts of the Earth than previous projects, and in particular the depth interval 50–300 km, which is below the crystalline crust. The investigations have included many geophysical features such as teleseismic P-wave tomography, Rayleigh wave velocities, shear wave splitting and wave scattering. We have distinguished between relatively high- and low-velocity zones, which also show variations in anisotropy and scatter characteristics. Generalised high-velocity zones correspond to the lithosphere, while generalised relatively low-velocity zones are equivalent to the asthenosphere.

The main outcome of the combined studies is that the deep lithosphere can be divided into three blocks separated approximately along the national boundaries between Sweden and Denmark and between Denmark and Germany. The boundaries between the blocks are steep, almost vertical. The Denmark block has lithosphere properties between those to the north and south. Based on previous crustal studies and the Tor results, we suggest that the Denmark block has evolved by stretching. The details in the new evaluation are derived from teleseismic tomography. Here we present a synthesis of the many derived models in the light of the new evaluation.

Lower lithosphere: data and interpretation

The area of investigation is shown in Fig. 1 and examples of analyses of P-wave data are presented in Fig. 2. The first and most important part of the data treatment is correction for the rather well-known structure of the crust, see Fig. 2, middle frames (e.g. EUGENO-S working group 1988; Thybo 2000). The end products of the analyses are two patterns of travel-time residuals for the lower lithosphere (bottom frames of Fig. 2). Together with approximately 50 similar patterns of P-wave travel-time residuals, each for one earthquake, these constitute the data for the model-velocity computations.

Several tomographic velocity calculations have been made in 2-D cross-sections along the line of seismographs shown in Fig. 1 (e.g. Arlitt 1999; Busche 2001; Shomali *et al.* 2002; Nielsen 2007). The results of Nielsen's (2007) work are shown in Figs 3 and 4, which are, respectively, a cross-section with P-wave velocity deviations from a laterally homogeneous Earth, and the horizontal gradients of these P-wave velocities. Figure 4 pinpoints the sharpest boundaries between different lithosphere/asthenosphere characteristics.

The teleseismic tomography has a poor resolution in the upper 50 km of the Earth, and the interval from 0 to 50 km

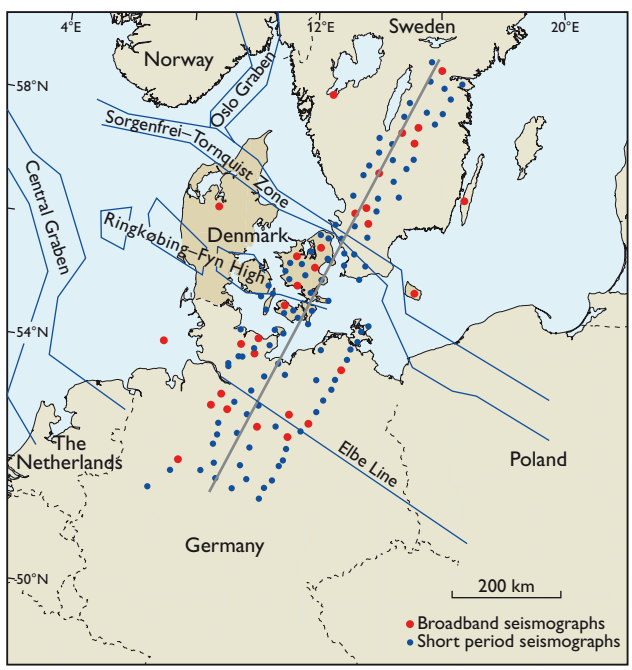

Fig. 1. The location of seismographs during field work of the Tor project 1996–1997. The 2-D interpretation profiles of Figs 3 and 4 follow the line in the middle of the cloud of seismographs from 59°N, 16°E to 51°N, 9°E, crossing the Sorgenfrei–Tornquist Zone at a right angle. The Ringkøbing–Fyn High is a basement high separating sedimentary basins to its north and south. The Elbe Line is a geophysically recognised lineament. Other important broad-scale features are the Permian Oslo Graben and the Mesozoic Central Graben.

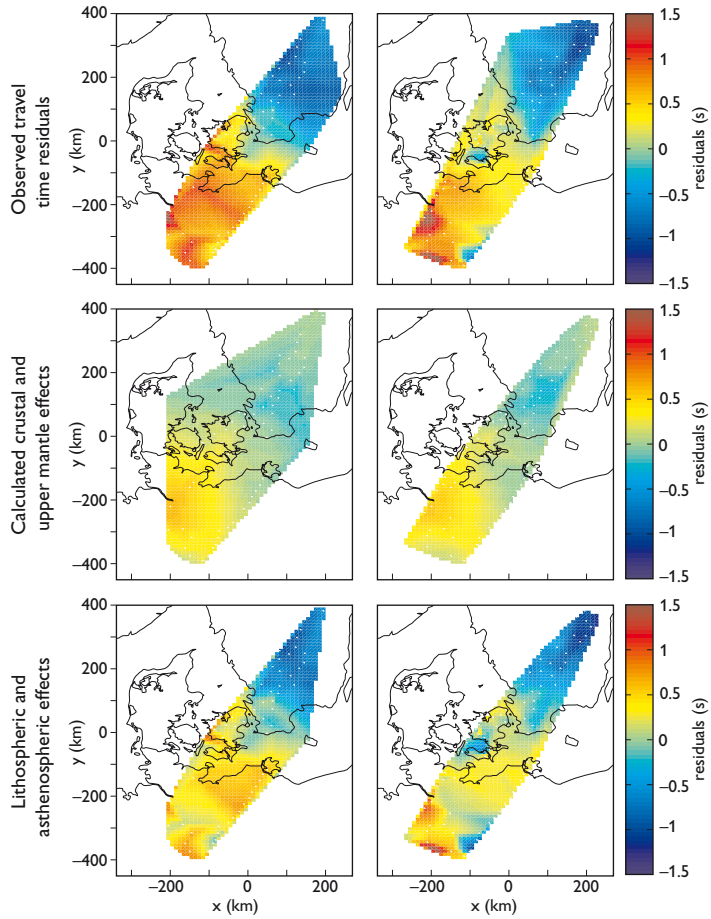

Fig. 2. P-wave travel time residuals from two earthquakes, in Japan (19 October 1996, 32°N 132°E, wave arrival to Tor area from north-east) and in Mexico (11 January 1997, 18°N 103°W, wave arrival to Tor area from north-west), each in one column. For each of the earthquakes the upper diagram shows total observed residuals (observed arrival times minus expected arrival times according to the global average tables IASP91). The middle diagram shows computed crustal residuals to 50 km depth (from Pedersen *et al.* 1999), which, when subtracted from the observed ones, yield the lower lithosphere residuals below 50 km depth which are shown in the lower diagram (from Pedersen *et al.* 1999).

depth is not shown on Figs 3 and 4. However, many previous investigations based on other data have provided rather detailed information about shallower structures (Arlitt *et al.* 1999; Pedersen *et al.* 1999). A dipping crustal transition from the Baltica crust in the north-east to the Avalonia crust in the south-west has been interpreted in the broad box A area. The blue and red P-velocity anomalies are computed with reference to a one-dimensional global travel-time model. Two sharp and steep velocity changes, or red to blue steps, are seen in Figs 3 and 4, and are outlined by boxes B and C. A third step at 57°N, seen as a colour change from light blue to dark blue, which was discussed by Gregersen *et al.* (2006), may not be significant (Fig. 4). The uncertainties of the exact locations of the transitions and their slopes are illustrated by the sizes of the boxes (B and C) in the transition regions.

A low-velocity asthenospheric layer, as deduced from higher mode surface-wave studies mentioned by Gregersen *et al.* (2006), is indicated by box D. This low-velocity layer does not extend to the north-east. This is consistent with the earlier interpretation of fundamental mode Rayleigh waves that showed absence of low-velocity asthenospheric layers below the Baltic Shield at this depth (Cotte *et al.* 2002).

It can be difficult to evaluate which features in the models should be regarded as well defined and appropriate to interpret in geological terms. Issues of spatial resolution, accuracy and uniqueness of the models are important. Within the Tor project considerable efforts have therefore been dedicated to examining these issues using, for example, tomographic inversions. In such an inversion it is straightforward to calculate the variance of model parameters, which quantifies the reliability of each parameter. This variance of a model parameter has only limited value, partly because mathematical assumptions of linearity are simplified, and partly because the often complicated interactions between model parameters are ignored.

The estimation of resolution also depends on choices in the mathematical inversion procedure. The resolution is limited by station spacing, ray geometry between earthquakes and seismic stations, and the frequency content of data, and it is different for various parts of the model. These complex problems mean that different approaches must be considered to quantify reliability. This has been carried out in previous analyses and evaluated by Nielsen (2007).

Suggested evolution of the lithosphere under Denmark

The broad-scale division of the lithosphere into three different blocks, with Denmark as the middle one of intermediate structure, has been confirmed by several studies. One major outcome of the Tor project is therefore unquestionably that the Sorgenfrei–Tornquist Zone is connected to a very deep and prominent lithospheric velocity difference (box C in Figs 3 and 4). Another marked change in lithosphere-asthenosphere properties is found in the depth range 0–120 km between the southern part of the Ringkøbing–Fyn High and

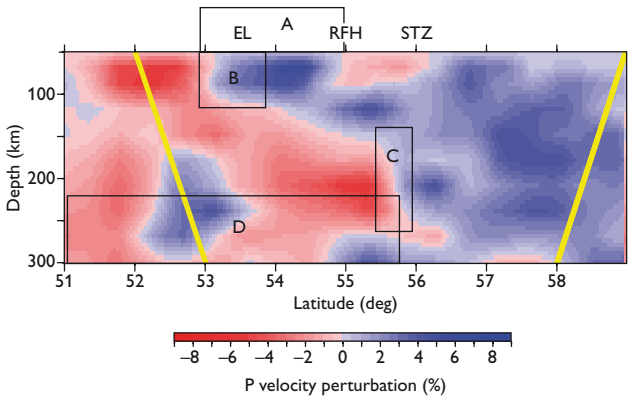

Fig. 3. Tomographic image of the lithosphere/asthenosphere system in a profile along the Tor array from 59°N, 16°E to 51°N, 9°E. Blue colours are areas with high P-wave velocities, while red colours are areas with low P-wave velocities with respect to the laterally homogeneous IASP91 model (Kennett & Engdahl 1991). The boxes show the uncertainty around the lateral changes (see text). **STZ**, Sorgenfrei–Tornquist Zone; **RFH**, Ringkøbing–Fyn High; **EL**, Elbe Line.

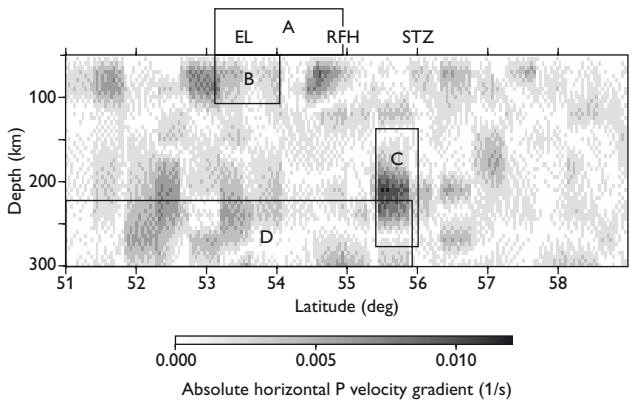

Fig. 4. Tomographic image along the Tor array. For location see Fig. 1. Dark areas show the largest horizontal gradients in P-wave velocities, corresponding to large changes in material. The boxes show the uncertainty around the lateral changes (see text).

the Elbe Line (boxes A and B in Figs 3 and 4). These interpretations together with the well-known surface geology and crustal structure (e.g. EUGENO-S working group 1988; Thybo 2000) have been discussed at many Europrobe meetings. The outcome of these discussions is that the evolution of the lithosphere-asthenosphere system can be summarised in graphical form (Fig. 5), with collision, spreading, shearing and compression over the last 500 million years.

Based on the Tor-project studies by Cotte *et al.* (2002) and Gregersen *et al.* (2002, 2006) we suggest that together with the other geophysical data the surface wave results and the tomography results (Figs 3 and 4) indicate a lithosphere thickness of a little less than 100 km in the south-western part of the profile, a little over 100 km in the middle, and a lithosphere thickness of more than 200 km in the north-eastern part of the region. The Baltic Shield in Sweden, i.e. the part of the craton exposing old, Precambrian crystalline rocks, terminates to the south-west at the Sorgenfrei–Tornquist Zone. From deep drilling data and seismic crustal studies, it is deduced that material originating from the craton extends southwards from the Sorgenfrei–Tornquist Zone, gradually thins where overlying sediments are thick and terminates just south of the Ringkøbing–Fyn High. In the late Precambrian to early Palaeozoic (*c.* 600 Ma), the eastern European craton including the Baltic Shield formed the core of the palaeo-continent Baltica, and the Tor study region was a passive continental margin.

The tomographic images reveal the structure originating from this episode, reworked by a number of later events, as illustrated by Fig. 5. The evolution can be divided into four stages. During stage 1 two separate lithospheric plates collided in late Palaeozoic times. In stage 2 the area was deformed by lithospheric stretching and transcurrent faulting, the Ringkøbing–Fyn High with its thick crust was detached from the Baltic craton, and the various blocks of the Ringkøbing–Fyn High rotated slightly. In the ensuing stage 3, lithospheric stretching was perpendicular to the trend of the plate transition and the Ringkøbing–Fyn High. The compressional stage 4 is very different, involving inversion of the Sorgenfrei–Tornquist Zone.

Conclusions

Our essential contributions from geophysics to the geological evolutionary account are the measurements of crustal and lithospheric thinning. In previous studies of the crustal structure (EUGENO-S working group 1988) it was suggested that the crust in Denmark between the Sorgenfrei–Tornquist Zone and the Ringkøbing–Fyn High had been stretched during the late Palaeozoic and the Mesozoic. Preliminary modelling of the stretching of the sedimentary basins and the crystalline crust has been carried out by Nielsen & Balling (1990). Fuller modelling, including the entire lithosphere, has been undertaken by Frederiksen *et al.* (2001). Since the results of the Tor project also show a distinct thinning of the lower lithosphere from the Swedish to the Danish area, we see this as evidence of essentially full lithospheric stretching. The reasoning has developed historically from recognition of stretching in sedimentary basin evolution, and then stretching of the crust (EUGENO-S working group 1988), to the present claim of stretching of the entire lithosphere. This account can now be reversed in a well-founded story of cause and effect: the lithosphere is stretched, and the crystalline crust is thereby stretched, creating the sedimentary basins.

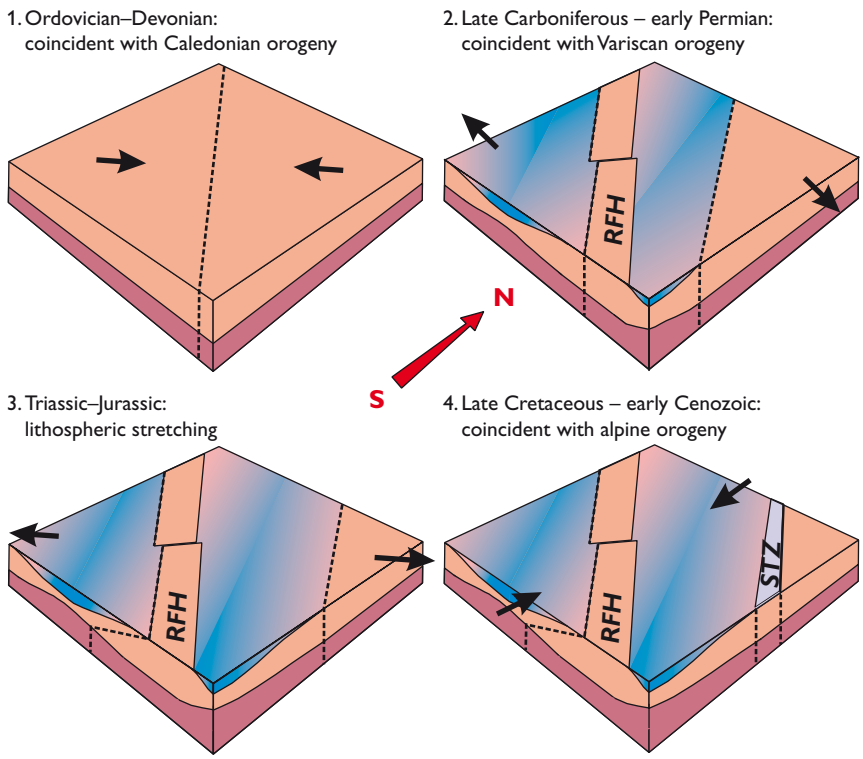

Fig. 5. Generalised summary diagram of the large-scale geological development of the Tor area (Fig. 1). Blue shows areas with sediments, orange shows areas of crystalline crust, and red is the uppermost mantle lithosphere. The Sorgenfrei–Tornquist Zone (**STZ**) and the Ringkøbing–Fyn High (**RFH**) act through time as compression, spreading and shearing zones. The arrows show the regional stress field (from Gregersen *et al.* 2006).

References

Arlitt, R. 1999: Teleseismic body wave tomography across the Trans-European Suture Zone between Sweden and Denmark, 109 pp. Unpublished Ph.D. thesis, Swiss Federal Institute of Technology, Zurich, Switzerland.

Arlitt, R., Kissling, E., Ansorge, J. & TOR Working Group 1999: 3-D crustal structure beneath the TOR array and effects on teleseismic wavefront. Tectonophysics **314**, 309–319.

Busche, H. 2001: Manteltomographie: Verspätungen von Wellenzügen im Norddeutsch–Dänischen Becken, 105 pp. Unpublished Ph.D. thesis, Christian-Albrechts-Universität Kiel, Germany.

Cotte, N., Pedersen, H.A. & Tor Working Group 2002: Sharp contrast in lithospheric structure across the Sorgenfrei–Tornquist Zone as inferred by Rayleigh wave analysis of TOR1 project data. Tectonophysics **360**, 75–88.

EUGENO-S working group 1988: Crustal structure and tectonic evolution of the transition between the Baltic Shield and the north German Caledonides (The EUGENO-S Project). Tectonophysics **150**, 253–348.

Frederiksen, S., Nielsen, S.B. & Balling, N. 2001: A numerical model for the Norwegian–Danish Basin. Tectonophysics **343**, 165–183.

Gregersen, S., Voss, P., Shomali, Z.H. & Tor Working Group 2002: Summary of Project Tor: Delineation of a stepwise, sharp, deep lithosphere transition across Germany–Denmark–Sweden. Tectonophysics **360**, 61–73.

Gregersen, S., Voss, P., Shomali, Z.H., Grad, M., Roberts, R.G. & Tor Working Group 2006: Physical differences in the deep lithosphere of northern and central Europe. In: Gee, D.G. & Stephensson, R.A. (eds): European lithosphere dynamics. Geological Society Memoirs (London) **32**, 313–322.

Kennett, B.L.N. & Engdahl, E.R. 1991: Traveltimes for global earthquake location and phase identification. Geophysical Journal International **105**, 429–465.

Nielsen, L.V. 2007: Teleseismic P wave tomography across the Sorgenfrei–Tornquist Zone. Evaluation of Tor project results, 109 pp. Unpublished cand. scient. thesis, University of Copenhagen, Denmark.

Nielsen, S.B. & Balling, N. 1990: Modelling subsidence, heat flow, and hydrocarbon generation in extensional basins. First Break **8**, 23–31.

Pedersen, T., Gregersen, S. & Tor Working Group 1999: Project Tor: Deep lithospheric variation across the Sorgenfrei–Tornquist Zone, southern Scandinavia. Bulletin of the Geological Society of Denmark **46**, 13–24.

Shomali, Z.H., Roberts, R.G. & Tor Working Group 2002: Non-linear body wave teleseismic tomography along the TOR array. Geophysical Journal International **148**, 562–574.

Thybo, H. 2000: Crustal structure and tectonic evolution of the Tornquist Fan region as revealed by geophysical methods. Bulletin of the Geological Society of Denmark **46**, 145–160.

Voss, P., Mosegaard, K., Gregersen S. & TOR working group 2006: The Tornquist Zone, a north-east-inclining lithospheric transition at the south-western margin of the Baltic Shield: revealed through a non-linear teleseismic tomographic inversion. Tectonophysics **416**, 151–166.

Authors' addresses

S.G. & P.V., *Geological Survey of Denmark and Greenland, Øster Voldgade 10, DK-1350 Copenhagen K, Denmark.* E-mail: *sg@geus.dk*

L.V.N., *Niels Bohr Institute, University of Copenhagen, Juliane Maries Vej 30, DK-2100 Copenhagen Ø, Denmark.*

Environmental response to the cold climate event 8200 years ago as recorded at Højby Sø, Denmark

Peter Rasmussen, Mikkel Ulfeldt Hede, Nanna Noe-Nygaard, Annemarie L. Clarke and Rolf D. Vinebrooke

The need for accurate predictions of future environmental change under conditions of global warming has led to a great interest in the most pronounced climate change known from the Holocene: an abrupt cooling event around 8200 years before present (present = A.D. 1950), also known as the '8.2 ka cooling event' (ka = kilo-annum = 1000 years). This event has been recorded as a negative $\delta^{18}O$ excursion in the central Greenland ice cores (lasting 160 years with the lowest temperature at 8150 B.P.; Johnsen *et al.* 1992; Dansgaard 1993; Alley *et al.* 1997; Thomas *et al.* 2007) and in a variety of other palaeoclimatic archives including lake sediments, ocean cores, speleothems, tree rings, and glacier oscillations from most of the Northern Hemisphere (e.g. Alley & Ágústsdóttir 2005; Rohling & Pälike 2005). In Greenland the maximum cooling was estimated to be 6 ± 2°C (Alley *et al.* 1997) while in southern Fennoscandia and the Baltic countries pollen-based quantitative temperature reconstructions indicate a maximum annual mean temperature decrease of around 1.5°C (e.g. Seppä *et al.* 2007).

Today there is a general consensus that the primary cause of the cooling event was the final collapse of the Laurentide ice sheet near Hudson Bay and the associated sudden drainage of the proglacial Lake Agassiz into the North Atlantic Ocean around 8400 B.P. (Fig. 1; Barber *et al.* 1999; Kleiven *et al.* 2008). This freshwater outflow, estimated to amount to *c.* 164,000 km^3 of water, reduced the strength of the North Atlantic thermohaline circulation and thereby the heat transported to the North Atlantic region, resulting in an atmospheric cooling (Barber *et al.* 1999; Clark *et al.* 2001; Teller *et al.* 2002). The climatic consequences of this meltwater flood are assumed to be a good geological analogue for future climate-change scenarios, as a freshening of the North Atlantic is projected by almost all global-warming models (e.g. Wood *et al.* 2003; IPCC 2007) and is also currently being registered in the region (Curry *et al.* 2003).

In an ongoing project, the influence of the 8.2 ka cooling event on a Danish terrestrial and lake ecosystem is being investigated using a variety of biological and geochemical proxy data from a sediment core extracted from Højby Sø, north-west Sjælland (Fig. 2). Here we present data on changes in lake hydrology and terrestrial vegetation in response to climate change, inferred from macrofossil data and pollen analysis, respectively.

Materials and methods

Højby Sø is located in Odsherred, north-west Sjælland, approximately 2.5 km from the sea. Today the lake has a surface area of *c.* 40 ha with a mean water depth of 1.8 m. The lake has no natural inlets or outlets. In 2005 a 13.6 m long sediment

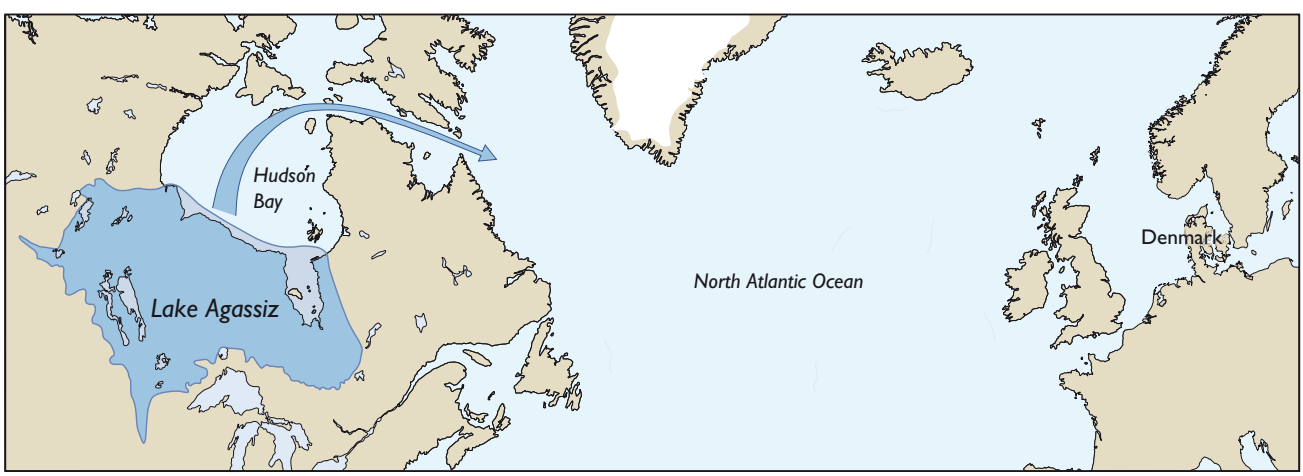

Fig. 1. Map showing Lake Agassiz in North America and the route of the meltwater outburst into Hudson Bay and the North Atlantic Ocean when the lake drained at about 8400 B.P. (modified from Kleiven *et al.* 2008).

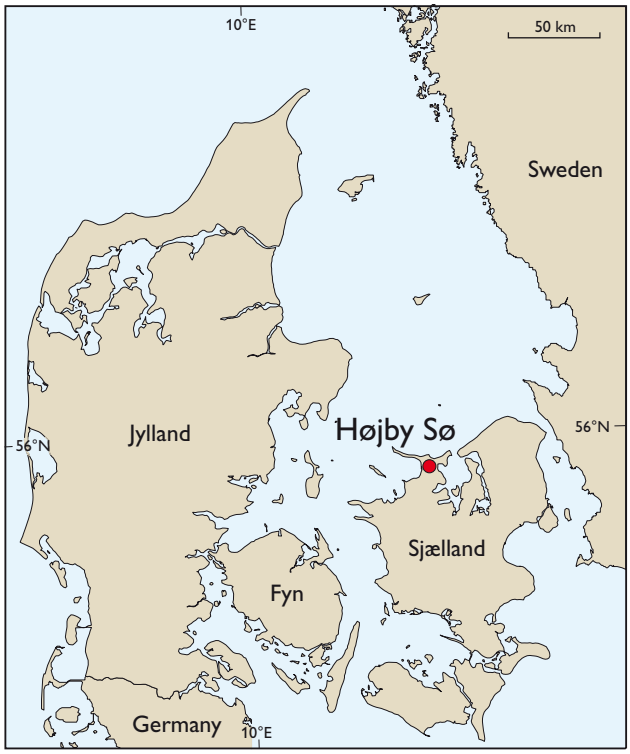

Fig. 2. Map of Denmark showing the location of Højby Sø in north-west Sjælland.

core consisting mainly of calcareous gyttja was retrieved from the lake. From the entire core 28 samples were dated by Accelerator Mass Spectrometry (AMS) ^{14}C using terrestrial plant material. The whole sediment sequence covers the time period *c.* 12,000–2000 years B.P.; here we focus on time slices of relevance to the 8.2 ka cooling event. The core content of plant and animal macrofossils is shown as accumulation rates. Pollen data were calculated as percentages, concentrations (grains/cm^3) and accumulation rates (grains/cm^2 per year); only the accumulation rate data are presented here. At least 500 pollen grains from terrestrial plants were counted per sample.

Results and discussion

Lake hydrology and climate change

Sedimentary macrofossil data can be used as proxy evidence for changes in catchment and lake hydrology (e.g. Hannon & Gaillard 1997). At Højby Sø the abundance of macrophyte remains – *Ceratophyllum* (hornwort), *Nymphaea* (white water-lily), *Nuphar* (yellow water-lily), *Najas marina* (holly-leaved naiad), *Chara* (stonewort) – and *Daphnia* resting eggs (ephippia) exhibits an abrupt increase around 8400 B.P. (Fig. 3). This pronounced change testifies to a sudden precipitation-induced lake level rise, as a higher water table would, on the one hand, result in an extension of shallow areas suitable for macrophyte growth, and on the other hand enhance conditions for the pelagic-living *Daphnia*. This inferred change to moist conditions and increased lake level are supported by simultaneous and marked increases in sediment accumulation rates of minerogenic matter and the alga *Pediastrum* (not illustrated). These data from Højby Sø add to the growing evidence that the brief 8.2 ka cooling event observed and defined in the Greenland ice cores (8247–8086 B.P.; Thomas *et al.* 2007) took place during a period of longer-term climatic perturbation which started some hundred years earlier (e.g. Rohling & Pälike 2005; Lal *et al.* 2007). Interestingly, the start of the moist climatic period inferred from Højby Sø (*c.* 8400 B.P.) is contemporary (within dating uncertainties) with the weakening of the thermohaline circulation (Kleiven *et al.* 2008) and a global CO_2 decline of *c.* 25 ppmv as inferred from stomata analysis from Lille Gribsø, north-east Sjælland (Wagner *et al.* 2002).

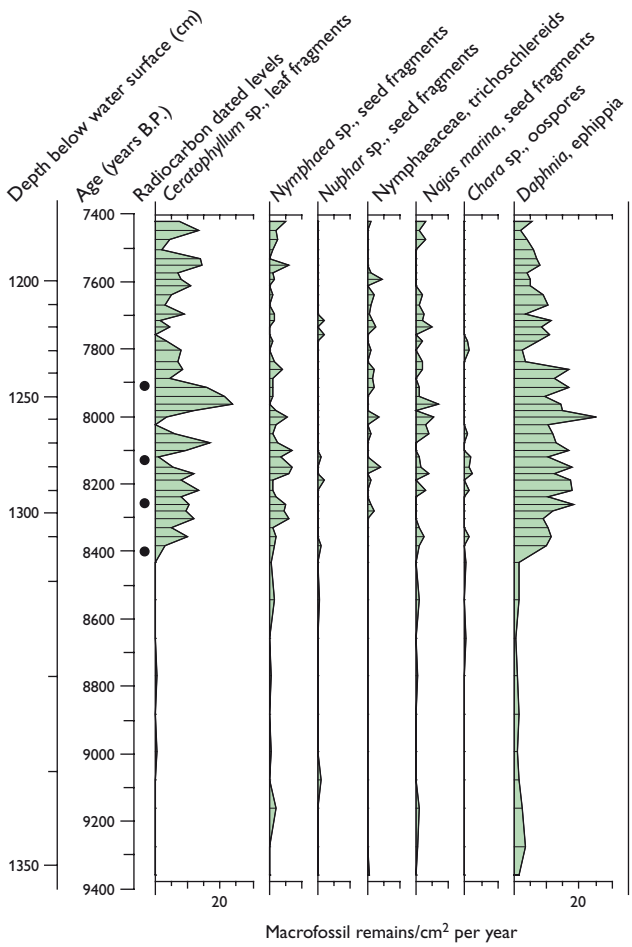

Fig. 3. Macrofossil accumulation diagram (remains/m^2 per year) from Højby Sø covering the time period *c.* 9400–7400 years B.P. Only selected taxa are shown. The age-depth model will be published in a forthcoming paper.

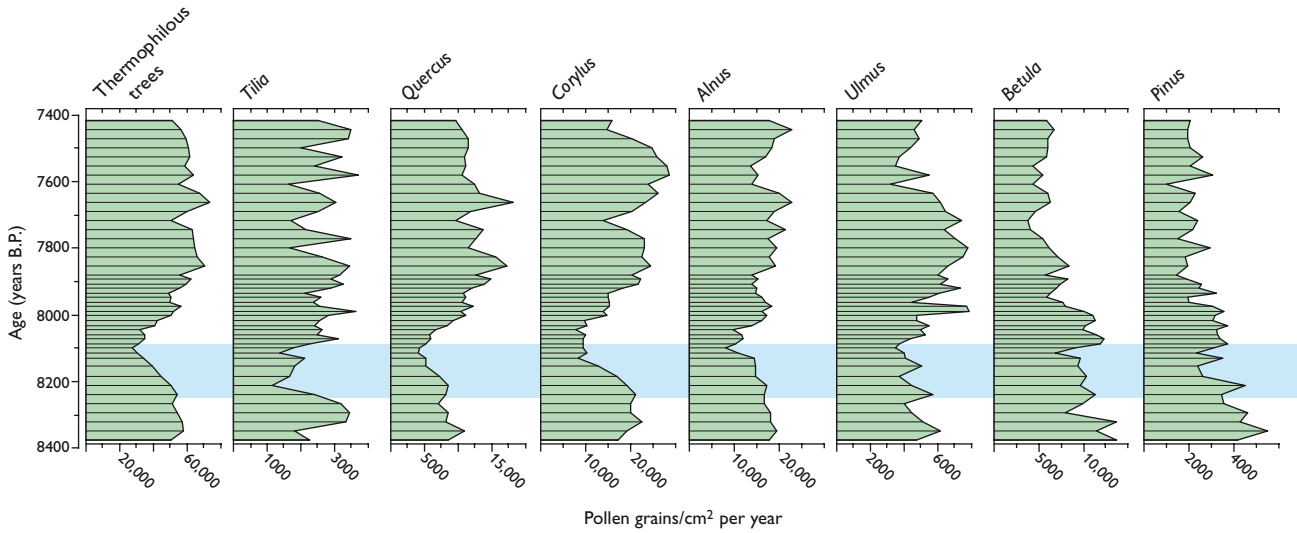

Fig. 4. Pollen accumulation rates (grains/cm^2 per year) of sum of thermophilous trees and dominant tree taxa at Højby Sø during the time interval *c.* 8400–7400 B.P. Note different horizontal scales. The time period of the 8.2 ka cooling event according to the Greenland ice core chronology is indicated by blue (8247–8086 B.P.; Thomas *et al.* 2007).

Vegetation and climate change

Figure 4 illustrates the pollen accumulation rates for selected tree taxa and groups of taxa at Højby Sø in the time interval 8400–7400 years B.P. In this study period the overall trends in the pollen data are similar whether calculated as accumulation rates, percentages or concentrations. In the Atlantic chronozone (9000–5900 years B.P.), the Danish landscape was characterised by broad-leaved, closed-canopy woodlands, also called the 'stable primeval forest' (Iversen 1973). Within the dating uncertainty of our chronology the pollen stratigraphy at Højby Sø provides clear evidence for vegetational disturbances coeval with the 8.2 ka cooling event. Between *c.* 8250 and 7900 years B.P. there is a pronounced decline and subsequent recovery in the pollen accumulation rates for *Tilia* (lime), *Quercus* (oak), *Corylus* (hazel) and *Alnus* (alder). The beginning of the decline in each of the mentioned taxa and the subsequent recovery are as follows: *Tilia c.* 8250/8100 B.P., *Quercus c.* 8200/8000 B.P., *Corylus c.* 8250/7900 B.P. and *Alnus c.* 8100/8000 B.P. By contrast, *Ulmus* (elm) accumulation rates are more variable and do not show a similarly clear decrease, although the taxon has a minimum frequency about 8100 B.P. Two taxa, *Betula* (birch) and *Pinus* (pine), exhibit a clear maximum in the time interval *c.* 8100–8000 B.P. Our data suggest that the primary response to the 8.2 ka cooling event was a decrease in the total pollen accumulation rates of thermophilous ('warm-loving'), deciduous tree taxa in the time period *c.* 8200–8000 B.P. (Fig. 4). This tree pollen recession is probably not a reflection of reduced forest cover as the abundance of open ground herbs – e.g. *Artemisia* (mugwort), *Rumex acetosella* (sheep's sorrel) and Poaceae (grasses) – does not exhibit a contemporary increase (not illustrated). As discussed by several authors, the decrease in pollen abundance of a number of thermophilous broad-leaved tree taxa during the 8.2 ka cooling event need not be synonymous with a change in population size. Instead it might, solely or partly, represent reduced pollen production due to unfavourable climatic conditions (e.g. Snowball *et al.* 2002; Seppä *et al.* 2007). The various taxa referred to above do not respond simultaneously to changing environmental conditions, which might be due to differences in their physiological tolerance towards changes in, for example, temperature and hydrology. The decrease in pollen accumulation rates for *Tilia* and *Quercus*, which flower in July and May/June respectively, strongly suggests that the forest ecosystem in our study area was stressed by low temperatures during the summer season. Many European palaeoclimate records and model simulations indicate that the temperature drop during the 8.2 ka cooling event was primarily a winter and early spring phenomenon (Alley & Ágústsdóttir 2005; Wiersma & Renssen 2006). Thus, our findings at Højby Sø constitute one of the rare examples of the 8.2 ka cooling event *also* being a summer phenomenon.

The decline in the pollen accumulation rates of the early flowering taxa *Corylus*, *Alnus* and *Ulmus* (start flowering February–April) was most likely caused by long winters with late spring frosts that would have damaged flowers and catkins, leading to a reduction in pollen productivity. Increases in pollen accumulation rates for *Betula* and *Pinus* during the 8.2 ka cooling event are presumably due to the fact that these two taxa are the most frost-resistant tree taxa in northern Europe. However, the fact that the accumulation rates for the latter taxa actually increase compared to levels

immediately before the cooling event, is cause for speculation. The elevated accumulation rates during the 8.2 ka cooling event might reflect an increase in actual population size and not just an increase in pollen productivity. If this is correct, the cause of the population expansion could be a hydrological change towards drier conditions. This hypothesis finds some support in the clear inverse relationship between the decrease in *Alnus* and the increase in *Betula* and *Pinus*, suggesting a causal link between these taxa. *Alnus* is a tree usually associated with damp or waterlogged soils and therefore sensitive to changes in the water table; the *Alnus* decrease might therefore, solely or partly, be related to a water-level lowering in this period, and with an exposure of the former littoral zone around the lake *Betula* and *Pinus* may have expanded into this habitat.

Conclusions and future work

Due to good chronological control (not presented here) combined with high sampling resolution of the sediment sequence from Højby Sø, it has been possible to identify the 8.2 ka cooling event in a Danish palaeo-record. The pollen data reveal that the forest ecosystem was affected by low temperatures during both the summer and winter – early spring; the result was reduced pollen production from thermophilous, deciduous trees. Possible changes in population size due to climatic-induced hydrological changes are also suggested. Furthermore, our investigation indicates that the short 8.2 ka cooling event took place during a period of longer-term climatic deterioration which started around 8400 B.P., coeval with the catastrophic drainage of Lake Agassiz. Using diatom and algal pigment analyses, ongoing work in the Højby Sø project aims to explore if and how the aquatic ecosystem responded to the climate change 8200 B.P.

Acknowledgements

Geocenter Copenhagen and the Carlsberg Foundation are gratefully acknowledged for financial support.

References

Alley, R.B. & Ágústsdóttir, A.M. 2005: The 8k event: cause and consequences of a major Holocene abrupt climate change. Quaternary Science Reviews **24**, 1123–1149.

Alley, R.B., Mayewski, P.A., Sowers, T., Stuiver, M., Taylor, K.C. & Clark, P.U. 1997: Holocene climate instability: a prominent widespread event 8200 years ago. Geology **25**, 483–486.

Barber, D.C. *et al.* 1999: Forcing of the cold event 8,200 years ago by catastrophic drainage of Laurentide lakes. Nature **400**, 344–348.

Clark, P.U., Marshall, S.J., Clarke, G.K.C., Hostetler, S.W., Licciardi, J.M. & Teller, J.T. 2001: Freshwater forcing of abrupt climate change during the last glaciation. Science **293**, 283–287.

Curry, R., Dickson, B. & Yashayaev, I. 2003: A change in the freshwater balance of the Atlantic Ocean over the past four decades. Nature **426**, 826–829.

Dansgaard, W. 1993: Evidence for general instability of past climate from a 250-kyr ice core record. Nature **364**, 218–220.

Hannon, G.E. & Gaillard, M.-J. 1997: The plant-macrofossil record of past lake-level changes. Journal of Paleolimnology **18**, 15–28.

IPCC (Intergovernmental Panel on Climate Change) 2007: Climate Change 2007. (www.ipcc.ch).

Iversen, J. 1973: The development of Denmark's nature since the last glacial. Danmarks Geologiske Undersøgelse V. Række **7-C**, 126 pp.

Johnsen, S.J., Clausen, H.B., Dansgaard, W., Fuhrer, K., Gundestrup, N., Hammer, C.U., Iversen, P., Jouzel, J., Stauffer, B. & Steffensen, J.P. 1992: Irregular glacial interstadials recorded in a new Greenland ice core. Nature **359**, 311–313.

Kleiven, H.F., Kissel, C., Laj, C., Ninnemann, U.S., Richter, T.O. & Cortijo, E. 2008: Reduced North Atlantic deep water coeval with the glacial Lake Agassiz freshwater outburst. Science **319**, 60–64.

Lal, D., Large, W.G. & Walker, S.G. 2007: Climatic forcing before, during, and after the 8.2 Kyr B.P. global cooling event. Journal of Earth System Science **116**, 171–177.

Rohling, E.J. & Pälike, H. 2005: Centennial-scale climate cooling with a sudden cold event around 8,200 years ago. Nature **434**, 975–979.

Seppä, H. *et al.* 2007: Spatial structure of the 8200 cal yr BP event in northern Europe. Climate of the Past **3**, 225–236.

Snowball, I., Zillén, L. & Gaillard, M.-J. 2002: Rapid early-Holocene environmental changes in northern Sweden based on studies of two varved lake-sediment sequences. The Holocene **12**, 7–16.

Teller, J.T., Leverington, D.W. & Mann, J.D. 2002: Freshwater outbursts to the oceans from glacial lake Agassiz and their role in climate change during the last deglaciation. Quaternary Science Reviews **21**, 879–887.

Thomas, E.R., Wolff, E.W., Mulvaney, R., Steffensen, J.P., Johnsen, S.J., Arrowsmith, C., White, J.W.C., Vaughn, B. & Popp, T. 2007: The 8.2 ka event from Greenland ice cores. Quaternary Science Reviews **26**, 70–81.

Wagner, F., Aaby, B. & Visscher, H. 2002: Rapid atmospheric CO2 changes associated with the 8,200-years-B.P. cooling event. Proceedings of the National Academy of Sciences of the United States of America **99**, 12,011–12,014.

Wiersma, A.P. & Renssen, H. 2006: Model-data comparison for the 8.2 ka BP event: Confirmation of a forcing mechanism by catastrophic drainage of Laurentide lakes. Quaternary Science Reviews **25**, 63–88.

Wood, R.A., Vellinga, M. & Thorpe, R. 2003: Global warming and thermohaline circulation stability. Philosophical Transactions of the Royal Society **A361**, 1961–1974.

Authors' addresses

P.R., *Geological Survey of Denmark and Greenland. Øster Voldgade 10, DK-1350 Copenhagen K, Denmark.* E-mail: *per@geus.dk*

M.U.H. & N.N.-N., *Department of Geography and Geology, University of Copenhagen, Øster Voldgade 10, DK-1350 Copenhagen K, Denmark.*

A.L.C., *APEM Manchester Lab, Riverview, A17 Embankment Business Park, Heaton Mersey, Stockport, SK4 3GN, UK.*

R.V., *Department of Biological Science - Freshwater Biodiversity Laboratory, University of Alberta, Edmonton, Alberta T6G 2E9, Canada.*

A new programme for monitoring the mass loss of the Greenland ice sheet

Andreas P. Ahlstrøm and the PROMICE project team*

The Greenland ice sheet has been losing mass at a dramatic rate in recent years, raising political concern worldwide due to the possible impact on global sea level rise and climate dynamics (Luthcke *et al.* 2006; Rignot & Kanagaratnam 2006; Velicogna & Wahr 2006; IPCC 2007; Shepherd & Wingham 2007). The Arctic region as a whole is warming up much more rapidly than the globe at large (ACIA 2005) and it is desirable to quantify these changes in order to provide the decision-makers with a firm knowledge base. To cover this need, the Danish Ministry of Climate and Energy has now launched a new *Programme for Monitoring of the Greenland Ice Sheet* (PROMICE), designed and operated by the Geological Survey of Denmark and Greenland (GEUS) in collaboration with the National Space Institute at the Technical University of Denmark and Asiaq (Greenland Survey). The aim of the programme is to quantify the annual mass loss of the Greenland ice sheet, track changes in the extent of local glaciers and ice caps, and track changes in the position of the ice-sheet margin.

Observing and modelling the ice-sheet surface-mass balance

Surface mass balance will be estimated using data from a new network of automatic mass-balance stations (AMS) on the margin of the Greenland ice sheet (Fig. 1). The final station network will include a total of 14 stations located in seven climatically different regions of the Greenland ice sheet and is intended to be fully operational from 2011. At each location, one station will be placed in the lower ablation zone, and another in the higher ablation zone near the equilibrium-line altitude. Currently, six of these stations are operational in four regions of the ice-sheet margin (Fig. 1). The PROMICE network will complement the U.S. Greenland Climate Network (GC-Net) which consists of *c.* 15 stations, mainly in the accumulation zone of the ice sheet (Steffen & Box 2001) and the Dutch K-transect of three stations on the ice-sheet margin near Kangerlussuaq, West Greenland (Fig. 1; van de Wal *et al.* 2005). This collaboration means that ice-

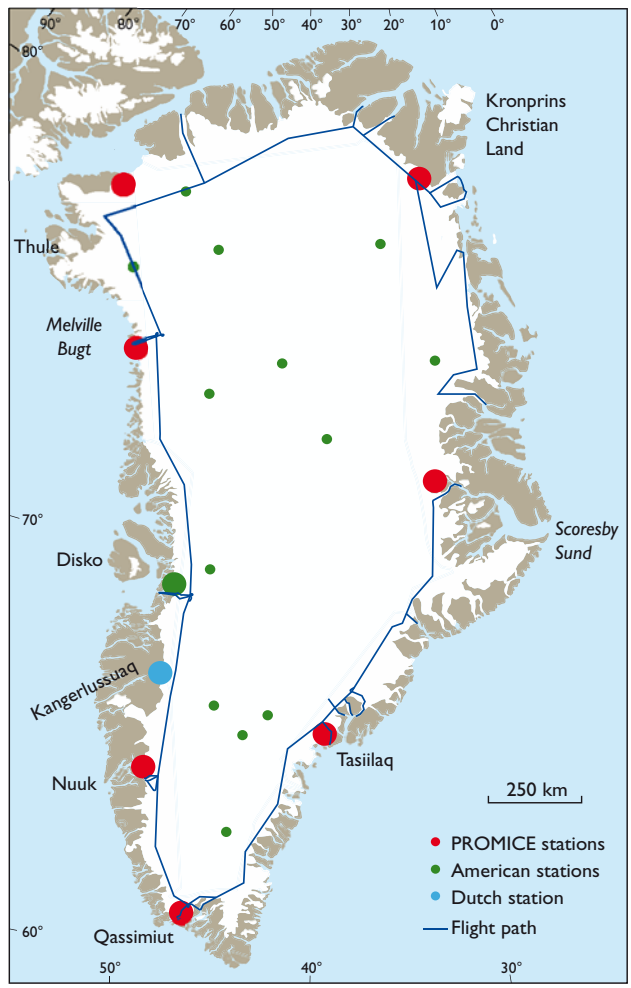

Fig. 1. Overview map showing current and future PROMICE activities. Large dots signify several stations along transects in the ablation zone of the ice sheet, small dots signify individual stations in the accumulation area. By summer 2007, six PROMICE stations were in operation on the ice-sheet margin: two near Tasiilaq, two near Nuuk, one in Melville Bugt and one in South Greenland near Qassimiut. The dots near Thule, Kronprins Christian Land and inner Scoresby Sund signify locations of future station transects to be established over the next three years. The flight lines show the PROMICE flight in August 2007, covering the entire margin apart from a short high elevation segment in East Greenland. Note that the flight paths also pass down 20 of the most significant outlet glaciers from the Greenland ice sheet.

*Peter Gravesen, Signe Bech Andersen, Dirk van As, Michele Citterio, Robert S. Fausto, Søren Nielsen, Hans F. Jepsen, Steen Savstrup Kristensen, Erik Lintz Christensen, Lars Stenseng, Rene Forsberg, Susanne Hanson and Dorthe Petersen

sheet surface melting and its climatic causes can be effectively monitored in all geographical regions of the Greenland ice sheet. The observations from the station network provide the input to perform the spatially distributed modelling of the surface melting necessary to quantify the total meltwater runoff from the Greenland ice sheet. Such modelling has previously relied on observational data from coastal stations in a maritime climate quite different from stations located at the ice-sheet margin and from stations in the accumulation zone, complemented only by the measurements from the few U.S. and Dutch stations on the ice-sheet margin in West Greenland (Box *et al.* 2006). The innovative GEUS station setup includes measurement of air temperature, relative humidity, wind speed and direction, atmospheric pressure, incoming and outgoing short- and long-wave radiation, ice temperature, surface velocity, snow depth and ice ablation (Fig. 2). The climate and ice temperature data allow calculation of the complete surface-energy balance. Together with the snow depth measurement, these data make it possible to determine the specific cause of an observed change in surface melt. This implies that we will be able to answer questions such as whether the impact on ice-sheet ablation of rising air temperatures is offset by a corresponding increase in snow precipitation. The data are stored locally in the data logger, but are also transmitted by satellite to GEUS at regular intervals during the melt season, when solar panels deliver the necessary additional power and the data are most crucial. Figure 3 shows some samples of transmitted data. Station power and

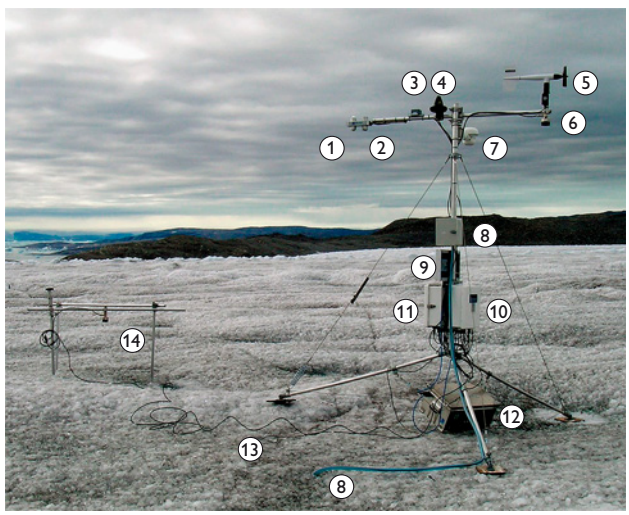

Fig. 2. The new PROMICE automatic mass-balance station, in this case the station with the lowest elevation on the Greenland ice-sheet margin near Tasiilaq, East Greenland. **1**, short-wave radiation (in/out); **2**, long-wave radiation (in/out); **3**, station tilt; **4**, satellite transmitter; **5**, wind speed and direction; **6**, snow height (sonar); **7**, air temperature and relative humidity; **8**, ablation (pressure sensor); **9**, solar panel; **10**, dogger logger enclosure; **11**, GPS and multiplexer enclosure; **12**, battery box; **13**, ice temperature 0–10 m (thermistors); **14**, ablation (sonar and stakes).

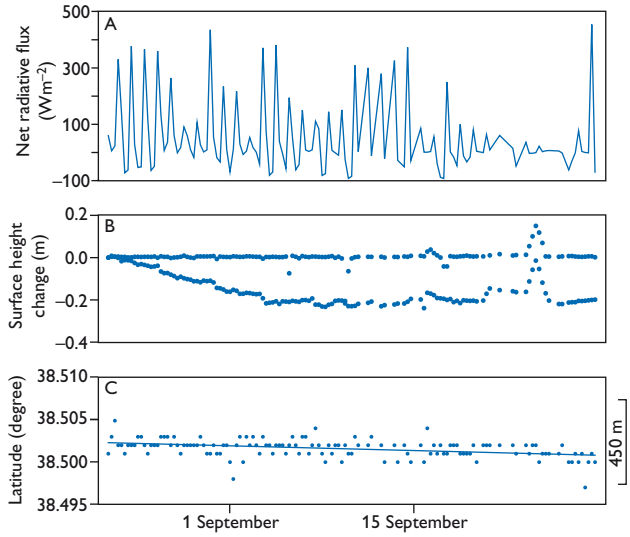

Fig. 3. **A**: Net radiative flux measured by a CNR-1 instrument, used on the PROMICE stations in 2007. The CNR-1 measures incoming and outgoing short- and long-wave radiation and enables calculation of the surface albedo. **B**: Snow depth and ablation, measured respectively by a SR-50 sonic ranging device installed on the station tripod and on stakes drilled into the ice. **C**: Latitudinal movement of the station recorded by the GPS. All graphs have been produced from satellite-transmitted data received at GEUS.

tilt are also monitored in order to minimise costly maintenance visits.

Generally, station visits by helicopter constitute the main expense in operating the network on the ice-sheet margin. This fact has prompted the development of a new type of ablation sensor at GEUS, based on measuring the pressure of anti-freeze liquid at the end of a flexible, closed hose inserted into the ice to a depth of 30–40 m. As the ice melts, the length of the hose in the ice diminishes, lowering the pressure exerted by the liquid column on the sensor at the bottom of the hose. The top of the hose is connected to a liquid reservoir at a fixed level on the station, making it possible to deduce ice-sheet surface melt from pressure change. An early version of the system has been described by Bøggild *et al.* (2005). Once this system is operational, it should in theory be possible to leave the station unattended for as long a time as it takes the hose to melt out of the ice, i.e. more than 5 years, as the remaining part of the station is 'floating' on the ever-changing ice surface. In practice, stations can rarely be left unattended in the harsh environment on the ice-sheet margin for that long, and most instruments would in any case require calibration or maintenance at more regular intervals. However, even a reduction of visits from every year to every second year is substantial. Currently, the pressure-sensor system is supplemented by a more traditional set up with a sonic ranging device mounted on stakes drilled into the ice. The

sonic-ranger system requires annual visits for re-drilling of stakes, but is necessary as long as the pressure-sensor system is not completely reliable. Both systems record ice melt on an hourly basis, yielding the perfect validation data for determining the individual energy-balance components from the climate data collected.

Quantifying the mass loss caused by iceberg calving

Iceberg calving from the outlet glaciers of the Greenland ice sheet, often termed the ice-dynamic mass loss, is responsible for most of the acceleration in the mass loss during the last decade (Rignot & Kanagaratnam 2006). To quantify this part of the mass loss, we combine an airborne survey yielding surface elevation and ice depth across the entire ice-sheet margin, with ice-sheet surface velocity derived from satellite radar. The ice-dynamic mass loss is then derived by calculating the ice flux from the interior of the ice sheet towards the outlet glaciers, while correcting for the surface melt between the flux gate and the calving front of the glacier (Rignot & Kanagaratnam 2006). The route chosen complements the airborne ice-sheet elevation measurements carried out by U.S. researchers. The route was designed to cover the accumulation zone and the centre line of the main outlet glaciers of the Greenland ice sheet (Krabill *et al.* 2004). The first airborne survey within PROMICE was carried out in August 2007, measuring ice-sheet elevation with a Riegl scanning laser altimeter (Forsberg *et al.* 2001) and ice-sheet thickness with a 60 MHz coherent ice-penetrating radar (Christensen *et al.* 2000). An example of the radar data is shown in Fig. 4. The airborne survey will be repeated every two or three years to monitor temporal changes in the elevation of the Greenland ice-sheet margin. The radar had difficulties penetrating the ice sheet in the southernmost part of Greenland, probably due to the extensive surface melting experienced in 2007 and the fact that the survey was carried out in August at the peak of the melt season. The time of year had been selected to minimise the influence of snow depth on the elevation measurements, but may have to be shifted to the spring for future surveys in order to obtain the ice-sheet thickness.

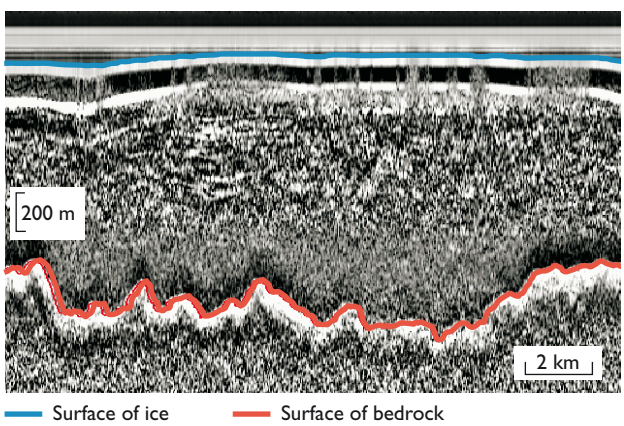

Fig. 4. Data from an ice-penetrating radar. The data have been post-processed and interpreted to determine the base and surface of the ice sheet at a site in West Greenland. Eventually the ice thickness is determined using the radar reflection from the bedrock in combination with laser altimeter measurements of the ice-sheet surface.

A new P-band radar is currently being developed at the Technical University of Denmark for the European Space Agency. This may replace the older 60 MHz radar on future surveys, if it is more successful in retrieving bedrock returns beneath the ice sheet and is made available for our use.

Monitoring the change of glaciers and ice caps in Greenland

In addition to the Antarctic and Greenland ice sheets, melting of glaciers and ice caps around the world is contributing significantly to the present-day sea-level rise, and yet almost nothing is known about the current state of the *c.* 20 000 glaciers and ice caps in Greenland. To remedy this lack of knowledge, PROMICE aims at delivering glacier and ice-sheet outlines to the Global Land Ice Measurements from Space (GLIMS) project, in order to compile a complete inventory of Greenland glaciers and ice caps as well as the ice-sheet margin. Representative glaciers can be selected from the inventory for detailed volume-change studies of the reaction to climate change and used for up-scaling to larger regions.

The island of Disko in West Greenland was chosen as a test region to develop the methodology for a number of reasons: (a) vectorised maps and elevation contours are available from an airborne survey in 1985; (b) the island is covered by a recent Landsat 7 ETM+ satellite image, facilitating a comparison over a 16-year period; (c) the island is covered by the Glacier Inventory of West Greenland (WGGI) (Weidick *et al.* 1992); and (d) the island exhibits a wide range of glacier types and problems representative for Greenland as a whole. The WGGI covers more than 5000 glaciers, and is published as a map compilation including a table summarising glacier specific data, such as area, elevation span and orientation. A digital version of the table was checked for errors and included in the Geographic Information System, ArcGIS. Glacier positions needed manual correction due to the limited precision listed in the inventory table. The relevant inventory maps were scanned, geo-referenced and likewise imported into ArcGIS, in order to yield additional information on glacier extent during the Little Ice Age (LIA) as derived from aerial photographs. A Landsat 7 ETM+ image from 2001 available from the Global Land Cover Facility was utilised to obtain a more recent inventory of the glaciers on

Disko, using the GLIMS algorithm (Paul & Kääb 2005). A 50 m resolution digital elevation model was created from the 100 m elevation contours of the 1985 map, to assist in determining ice-flow divides and orientation controls on glacier sensitivity to climate change.

Preliminary results show that in the period 1985–2001, glaciers on Disko retreated by 8%, whereas no significant areal change could be determined (<0.5%). It was also found that the WGGI could not be used for determination of glacier area change since the LIA, but that the glaciers on the island of Disko had retreated 44% between the LIA and 2001. The initial results thus point to at a more limited reaction to recent warming trends in West Greenland, compared to the strongly responding glaciers and ice caps in Alaska (Arendt *et al.* 2002).

Outlook

The data acquired by the monitoring programme will be stored in a database constructed for the purpose at GEUS. So far, the process of defining the database requirements and user needs has been initiated. Once the monitoring programme is operational, data will be made available within a year from acquisition through this database. Already at this early stage, PROMICE has been woven into a number of research activities, national as well as international, utilising the existing field operations as a vehicle for scientific projects. Through the extensive monitoring programme, GEUS has become a natural partner in most international glaciological research activities on the Greenland ice sheet. The effort is also a strong asset for current and future hydropower investigations by the Greenland Home Rule, as well as for prospecting activities near the ice margin.

Over the next three years, the full station network will be established, the ice-sheet surface velocity software will be finalised and the glaciological modelling tools for estimating melting and dynamic mass loss will be developed and applied. With the new monitoring programme of the Greenland ice sheet, we will not only be able to provide an answer to how much the Greenland ice sheet contributes to global sea-level rise, but also make it possible for the global research community to gain access to key data sets to conduct their own investigations.

Acknowledgement

The Programme for Monitoring of the Greenland ice sheet (PROMICE) is partly funded by DANCEA under the Danish Ministry of Climate and Energy.

References

ACIA 2005: Arctic climate impact assessment, 1042 pp. Cambridge: Cambridge University Press.

Arendt, A.A., Echelmeyer, K.A., Harrison, W.D., Lingle, C.S. & Valentine, V.B. 2002: Rapid wastage of Alaska glaciers and their contribution to rising sea level. Science **297**, 382–386.

Bøggild, C.E., Olesen, O.B., Ahlstrøm, A.P. & Jørgensen, P. 2005: Automatic glacier mass balance observations using pressure sensors. Journal of Glaciology **50**(169), 303–305.

Box, J.E., Bromwich, D.H., Veenhuis, B.A., Bai, L.-S., Stroeve, J.C., Rogers, J.C., Steffen, K., Haran, T. & Wang, S.-H. 2006: Greenland ice sheet surface mass balance variability (1988–2004) from calibrated polar MM5 output. Journal of Climate **19**, 2783–2800.

Christensen, E.L., Reeh, N., Forsberg, R., Jørgensen, J.H., Skou, N. & Woelders, K. 2000: A low cost glacier mapping system. Journal of Glaciology **46**(154), 531–537.

Forsberg, R., Keller, K. & Jacobsen, S.M. 2001: Laser monitoring of ice elevations and sea-ice thickness in Greenland. International Archives of Photogrammetry and Remote Sensing **34**, 163–169.

IPCC 2007: Climate change 2007: the physical science basis. Contribution of working group I to the fourth assessment report of the Intergovernmental Panel on Climate Change [Solomon, S. *et al.* (eds)]. Cambridge: Cambridge University Press.

Krabill, W. *et al.* 2004: Greenland ice sheet: increased coastal thinning. Geophysical Research Letters **31**, L24402, doi:10.1029/2004GL021533.

Luthcke, S.B., Zwally, H.J., Abdalati, W., Rowlands, D.D., Ray, R.D., Nerem, R.S., Lemoine, F.G., McCarthy, J.J. & Chinn, D.S. 2006: Recent Greenland ice mass loss by drainage system from satellite gravity observations. Science **314**, 1286–1289.

Paul, F. & Kääb, A. 2005: Perspectives on the production of a glacier inventory from multispectral satellite data in the Canadian Arctic: Cumberland Peninsula, Baffin Island. Annals of Glaciology **42**, 59–66.

Rignot, E. & Kanagaratnam, P. 2006: Changes in the velocity structure of the Greenland ice sheet. Science **311**, 986–990.

Shepherd, A. & Wingham, D. 2007: Recent sea-level contributions of the Antarctic and Greenland ice sheets. Science **315**, 1529–1532.

Steffen, K. & Box, J.E. 2001: Surface climatology of the Greenland ice sheet: Greenland climate network 1995–1999. Journal of Geophysical Research, **106**(D24), 33,951–33,964.

van de Wal, R.S.W., Greuell, W., van den Broeke, M.R., Reijmer, C.H. & Oerlemans, J. 2005: Surface mass-balance observations and automatic weather station data along a transect near Kangerlussuaq, West Greenland. Annals of Glaciology **42**, 311–316.

Velicogna, I. & Wahr, J. 2006: Acceleration of Greenland ice mass loss in spring 2004. Nature **443**, 329–331.

Weidick, A., Bøggild, C.E. & Knudsen, N.T. 1992: Glacier inventory and atlas of West Greenland. Rapport Grønlands Geologiske Undersøgelse **158**, 194 pp.

Authors' addresses

A.P.A., P.G., S.B.A., D.v.A., M.C., R.S.F., S.N. & H.F.J., *Geological Survey of Denmark and Greenland, Øster Voldgade 10, DK-1350 Copenhagen K, Denmark.* E-mail: *apa@geus.dk*

S.S.K., E.L.C., L.S., R.F. & S.H., *National Space Institute, Technical University of Denmark, Ørsteds Plads, Bldg. 348, DK-2800 Kgs. Lyngby, Denmark.*

D.P., *ASIAQ – Greenland Survey, P.O. Box 1003, Qatserisut 8, DK-3900 Nuuk, Greenland.*

The north-east Baffin Bay region, offshore Greenland – a new frontier petroleum exploration region

Ulrik Gregersen

In recent years the Arctic has come into focus for hydrocarbon exploration, and areas offshore both West and East Greenland have been evaluated as promising frontier hydrocarbon provinces. Seven hydrocarbon exploration and exploitation licenses were awarded in 2007–2008 offshore the Disko–Nuussuaq region (Fig. 1), and two more have been awarded in the open-door region offshore south-western Greenland. In 2007, an extensive amount of new seismic and aeromagnetic data was acquired by the TGS-NOPEC Geophysical Company in the north-eastern Baffin Bay region.

Geophysical mapping has been initiated by the Geological Survey of Denmark and Greenland (GEUS) in the Melville Bugt region offshore North-West Greenland (Fig. 1) with the purpose of evaluating the hydrocarbon prospectivity. Initial interpretation of seismic and gravity data suggests the presence of deep sedimentary basins separated by structural highs.

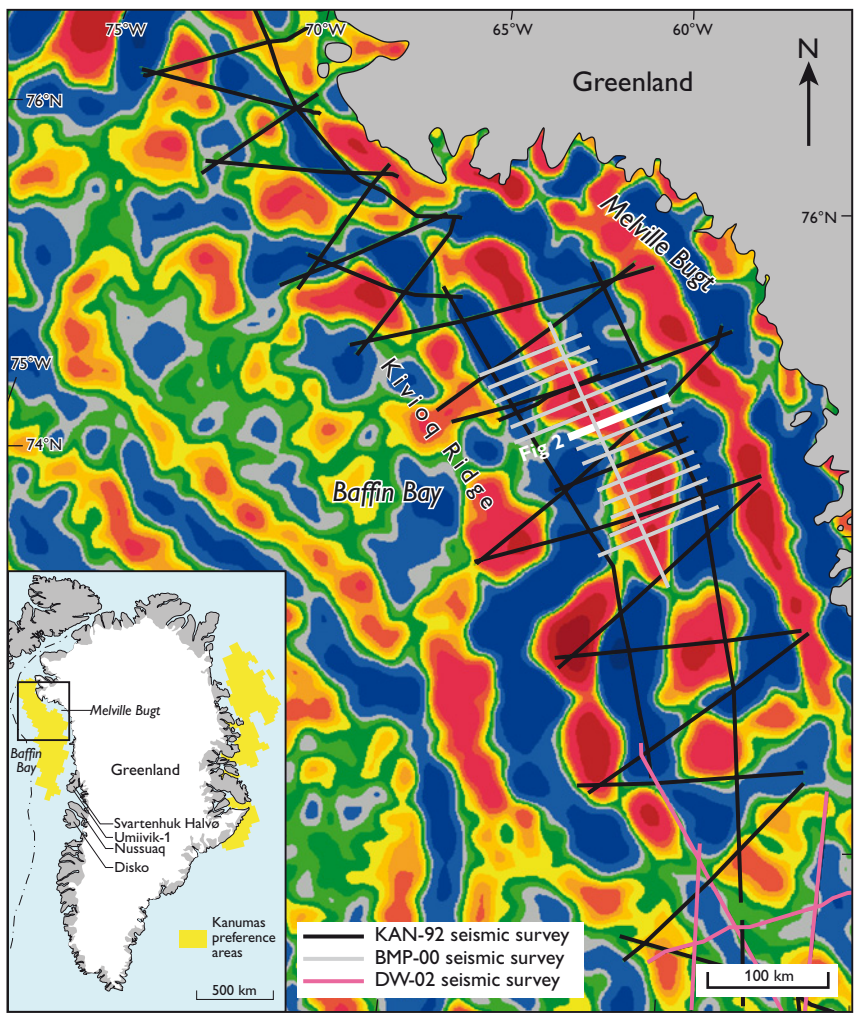

Fig. 1. Gravity map (100 km filtered bouguer gravity data) of the study region, showing the seismic grid. The location of the seismic line shown in Fig. 2 is indicated. Large areas with marked high gravity values (red) often indicate structural highs, whereas areas with low values (blue) mostly indicate deep sedimentary basins. Most basins and marked highs indicated by gravity data are confirmed by seismic data (Fig. 2). The gravity data are public domain data from the Danish National Space Center and have been filtered by GEUS.

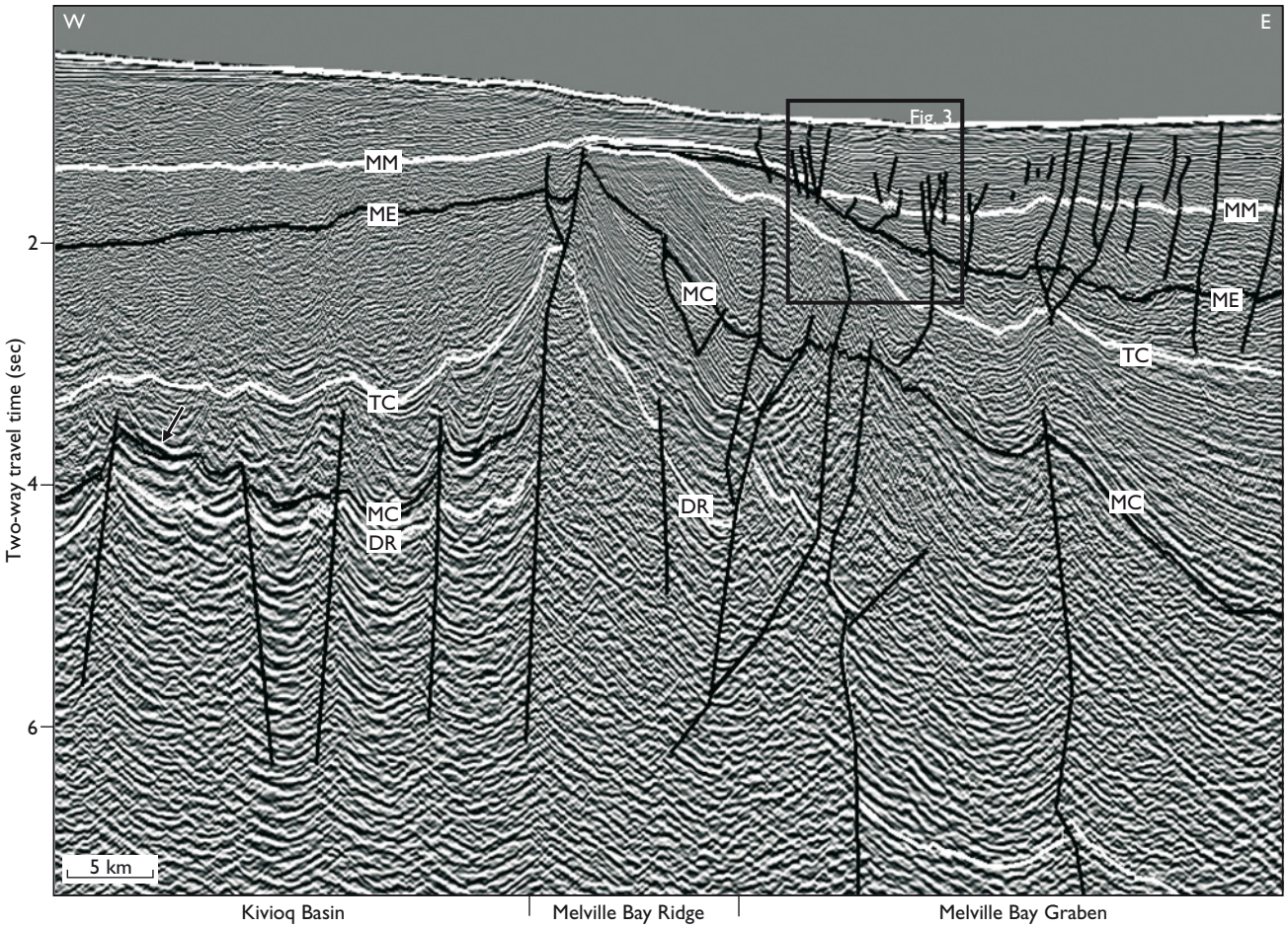

Fig. 2. Seismic section BMP00-209, Melville Bugt region, eastern Baffin Bay, illustrating the structural elements (for location of line, see Fig. 1). Intervals below the 'mid-Cretaceous' (**MC**) and just below and above the 'top Cretaceous' (**TC**) horizons may, by analogy with surrounding regions, contain reservoir levels. Structural closures are present at levels near the 'mid-Cretaceous' and the 'top Cretaceous' horizons in the basin and the graben areas. Cretaceous structures are locally affected by Palaeogene tectonic reactivation indicated by convex flexures above the TC horizon. The 'mid-Eocene' (**ME**) and the 'mid-Miocene' (**MM**) horizons truncate structures, especially over the Melville Bay Ridge, and the horizons are locally affected by Neogene faulting. Local U-shaped marked reflections with high amplitudes at the 'mid-Cretaceous' horizon may indicate intrusions, e.g. in the Kivioq Basin (arrowed). The succession below the 'deep reflection' (**DR**) horizon loses seismic reflector continuity, and probably reflects mostly the crystalline basement. Local scattered, low continuity reflections at the DR horizon may result from deeply buried Proterozoic to Palaeozoic sediments and volcanics, probably comparable to some of those known north of the study area. The frame marks the location of Fig. 3.

Geological information on source rock, reservoir rock and seal intervals from surrounding regions suggest that the Melville Bugt region is likely to have a significant petroleum potential. The study is based on public domain magnetic and gravity data, and all proprietary and public 2-D seismic data (Fig. 1) acquired before 2003. Seismic horizons from the 'seismic basement' to 'base Quaternary' are being interpreted regionally. Based on the seismic interpretation, a structural element map, depth-structure maps and isopach maps will be produced in order to assess the prospectivity of the Melville Bugt region.

Structures and basin development

Interpretations of structures and basin development are mainly based on seismic data supplemented by gravity and magnetic data. Because no wells have been drilled in eastern Baffin Bay, interpretations of the geological development and petroleum prospectivity are based partly on correlations to wells farther south and partly on the onshore geology of the surrounding region. The mapping and regional analyses show deep basins and mainly north-north-west-trending major structural highs (Figs 1, 2). The Melville Bugt region is proba-

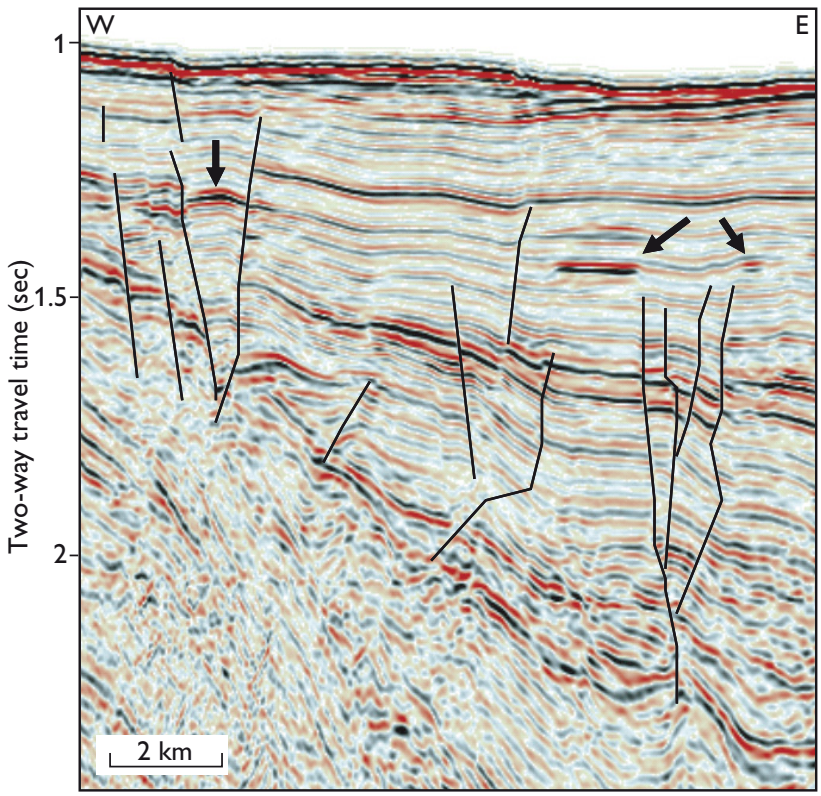

Fig. 3. Detail of the seismic section in Fig. 2 showing abnormal seismic amplitude values (arrowed), interpreted as possible 'bright spots'.

bly characterised by continental crust, whereas oceanic crust may be present farther west, in the central part of Baffin Bay (Whittaker *et al.* 1997; Oakey 2005). The highs and basins in the Melville Bugt region probably developed during several phases of mainly Cretaceous to Paleocene rifting and compressional strike-slip related Palaeogene tectonism.

The first rift phase probably occurred during Early to mid-Cretaceous time and resulted in mainly extensional faulting that created the two major structural highs in the region, the Melville Bay Ridge and the Kivioq Ridge, and some normal faults in the adjacent grabens (Fig. 2). The second rift phase occurred in Late Cretaceous and possibly in early Paleocene time and resulted in normal faulting, partly reactivating earlier Cretaceous faults. During the Palaeogene, flexures and thrust faults developed related to compressional tectonics, which affected especially the central and northern parts of the region. The Melville Bay Ridge was uplifted during the Late Cretaceous and Palaeogene (Fig. 2). The boundary fault east of the Melville Bay Graben was active at least during the Cretaceous and early Palaeogene, giving way to major graben subsidence. In the graben, more than 12 km of sediments accumulated that probably comprise mainly Mesozoic and Cenozoic deposits. In the lower part of the graben, some Palaeozoic and Proterozoic deposits similar to those known in North-West and North Greenland may be present (Peel & Sønderholm 1991; Dawes 1997).

A more than 1.3 km thick succession of Palaeogene basalts occurs in the southern part of the region and thickens southeastwards towards Svartenhuk Halvø. On Svartenhuk Halvø, Nuussuaq and Disko a thick Palaeogene basalt succession is exposed (Larsen & Pulvertaft 2000; Pedersen *et al.* 2006), and thick, tilted basalt successions are interpreted to extend out onto the adjacent offshore area (Skaarup & Pulvertaft 2007). Offshore, the basalts occur in the upper part of some fault blocks that are on-lapped by subsequent deposits below the suggested mid-Eocene horizon, indicating a mainly early Eocene age of faulting and tilting of the blocks, which is also described by Skaarup & Pulvertaft (2007). Deposition of thick sedimentary successions took place during the Late Cretaceous and in parts of the Palaeogene. A major unconformity has been recognised at a mid-Eocene level both in the Baffin Bay region (Fig. 2) and offshore West Greenland (Dalhoff *et al.* 2003). Neogene deposition is characterised by westwards and southwards prograding depositional systems, as also seen farther south offshore West Greenland (Dalhoff *et al.* 2003).

Prospectivity

The Melville Bugt region in eastern Baffin Bay probably has a considerable hydrocarbon potential. Major structures have been located at a suggested mid-Cretaceous level (Fig. 2), some with large structural closures at depths of *c.* 1–4 km. Most of the structures have an attractive combination of size, short distance to potential mature source kitchens and a thick overburden. Several potential reservoir rock levels may be present if Cretaceous and Palaeogene sand dominated units equivalent to those found farther south offshore and onshore West Greenland are also present here (Dalhoff *et al.* 2003; Scherstén & Sønderholm 2007).

The deep basins of the Melville Bugt region contain thick successions of sedimentary rocks that may include prolific source rocks. Several indications of an active hydrocarbon system with mature source rocks are known from Canada and western Greenland. In the Arctic islands of Canada these comprise exposed oil-prone source rocks of the Kanguk Formation (Núñez-Betelu *et al.* 1993) and the Scott Trough oil seep (MacLean *et al.* 1981).

In West Greenland the presence of mature source rocks is proven by oil seeps onshore Nuussuaq, Disko and Svartenhuk Halvø (Bojesen-Koefoed *et al.* 1999, 2007). Oil and gas have been encountered in boreholes on Nuussuaq and Svartenhuk Halvø (e.g. wet gas in the Umiivik-1 borehole; Dam *et al.* 1998). 'Bright spots' (Fig. 3) and other hydrocarbon indicators related to structural closures or faults in the Melville Bugt region also suggest an active hydrocarbon system. A 'bright spot' is a type of hydrocarbon indicator that may point to, for example, gas in sands. Potential mid-Cretaceous source intervals may, as farther south, be in the 'late oil window' (Gregersen *et al.* 2007), whereas the more deeply buried parts may be in the 'gas window'. The distances from the source kitchens to the mapped structures are mostly less than 50 km. The Cenozoic sediment cover generally exceeds 900 m over the Cretaceous structures. The potential seal sections of Late Cretaceous and Palaeogene ages are probably dominated by mudstones with local sands as known from outcrops and a few wells farther south (Dalhoff *et al.* 2003; Gregersen *et al.* 2007).

The seismic data from the eastern Baffin Bay region (BMP-00 from the year 2000) have increased our knowledge about the main structures and faults and have facilitated the interpretation of the basins, but new data are needed to increase our understanding of the geology and prospectivity of the region.

References

Bojesen-Koefoed, J.A., Christiansen, F.G., Nytoft, H.P. & Pedersen, A.K. 1999: Oil seepage onshore West Greenland: evidence of multiple source rocks and oil mixing. In: Fleet, A.J. & Boldy, S.A.R. (eds): Petroleum geology of Northwest Europe: Proceedings of the 5th conference, 305–314. London: Geological Society.

Bojesen-Koefoed, J.A., Bidstrup, T., Christiansen, F.G., Dalhoff, F., Gregersen, U., Nytoft, H.P., Nøhr-Hansen, H., Pedersen, A.K. & Sønderholm, M. 2007: Petroleum seepages at Asuk, Disko, West Greenland – implications for regional petroleum exploration. Journal of Petroleum Geology **30**, 219–236.

Dalhoff, F., Chalmers, J.A., Gregersen, U., Nøhr-Hansen, H., Rasmussen, J.A. & Sheldon, E. 2003: Mapping and facies analysis of Paleocene – Mid-Eocene seismic sequences, offshore southern West Greenland. Marine and Petroleum Geology **20**, 935–986.

Dam, G., Nøhr-Hansen, H., Christiansen, F.G., Bojesen-Koefoed, J.A. & Laier, T. 1998: The oldest marine Cretaceous sediments in West Greenland (Umiivik-1 borehole) – record of the Cenomanian–Turonian anoxic event? Geology of Greenland Survey Bulletin **180**, 128–137.

Dawes, P.R. 1997: The Proterozoic Thule Supergroup, Greenland and Canada: history, lithostratigraphy and development. Geology of Greenland Survey Bulletin **174**, 150 pp.

Gregersen, U., Bidstrup, T., Bojesen-Koefoed, J.A., Christiansen, F.G., Dalhoff, F. & Sønderholm, M. 2007: Petroleum systems and structures offshore central West Greenland: implications for hydrocarbon prospectivity. Geological Survey of Denmark and Greenland Bulletin **13**, 25–28.

Larsen, J.G. & Pulvertaft, T.C.R. 2000: The structure of the Cretaceous–Palaeogene sedimentary-volcanic area of Svartenhuk Halvø, central West Greenland. Geology of Greenland Survey Bulletin **188**, 40 pp.

MacLean, B., Falconer, R.K. & Levy, E.M. 1981: Geological, geophysical and chemical evidence for natural seepage of petroleum off the northeast coast of Baffin Island. Bulletin of Canadian Petroleum Geology **29**, 75–95.

Núñez-Betelu, L.K, Riediger, C.L. & Hills, L.V. 1993: Rock-eval analysis of the Cretaceous Bastion Ridge and Kanguk Formations, Axel Heiberg and Ellesmere Islands, Canadian Arctic Archipelago. Abstract (A-78), Annual Meeting of the Geological Association of Canada, Edmonton.

Oakey, G.N. 2005: Cenozoic evolution and lithosphere dynamics of the Baffin Bay – Nares Strait region of Arctic Canada and Greenland, 233 pp. Unpublished Ph.D. thesis, Vrije Universiteit, Amsterdam, The Netherlands.

Pedersen, A.K., Larsen, L.M., Pedersen, G.K. & Dueholm, K.S. 2006: Five slices through the Nuussuaq Basin, West Greenland. Geological Survey of Denmark and Greenland Bulletin **10**, 53–56.

Peel, J.S. & Sønderholm, M. (eds) 1991: Sedimentary basins of North Greenland. Bulletin Grønlands Geologiske Undersøgelse **160**, 164 pp.

Scherstén, A. & Sønderholm, M. 2007: Provenance of Cretaceous and Paleocene sandstones in the West Greenland basins based on detrital zircon dating. Geological Survey of Denmark and Greenland Bulletin **13**, 29–32.

Skaarup, N. & Pulvertaft, T.C.R. 2007: Aspects of the structure on the coast of the West Greenland volcanic province revealed in seismic data. Bulletin of the Geological Society of Denmark **55**, 65–80.

Whittaker, R.C., Hamann, N.E. & Pulvertaft, T.C.R. 1997: A new frontier province offshore northwest Greenland; structure, basin development, and petroleum potential of the Melville Bay area. American Association of Petroleum Geologists Bulletin **81**, 978–998.

Author's address

Geological Survey of Denmark and Greenland, Øster Voldgade 10, DK-1350 Copenhagen K, Denmark. E-mail: *ug@geus.dk*

Geochemistry of greenstones in the Tasiusarsuaq terrane, southern West Greenland

Anders Scherstén, Henrik Stendal and Tomas Næraa

Tonalite-trondhjemite–granodiorite (TTG) gneisses and melanocratic to ultramafic greenstones dominate the Archaean basement of southern West Greenland. The greenstones are likely to represent different original environments, which is important as the mineral deposits they may host depend on this. For example, massive sulphide deposits associated with gold and base metals are commonly volcanogenic, while chrome, nickel and platinum group elements are more commonly associated with layered intrusions (Robb 2005). Current investigations by the Geological Survey of Denmark and Greenland (GEUS) in southern West Greenland are therefore focused on the origin of greenstones and their relationship to associated TTG gneisses.

Here, we report on work in progress on greenstones within the Tasiusarsuaq terrane (Fig. 1; Friend *et al.* 1996). They differ from many other greenstone belts in southern West Greenland in their spatial association with the TTG gneisses. Unlike the Isua, Ivisârtoq and Storø greenstone belts in the central and northern Nuuk region, the Tasiusarsuaq greenstones are not proximal to terrane boundaries but form dismembered blocks and slivers within the terrane (Fig. 1). Contact relationships to the gneisses are almost exclusively tectonic, and primary textures are, with rare exceptions, obliterated by amphibolite to granulite facies metamorphism.

Field relationships

Stendal & Scherstén (2007) documented one of the rare examples of well-preserved field relationships for a volcanic pile of pillow basalts, rhyolites (*sensu lato*) and melanocratic-ultramafic tuffs and flows on 'Nunatak 1390' (Fig. 1). The rhyolite was extruded at 2.876 ± 0.005 Ga (Næraa & Scherstén 2008 – this volume), which is the minimum age for the basalts and within the known age range for the Tasiusarsuaq terrane.

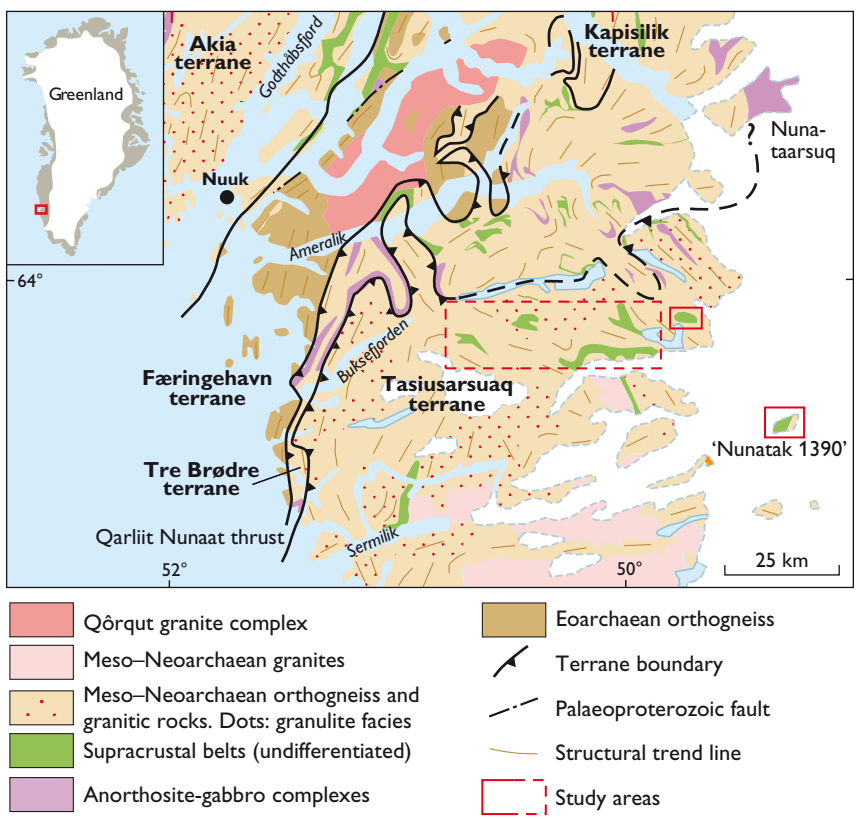

Fig. 1. Generalised map of the northern part of the Tasiusarsuaq terrane. The northern boundary as suggested by Friend *et al.* (1996) is outlined with solid and stippled lines for more or less well-determined demarcations of the terrane. It is likely that the border extends farther to the north in the eastern part (cf. Næraa & Scherstén 2008 – this volume; B. Windley and A.A. Garde, personal communication 2008). Sampling areas are highlighted by red boxes, and the two main sampling areas are indicated by solid lines.

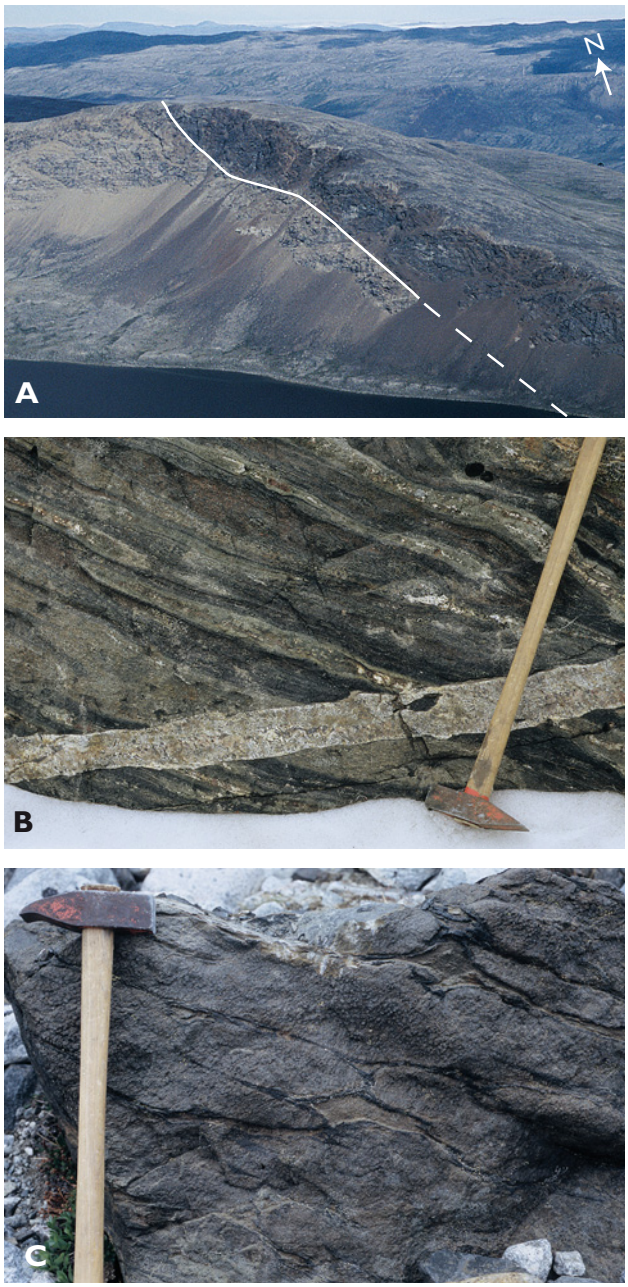

Fig. 2. **A**: Tasiusarsuaq greenstones displaying a tectonic contact with the Tasiusarsuaq grey TTG gneises; the greenstones seem to have been thrust northwards. **B**: Variably deformed pillows, sometimes with elongate calc-silicate aggregates, demonstrating a supracrustal origin for the greenstones. Such rocks are found throughout the area (cf. Stendal & Scherstén 2007, fig. 4). The flattened pillows are cross-cut by a granite dyke of unknown age. **C**: Pillow-like structures among ultramafic rocks.

Here, we make the assumption that the rhyolite date establishes the age for the majority of the greenstones within the Tasiusarsuaq terrane.

To the north-west of 'Nunatak 1390', a melanocratic to ultramafic complex forms a tectonic lens, with internal top-to-the-north thrust planes that reflect tectonic emplacement against the gneisses (Figs 1, 2A). The rocks range from ultramafic olivine-pyroxene-rich cumulates to basaltic amphibolites, sometimes with flattened pillow lavas and calc-silicates (Fig. 2B). Ultramafic rocks with pillow-like structures were also observed, and the complex is interpreted to be dominated by basaltic to komatiitic flows and shallow sills (Fig. 2C).

Similar dismembered bodies are scattered within the Tasiusarsuaq terrane but are commonly more deformed and do not preserve primary textures. The ultramafic rocks have been divided into two groups on the basis of their field appearance, with the first group containing ultramafic rocks of cumulate or undetermined origin and the second comprising ultramafic rocks with eruptive features such as pillow structures. Only the eruptive ultramafic rocks will be considered here.

Whole-rock geochemistry

The rocks considered here are dominated by tholeiitic metavolcanic amphibolites and meta-ultramafic rocks of komatiitic composition. The ultramafic rocks are signified by MgO >16 wt%, Al_2O_3 <5.5 wt%, high Ni and Cr (>500 and >1500 ppm, respectively), and Al_2O_3/TiO_2 ratios <10, while the amphibolites have MgO <10 wt%, Al_2O_3 >10 wt%, Ni and Cr (<250 and <500 ppm, respectively) and Al_2O_3/TiO_2 ratios of 7–37, of which most ratios are >10 (Fig. 3). The ultramafic rocks are aluminium depleted and show strong positive correlation between Ni and MgO (Fig. 3), which is presumably controlled by olivine and pyroxene fractionation. Al_2O_3/TiO_2 ratios of 10–40 for the amphibolites and <10 for the ultramafic eruptives imply a deeper melt origin (>5 GPa, i.e. >150 km) for the ultramafic rocks (Walter 1998). On 'Nunatak 1390' at least some of the ultramafic rocks seem to be intercalated with basaltic pillow lavas, which might suggest that they formed sills that are younger than the basalts (Stendal & Scherstén 2007). This could imply that the depth of melting increased with time (presuming that the ultramafic rocks are indeed slightly younger than the pillow lavas), or that shallow melting was induced by the deeper melts if they were contemporaneous.

The ultramafic rocks have smooth trace element patterns, but with Nb/Th ratios that are lower than the primitive mantle (PM; Fig. 4). This implies some degree of enrichment in the mantle source, or that the Nb/Th ratios have decreased due to shallow continental crustal contamination. The light rare-earth element (REE) signatures are horizontal, whereas the mid- to heavy REE signature slopes towards lower abundances, indicating a garnet residue during mantle melting, which is consistent with their deep origin as discussed above (Fig. 4). The REE signatures of the amphibolites are similar to those of the ultramafic rocks, but with slightly higher con-

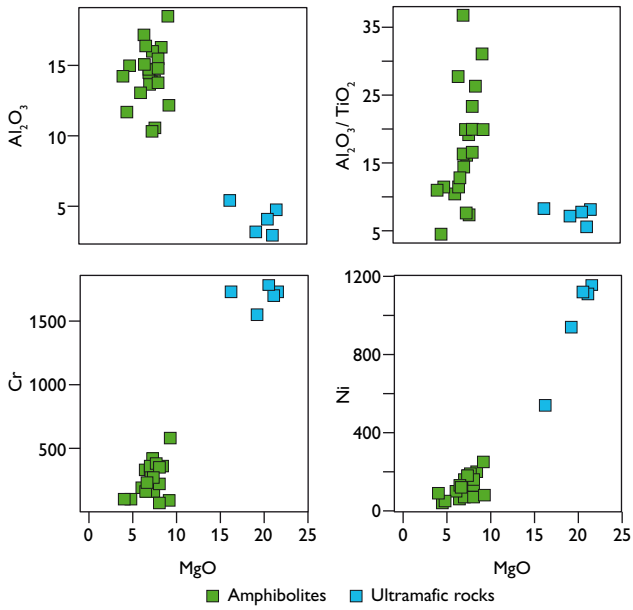

Fig. 3. MgO bivariate plots for a selected oxide, an oxide ratio and compatible trace elements. See text for further discussion.

centrations, and lacking the garnet signature noted for the ultramafic rocks (Fig. 4). Nb/Th ratios are generally PM-like. Overall, the amphibolites are generally more mid-oceanic ridge basalt (MORB)-like in their range of trace element ratios and abundances. In particular, one core of a pillow basalt from 'Nunatak 1390' consistently lacks continental crustal (or arc-like) trace element patterns.

Crustal contamination

The general geochemical signatures and the subaqueous nature of the amphibolites and ultramafic rocks are consistent with an ocean-floor origin in its broadest sense. The MORB-like signatures of the amphibolites might be suggestive of an ocean basin, a back-arc basin or even a primitive tholeiitic arc. However, a major extensional setting such as a mid-ocean ridge is at odds with major simultaneous continental crust formation, which is indicated by e.g. massive volumes of presumably contemporaneous TTG crystallisation (Næraa & Scherstén 2008 – this volume), while a back-arc basin seems more conceivable. The trace-element arrays indicate source enrichment, i.e. variable amounts of enriched subduction components, or local contamination during emplacement (Fig. 4). Positive correlations for Nb/Th and Nb/La against the Th or La concentration reciprocals lie between mantle and continental crustal end-members, and these ratios are the most sensitive to small degrees of conta-

Fig. 4. Primitive mantle (Palme & O'Neill 2004) normalised trace element diagram for Tasiusarsuaq greenstones, one pillow lava from 'Nunatak 1390' and selected reference rocks and reservoirs. For comparison plots of N-MORB (Hofmann 1988), OIB (Sun & McDonough 1989), Archaean TTG (Martin 1995; Martin *et al.* 2005), Lau basin back-arc (Regelous *et al.* 2008) and median Tonga arc basalts (http://georoc.mpch-mainsz.gwdg.de/georoc) are shown. **Inset**: N-MORB, Lau basin back-arc basalts and OIB are characterised by Nb/Th ratios that are higher than PM, while median Tonga arc basalts and TTG have ratios that are lower than PM. The Tasiusarsuaq ultramafic rocks and one pillow lava have arc-like ratios lower than PM Nb/Th, while the amphibolites are variable with both sub- and supra-PM ratios. Minor TTG contamination of magmas with MORB-like ratios would rapidly decrease Nb/Th with associated increasing La/Sm, as these ratios are extreme in TTG. A plot of Nb/Th against chondrite normalised La/Sm is shown in the figure inset for the Tasiusarsuaq data, displaying a moderate fit with a mixing scenario as discussed above.

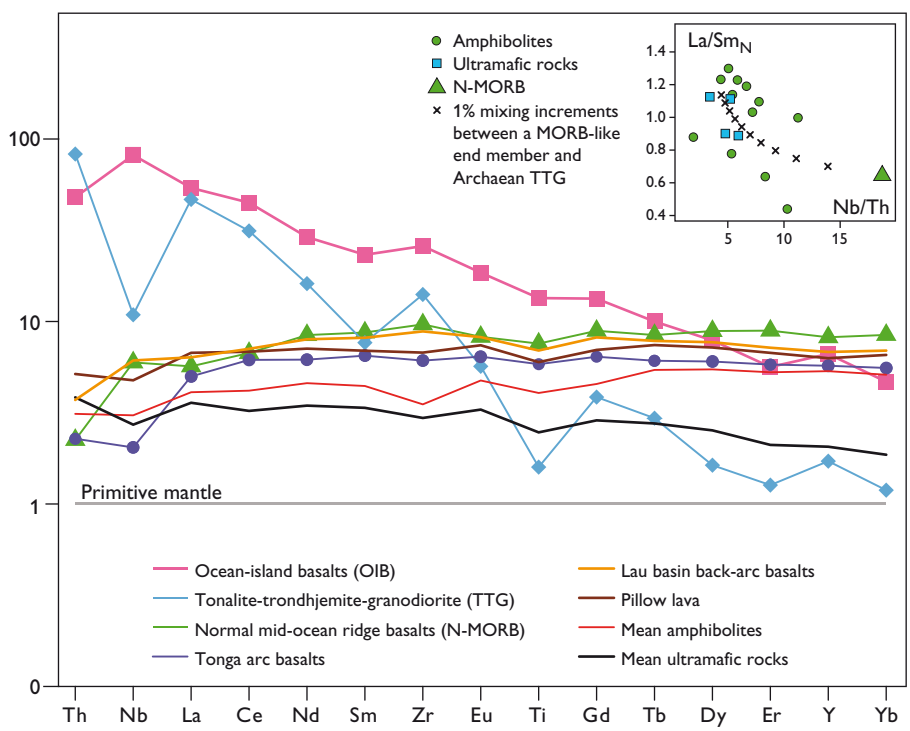

mination. Assuming a TTG crustal component as the contaminant, the array can be explained by <5% contamination for all but one sample, supposing that the most primitive ultramafic rocks are uncontaminated.

Tectonic implications

If the basalt–komatiite magmatism in the Tasiusarsuaq terrane is indeed concurrent with TTG-formation, an arc environment for the former magmatism is favoured (cf. Stendal & Scherstén 2007; Næraa & Scherstén 2008 – this volume), and such a hypothesis is still viable in the light of the current geochemical data. The origin of komatiites remains controversial, although most authors advocate a mantle-plume related origin. The komatiite-like rocks documented here do not readily fit such an origin as they seem to be primarily associated with subduction and growth of continent crust. Alternatively, renewed models for subduction-related komatiite genesis might be considered. However, this scenario typically involves shallow melting (Grove & Parman 2004), while the REE ratios observed here favour deep melting with residual garnet.

Outlook

Further work with detailed field studies and geochronology over the next few years will hopefully shed new light on these outstanding issues. Emphasis will be placed on searching for primary relationships between the TTG gneisses and the ultramafic rocks and amphibolites in conjunction with detailed geochronology and geochemistry.

References

Friend, C.R.L., Nutman, A.P., Baadsgaard, H., Kinny, P.D. & McGregor, V.R. 1996: Timing of late Archaean terrane assembly, crustal thickening and granite emplacement in the Nuuk region, southern West Greenland. Earth and Planetary Science Letters **142**, 353–365.

Grove, T.L. & Parman, S.W. 2004: Thermal evolution of the Earth as recorded by komatiites. Earth and Planetary Science Letters **219**, 173–187.

Hofmann, A.W. 1988: Chemical differentiation of the Earth: the relationship between mantle, continental crust, and oceanic crust. Earth and Planetary Science Letters **90**, 297–314.

Martin, H. 1995: Archean grey gneisses and the genesis of continental crust. In: Condie, K.C. (ed.): Archean crustal evolution, 205–260. Amsterdam: Elsevier.

Martin, H., Smithies, R.H., Rapp, R., Moyen, J.-F. & Champion, D. 2005: An overview of adakite, tonalite-trondhjemite-granodiorite (TTG), and sanukitoid: relationships and some implications for crustal evolution. Lithos **79**, 1–24.

Næraa, T. & Scherstén, A. 2008: Zircon age perspective on the Tasiusarsuaq terrane, southern West Greenland. Geological Survey of Denmark and Greenland Bulletin **15**, 73–76.

Palme, H. & O'Neill, H.S.C. 2004: Cosmochemical estimates of mantle composition. In: Carlson, R.W. (ed.): Treatise on geochemistry **2**, 1–38. Amsterdam: Elsevier.

Regelous, M., Turner, S., Falloon, T.J., Taylor, P., Gamble, J. & Green, T. 2008: Mantle dynamics and mantle melting beneath Niuafo'ou Island and the northern Lau back-arc basin. Contributions to Mineralogy and Petrology. DOI: 10.1007/s00410-007-0276-7.

Robb, L. 2005: Introduction to ore-forming processes, 373 pp. Oxford: Blackwell Science Ltd.

Stendal, H. & Scherstén, A. 2007: A well-preserved bimodal volcanic succession in the Tasiusarsuaq terrane, South-West Greenland. Geological Survey of Denmark and Greenland Bulletin **13**, 53–56.

Sun, S.-s. & McDonough, W.F. 1989: Chemical and isotopic systematics of oceanic basalts: implications for mantle composition and processes. In: Saunder, A.D. & Norry, M.J. (eds): Magmatism in the ocean basins. Geological Society Special Publication (London) **42**, 313–345.

Walter, M.J. 1998: Melting of garnet peridotite and the origin of komatiite and depleted lithosphere. Journal of Petrology **39**, 29–60.

Authors' address

Geological Survey of Denmark and Greenland, Øster Voldgade 10, DK-1350 Copenhagen K, Denmark. E-mail: *asch@geus.dk*

New zircon ages from the Tasiusarsuaq terrane, southern West Greenland

Tomas Næraa and Anders Scherstén

In the last three field seasons the Geological Survey of Denmark and Greenland (GEUS) has undertaken mapping in the south-eastern part of the Nuuk region in southern West Greenland, and here we present new zircon ages that help constrain the northern boundary of the Tasiusarsuaq terrane. The Archaean geology of the Nuuk region is commonly interpreted as a tectonic collage assembled through lateral accretion and collision of oceanic and continental slivers and blocks (e.g. Friend & Nutman 2005). Popular jargon describes these as terranes, bounded by faults or mylonite zones and characterised by rocks of contrasting origin on either side of their tectonic boundaries (Coney *et al.* 1980). The Isukasia and Færingehavn terranes (Figs 1, 2) are the oldest terranes at ≥3.75 Ga, and extend from the outer part of Godthåbsfjord in the south-west to the margin of the Inland Ice in the north-east, but they might not have a common geological history (Friend & Nutman 2005). The Tre Brødre terrane is mainly represented by the Ikkatoq gneiss and occurs in close spatial relationship with the Færingehavn terrane, and also as a pronounced thrust unit along the Qarliit Nunaat thrust between the Færingehavn and Tasiusarsuaq terranes (Fig. 1; Nutman *et al.* 1989). The terrane boundaries in the inner fjord region near the Inland Ice margin are less well constrained; the Tre Brødre terrane extends into the region from the south-west, the Kapisilik terrane is defined from the northern and eastern part and borders the Tasiusarsuaq terrane to the south and possibly to the east.

The terrane accretion is believed to have taken place in two events. The first terrane accretion is defined from the northern part of the region, and possibly involves the Isukasia, Kapisilik and Akia terranes. The thermal event stitching these terranes is dated to *c.* 2.99–2.95 Ga (Fig. 2; Hanmer *et al.* 2002; Friend & Nutman 2005). The second accretion phase of the major continental blocks is believed to have occurred at around 2.725–2.71 Ga. This second event is well described, and includes anatexis and emplacement of continental crust-derived granites, which are associated with contemporaneous metamorphism (Friend *et al.* 1996).

Figure 2 outlines regional plutonic, metamorphic and supracrustal events. Individual terranes were formed during relatively short time periods with active geological processes of creation and recycling of continental crust, and most of the terranes follow a similar pattern of development. The first plutonic events consisted of primitive magmas and produced tonalite–trondhjemite–granodiorite (TTG) and dioritic gneisses. Younger, more evolved granitic magmas were often intruded simultaneously with high-grade metamorphism. This development may reflect a stabilisation of the individual terranes.

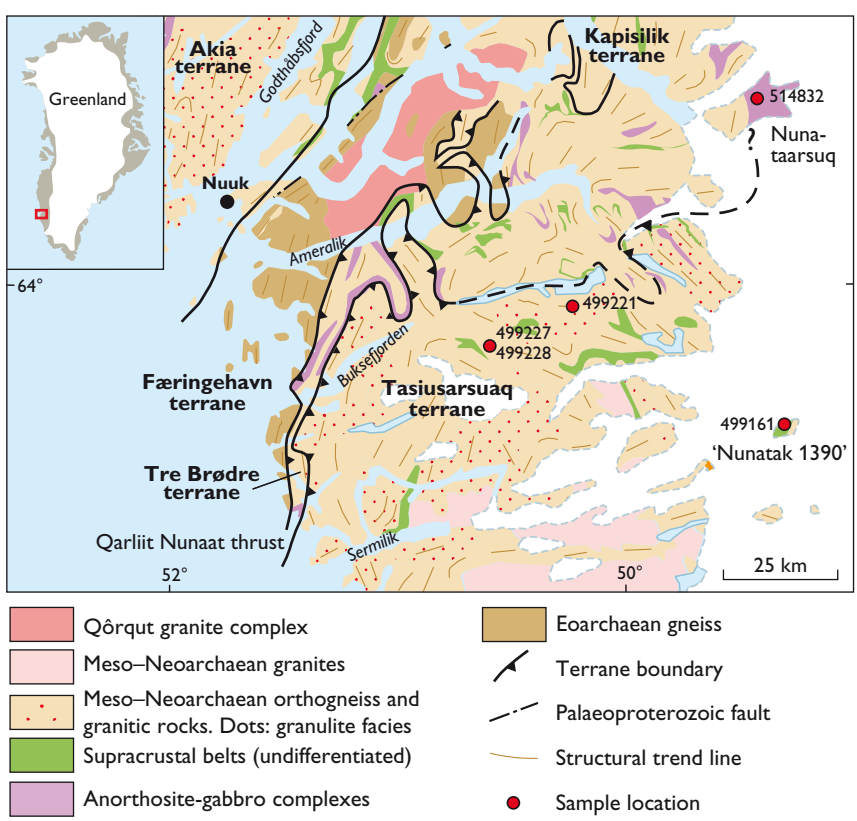

Fig. 1. Geological map of the southern Nuuk region (modified from Escher & Pulvertaft 1995), with locations and numbers of samples discussed in this paper.

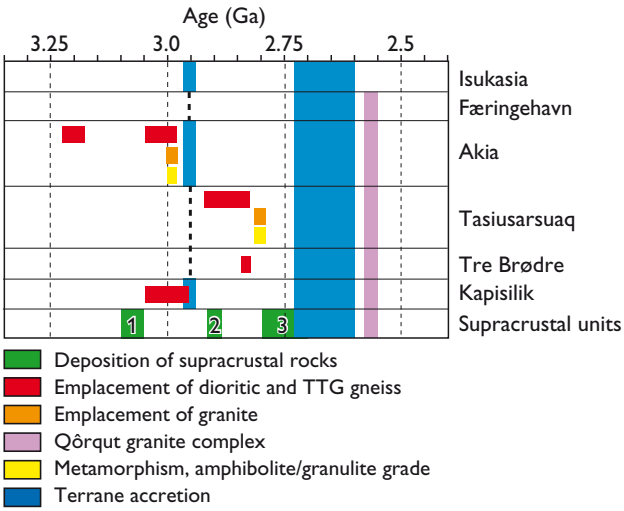

Fig. 2. Time lines for igneous and metamorphic events in the Nuuk region. Numbers for the supracrustal units refer to (1) Ivisaartoq and Qussuk, (2) 'Nunatak 1390' and (3) Storø. Data from Pidgeon & Kalsbeek (1978), Friend & Nutman (2001), Crowley (2002), Hanmer *et al.* (2002), Friend & Nutman (2005), Polat *et al.* (2008), Nutman & Friend (2007), Garde (2007) and Knudsen *et al.* (2007).

The Tasiusarsuaq terrane

The Tasiusarsuaq terrane is dominated by 2.92–2.84 Ga tonalite and granodiorite gneisses (Friend & Nutman 2001; Crowley 2002). The main regional metamorphism is of amphibolite facies grade, however, granuite facies or retrogressed granulite facies rocks are present in large areas (Fig. 1). Peak granulite facies conditions have been dated at 2.81–2.79 Ga (Pidgeon & Kalsbeek 1978; Crowley 2002). Greenschist facies rocks have been observed on 'Nunatak 1390', which we in the present article suggest is part of the Tasiusarsuaq terrane.

Northern boundary of the Tasiusarsuaq terrane

The north-western boundary of the Tasiusarsuaq terrane in the Buksefjorden area (Fig. 1) has been described in some detail. Narrow mylonite zones define a boundary between granulite facies gneisses of the Tasiusarsuaq terrane and prograde amphibolite facies gneisses of the Tre Brødre terrane. Prograde amphiolite facies metamorphism dated at around 2.74–2.70 Ga is presumably related to the terrane accretion and has not been recorded within the Tasiusarsuaq terrane itself (Crowley 2002), which was thrust upon the Tre Brødre terrane during orogenesis (Nutman *et al.* 1989). The eastern extension of the northern Tasiusarsuaq terrane boundary remains speculative. Here we present zircon U-Pb age data from six selected rock samples collected in the vicinity of the proposed eastern extension of the northern Tasiusarsuaq terrane boundary.

Tasiusarsuaq tonalite

A migmatised tonalite representative of the basement gneisses in the northern part of the terrane was collected for zircon U-Pb age determination (Fig. 1; sample 499221 in the Survey numbering system). The rock contains lenses of amphibolite and has abundant migmatite veins. Palaeosome was separated from neosome by sawing slabs of each, and both sub-samples were dated. The internal zircon textures are very similar in both palaeosome and neosome. Zircon grains have complex internal textures often with dark shells separating the core from the rim (Fig. 3a, b). The cores display igneous oscillatory zonation to homogeneous textures. The age data for the palaeosome are concordant within 10% for 63 spots (n = 65), and regress to an essentially zero age lower intercept. We therefore use the $^{207}Pb/^{206}Pb$ ratios, which yield an age of 2.868 ± 0.004 Ga (Fig. 4a; n = 62/65, ± 2σ, MSWD = 1.5). The outliers are slightly younger, presumably due to ancient Pb loss. The neosome data are concordant within 10% for 55 spots (n = 57; Fig. 4b); close inspection of the $^{207}Pb/^{206}Pb$ age data indicates that two ages at *c.* 2.87 and *c.* 2.80 Ga can be differentiated (Fig. 4b). However, this is speculative as the data suffer from insufficient precision in conjunction with an apparent 'age smear' as noted in the palaeosome, presumably due to ancient Pb-loss. Nevertheless, the two suggested ages at *c.* 2.87 and *c.* 2.80 Ga are in excellent agreement with the palaeosome date and known ages for granulite facies metamorphism in the region (Pidgeon & Kalsbeek 1978; Crowley 2002). Discordant granite sheets 2.72 Ga old cut the gneisses in this part of the Tasiusarsuaq terrane (Friend *et al.* 1996), but no such age component was found in this rock.

'Nunatak 1390' and Nunataarsuk

'Nunatak 1390' comprises rocks with some of the best preserved primary textures and structures found in the Tasiusarsuaq terrane. In brief, 'Nunatak 1390' contains a volcanic series with variably preserved pillow lava sequences that are succeeded by melanocratic-ultramafic ash and rocks with flow structures (Stendal & Scherstén 2007). Rhyolitic rocks

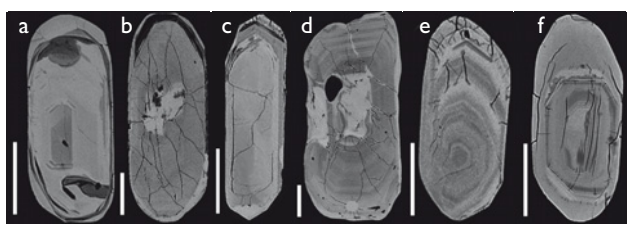

Fig. 3. Backscattered electron images of representative zircon grains for each dated sample. Zircons were separated, picked, mounted in epoxy and polished to expose the central part of the grains. Scale bars = 50 µm. (a) 499221 palaeosome; (b) 499221 neosome; (c) 499161; (d) 514832; (e) 499227; (f) 499228.

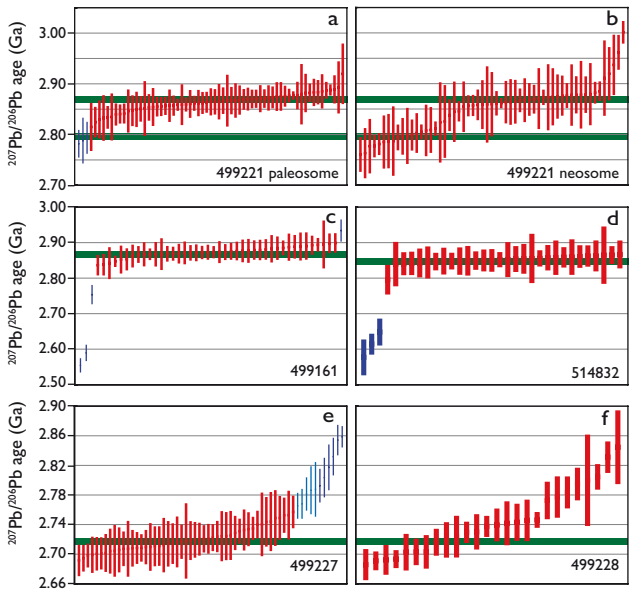

Fig. 4. Zircon 207Pb/206Pb ages. All errors presented at 2 sigma levels. (a) Sample 499221 palaeosome. The red bars represent data used to calculate crystallisation age (green horizontal bar). Five blue bars are rejected due to assumed ancient lead loss. (b) Sample 499221 neosome. The upper green horizontal bar represents the crystallisation age for the paleosome and the lower green horizontal bar represents the known granulite facies event for the Tasiusarsuaq terrane. (c, d) Samples 499161 and 514832. The red bars represent data used to calculate crystallisation ages (green horizontal bar) and the blue bars were rejected due to assumed ancient lead loss. (e) Sample 499227: Red bars represent data used to calculate crystallisation or metamorphic age (green horizontal bar), and the blue bars are assumed to be inherited from an older source. (f) Sample 499228. The red bars define an ancient lead loss trend with age components as in sample 499227. Age determinations were carried out on the Element 2 Laser ICPMS at GEUS. Detailed analytical procedures are described in Frei et al. (2006).

are intercalated with the pillow lava sequences, and were interpreted as ignimbrites by Stendal & Scherstén (2007). In 2007, however, intrusive discordant dykes that appear to feed into the rhyolites were discovered, and it may be that some or all of these rocks are significantly younger sills. Zircons were extracted from a rhyolite sample (499161) for dating, and in spite of the alternative interpretations either date the pillow lava sequence or provide a minimum age for it. The zircon grains have bright homogeneous cores and darker rims and/or zones within the cores (Fig. 3c). The dark areas may extend into the bright areas and contain minor amounts of Ca and Al, which could indicate destabilisation and partial zircon breakdown. Of 48 age determinations 43 define a recent Pb loss line and a ^{207}Pb/^{206}Pb age of 2.873 ± 0.005 Ga (n = 43/48, ± 2σ, MSWD = 1.7). One grain (two analyses) is concordant at *c.* 3.2 Ga. We interpret the 2.873 ±0.005 Ga age to represent the time of crystallisation of the rhyolite. The origin of the 3.2 Ga old grain is unclear, but we speculate that it is inherited from rocks of this age. Gneisses with palaeosomes of this age have been found farther to the west in the Tasiusarsuaq terrane (Næraa & Scherstén, unpublished data).

Eastern Nunataarsuk is characterised by an anorthosite-amphibolite-granite succession. Granite sample 514832 for geochronology is from an area where granite and slices of amphibolite with local pillow structures in low-strain areas form the major successions; the granite-amphibolite contact is either an irregular and intrusive or a boudinaged contact parallel to the foliation, and the granite is interpreted as late to posttectonic relative to a locally defined S1 foliation (Kolb & Stendal 2007). Zircon grains from the granite have oscillatory-zoned cores surrounded by thin homogeneous rims (Fig. 3d). Oscillatory-zoned grains plot along a recent Pb-loss line and yielded a ^{207}Pb/^{206}Pb age of 2.852 ± 0.005 Ga (n = 30/33, ± 2σ, MSWD = 0.30, concordant within 10%), which we interpret as the intrusive age of the granite. The rims were generally too narrow to be analysed with our standard 20 µm laser spot; however, three analyses gave a poorly defined upper intercept age of 2.58 ± 0.04 Ga.

Veined gneiss and cross-cutting tonalitic schist

In the southern part of the region, a slightly schistose tonalite (499227) has an intrusive cross-cutting relationship to a veined tonalitic gneiss (499228) with amphibolite enclaves. Abundant veins of granitic pegmatite appear to have formed by partial melting of the veined gneiss along amphibolite boudin necks, along the foliation and along the tonalite-gneiss contacts. The zircon grains from the tonalite (499227) have complex internal textures. Many of them have oscillatory zoned cores and homogeneous rims and/or internal zones (Fig. 3e). A total of 49 of 60 U-Pb zircon age determina- tions define a ^{207}Pb/^{206}Pb age of 2.719 ± 0.005 Ga (n = 49/60, ± 2σ, MSWD = 2.2, concordant from 91 to 113%). The remaining 11 age determinations form an array towards older ages and presumably represent ancient Pb-loss in grains as old as *c.* 2.859 ± 0.014 Ga (single grain ^{207}Pb/^{206}Pb age; Fig. 4e). The zircon grains from the veined gneiss (499228) generally have thick, homogeneous, bright rims surrounding cores that are highly cracked and commonly metamict; only a few cores show remains of oscillatory zonation (Fig. 3f). The spread in ages indicates ancient lead loss from 2.85 to 2.7 Ga with no obvious ^{207}Pb/^{206}Pb age plateau (Fig. 4f); one grain was dated at *c.* 3.1 Ga. The interpretation of the age data remains speculative, but given the altered appearance, the metamorphic rims and the relationship with the tonalite (499227), it seems reasonable to assume a metamorphic overprinting of the rock at *c.* 2.72 Ga, perhaps related to the accretion with the Tre Brødre terrane.

Discussion and summary

The zircon crystallisation age of 2.87–2.85 Ga for samples 499221, 499161 and 514832 and a somewhat speculative metamorphic age at 2.80 Ga for sample 499221 correlate very well with known crystallisation ages and granulite facies events within the Tasiusarsuaq terrane. These ages are significantly younger than ages of rocks from the Kapisilik terrane but older than those of the Tre Brødre terrane. It is thus tempting to ascribe these areas to the Tasiusarsuaq terrane. To include the 'Nunatak 1390' is straightforward, while including Nunataarsuk implies a major northerly extension of the terrane that requires confirmation by further work. Age data alone naturally do not justify the inclusion of these areas into the Tasiusarsuaq terrane, but it appears to be the most straightforward option based on the available information. More importantly, the ages obtained from the rhyolite and granite at 'Nunatak 1390' (2.873 Ga) and Nunataarsuk (2.853 Ga) provide minimum extrusive ages for the associated mafic greenstones and might reflect the onset of crustal growth in this block. Furthermore, the emerging terrane configuration might indicate that the Tasiusarsuaq terrane accreted with the Kapisilik terrane in the north-east and with the Tre Brødre terrane in the south-west.

The ages from the schistose tonalite (499227) and the veined gneiss (499228) are too young to readily represent known events within the Tasiusarsuaq terrane. The inferred metamorphic ages rather correlate with the thermal event associated with prograde amphibolite facies metamorphism within the Tre Brødre terrane. However, situated well within the Tasiusarsuaq terrane these rocks would not have experienced a prograde metamorphic path during terrane accretion. Furthermore, there is evidence for ≥2.85 Ga old zircons, which are too old to readily fit with known ages of the Tre Brødre terrane. We speculate that the northern part of the Tasiusarsuaq terrane may represent a nappe complex, and that the investigated rocks either represent a tectonic window exposing footwall rocks that experienced prograde metamorphism and partial melting during overthrusting, or that fluids released from footwall-induced zircon Pb-loss and/or partial melting in the overriding nappe.

References

Coney, P.J., Jones, D.L. & Monger, J.W. 1980: Cordilleran suspect terranes. Nature **288**, 329–332.

Crowley, J.L. 2002: Testing the model of late Archean terrane accretion in southern West Greenland: a comparison of the timing of geological events across the Qarliit nunaat fault, Buksefjorden region. Precambrian Research **116**, 57–79.

Escher, J.C. & Pulvertaft, T.C.R. 1995: Geological map of Greenland, 1:2 500 000, Copenhagen: Geological Survey of Greenland.

Frei, D., Hollis, J.A., Gerdes, A., Harlov, D., Karlsson, C., Vasquez, P., Franz, G., Johansson, L. & Knudsen, C. 2006: Advanced in situ geochronological and trace element microanalyses by laser ablation techniques. Geological Survey of Denmark and Greenland Bulletin **10**, 25–28.

Friend, C.R.L. & Nutman, A.P. 2001: U-Pb zircon study of tectonically bounded blocks of 2940–2840 Ma crust with different metamorphic histories, Paamiut region, South-West Greenland: implications for the tectonic assembly of the North Atlantic craton. Precambrian Research **105**, 143–164.

Friend, C.R.L. & Nutman, A.P. 2005: New pieces to the Archaean terrane jigsaw puzzle in the Nuuk region, southern West Greenland: steps in transforming a simple insight into a complex regional tectonothermal model. Journal of the Geological Society (London) **162**, 147–162.

Friend, C.R.L., Nutman, A.P., Baadsgaard, H., Kinny, P.D. & McGregor, V.R. 1996: Timing of late Archaean terrane assembly in the Nuuk region, southern West Greenland. Earth and Planetary Science Letters **142**, 353–365.

Garde A.A. 2007: A mid-Archaean island arc complex in the eastern Akia terrane, Godthåbsfjord, southern West Greenland. Journal of the Geological Society (London) **164**, 565–579.

Knudsen, C., van Gool, J.A.M., Østergaard, C., Hollis, J.A., Rink-Jørgensen, M., Persson, M. & Szilas, K. 2007: Gold-hosting supracrustal rocks on Storø, southern West Greenland: lithologies and geological environment. Geological Survey of Denmark and Greenland Bulletin **13**, 41–44.

Kolb, J. & Stendal H. 2007: Geological environments and hydrothermal mineralisation in Nunataarsuk, Qarliit Nunaat and Ameralik, Nuuk region, SW Greenland – a field report 2007. Mineral resource assessment of the Archaean Craton (66° to 63°30´N), SW Greenland. Contribution no. 2. Danmarks og Grønlands Geologiske Undersøgelse Rapport **2007/58**, 44 pp.

Nutman, A.P. & Friend, C.R.L. 2007: Adjacent terranes with ca. 2715 and 2650 Ma high-pressure metamorphic assemblages in the Nuuk region of the North Atlantic Craton, southern West Greenland: Complexities of Neoarchaean collisional orogeny. Precambrian Research **155**, 159–203.

Nutman, A.P., Friend, C.R.L., Baadsgaard, H., & McGregor, V.R. 1989: Evolution and assembly of Archaean gneiss terranes in the Godthåbsfjord region, southern West Greenland: structural, metamorphic and isotopic evidence. Tectonics **8**, 573–589.

Pidgeon, R.T. & Kalsbeek, F. 1978: Dating of igneous and metamorphic events in the Fiskenaesset region of southern West Greenland. Canadian Journal of Earth Sciences **15**, 2021–2025.

Polat A., Frei, R., Appel, P.W.U., Dilek, Y., Fryer, B., Ordóñez-Calderón, J.C. & Yang, Z. 2008: The origin and composition of Mesoarchean oceanic crust: Evidence from the 3075 Ma Ivisaartoq greenstone belt, SW Greenland. Lithos **100**, 293–321.

Stendal, H. & Scherstén, A. 2007: A well-preserved bimodal Archaean volcanic succession in the Tasiusarsuaq terrane, South-West Greenland. Geological Survey of Denmark and Greenland Bulletin **13**, 53–56.

Authors' address

Geological Survey of Denmark and Greenland, Øster Voldgade 10, DK-1350 Copenhagen K, Denmark. E-mail: *tomn@geus.dk*

Hans Ø, celebrated island of Nares Strait between Greenland and Canada: from dog-sledge to satellite mapping

Peter R. Dawes and Tapani Tukiainen

Hans Ø – or Tartupaluk to the indigenous population of North-West Greenland – is a small steeply sided island in Nares Strait at *c.* 80°50´N. Charted in 1871 and named after Greenlander Hans Hendrik, it is one of five limestone islands forming an integral part of the Greenland Silurian succession. Rising less than 170 m above normally ice-infested waters, the 1.25 km^2 island is physiographically far overshadowed by nearby Franklin Ø (Fig. 1).

The island's notoriety results from its placing more or less equidistant between the coasts of Kennedy Channel on the political boundary between Greenland and Canada. For 40 years the rocky patch has been the subject of a dispute between the Danish/Greenland and Canadian governments regarding sovereignty rights, an issue that remains unresolved. However, there is mutual understanding between Canada and Denmark that "since the question of sovereignty over the island has not yet been solved no action should be taken by either side which might prejudge the settlement of the issue" (Brückner 1984). Formally, this remains the position today.

2007 developments and this article

In 2007, two geological map sheets entitled 'Hans Island, Nunavut' were released by the Canadian government. Forming part of a richly illustrated report, the maps with structural cross-sections portray the island's geology and that of Kennedy Channel at scales 1:5000 and 1:100 000, respectively (Harrison *et al.* 2007). Also released are offshore geophysical and bathymetric data, including seismic and refraction profiles, obtained with the Canadian Coast Guard ice-breaker *Louis S. St-Laurent*.

The new data are an important addition to scientific knowledge of Nares Strait. However, the section 'History of geological research' does not match the excellence of the rest of Harrison *et al.'s* report. Beginning with Canadian geodetic activities in 1953, the section continues: "It has been reported that Robert L. Christie of the Geological Survey of Canada visited Hans Island between 1957 and 1966 during geological mapping on northeastern Ellesmere Island (see Dawes, 2004)". Yet, Dawes (2004) makes no mention of any such visit. Indeed, this author – who worked very closely with the late Dr. Christie on the history of exploration of Nares Strait and participated in his field programme in 1965 and 1966 – doubts that he ever set foot on the island or even planned to. Harrison *et al.* (2007) list further Canadian activity on and around Hans Ø but limit comment on Danish geological research to: "It is evident that Danish geologists have also visited Hans Island. There is a bedding attitude recorded on the island on the map of Dawes and Garde (2004) who consider bedrock here to be an exposure of the Cape Morton Formation of Silurian age". However, in a postscript, acknowledgement is given to Lauge Koch's map from 1922 with reference to Dawes & Haller (1979).

By any standards this is meagre reporting, particularly so since the island was initially mapped by Danish geologists and has appeared as an integral part of the Silurian of Washington Land on Danish maps for more than 75 years (e.g. Koch 1931; Troelsen 1950; Jepsen *et al.* 1983). The lack of reference to these studies seems even more odd when early Canadian geological maps of north-eastern Ellesmere Island covering the latitude of Hans Ø – for example, Christie (1964, 1967) – do not portray the island, and neither does the 1:250 000 map of Kennedy Channel that is part of the Canadian national map sheet coverage (Kerr 1973).

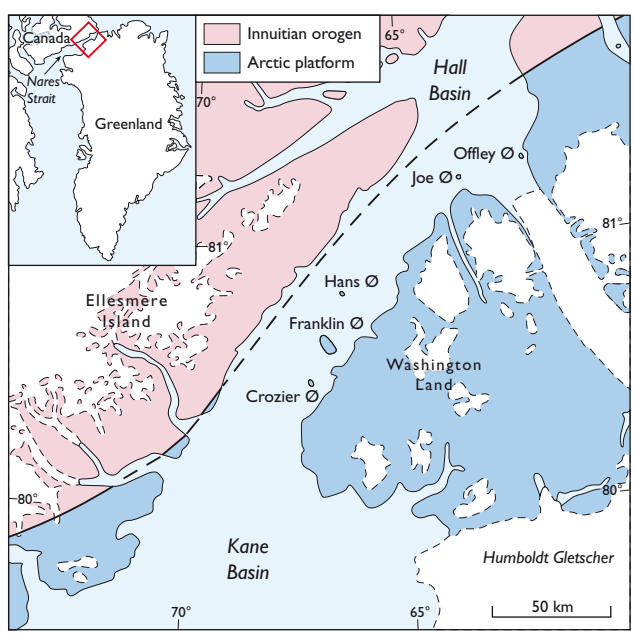

Fig. 1. Geological map showing two main structural provinces of Kennedy Channel and five carbonate islands, with Hans Ø in mid-channel.

This article is stimulated by the realisation that the early mapping of this part of the High Arctic is apparently little known internationally. The aim is two-fold. Firstly, to briefly summarise Danish geological work at Kennedy Channel, illustrated by the first map featuring Hans Ø (Fig. 2), and secondly, to illustrate how the Geological Survey in Copenhagen employs modern research techniques to maintain its interest in the far north.

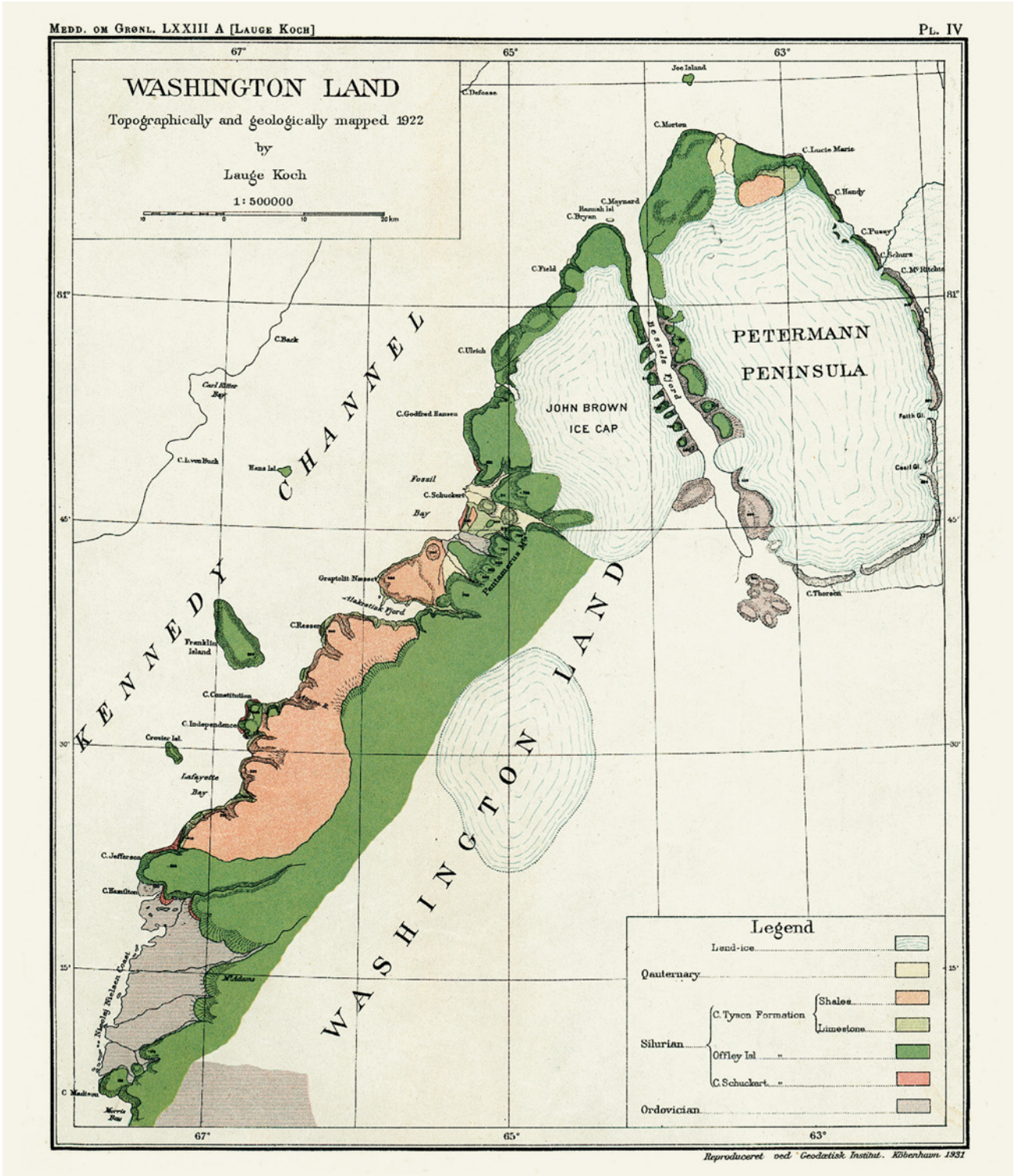

Fig. 2. The first geological map showing Hans Ø. Printed in 1931 and annotated for publication in volume 73, the map appeared in *Meddelelser om Grønland* volume 200 (Dawes & Haller 1979, plate 2; for explanation see text). From Dawes (1984; copies in Survey archives and The Royal Library, Copenhagen, are 28 × 23 cm).

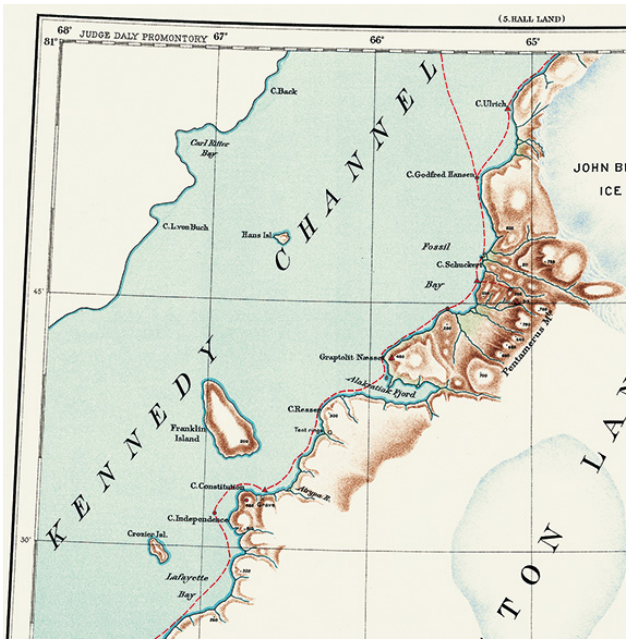

Fig. 3. Extract of 'Cape Constitution', sheet 11 of the topographical map of North Greenland, scale 1:300 000, showing Hans Ø. From Koch (1932). The original size of the extract is 21 × 23 cm.

First geological map of Hans Ø

The initial Danish mapping of northern Greenland took place via Nares Strait on two dog-sledge expeditions: the 2nd Thule Expedition 1916–1918 and the Bicentenary Jubilee Expedition 1920–1923. The expeditions carried strong political overtones and for the purpose of fund raising national pride was a timely motif. The overriding aim was regional mapping of the national territory of Denmark, with the ambitious plan becoming the lot of geologist and cartographer Lauge Koch. The scientific results were outstanding. For example, a topographical series of 19 sheets at 1:300 000 and a geological series of five sheets at varying scale were printed: geology in two batches, in 1929 and 1931, and topography in 1932 (Dawes & Haller 1979, fig. 3). Hans Ø, coloured as part of Greenland, appears on topographic sheet 11 'Cape Constitution' and on geological sheet 'Washington Land' where it is referred to the Offley Island Formation (Figs 2, 3). The five geological sheets with map descriptions were intended for publication in volume 73 of *Meddelelser om Grønland*, and the maps were annotated accordingly. Two were published as planned (Koch 1929, 1933). The fate of the remaining maps is intimately bound up with the destruction of stockpiles in Copenhagen during the German occupation in the 2nd World War destining the Washington Land map – compiled in 1922 and printed in 1931 – to be released years later in another volume of *Meddelelser om Grønland* (Dawes & Haller 1979).

Later Danish geological work

During the Thule and Ellesmere Land Expedition 1939–1941, Danish geologist Johannes C. Troelsen examined and refined Koch's (1929) Lower Palaeozoic lithostratigraphy in southern Washington Land. Hans Ø and the four other islands were included on his map in the same colour as the Silurian limestone and shale of the Greenland coast (Troelsen 1950). Air-supported regional mapping by the Geological Survey of Greenland in 1975–1977 and 1984–1985 included visits to Hans Ø and other islands, for example in 1975 and 1984, for the purpose of studying the bedrock with a view to correlation with the lithostratigraphic framework established on Washington Land and farther north (Peel 1984). Hans Ø was referred to the Cape Morton Formation of the Washington Land Group and so portrayed on the 1:250 000 map sheet of Jepsen *et al.* (1983).

ASTER satellite data and 3-D modelling

Combined with traditional information from aerial photographs, satellite data form an important tool in geological and commodity mapping in Greenland. Recently, ASTER (Advanced Spaceborne Thermal Emission and Reflection Radiometer), the imaging instrument on NASA's Terra satellite launched in December 1999, has proved to be particularly attractive due to its availability and low cost. It provides high-resolution images in 14 different bands of the electromagnetic spectrum ranging from visible to reflected and thermal infrared light. The image resolution ranges between 15 and 90 m and can be used to create detailed maps of surface temperature of land, reflectance and elevation. The imaging power of ASTER data is illustrated by Fig. 4.

Concluding remarks

Initial surveying of the now celebrated island of Nares Strait can be attributed to the Inughuit with their specialised travel techniques since their historic name Tartupaluk, meaning 'kidney-shaped', precisely describes the island's coastal outline. Danish geological research along Nares Strait spans 90 years from the same dog-sledging era through helicopter operations to satellite mapping. Modern remote-sensing techniques provide an accurate perspective of an island traditionally visited by indigenous folk and a handful of explorers and geoscientists, but now – as a disputed border – by politicians and military personnel.

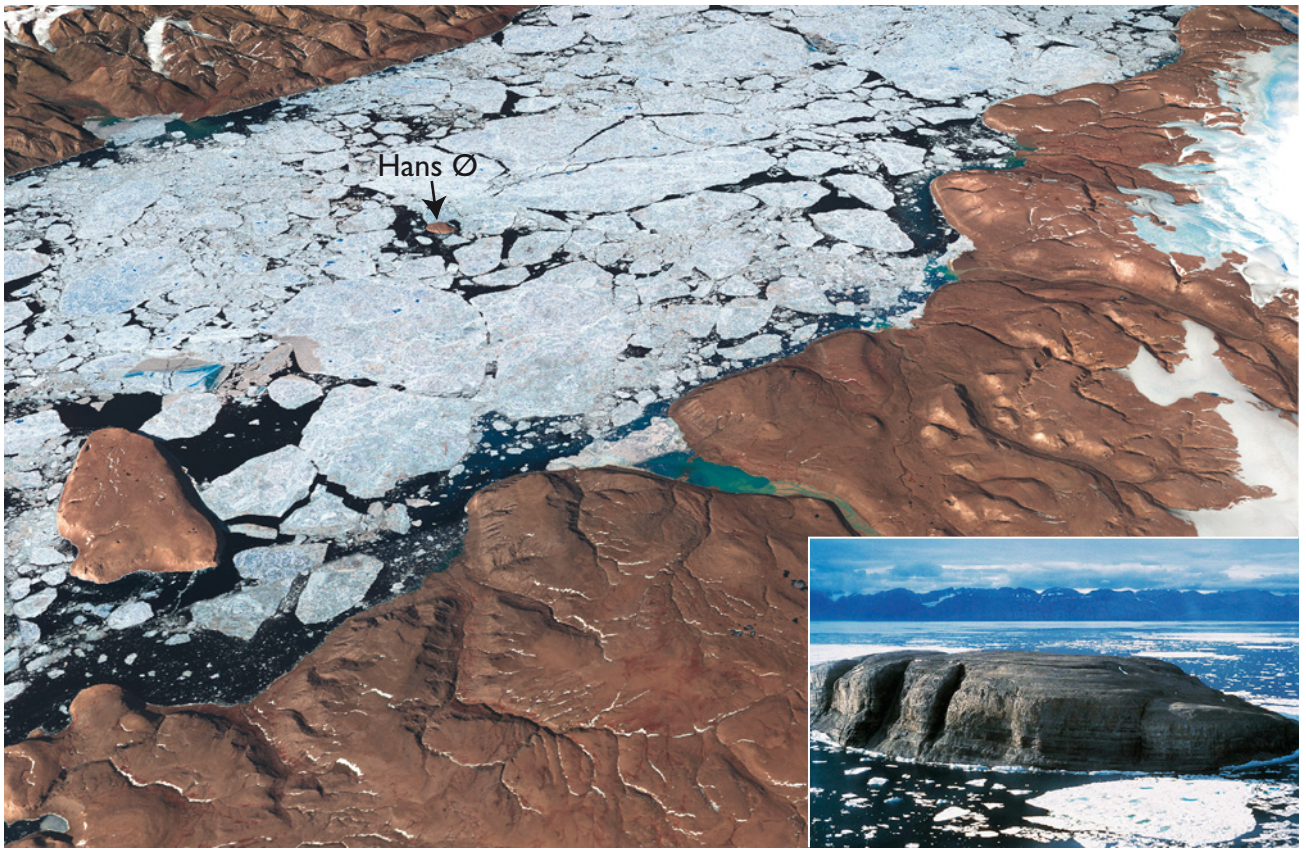

Fig. 4. Perspective view of Kennedy Channel showing Hans Ø and Franklin Ø viewed from the south towards Canada. The colour composite of the visible and near-infrared ASTER image data draped over the digital elevation model are extracted from four ASTER images taken between 26 June and 30 July 2003. Inset: Hans Ø viewed from the south-east.

References

Brückner, P. 1984: Hans Island, Kennedy Channel. Journal of Glaciology **30**(105), p. 256 only.

Christie, R.L. 1964: Geological reconnaissance of northeastern Ellesmere Island, District of Franklin. Geological Survey of Canada Memoir **331**, 79 pp. + map.

Christie, R.L. 1967: Reconnaissance of the surficial geology of northeastern Ellesmere Island, Arctic Archipelago. Geological Survey of Canada Bulletin **138**, 50 pp. + map.

Dawes, P.R. 1984: Notes on Hans Ø, Kennedy Channel: discovery and naming, early geological maps and a 1983 fly-past, 14 pp. + maps. Unpublished report, Geological Survey of Greenland, Copenhagen.

Dawes, P.R. 2004: Explanatory notes to the Geological map of Greenland, 1:500 000, Humboldt Gletscher, Sheet 6. Copenhagen: Geological Survey of Denmark and Greenland, 48 pp. + map.

Dawes, P.R. & Garde, A.A. 2004: Geological map of Greenland, 1:500 000, Humboldt Gletscher, Sheet 6. Copenhagen: Geological Survey of Denmark and Greenland.

Dawes, P.R. & Haller, J. 1979: Historical aspects in the geological investigation of northern Greenland. Part 1: New maps and photographs from the 2nd Thule Expedition 1916–1918 and the Bicentenary Jubilee Expedition 1920–1923. Meddelelser om Grønland **200**(4), 38 pp. + 4 plates.

Harrison, J.C., Dewing, K. & Mayr, U. 2007: Geology of Hans Island and adjacent parts of Kennedy Channel, northwest Greenland (Kalaallit Nunaat) and northern Nunavut (Canada). Geological Survey of Canada Open File **5321**, 33 pp. + maps.

Jepsen, H.F., Henriksen, N., Hurst, J.M. & Peel, J.S. 1983: Geology, 1:250 000 map, Washington Land and Daugaard-Jensen Land. Copenhagen: Geological Survey of Greenland.

Kerr, J.W. 1973: Geology, Kennedy Channel and Lady Franklin Bay, District of Franklin, Map **1359A**, 1:250 000. Ottawa: Geological Survey of Canada.

Koch, L. 1929: The geology of the south coast of Washington Land. Meddelelser om Grønland **73**(1/1), 39 pp. + plates.

Koch, L. 1931: Washington Land. Geological map at 1:500 000. Copenhagen: Geodetic Institute.

Koch, L. 1932: Map of North Greenland, 1:300 000, 19 sheets. Copenhagen: Geodetic Institute.

Koch, L. 1933: Geology of Inglefield Land. Meddelelser om Grønland **73**(1/2), 38 pp. + plates.

Peel, J.S. 1984: Preliminary report. Geological reconnaissance on Hans Ø, North Greenland, 4 pp. + map. Unpublished report, Geological Survey of Greenland, Copenhagen.

Troelsen, J.C. 1950: Contributions to the geology of Northwest Greenland, Ellesmere Island and Axel Heiberg Island. Meddelelser om Grønland **149**(7), 85 pp. + map.

Authors' address

Geological Survey of Denmark and Greenland, Øster Voldgade 10, DK-1350 Copenhagen K, Denmark. E-mail: *prd@geus.dk*

From science to practice in implementing the European Union's Water Framework Directive

Lisbeth Flindt Jørgensen, Jens Christian Refsgaard and Anker Lajer Højberg

The Water Framework Directive (WFD) of the European Union aims to achieve a 'good' status for all inland and coastal waters by the year 2015 (EC 2000). The directive defines how this should be achieved through the establishment of environmental objectives and ecological targets.

Successful implementation of the WFD requires integration into already existing national legislation and a sound combination of issues on technical feasibility, scientific knowledge and socio-economic aspects requiring intensive stakeholder involvement. This calls for appropriate tools such as models to support management of technical and social aspects of different phases of the implementation (Rekolainen *et al*. 2003; Quevauviller *et al*. 2005). It is therefore necessary to provide an overview of already existing methods and tools and develop new ones. Research programmes funded by the European Commission (EC) often address issues of current interest for practitioners, such as the Fifth Framework Programme, where a number of research projects to support the practical implementation of the WFD were initiated under the theme 'Energy, Environment and Sustainable Development'. The funding part (the Directorate-General for Research, DG Research) and the responsible authority for the WFD at European level (Directorate-General of Environment) saw the need to cluster these research projects and related activities, and initiated the *Harmoni-CA* project, a so-called 'Concerted Action' (i.e. Harmonised Modelling Tools for Integrated River Basin Management).

The objectives of this paper are (a) to briefly describe the overall purpose of the *Harmoni-CA* project and some of its overarching outputs, and (b) to further illustrate how the implementation of the WFD can be enhanced by combining monitoring and modelling disciplines and by bringing practitioners and researchers together.

Harmoni-CA

The *Harmoni-CA* project started in October 2002 and concluded with a major conference in Brussels in September 2007. The main objectives of the project were: (1) to build a bridge from research to practice; (2) to create a forum for related research projects to exchange ideas, to optimise and co-ordinate activities in ongoing research projects, and to initiate new spin-off projects; and (3) to gather already existing information, experience and research on both national and European levels that can support the implementation of the WFD (Arnold *et al*. 2005).

Bridging research and practice

A central activity of the project was to bring practitioners and researchers together at a large number of targeted workshops and open annual conferences. The main purpose was to open the floor for discussions on the needs of those working with integrated water management and the related outputs from the scientific community. Several opportunities and new ideas arose from the workshops. However, obstacles and bottlenecks were also recognised, such as insufficient dialogue between the scientific and policy-making communities due to different interests and languages, lack of translation of scientific outputs into tools readily applicable to policy-makers, and the lack of a structure within which the groups responsible for the implementation of the WFD could be brought together with the scientists (Arnold *et al*. 2005).

While the open annual conferences had broad themes, the workshops concentrated on the following tasks of *Harmoni-CA*: (1) establishment of a 'tool box' to provide easy and guided access to information and communication technologies for the development of river basin management plans (van Griensven & Vanrolleghem 2006); (2) development of a generalised methodological framework for harmonised model support in integrated river basin management (Hattermann & Kundzewicz 2006); (3) better integration between monitoring and modelling in water management (Højberg *et al*. 2007a, Jørgensen *et al*. 2007); and (4) investigation of how the science–policy interface can be bridged in current water management (Borowski & Hare 2007). More than 20 targeted workshops addressing these issues were held, resulting in workshop reports, synthesis reports and *Harmoni-CA* guidances.

Forum for research projects

The activities in *Harmoni-CA* and other related research projects were integrated in a cluster called CatchMod. The projects in this cluster produced outputs that could support the implementation of the WFD in different ways. This co-ordi-

nation of research and technology development activities supported researchers in exchanging ideas on modelling tools to support the WFD. It aimed to increase the output and benefit of ongoing research, to speed up the (re-)use of developed products, to avoid major overlaps between projects,and to reduce the risk of duplicating activities. *Harmoni-CA* achieved this by, amongst other things, organising two technical CatchMod workshops for the projects involved, where a dialogue was established among the scientific communities and gaps were reduced between different research disciplines. The workshops were also often used as an instrument to prepare input to guidance documents and synthesis reports.

Support to the implementation of the WFD

Another important task of the project was to collect already existing knowledge on issues related to the different steps of the WFD. This was partly done by producing a number of reports and guidances and partly by establishing a web portal.

Synthesis reports and guidances. A large number of synthesis reports and guidances was initiated by *Harmoni-CA*. The following groups can be distinguished: (1) Reports supporting modelling activities and development, e.g. quality assurance, sensitivity analysis, and decision support development; (2) Reports supporting the collaboration between different scientific/policy fields such as monitoring, modelling, agriculture, economy and (3) Reports on the science–policy interface and end-user involvement. The reports harmonise available knowledge, provide added value by picking up recent insights and are essential in order to improve the quality of communication between science and practice. Most of the reports have been commissioned to small task groups consisting of both scientists and end-users and include outcomes of discussions held at various workshops and conferences. Some reports will be published in the International Water Association publication series, improving the visibility of European research. Examples are: 'Uncertainty Analysis' (Refsgaard *et al*. 2005), 'Model-supported implementation of the Water Framework Directive – A water manager's guide' (Hattermann & Kundzewicz 2007), 'Integration of the human dimension in model-supported water management' (Bots *et al*. 2007) and 'Good practice in joint use of monitoring and modelling' (Højberg *et al*. 2007b).

The WISE-RTD web portal. It is often a difficult task for practitioners dealing with new or challenging steps of the WFD, to find their way through the jungle of existing knowledge and experiences, when they look for assistance or good examples. *Harmoni-CA* has therefore developed a web portal (www.wise-rtd.info) that mainly acts as an entry to tools, experiences, guidances and research activities or results that can help water managers or others interested in finding information relevant to the WFD implementation.

Fig. 1. Map of Europe showing the locations of the six case studies discussed.

There are several ways to search for help in the portal. Users can enter in their capacity as water managers, scientists or stakeholders. Another option is to search by keywords derived from the 'Common Implementation Strategy Guidance Documents' developed by the EC to support the implementation of the WFD. Information on tests or pilot projects can also be found, such as the 'Pilot River Basins', where different steps of the WFD have been tested before final implementation. The portal is hosted and supported by the European Commission and is expected to become *the* support portal for WFD implementation.

Joint use of monitoring and modelling

While a combination of monitoring and modelling is often seen in research, there seems to be more hesitance to use modelling in practical water management where, on the other hand, a lot of data acquisition takes place. One of the tasks within *Harmoni-CA* was to try to integrate the monitoring and modelling disciplines in water management to a higher degree than currently seen.

For this purpose five workshops have been arranged over a period of three years. A total of more than 80 water managers, stakeholders, consultants, policy makers and scientists participated, representing 24 mainly European countries. The first three workshops investigated the status of monitoring programmes and the present use or knowledge of modelling support to monitoring. It was recognised that monitoring programmes often date back several decades and have traditionally been considered an independent discipline. However, within

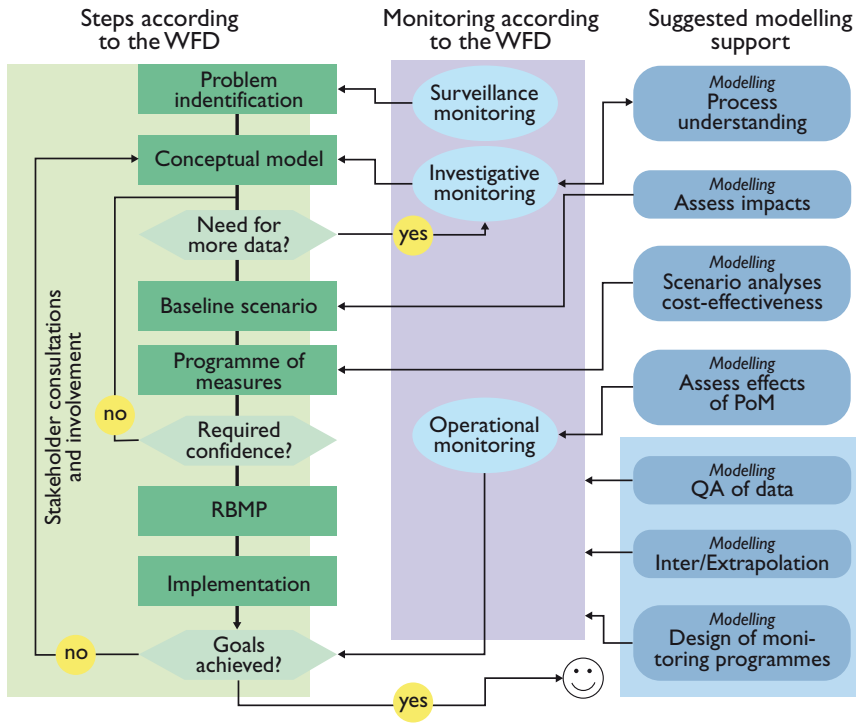

Fig. 2. Flowchart for integrating monitoring and modelling activities when implementing the European Union's Water Framework Directive. The chart is a result of workshops on six case studies from different parts of Europe. The workshops addressed diverse challenges and problems of current interest. **RMBP**, River Basin Management Plans; **PoM**, Programme of Measures; **QA**, Quality Assurance.

the last few decades modelling has entered the arena as a supplementary tool to help extract information from observation data. This is generally accepted in the research community. However, in practical water management there is considerable reluctance to employ models due to various obstacles such as lack of skill, lack of time, lack of awareness on what models can do and also lack of confidence in models (Brugnach *et al*. 2007).

It was therefore decided to use the last two workshops to discuss six case studies from different areas of Europe (Fig. 1), in order to explore the possibility of developing an outline for a common approach in implementing the WFD and combining monitoring and modelling activities. These case studies are briefly presented here:

Hørup well field (Denmark). Groundwater extraction for drinking water results in low base flows in nearby streams in dry seasons. There are threats to the groundwater quality from diffuse pesticide pollution and from point sources (contaminated sites in a nearby city). The challenges in this case study were to ensure sustainable extraction without unacceptably affecting nearby streams and to protect the groundwater against pollution.

Ezousas aquifer (Cyprus). Heavy abstraction for irrigation causes saline intrusion into the aquifer. Groundwater recharge is low due to a decline in precipitation and damming of the river that previously supplied most of the recharge. The challenges were to convince stakeholders of the positive effects of a planned artificial recharge programme using cleaned wastewater, to optimise this programme to avoid saline intrusion and to evaluate the present monitoring programme.

Pärnu River Basin (Estonia). Threats to wetland and groundwater quality due to agricultural activities with both diffuse and point sources of pollution. Peat mining in the area leads to local acidification of surface waters. The challenges were to differentiate diffuse and point source contamination in surface water and groundwater and to address the acidification problem.

Nevesis River Basin (Lithuania). Surface waters are threatened by high nutrient loads from diffuse agricultural sources and from sewage from small villages without waste water treatment. The challenge was to differentiate between diffuse and point source contamination in surface water.

Campania (Italy). The groundwater, and thus the drinking water, is polluted by agriculture and horticulture, and outlets of untreated waste water from small villages contribute to poor groundwater quality. The challenge was to differentiate between diffuse and point source pollution.

Ialomita River Basin (Romania). High levels of nutrients, especially nitrate, in both surface and groundwater, caused by aerial deposition from neighbouring areas with agricultural activities as well as by diffuse pollution from the local agriculture. In addition, a special problem arises from high nitrate levels in the groundwater due to extensive use of nutrients in the past. The challenges were to differentiate between contamination caused by aerial deposition, local sources, and the inherited high nitrate concentrations from earlier agricultural activities.

Each case study was elaborated by a small group of participants, and flowcharts were prepared showing how to implement the WFD, with special reference to combining models and monitoring. The groups working on the six cases focussed on different aspects. In spite of this, their flowcharts showed many similarities in their approaches, which allowed the construction of a common flowchart representing the key

aspects of all the six cases (Fig. 2). This flowchart may be applicable in most areas of Europe that face different challenges in the implementation of the WFD.

As shown in Fig. 2, models can support a variety of different tasks. A numerical model can be used to test different conceptual models and to check whether these are consistent with all available data. A model can be used to evaluate the effects of already implemented or planned measures, and by undertaking analyses of different scenarios help to choose the best programme of future measures to improve the status of the environment. Incorporation of data in models provides an additional check of the consistency and quality of the data, and since such data are often discrete in time and space, models are more applicable for interpolation and extrapolation than statistical methods. Models can also help to achieve an optimal design of monitoring programmes by providing input on when and how often to monitor. They can also help to find a predefined confidence level, taking uncertainty into consideration.

Thus models can support data acquisition in many ways, and this support may go much further than the traditional prediction of effects of various alternative initiatives.

Although the six case studies were real-life situations addressing topics of current interest, a major limitation was the fact that the participants did not have to consider political or economic constraints. Nevertheless, people with different backgrounds – scientists, practitioners, monitoring, modellers and experts – could easily work together in combining monitoring and modelling in an effective manner. All participants found the use of models to be beneficial in most of the situations mentioned above.

Concluding remarks

Different professional communities have different interests, traditions and working cultures. This constrains the uptake and acceptance of research results by practitioners and hinders the interaction of different disciplines such as monitoring and modelling. Experience from *Harmoni-CA* workshops on monitoring and modelling shows that when researchers and practitioners are brought together to elaborate on real life cases, they can easily work together in a very inspiring and constructive way. A key conclusion from the project is that it is possible to bridge some of the gaps between research and practice and between different disciplines, but that this requires continuous attention and positive co-operation from all parties involved.

Acknowledgement

The present work was carried out within the Concerted Action *Harmoni-CA*, which was funded under the European Commission's 5th Framework Programme (Contract EVK1-CT2001-00192).

References

Arnold, G.E., de Lange, W.J. & Blind, M.W. 2005: The concerted action Harmoni-CA: Facilitating the dialogue and bridging the gap between research and WFD implementation. Environmental Science and Policy **8**, 213–218.

Borowski, I. & Hare, M. 2007: Exploring the gap between water managers and researchers: difficulties of model-based tools to support practical water management. Water Resources Management **21**, 1049–1074.

Bots, P., Gooch, G., McIntosh, B.S. & Pahl-Wostl, C. 2007: Integration of the human dimension in model supported water management. A Harmoni-CA Guiding document. Available on: www.harmoni-ca.info.

Brugnach, M., Tagg, A., Keil F. & de Lange, W.J. 2007: Uncertainty matters: computer models in the science-policy interface. Water Resources Management **21**, 1075–1090.

EC 2000: European Commission, Directive 2000/60/EC of the European Parliament and of the Council of October 23, 2000 establishing a framework for Community action in the field of water policy. Official Journal of the European Communities 2000, 22.12.2000, L327/1–L327/72.

Hattermann, F.F. & Kundzewicz, Z.W. 2006: Model-supported integrated river basin management – methodological framework. In: Kundzewicz, Z.W. & F.F. Hattermann (eds): Natural systems and global change. Poznan: RCAFE PAS, 65–74.

Hattermann, F.F. & Kundzewicz, Z.W. (eds) 2007: Model-supported implementation of the Water Framework Directive – a water manager's guide. A Harmoni-CA Guideline. Available on: www.harmoni-ca.info.

Højberg, A.L., Refsgaard, J.C., van Geer, F., Jørgensen, L.F. & Zsuffa, I. 2007a: Use of models to support the monitoring requirements in the Water Framework Directive. Water Resources Management **21**, 1649–1672.

Højberg, A.L., Refsgaard, J.C., Jørgensen, L.F., van Geer, F. & Zsuffa, I. 2007b: Good practice in joint use of monitoring and modelling. A catchment modelling guidance. Available on: www.harmoni-ca.info.

Jørgensen, L.F., Refsgaard, J.C. & Højberg, A.L. 2007: The inadequacy of monitoring without modelling. Journal of Environmental Monitoring **9**, 931–942.

Quevauviller, P. *et al.* 2005: Science-policy integration needs in support of the implementation of the EU Water Framework Directive. Environmental Science & Policy **8**, 203–211.

Refsgaard, J.C., van der Sluijs, J.P., Højberg, A.L. & Vanrolleghem, P.A. 2005: Uncertainty analysis. A catchment modelling guidance. Available on: www.harmoni-ca.info.

Rekolainen, S., Kämäri, J. & Hiltunen, M. 2003: A conceptual framework for identifying the need and role of models in the implementation of the Water Framework Directive. International Journal on River Basin Management **1**, 347–352.

van Griensven, A. & Vanrolleghem, P.A. 2006: The CatchMod toolbox: easy and guided access to ICT tools for Water Framework Directive Implementation. Water Science & Technology **53**, 285–292.

Authors' address

Geological Survey of Denmark and Greenland, Øster Voldgade 10, DK-1350 Copenhagen K, Denmark. E-mail: *lfj@geus.dk*

KenSea – tsunami damage modelling for coastal areas of Kenya

John Tychsen, Ole Geertz-Hansen and Frands Schjøth

On 26 December 2004, the eastern part of the Indian Ocean was hit by a tremendous tsunami created by a submarine earthquake of magnitude 9.1 on the Richter scale off the west coast of Sumatra. The tsunami also reached the western part of the Indian Ocean, including the coastal areas of eastern Africa. Along the coast of Kenya (Figs 1, 2) it resulted in a sudden increase in water level comparable to a high tide situation. This rather limited consequence was partly due to the great distance to the epicentre of the earthquake, and partly due to the low tide at the time of the impact. Hence the reefs that fringe two thirds of the coastline reduced the energy of the tsunami waves and protected the coastal areas.

During the spring of 2005, staff members from the Geological Survey of Denmark and Greenland (GEUS) carried out field work related to the project *KenSea – development of a sensitivity atlas for coastal areas of Kenya* (Tychsen 2006; Tychsen *et al.* 2006). Local fishermen and authorities often asked what would have been the effect if the tsunami had hit the coastal area during a high tide, and to answer the question GEUS and the Kenya Marine and Fisheries Research Institute (KMFRI) initiated a tsunami damage projection project. The aim was to provide an important tool for contingency planning by national and local authorities in the implementation of a national early warning strategy.

The tsunami damage projection project used the database of coastal resources – KenSeaBase – that was developed during the KenSea project. The topographical maps of Kenya at a scale of 1:50 000 have 20 m contour lines, which is insufficient for the tsunami run-up simulation modelling undertaken by the new tsunami project. Therefore new sets of aerial photographs were obtained, and new photogrammetric maps with contour lines with an equidistance of 1 m were drawn for a 6–8 km broad coastal zone.

The tsunami modelling is based on the assumption that the height of a future tsunami wave would be comparable with the one that reached the coastal area of Kenya in December 2004. Based on the regional geology of the Indian Ocean, it appears that the epicentre for a possible future earthquake that could lead to a new tsunami would most likely be situated in the eastern part of the ocean. Furthermore, based on a seismological assessment it has been estimated that the largest tsunami that can be expected to reach eastern Africa would have a 50% larger amplitude than the 2004 tsunami.

It was therefore decided to carry out the simulation modelling with a tsunami wave similar to that of the 2004 event, but with the wave reaching the coast at the highest astronomical tide (scenario 1) and a worst case with a 50% larger

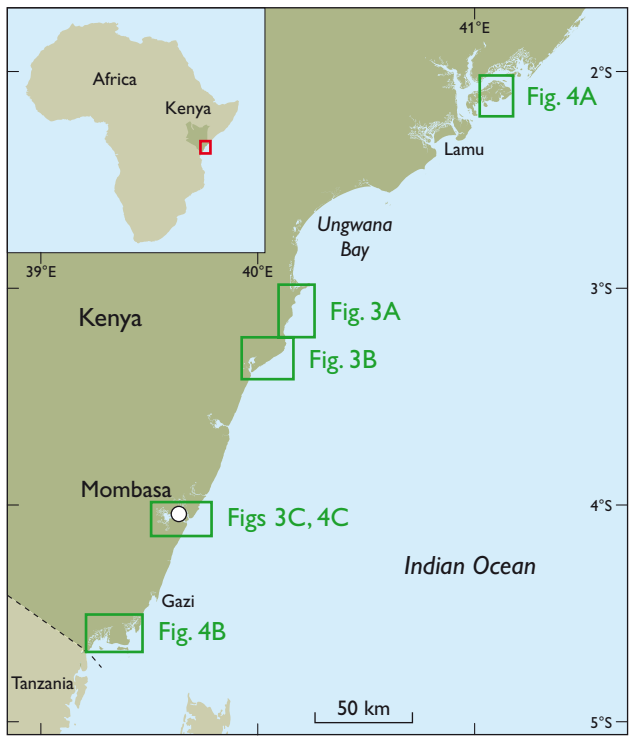

Fig. 1. Map of the coastal area of Kenya (red frame on index map). The green frames show the locations of the maps shown in Figs 3–4.

Fig. 2. A fishing vessel lying on the beach east of Ngomeni. The vessel was wrecked by the tsunami in December 2004 (see Fig. 3A for location).

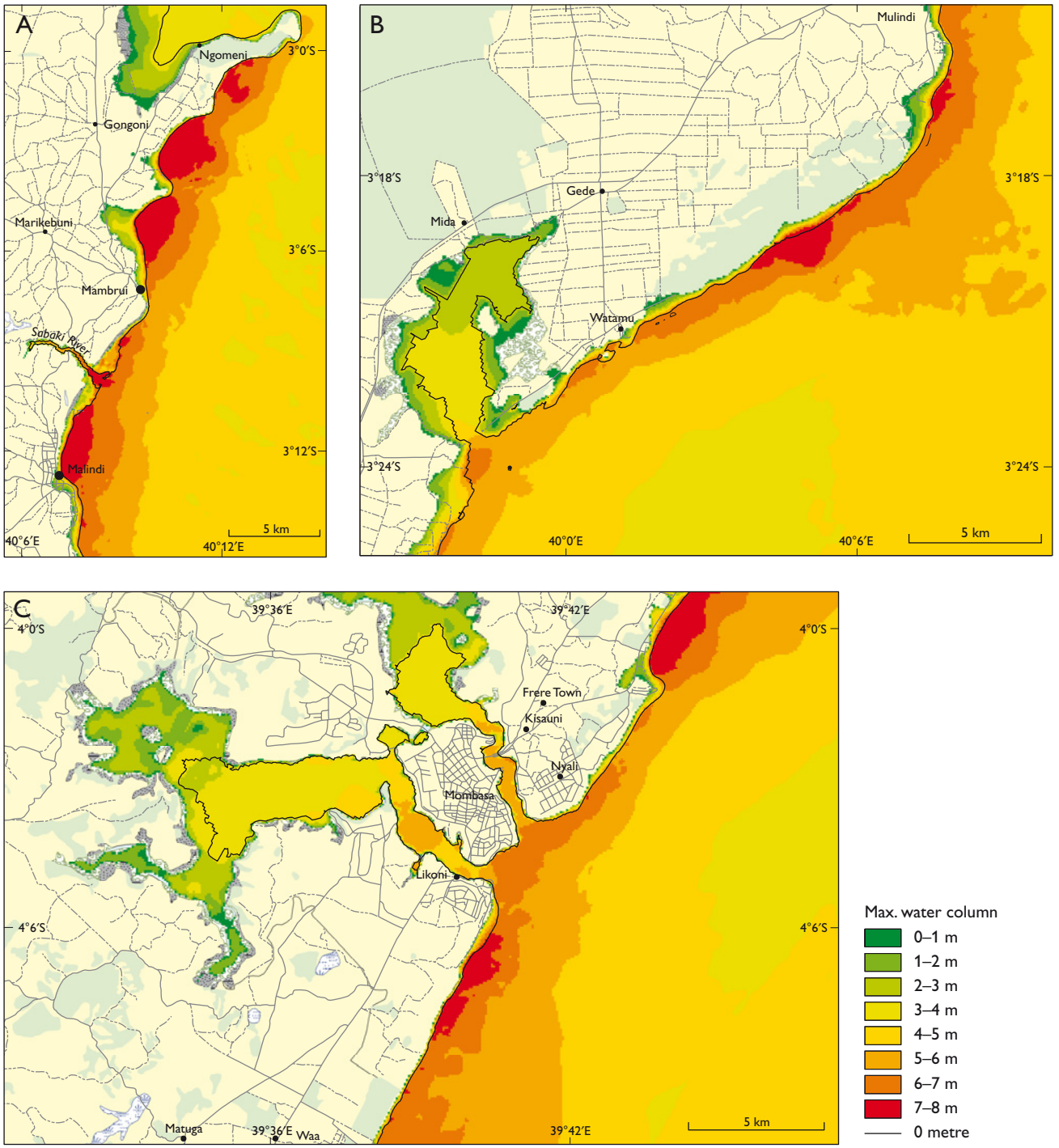

Fig. 3. Scenario 2, showing maximum simulated water levels north of Sabaki River, in the Watamu-Malindi area, and around Mombasa for a tsunami reaching the coast at high tide, and with a 50% larger amplitude than the 2004 tsunami. At sea, sea surface elevation is shown relative to mean sea level, whereas on land the water level is relative to the land surface and therefore shows flooding heights (see Fig. 1 for location).

amplitude (scenario 2: Fig. 3). The 2004 tsunami documented that the coastal belt of mangrove swamps provided some protection to the coastline by reducing the energy of the tsunami. Hence we included in this study a scenario 3 (Fig. 4), in which the mangrove areas along the coastline were removed. Maps for the three scenarios have been produced and show the areas that would be flooded, the degree of flooding, and the distribution of buildings such as schools and hospitals in the flooded areas. In addition, the force and velocity of the wave were calculated (COWI 2006).

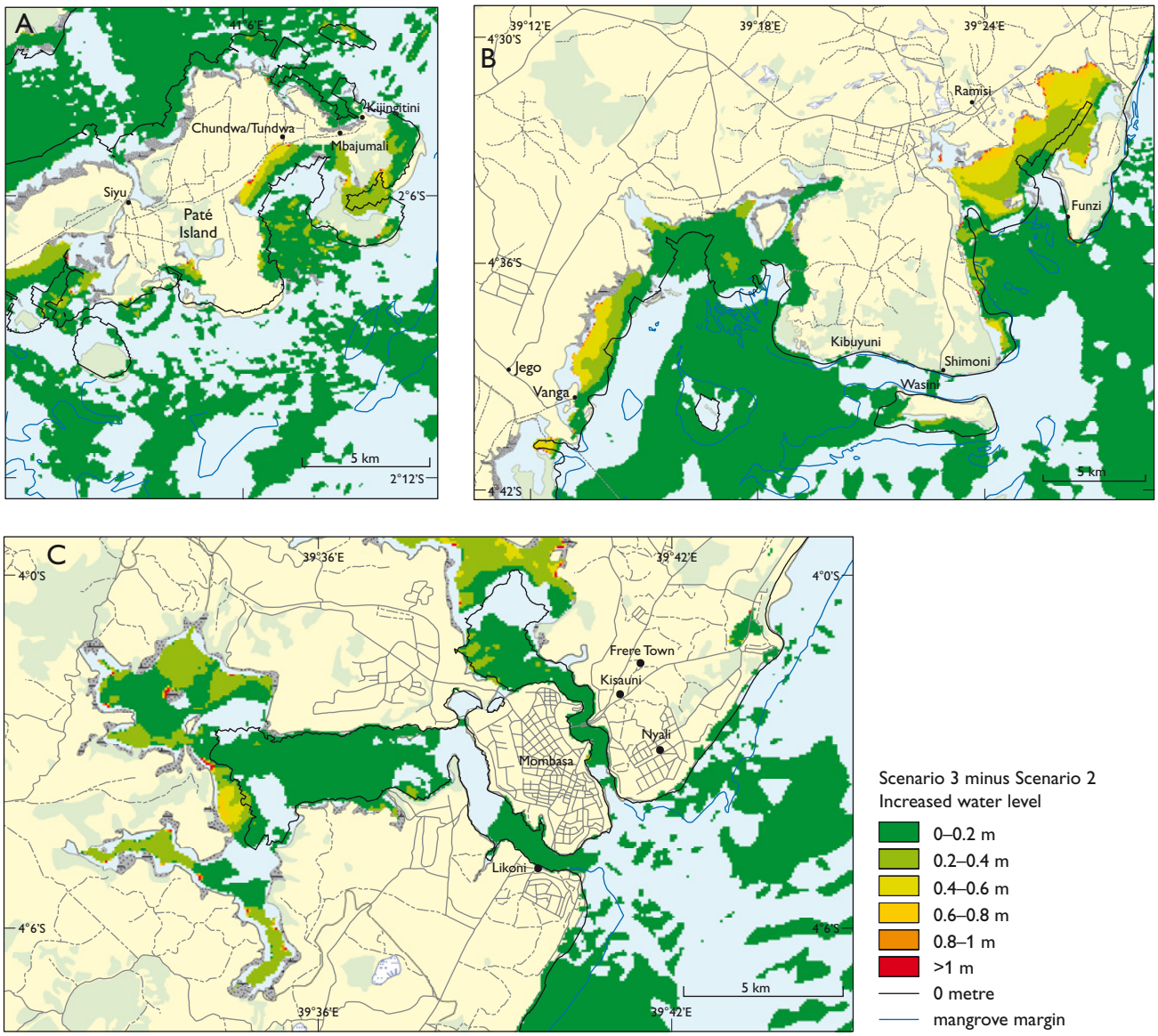

Fig. 4. The effect of mangroves. The figure shows the difference between scenario 3 (all mangrove removed) and scenario 2 (mangrove present) for three important mangrove areas (Paté Island, the Vanga-Shimoni-Funzi area and the Mombasa area). The green 0–0.2 m signature in open water can mostly be regarded as noise from the model. The only marked difference between the models is seen behind areas with dense mangroves (see Fig. 1 for location).

The run-up simulation model

The study used the MIKE 21 BW model, which is a 2-D hydrodynamic model from the MIKE modelling suite developed by the Danish Hydraulic Institute. The modelling was undertaken by COWI A/S in Denmark (COWI 2006). The model setup included detailed bathymetry and topography of the area and data on the surface properties (e.g. sand, reef, rock, mangrove, forest, town), which provide information on bed resistance. The model covers an area of 49 000 km^2 with a grid size of 100 x 100 m. Thus the total number of grid cells is 4 900 000. The topographical data mainly derive from the detailed topographic maps that were drawn from the new aerial photographs. Where necessary these data were complemented with data extracted from existing topographic maps. The topographical data thus only cover elevations above mean sea level. Bathymetrical data were extracted from C-Map, a world wide digital navigational chart, by a module that produces bathymetrical data that can be used directly by the MIKE models. The C-Map data include water depths at and below the chart datum. The topography between mean sea level and chart datum was interpolated.

No measured boundary data were available, and a normal calibration of the model was therefore not possible. Only one single high-resolution time series of water level changes during the 2004 tsunami incident is available, from the port of Lamu in the north. The offshore boundary conditions off

Lamu were back-calculated by a trial and error approach until the model reproduced the recorded time series at Lamu. By this approach, bed resistances could not be used for calibration, but were set to well-established values for the various types of sea bed and land surfaces mapped and described by Tychsen (2006). The resulting boundary conditions (i.e. the offshore tsunami wave train) were then applied to the full length of the Kenyan coast.

Model results

A few examples of the model results are illustrated here, and more details can be found in the project reports (COWI 2006; GEUS 2007). All data and results are stored in electronic form in the KenSea database located at KMFRI in Kenya. Three areas have been selected to give an impression of the effects of a possible new tsunami. The risk of a scenario 2 incident is extremely small, but the model helps to pinpoint the most sensitive areas along the coast (Fig. 3).

Effects of mangrove

The mitigating effects of mangrove forests on the destructive powers of tsunamis have been described and discussed by several authors following the December 2004 tsunami (e.g. Kathiresan & Rejendran 2005). Scenario 2 was therefore remodelled with all mangroves removed, i.e. with bed resistance corresponding to normal sea bed (scenario 3).

The difference between models with and without mangrove is not obvious, and it was therefore decided to subtract scenario 2 from scenario 3 to isolate the mangrove effects. This method creates some noise and artefacts, but the conclusion is that the effect on water level is small, less than 20 cm in most places; however, behind wide and somewhat exposed mangroves the difference can be up to 60 or 70 cm. In addition, the flooding extends up to 300 m farther inland when the mangrove is removed. The most significant effect is found behind the mangrove areas north of Vanga, behind Funzi, near Gazi, in the south-western part of Ungwana Bay, and on Paté Island (Fig. 4).

The effects in Kenya of removing the mangrove are smaller than expected from other studies (Gelfenbaum *et al.* 2007). This is not because the mangroves do not mitigate tsunami waves, but because mangroves along the coast of Kenya are mostly found in areas already protected from direct wave exposure, as found in sheltered bays and lagoons, and behind islands or wide reefs. Mangroves do not usually grow naturally along the most exposed coastlines characterised by erosion. This is partly due to the exposure, but mainly due to the lack of suitable substrates for the roots.

Recommendations

An important output of the project was the following set of recommendations to the Government of Kenya:

- It is recommended that an Indian Ocean tsunami warning system is developed, similar to the well-developed system in the Pacific Ocean.
- A post-2004 tsunami study showed a marked lack of knowledge of tsunamis among the coastal communities. Hence there is a need to create public awareness of the causes and potential impacts of tsunamis to enable the local population to take appropriate action when an alarm is raised and thus to minimise the effects of future tsunamis.
- Mangrove forests play an important role in mitigating the impact of tsunami waves. It is recommended that the Department of Forestry in conjunction with local communities rehabilitate areas where mangrove has been cut down.
- In high-risk areas, the provincial administration in collaboration with the Disaster and Tsunami Management Committee should educate the population living in those areas. This would help them to cope better with a tsunami disaster, both physically and psychologically.

References

COWI 2006: Tsunami run-up simulation model for the near shore part of the coastal area of Kenya, 49 pp. Unpublished report, COWI for the Geological Survey of Denmark and Greenland, Copenhagen.

Gelfenbaum, G., Vatvani, D., Jaffe, B. & Dekker, F. 2007: Tsunami inundation and sediment transport in vicinity of coastal mangrove forest. In: Kraus, N.C. & Rosati, J.D. (eds): Coastal sediments '07. Proceedings of the Sixth International Symposium on Coastal Engineering and Science of Coastal Sediment Processes, 1117–1128. 13–17 May 2007, New Orleans, Louisiana.

GEUS 2007: The KenSea II project. Tsunami damage projection for the coastal area of Kenya, 70 pp. Unpublished report, Geological Survey of Denmark and Greenland, Copenhagen.

Kathiresan, K. & Rejendran, N. 2005: Coastal mangrove forests mitigated tsunami. Estuarine, coastal and shelf processes **65**, 601–606.

Tychsen, J. 2006 (ed.): KenSea – environmental sensitivity atlas for coastal area of Kenya, 76 pp. Copenhagen: Geological Survey of Denmark and Greenland.

Tychsen, J., Geertz-Hansen, O. & Kofoed, J. 2006: KenSea – development of an environmental sensitivity atlas for coastal areas of Kenya. Geological Survey of Denmark and Greenland Bulletin **10**, 65–68.

Authors' addresses

J.T. & F.S., *Geological Survey of Denmark and Greenland, Øster Voldgade 10, DK-1350 Copenhagen K, Denmark.* E-mail: *jt@geus.dk*

O.G.-H., *AquaSim, Slagslunde Bygade 37, DK-3660 Stenløse, Denmark.*

Laser ablation analysis of bivalve shells – archives of environmental information

Maiken Hansen Klünder, Dorothee Hippler, Rob Witbaard and Dirk Frei

Reconstructing past secular environmental variations is an important issue in palaeoclimate research. However, most key variables for palaeoclimate reconstructions cannot be measured directly, and reconstructions are therefore based on proxy data. Here, we demonstrate the potential of bivalve shells as an archive of environmental parameters. The Geological Survey of Denmark and Greenland (GEUS) has developed a fast and reliable method for chemical analyses of shell material by laser ablation - inductively coupled plasma - mass spectrometry (LA-ICP-MS), and here we present some examples of the use of this method.

In tropical and subtropical waters, corals can provide century-long archives of past water chemistry with annual resolution. A comparable archive for temperate and Arctic waters would be highly useful in climate research, and therefore it has been examined whether this can be provided by bivalve shells (e.g. Schoene *et al.* 2005). Long-lived species may provide archives with annual resolution extending over several hundred years, whereas short-lived, fast-growing species can provide archives with a seasonal or in some cases daily resolution over a period of a few years. Most bivalves are sessile, and shells are commonly preserved as fossils. There are, however, a number of challenges related to the use of bivalves as proxy archives: (1) many proxies show species specific behaviour (Seed 1980); (2) only very few proxies are dependent on a single variable (Wefer *et al.* 1999); and (3) the effects of biology and ontogeny on the uptake of trace elements and stable isotope fractionation in shell carbonate are largely unknown and have to be evaluated empirically. Therefore, any potential proxy must be calibrated individually for each species of interest before it can be used. A large number of chemical analyses are needed to calibrate a proxy. These are commonly obtained by solution ICP-MS, in which sample preparation is time-consuming and labour-intensive. The use of LA-ICP-MS is therefore a considerable advance in bivalve shell proxy research, as it greatly reduces the effort needed for sample preparation. At the same time, the method requires less material for analysis, thus providing better spatial and hence temporal resolution.

Proxies based on bivalve shell carbonate can be used in present-day environmental monitoring, and for environmental reconstructions from shells found as fossils. Shells from museum collections and shells found in archaeological middens can give information on historic and prehistoric environmental conditions (e.g. Carrell *et al.* 1987), and fossil shells can be used as archives of environmental parameters on geological timescales (e.g. Hendry *et al.* 2001).

Shell mineralisation

Bivalve shells consist mainly of calcium carbonate with impurities in the form of various elements substituting for calcium in the crystal structure. Calcium carbonate represents 95–99% by weight of the shell, the remaining 1–5% being organic matrix, which is dominated by proteins (Marin & Luquet 2004). The shell material is deposited sequentially in growth increments that are often visible in polished sections studied by computer-controlled scanning electron microscopy (CCSEM). As a consequence of the growth pattern the increments occur in chronological order, and a relative time line for chemical analyses can be established. A section with the different layers of the shell of the common blue mussel (*Mytilus edulis*) is shown in Fig. 1, where internal growth increments are also illustrated. Figure 2 shows an image of the actual shell structure.

The elements needed for shell mineralisation come from the water or from particles that the bivalve ingests. In order to be included in the shell, the elements have to cross two biological membranes, the outer and inner mantle epithelium. These membranes actively discriminate against certain elements, but for some elements this discrimination is influenced by external stimuli (e.g. Klein *et al.* 1996).

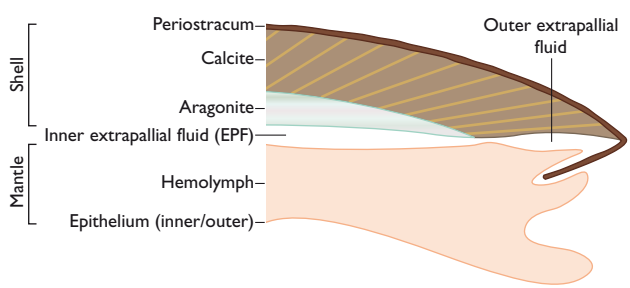

Fig. 1. Section through the margin of shell and mantle of a *Mytilus edulis*. The crystalline shell consists of two separate layers: a prismatic layer of calcite and an aragonitic layer of nacre. The outermost layer is a protective organic layer (periostracum). The shell is secreted in growth increments in the area between the shell and the mantle.

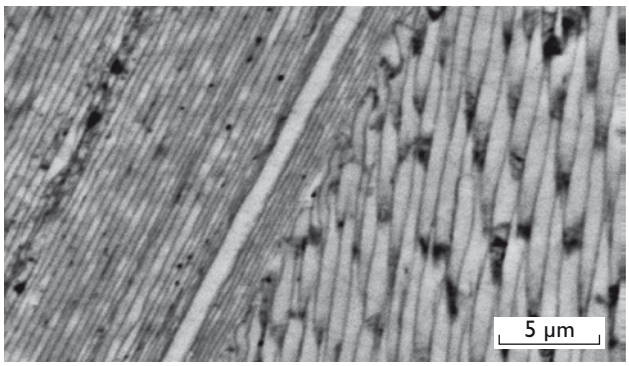

Fig. 2. SEM image of a *Mytilus edulis* shell in cross-section, showing aragonitic nacre (left side of image) and prismatic calcite (right side of image). The image illustrates the differences in structure between these two shell layers, and the direction of the growth increments.

The LA-ICP-MS method

Many previous studies of bivalve shells have utilised wet chemical analysis. Samples often consist of powder drilled from the shell with dentist drills and other microdrilling tools. Powder samples are routinely analysed by solution ICP-MS. LA-ICP-MS combines an analytical precision comparable to that of solution ICP-MS with a significantly shorter and easier sample preparation process. The laser technique is not only time-saving – the fewer steps needed in sample preparation also reduce the risk of contamination. Furthermore, the spatial resolution is much higher, as laser ablation in shell samples can be undertaken with a beam diameter of 30–65 µm, as opposed to the 200–300 µm diameter of a microdrill.

Sample preparation

Any sample of bivalve shell material can be analysed by LA-ICP-MS, but cross-sections through entire valves are preferred in order to constrain the growth history. The shell must be cleaned of soft tissues, epibionts or adhering sediment. The shell material is embedded in epoxy resin to prevent it from fracturing during handling. The shell is then cut with a diamond-tipped rock saw to produce a cross-section, and polished to show the shell structure (Fig. 3). Shells longer than 5 cm may have to be divided into two or more sections to fit into the sample chamber of commercially available laser ablation systems. After polishing, the section is cleaned with alcohol and treated ultrasonically to remove possible surface contamination.

Analytical techniques

The LA-ICP-MS equipment at GEUS is a Finnigan Element2 high resolution ICP-MS connected to a new wave research UP213 laser ablation system. For shell analyses, the NIST 612 and NIST 614 glasses are used as standard materials. The elemental concentrations for the standard glasses published by Pearce *et al.* (1997) are used for concentration calculations. There are potential problems in using non-matrix-matched standards, but at ablation times of less than 80 seconds, these problems are not significant in analyses carried out on calcium carbonate (Vander Putten *et al.* 1999). As an internal standard in the samples, calcium (^{43}Ca) is suitable for the measurement of several trace and minor elements in calcite (Longerich *et al.* 1996), and SEM analyses of *M. edulis* have shown that the calcium content in the calcite layer is uniform. We use the Glitter software package for final concentration calculations from the time-resolved raw data.

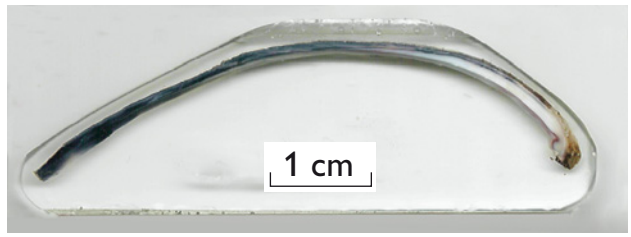

Fig. 3. Computer scan of shell sample *Mytilus edulis* B218 prepared for LA-ICP-MS analysis.

Relative age and growth rate

An advantage of calibrating a proxy on bivalve shells taken from laboratory or field culturing experiments is that measurements of the shell length can be made during the experiment, so that the chemical analyses can be time constrained. When applying the proxy to fossil shells, it is of course impossible to carry out multiple shell length measurements on the live individual, so other methods must be used. Many species form annual growth increments that can be used to set the relative age of a specimen. Furthermore, all species show micro-increments that are visible in a microscope. These narrow growth increments are not always regular, but in a number of species the increments show a periodicity related to moon phases or diurnal or tidal shifts. Utilising what is known about the periodicity of increment formation in the species analysed, one can assign relative ages to chemical analyses and calculate approximate growth rates for the analysed shell.

Examples

Mg/Ca thermometry

The use of the ratio between Mg and Ca in shells as a temperature proxy was first suggested because it was found that the Mg/Ca ratio in marine carbonates varies according to lat-

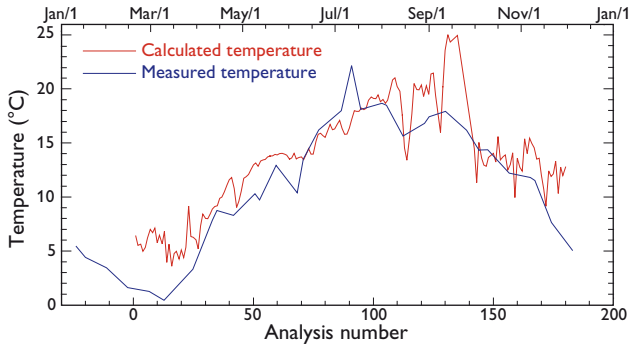

Fig. 4. Temperatures in Svendborg Sund, Denmark in the summer of 2005 calculated from Mg/Ca ratios in *Mytilus edulis* (red line) and compared to measured water temperatures (blue line). The calculated temperatures provide a fair estimate of the actual temperature.

itude (see Henderson 2002). Using calcite from *M. edulis* taken from field culturing experiments in the Wadden Sea, we found shell Mg/Ca ratios to be temperature dependent. The Mg/Ca ratio of *M. edulis* shells from Svendborg Sund, Denmark was then used to calculate seawater temperatures. The temperature was calculated from the Mg/Ca ratio using the equation T = 2.22 + 18.2 log (Mg/Ca) (unpublished data, M.H. Klünder). The calculated temperatures have been compared with water temperatures measured by the National Environmental Research Institute (Fig. 4). It is seen that the Mg/Ca thermometer gives a fair estimate of temperature changes during a summer.

Lead pollution

The concentration of Pb in shell increments of the bivalve *Mya arenaria* is a function of the Pb concentration in the water (Pitts & Wallace 1994), and hence the former concentration of Pb in the water can be calculated from the lead concentration in *M. arenaria* shells. Shell samples from a four-year old specimen from Limfjorden, Denmark, collected in 2005, have been analysed. The results indicate that the Pb concentration in Limfjorden has varied from 20 to 280 pmol/kg water over the sampled time span (Fig. 5). Hence analysing a single water sample may give a misleading picture of the Pb level. The concentration of Pb in Limfjorden is comparable to that found in the relatively uncontaminated Cape Cod Bay, eastern USA; it is up to ten times higher than pre-industrial levels in the Boston area, as calculated from the Pb content of sub-fossil shells from shell middens, and ten times lower than in Boston harbour (Pitts & Wallace 1994).

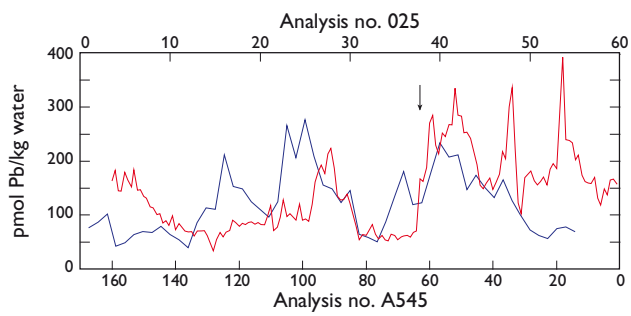

Fig. 5. Pb content in seawater calculated from shell Pb concentration using the equation of Pitts & Wallace (1994). One specimen of *Mya arenaria* (blue line, Limfjorden) and one specimen of *Arctica islandica* (red line, Baltic Sea, transplanted to the Netherlands) were analysed. The arrow shows the time of the transplantation.

The Pb proxy has also been applied to data from an *Arctica islandica* individual that was transferred from the Baltic Sea to a Dutch harbour (Fig. 5). The proxy has not yet been calibrated for *A. islandica*, and the results can only be regarded as qualitative. However, it is seen that the Pb concentration in shell material secreted after transplantation to the harbour is significantly higher than in that secreted in the Baltic. These results indicate that shells of *A. islandica* can be used to monitor Pb contamination of seawater.

Shell Mn/Ca and Ba/Ca – a link to primary production?

It has been suggested that the content of Mn and/or Ba in bivalve shells can be correlated with primary production (e.g. Stecher *et al.* 1996). This would suggest that Mn/Ca or Ba/Ca ratios are related to phytoplankton blooms, providing a proxy

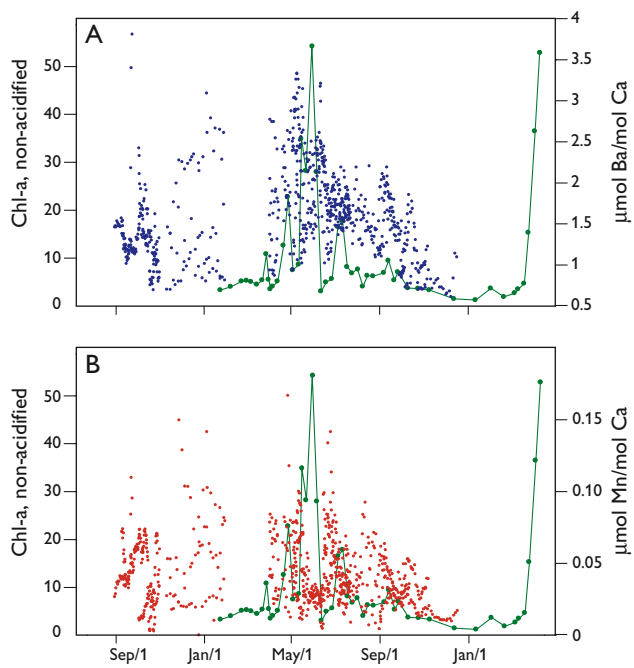

Fig. 6. Ba/Ca and Mn/Ca ratios of four *Mytilus edulis* specimens compared with the chlorophyll-a concentrations (red line) of the seawater. **A**: Ba/Ca ratios in *M. edulis* shells from the Dutch Wadden Sea. **B**: Mn/Ca measured in the same shells.

for the timing and size of such events. To test this theory, *M. edulis* shell samples from an aquaculture field experiment site in the Wadden Sea were analysed at GEUS and compared to the chlorophyll-a concentration of the ambient water (Fig. 6). The results are not conclusive, but they suggest that the relationships between the Mn/Ca or Ba/Ca ratios and the chlorophyll-a concentration are not simple linear functions. The Ba/Ca ratio in the shells seems to increase with the chlorophyll-a concentration in the water, but continues to remain at an elevated level after the end of the bloom; however, Mn/Ca seems to have a correspondence with the peaks of some less intensive algae blooms, but is quite low during the most pronounced bloom recorded in May. Clearly, further research is needed to better understand the link between Mn/Ca and Ba/Ca ratios in shell material and phytoplankton blooms.

Final remarks

The LA-ICP-MS method is a reliable and advantageous technique for the analysis of a wide range of trace elements in carbonates. The combination of relatively high precision, low detection limits, high spatial resolution, straightforward sample preparation and fast analysis makes the method especially suited for research and application of calcium carbonate based proxies. Further development of biogenic carbonate proxies will have benefits for both palaeo-climate research and investigation into the processes of biomineralisation, as well as for environmental studies.

Acknowledgements

We would like to thank M. Sejr for assistance and J. v. Iperen for the chlorophyll-a data. This paper is a contribution to the EuroCLIMATE project 04 ECLIM FP08 CASIOPEIA. The work has been supported financially by the European Science Foundation under the EUROCORES Programme EuroCLIMATE and the Danish Research Agency for Science, Technology and Innovation (FNU).

References

Carell, B., Forberg, S., Grundelius, E., Henrikson, L., Johnels, A., Lindh, U., Mutvei, H., Olsson, M., Svärtström, K. & Westermark, T. 1987: Can mussel shells reveal environmental history? Ambio **16**, 2–10.

Henderson, G.M. 2002: New oceanic proxies for paleoclimate. Earth and Planetary Science Letters **203**, 1–13.

Hendry, J.P., Perkins, W.T. & Bane, T. 2001: Short-term environmental change in a Jurassic lagoon deduced from geochemical trends in aragonite bivalve shells. Geological Society of America Bulletin **113**, 790–798.

Klein, R.T., Lohmann, K.C. & Thayer, C.W. 1996: Bivalve skeletons record sea-surface temperature and $\delta^{18}O$ via Mg/Ca and $^{18}O/^{16}O$ ratios. Geology **24**, 415–418.

Longerich, H.P., Günther, D. & Jackson, S.E. 1996: Elemental fractionation in laser ablation inductively coupled plasma mass spectrometry. Fresenius' Journal of Analytical Chemistry **355**, 538–542.

Marin, F. & Luquet, G. 2004: Molluscan shell proteins. Comptes Rendus Palevol **3**, 469–492.

Pearce, N.J.G., Perkins, W.T., Westgate, J.A., Gorton, M.P., Jackson, S.E., Neal, C.R. & Chenery, S.P. 1997: A compilation of new and published major and trace element data for NIST SRM 610 and NIST SRM 612 glass reference materials. Geostandards Newsletter **21**, 115–144.

Pitts, L.C. & Wallace, G.T. 1994: Lead deposition in the shell of the bivalve *Mya arenaria*: an indicator of dissolved lead in seawater. Estuarine, Coastal and Shelf Science **39**, 93–104.

Schoene, B.R., Fiebig, J., Pfeifer, M., Gless, R., Hickson, J., Johnson, A.L.A., Dreyer, W. & Oschmann, W. 2005: Climate record from a bivalved methuselah (*Arctica islandica*, mollusca, Iceland). Palaeogeography, Palaeoecology, Palaeoclimatology **228**, 130–148.

Seed, R. 1980: Shell growth and form in the bivalvia. In: Rhoads, D.C. & Lutz, R.A. (eds): Skeletal growth of aquatic organisms, biological records of environmental change, 23–67. New York: Plenum Press.

Stecher, H.A., Krantz, D.E., Lord, C.J., Luther, G.W. & Bock, K.W. 1996: Profiles of strontium and barium in *Mercenaria mercenaria* and *Spisula solidissima* shells. Geochimica et Cosmochimica Acta **60**, 3445–3456.

Vander Putten, E., Dehairs, F., André, L. & Bayens, W. 1999: Quantitative *in situ* microanalysis of minor and trace elements in biogenic calcite using infrared laser ablation – inductively coupled plasma mass spectrometry: a critical evaluation. Analytica Chimica Acta **378**, 261–272.

Wefer, G., Berger, W.H., Bijma, J. & Fischer, G. 1999: Clues to ocean history: a brief overview of proxies. In: Fischer, G. & Wefer, G. (eds): Use of proxies in paleoceanography: examples from the South Atlantic, 1–68. Berlin: Springer.

Authors' addresses

M.H.K. & D.F., *Geological Survey of Denmark and Greenland, Øster Voldgade 10, DK-1350 Copenhagen K, Denmark.* E-mail: *mhk@geus.dk*

D.H., *Faculty of Earth and Life Sciences, Vrije Universiteit Amsterdam, De Boelelaan 1085, 1081 HV Amsterdam, the Netherlands.*

R.W., *Royal Netherlands Institute for Sea Research (NIOZ), P.O. Box 59, 1790 AB Den Burg (Texel), the Netherlands.*

Fully automated analysis of grain chemistry, size and morphology by CCSEM: examples from cement production and diamond exploration

Nynke Keulen, Dirk Frei, Stefan Bernstein, Mark T. Hutchison, Christian Knudsen and Lucas Jensen

Computer-controlled scanning electron microscopy (CCSEM) combines the advantages of energy dispersive X-ray spectrometry (EDX) with those of digital image analysis of back-scattered electron (BSE) micrographs. CCSEM analysis of a wide range of geological or non-geological materials has been introduced at the Geological Survey of Denmark and Greenland (GEUS) as a fast and reliable method to determine both the chemistry of individual grains and bulk samples. The chemical analysis is combined with measurements of the two-dimensional size and morphology of every single grain.

The CCSEM technique was developed in the early 1980s for characterisation of coal minerals (Huggins *et al.* 1980; Lee & Kelly 1980) and studies of synthetic crystals for super-conductors and catalysts (Lin & Barnes 1984). Soon it found a broader application in the study of dust particles and fibres in lung tissue of mine workers (Friedrichs 1987), in the analyses of aerosols for air quality control and source emission characterisation (e.g. Heasman & Watt 1989) and the degree of sintering and consolidation of coal ash deposits (e.g. Huffman *et al.* 1994). CCSEM has been used in the earth sciences for the determination of the sediment budget of a lake (Yin & Johnson 1984), for the characterisation of soil and dust (Pirrie *et al.* 2004), for provenance analysis of ilmenite-bearing beach sands (Knudsen *et al.* 2005; Bernstein *et al.* 2008), and provenance studies on sandstones in oil-bearing basins (Frei *et al.* 2005). Other areas where CCSEM has been applied range widely and include characterisation of small inclusions, e.g. impurities in metal alloys or steel (Schwoeble *et al.* 1988), analyses of gun-shot residues (e.g. Steffen *et al.* 2007), and analyses of bladder stones obtained from a skeleton found in a Mesolithic cave-tomb (D'Alessio *et al.* 2005). In this paper, we demonstrate the benefits of the method with examples from the cement industry and from diamond prospecting.

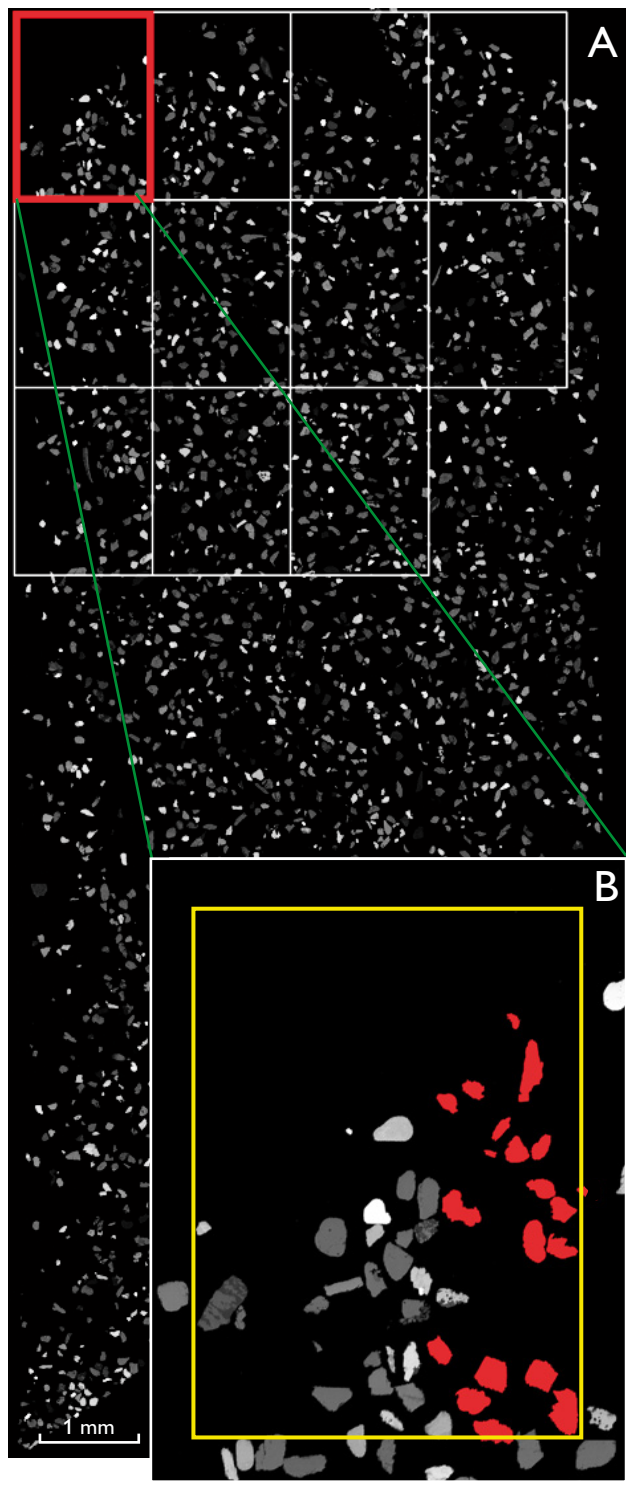

Fig. 1. **A**: CCSEM sample of beach sediment from Jylland, Denmark, divided into a number of frames in a grid. Part of the grid is outlined in white. Grains of different chemical compositions (different grey values) are embedded in epoxy resin. **B**: Enlargement of one of the frames of the grid (indicated in red in **A**). The guard region (yellow) prevents double or incomplete measurements of grains (see text). The grey-level threshold function selects the grains one by one from the matrix for analyses of chemical composition, size and shape. Analysed grains are shown in red; the image represents a snapshot of the CCSEM procedure.

Analytical technique

Sample preparation

Sample material may, for example, consist of (1) a representative part of a bulk sample, (2) carefully selected grains mounted on double-sided tape, or (3) a heavy mineral separation of a bulk sample. Grains, beads, and powders of both geological and non-geological origin can be analysed. For most studies, approximately 1 g of sample material was mounted in epoxy resin, using a technique that ensures that almost every grain is completely embedded in the epoxy, without touching any neighbouring grains (Frei *et al.* 2005). The epoxy mounts are cut to show a representative part of the mount, subsequently polished and coated with carbon to enhance their conductivity. However, it is also possible to use thin sections of sample material prepared in a similar way.

CCSEM analysis

The CCSEM analysis was undertaken using a Philips XL40 SEM equipped with two EDX detectors: a Thermo Nanotrace 30 mm^2 window and a Pioneer Voyager 2.7 10 mm^2 window Si(Li) detector. The tungsten filament of the SEM was operated with an acceleration voltage of 17 kV, a filament current of typically 50–70 µA, and the sample was placed at a distance of 10 mm from the detector. The Noran System SIX software package was used to automatically collect X-ray spectra, grain size and morphology of all particles and to recalculate the data following the Proza (φρZ) data correction and the filtering quantification technique. The technique described here is an improvement of the method described by Frei *et al.* (2005) and Bernstein *et al.* (2008).

The samples were studied in the BSE contrast mode of the electron microscope where the individual particles appear as different shades of grey in their black epoxy matrix (Fig. 1). Grey-level intensity thresholding by the image analysis function integrated in the software created a binary image of the BSE micrograph and allowed for the separation and selection of individual grains (Fig. 1B). A grid of image frames covering the whole sample area was defined by feeding the end-coordinates of the sample to the computer and by setting the required magnification (typically 30–100×) for the analysis (Fig. 1A). Grids consisted of 15 to 60 frames with approximately 20–35 grains per frame. A guard region between each frame ensured that double measurements of large particles in the sample was avoided and that only grains that lay completely within the image frame were included for analysis and thus recorded the true shape of grains. A 'hole-fill' function enabled more precise measurement of the grain size and shape from the binary image. Because the grains were mounted in epoxy resin in such a way that they do not touch each other, no grain separation techniques had to be used, as commonly applied in automatic particle analysis software. Thus, the original 2-D grain shape and grain size were completely available for analysis, without the introduction of artefacts by grain erosion and dilation or median filtering. All standard grain-shape factors can be measured. The smallest grains in the sample can be excluded from the analysis to avoid the measurement of particles that are only a few pixels in size, especially if a good grain morphology resolution is required.

The created binary image formed the basis for the measurements of the grain chemistry. The software forced the microscope to scan within the perimeter of each grain to obtain the chemistry of either the whole grain area or from a single point in the centre of the grain mass. A typical spectrum for one particle contained 1000–2000 counts for the highest peak. Spectra with a very low number of counts can be removed to ensure good measurement statistics. Commonly, 800–1200 grains were measured in approximately two hours.

The Noran software produces a results table that lists shape, size and chemistry for each individual grain. All spectrum files and image frames, with a typical size of 1024 × 774 pixels, are stored after analysis. Spectrum files can be reprocessed to include accidentally omitted elements retrospectively, without the need to physically reanalyse the sample. The chemical data are further reduced using a software package that is connected to a mineral library database for automatic phase recognition and data storage.

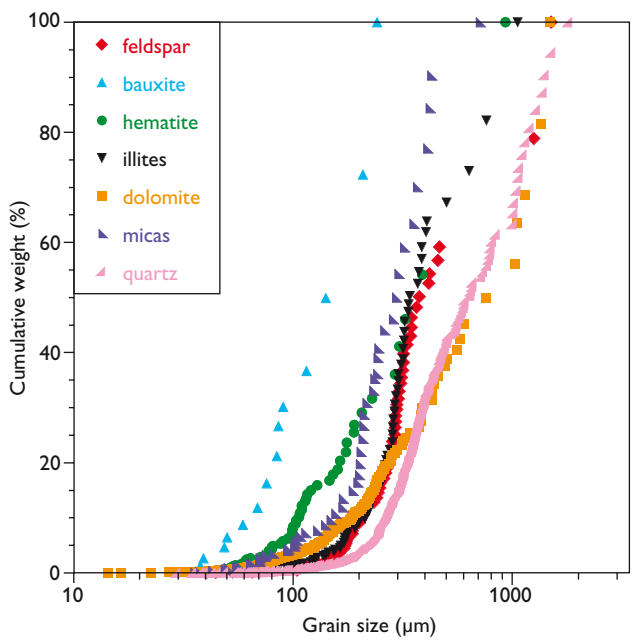

Fig. 2. Grain-size distribution diagram for seven minerals from raw materials used in the cement industry. Grain mineralogy and grain size were determined with CCSEM.

Application of CCSEM as a practical solution

Quality control of raw materials in cement production

For cement production, raw materials are crushed to fine grain sizes before they are mixed and reacted at high temperatures in a kiln. To optimise the performance of the grinding mill and the sintering process an investigation of the grain-size distribution of the limestone, iron ore, clay and sand fractions of the cement was undertaken. The grain-size distribution of the individual components in particular is of great importance for further processing of the raw material into cement clinker.

The raw material was sieved into different grain-size fractions and treated with hydrochloric acid to decrease the amount of calcium carbonate in the raw material. The size fraction of 10–2000 µm was analysed with CCSEM to determine the grain-size distribution and grain chemistry. Figure 2 shows the grain-size distribution for seven different minerals. The mica, illite, and feldspar grains show uniform grain-size distributions, whereas bauxite, hematite and particularly dolomite grains show ranges of size distributions over two orders of magnitude. The hematite grains display a bimodal-size distribution. These findings demonstrate that CCSEM is a suitable option for routine quality control and improvement of the production process.

CCSEM: a fast and reliable tool for diamond prospecting?

Determinations of the elemental composition of macro-crystalline phases in kimberlitic rocks or in detrital sediment samples are an important tool in diamond exploration. The major and minor element compositions of certain minerals are diagnostic for igneous rocks of mantle origin, and in some cases also represent a defined probability that the crystallisation of these phases occurred under conditions where diamond is stable. The ratios between Cr and Ca concentrations of Mg-rich garnets and the Cr and Ca concentrations of eclogitic garnets are examples where such probability fields have been defined (Fig. 3; Grütter *et al.* 2004). A standard method for analysing the composition of garnets and other macrocrystalline phases is to measure the concentration of approximately ten to fifteen oxides with an electron microprobe (EMP). EMP is a dependable, yet time-consuming and relatively expensive method. We therefore tested the potential of CCSEM analysis as a faster and cheaper method to measure the composition of macrocrystals in kimberlitic rocks.

We used indicator minerals from the 'Garnet Lake' kimberlite body in West Greenland, where diamonds are common (Hutchison 2005). A series of hand-picked pyrope (garnet)

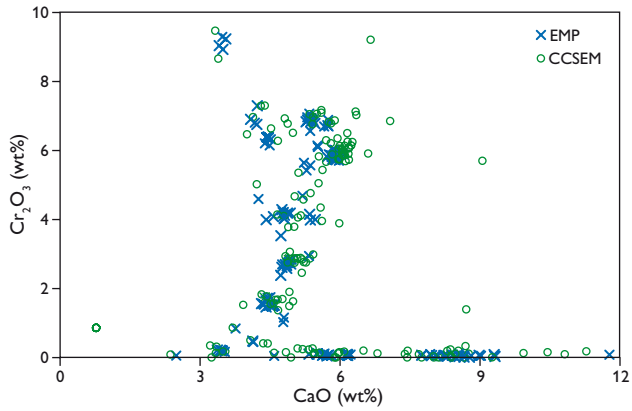

Fig. 3. Comparison of electron microprobe (EMP) and CCSEM measurements for chromium oxide and calcium oxide in Mg-rich garnets from diamond-bearing rocks. Note the good correlation between the results obtained with CCSEM and the EMP data.

grains were mounted in epoxy resin. The sample was analysed using CCSEM, with extended counting times to ensure good statistics: the relative error in the reproducibility of the measurements is *c.* 1–2% for major elements and *c.* 4–8% for minor elements. The accuracy of CCSEM was tested by comparing the results with compositional data obtained from electron microprobe analyses for the same minerals (as reported by Hutchison 2005). Even with extended counting time, a sample consisting of 200 grains can be analysed in 1–3 hours, with less than half an hour of operator time. An excellent reproduction of the EMP measurements was achieved by CCSEM (Fig. 3); the statistical correlation between the two methods for these elements is 70%. The few outliers reflect those garnet grains that show a compositional gradient from core to rim. The EMP point analyses were carried out on the cores of the grains, whereas the CCSEM analyses average the whole surface of the grains, therefore providing slightly different results that are closer to the bulk composition of the grains. The vast majority of the garnet grains analysed by CCSEM plot in the same classification field as do the grains according to the EMP measurements. CCSEM is therefore a good option for reliable and more rapid measurements of garnet minerals in diamond-bearing rocks.

Validity of the CCSEM measurements

Comparison between EMP and CCSEM shows high accuracy of the CCSEM for minor elements. Figure 4 shows the precision of the CCSEM method for a major element (93.71 wt%), a minor element (2.19 wt%) and a trace element (0.21 wt%), measured on the same sample. Five sets of measurements at nine different maximum peak count settings (equivalent to nine different time periods) were undertaken to evaluate the reproducibility of the data. For standard single spot or single grain analyses the relative errors are high com-

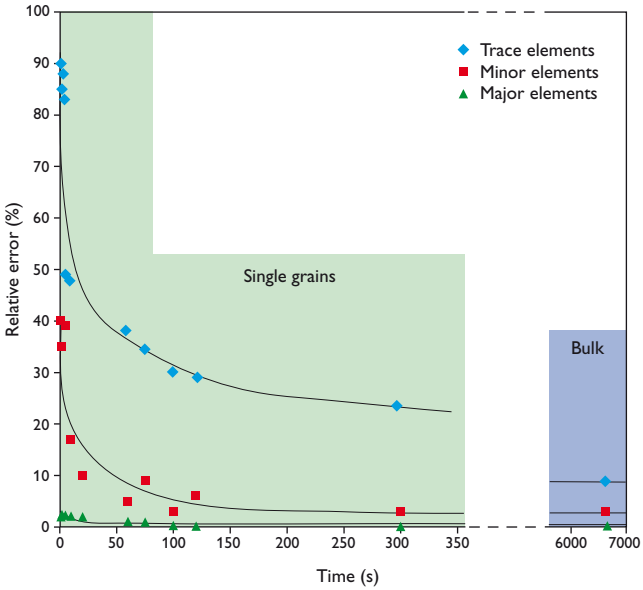

Fig. 4. Precision of single grain and bulk sample CCSEM analyses as a function of measurement times. Two detectors were used for the analyses. The precision increases with counting time.

pared to other analytical methods: 2–3% for major elements (>20 wt%), 5–10% for minor elements (>2 wt%) and 50–100% for elements present in smaller quantities. However, these figures can easily be improved by slightly increasing the counting time (Fig. 4). The precision of bulk sample CCSEM measurements is very high: as an effect of the long counting times the relative errors are reduced to <0.2% for major elements, <2% for minor elements and <15% for trace elements. This shows that the analysis time can be usefully tailored to the sample set depending on the required precision of the measurements and the time available. Applied to diamond prospecting, measurement times could be adjusted depending on how marginal the sample is in the diamond stability field.

The examples discussed above indicate that CCSEM provides an accurate and precise way to rapidly measure single grain and bulk compositions of minerals and of other geological and non-geological materials. Coupled with measurements of the grain size and other grain parameters for the individual particles, this technique is a potent tool to solve a wide range of problems.

Acknowledgement

Hudson Resources Inc. is thanked for provision of garnet samples.

References

Bernstein, S., Frei, D., McLimans, R.K., Knudsen, C. & Vasudev, V.N. 2008: Application of CCSEM to heavy mineral deposits: source of high-Ti ilmenite sand deposits of South Kerala beaches, SW India. Journal of Geochemical Exploration **96**, 25–42.

D'Alessio, A., Bramanti, E., Piperno, M. Naccarato, G. Vergamini, P. & Fornaciari, G. 2005: An 8500-year-old bladder stone from Uzzo cave (Trapani): fourier transform-infrared spectroscopy. Archaeomotry **47**, 127–136.

Frei, D., Rasmussen, T., Knudsen, C., Larsen, M., Whitham, A. & Morton, A. 2005: Linking the Faroese area and Greenland: new methods and techniques used in an innovative, integrated provenance study. Fróðskaparrit **43**, 96–108.

Friedrichs, K.H. 1987: Electron microscopic analyses of dust from the lungs and the lymph nodes of talc-mine employees. American Industry Hygiene Association Journal **48**, 626–633.

Grütter, H.S., Gurney, J.J., Menzies, A.H. & Winter, F. 2004: An updated classification scheme for mantle-derived garnet, for use by diamond explorers. Lithos **77**, 841–857.

Heasman I. & Watt, J. 1989: Particulate pollution case studies which illustrate uses of individual particle analysis by scanning electron microscopy. Environmental Geochemistry and Health **11**, 157–162.

Huffman, G.P. *et al.* 1994: Investigation of ash by microscopic and spectroscopic techniques. In: Williamson, J. & Wigley, F. (eds): The impact of ash deposition on coal fired plants. Proceedings of the Engineering Foundation Conference (20–25 June 1993, Solihull, Birmingham, UK), 409–423. London: Taylor & Francis.

Huggins, F.E., Kosmack, D.A., Huffman, G.P. & Lee, R.J. 1980: Coal mineralogy by SEM analysis. Scanning Electron Microscopy **1**, 531–540.

Hutchison, M.T. 2005: Diamondiferous kimberlites from the Garnet Lake area, West Greenland: exploration, methodologies and petrochemistry. In: Secher, K. & Nielsen, M.N. (eds): Workshop on Greenland's diamond potential. 7–9 November 2005 in Copenhagen. Extended abstracts. Danmarks og Grønlands Geologiske Undersøgelse Rapport **2005/68**, 33–42.

Knudsen, C., Frei, D., Rasmussen, T., Rasmussen, E. S. & McLimans, R. 2005: New methods in provenance studies based on heavy minerals: an example from Miocene sands in Jylland, Denmark. Geological Survey of Denmark and Greenland Bulletin **7**, 29–32.

Lee, R.J. & Kelly, J.F. 1980: Overview of SEM-based automated image analysis. Scanning Electron Microscopy **1**, 303 only.

Lin, M.C. & Barnes, R.G. 1984: Mössbauer spectroscopy and scanning electron microscopy study of iron-graphimet. Journal of Applied Physics **55**, 2294–2296.

Pirrie, D., Butcher, A.R., Power, M.R., Gottlieb, P. & Miller, G.L. 2004: Rapid quantitative mineral and phase analysis using automated scanning electron microscopy (QemSCAN); potential applications in forensic geoscience. In: Pye, K. & Croft, D.J. (eds): Forensic geoscience: principles, techniques and applications. Geological Society Special Publication (London) **232**, 123–136.

Schwoeble, A.J., Dalley, A.M., Henderson, B.C. & Casuccio, G.S. 1988: Computer-controlled SEM and microimaging of fine particles. Journal of Metals **40**, 11–14.

Steffen, S., Otto, M., Niewoehner, L., Barth, M., Brozek-Mucha, Z., Biegstraaten, J. & Horvath, R. 2007: Chemometric classification of gunshot residues based on energy dispersive X-ray microanalysis and inductively coupled plasma analysis with mass-spectrometric detection. Spectrochimica Acta **B62**, 1028–1036.

Yin, C. & Johnson, D.L. 1984: An individual particle analysis and budget study of Onondaga Lake sediments. Limnology & Oceanography **29**, 1193–1201.

Authors' addresses

N.K., D.F., M.T.H. & C.K., *Geological Survey of Denmark and Greenland, Øster Voldgade 10, DK-1350 Copenhagen K, Denmark.* E-mail: *ntk@geus.dk*

S.B., *Avannaa Resources Ltd., Geological Museum, University of Copenhagen, Øster Voldgade 5–7, DK-1350 Copenhagen K, Denmark.*

L.J., *FLSmidth A/S, Vigerslev Allé 77, DK-2500 Valby, Denmark.*